

Alma Mater Studiorum – Università di Bologna

DOTTORATO DI RICERCA IN

SCIENZE BIOTECNOLOGICHE, BIOCOMPUTAZIONALI,  
FARMACEUTICHE E FARMACOLOGICHE

Ciclo 33

**Settore Concorsuale:** 03/D1 CHIMICA E TECNOLOGIE FARMACEUTICHE, TOSSICOLOGICHE E  
NUTRACEUTICO - ALIMENTARI

**Settore Scientifico Disciplinare:** CHIM/08 – CHIMICA FARMACEUTICA

DESIGN AND SYNTHESIS OF (PRO)ELECTROPHILIC COMPOUNDS FOR  
INVESTIGATING THE MULTIFACTORIAL NATURE OF  
NEURODEGENERATIVE DISEASES: FOCUS ON INFLAMMATION-DRIVEN  
EVENTS

**Presentata da:** Filippo Basagni

**Coordinatore Dottorato**

Maria Laura Bolognesi

**Supervisore**

Michela Rosini

**Esame finale anno 2021**

# CONTENTS

<b>Preface</b>	iii
<b>Abstract</b>	iv
<b>Chapter 1 – Introduction</b>	1
<b>1.1 The inflammation-centred network: new opportunities arise from exploring nodes and connections</b>	3
1.1.1 Cytokines' imbalance: focus on NF- $\kappa$ B and CB <sub>2</sub> R as promising cellular watchmen of their release	5
1.1.2 Neuroinflammation and oxidative stress: a toxic intertwined relationship involving Nrf2 and MAO-B	10
1.1.3 Neuroinflammation and proteinopathies: focus on $\beta$ -amyloid	15
1.1.4 The role of excitotoxicity in neuroinflammation	19
<b>1.2 Electrophilic warheads: emerging tools in drug discovery</b>	21
1.2.1 Electrophilic-sensor targets to tackle neuroinflammatory processes	24
1.2.2 Electrophiles as pharmacological tools in neuroinflammation	27
<b>Chapter 2 – Aim of the thesis</b>	36
<b>2.1 Inhibition of <math>\beta</math>-amyloid aggregation: the key role of (pro)electrophilic warheads</b>	39
2.1.1 METHODS: Chemistry and Biology	42
2.1.2 RESULTS AND DISCUSSION	44
2.1.3 CONCLUSIONS	51
<b>2.2 Merging dihydroxy-cinnamic core into a coumarine nucleus to enclose CB<sub>2</sub>R modulatory properties</b>	52
2.2.1 METHODS: Chemistry and Biology	54
2.2.2 RESULTS AND DISCUSSION	56
2.2.3 CONCLUSIONS	63
<b>2.3 Double attack to the neurodegenerative cascade: MAO-B and Nrf2 as elected targets</b>	64
2.3.1 METHODS: Chemistry and Biology	67
2.3.2 RESULTS AND DISCUSSION	71
2.3.3 CONCLUSIONS	78
<b>2.4 Exploiting memantine as driving-motif to build up neuroprotective hybrids</b>	79
2.4.1 METHODS: Chemistry and Biology	83
2.4.2 RESULTS AND DISCUSSION	84

2.4.3 CONCLUSIONS	87
<b>Chapter 3 – Conclusions</b>	<b>88</b>
<b>Chapter 4 – Experimental section</b>	<b>91</b>
<b>4.1 Chemistry</b>	<b>91</b>
<b>4.2 Biology</b>	<b>111</b>
<b>Abbreviations and acronyms</b>	<b>117</b>
<b>Bibliography</b>	<b>119</b>
<b>Appendix</b>	<b>133</b>

## PREFACE

This PhD thesis has been carried out at the Department of Pharmacy and Biotechnology, Alma Mater Studiorum – University of Bologna (Italy) under the supervision of Prof. Michela Rosini and during the period abroad at Institute of Pharmacy and Food Chemistry, University of Würzburg (Germany), under the supervision of Prof. Michael Decker.

The dissertation research presented here is focused on the design, synthesis and evaluation of new (pro)electrophilic compounds for investigating mechanisms regulating the etiopathology of neurodegenerative diseases. This PhD work is focused on four main projects: i) study of the mechanistic underpinnings involved in catechol's inhibitory activity toward A $\beta$  aggregation through the synthesis and biological investigation of new nature-inspired dihydroxyl derivatives; ii) design, synthesis and characterization of new coumarine derivatives that merge antiaggregant with antiinflammatory properties; iii) development of pioglitazone-derived hybrids with putative neuroprotective properties and targeting both Nrf2 and MAO-B; iv) design, synthesis and characterization of memantine derivatives with antiinflammatory/immunomodulatory skills.

This thesis is organized in four different chapters.

The first chapter is an introduction about physiopathological aspects and the intertwined mechanisms underpinning neuroinflammatory processes in the context of neurodegenerative diseases, highlighting the underrated importance and potential of electrophilic modulation in this respect, both at physiological and pharmacological level.

Chapter 2 contains the drug design approaches used in each project as well as synthetic methods and biological evaluation assays of the new synthesized compounds. Results and discussion sections are also reported.

Chapter 3 draws overall final remarks.

Chapter 4 includes experimental procedures of synthesized compounds including chemical and biological methods.

I would like to sincerely thank Prof. Michela Rosini for guidance and encouragement throughout this exciting project realization. I would express my gratitude to Prof. Anna Minarini for helpful discussion and valuable support during this 3-years journey. I would also like to thank Prof. Michael Decker (University of Würzburg) for hosting and supporting me during my period abroad, where I carried out part of the synthesis of the project described in chapter 2.2, and for binding CBRs assays.

Thanks to Prof. Manuela Bartolini and Prof. Barbara Monti (University of Bologna) and their groups for biological investigations regarding  $\beta$ -amyloid aggregation and neurotoxicity/immunomodulation.

Thanks to Dr. Maria Luisa Di Paolo and Prof. Giorgio Cozza for biological investigations *in vitro* and *in silico* on hMAOs. Thanks to Prof. Cristina Lanni (University of Pavia) and Prof. Ian Mellor (University of Nottingham) and their groups for biological investigations on Nrf2- and NMDAR-related activities.

## ABSTRACT

Neuroinflammation constitutes a major player in the etiopathology of neurodegenerative diseases (NDDs), by orchestrating several neurotoxic pathways which in concert lead to neurodegeneration. A positive feedback loop occurs between inflammation, microglia activation and misfolding processes that, alongside excitotoxicity and oxidative events, represent crucial features of this intricate scenario. The multi-layered nature of NDDs requires a deeper investigation on how these vicious cycles work. This could further help in the search for effective treatments.

Electrophiles are critically involved in the modulation of a variety of neuroprotective responses. Thus, we envisioned their peculiar ability to switch on/off biological activities as a powerful tool for investigating the neurotoxic scenario driven by inflammation in NDDs. In particular, in this thesis project, we wanted to dissect at a molecular level the functional role of (pro)electrophilic moieties of previously synthesized thioesters of variously substituted trans-cinnamic acids, to identify crucial features which could interfere with amyloid aggregation as well as modulate Nrf2 and/or NF- $\kappa$ B activation. To this aim, we first synthesized new compounds to identify bioactive cores which could specifically modulate the intended target. Then, we systematically modified their structure to reach additional pathogenic pathways which could in tandem contribute to the inflammatory process. In particular, following the investigation of the mechanistic underpinnings involving the catechol feature in amyloid binding through the synthesis of new dihydroxyl derivatives, we incorporated the identified antiaggregating nucleus into constrained frames which could contrast neuroinflammation also through the modulation of CB<sub>2</sub>Rs. In parallel, Nrf2 and/or NF- $\kappa$ B antiinflammatory structural requirements were combined with the neuroprotective cores of pioglitazone, an antidiabetic drug endowed with MAO-B inhibitory properties, and memantine, which notably contrasts excitotoxicity. By acting as Swiss army knives, the new set of molecules emerge as promising tools to deepen our insights into the complex scenario regulating NDDs.

# CHAPTER 1

## INTRODUCTION

Neurodegenerative diseases (NDDs) are chronic disorders with a significant inflammatory component, whose incidence is constantly growing worldwide. This is partially due to the increase in lifespan, given the high impact on elderly population.<sup>1</sup> Unfortunately, no disease-modifying therapy is still available, in part due to the lack of a deep and overall comprehension of the triggering etiopathological networks. In the central nervous system (CNS), exogenous or endogenous stimuli initiate alterations in neuronal function and structure, leading to progressive deterioration if not discontinued by tailored physiological compensative mechanisms or pharmacological responses. For many NDDs, initiating events in reply to an insult involve inflammatory processes which aim to protect and fix the tissues affected.<sup>2</sup> Nevertheless, if the homeostasis is not restored and the insult persists, neuroinflammation becomes chronic, stirring up neurodegeneration and progressing to cognitive and motor declines.<sup>3</sup> The CNS inflammatory response is orchestrated by a complex interplay between glial cells, blood-brain barrier (BBB) and signaling molecules such as cytokines and chemokines that in liaison produce a counteracting reaction (Figure 1.1).<sup>4</sup>

Glial cells are non-neuronal cells, which maintain brain homeostasis through function of neuronal support as well as immunity duties. Among glial family there are oligodendrocytes, astrocytes and microglia. Oligodendrocytes in the CNS generate the myelin sheath wrapping axons. The myelin sheath is not continuous but interrupted by the nodes of Ranvier, which allow fast signal transmission between neurons (Figure 1.1). Oligodendrocytes are also the presumed target of autoimmune diseases such as multiple sclerosis (MS).<sup>5</sup> Astrocytes are multifaceted cells, which appear in different morphological forms (star-shaped, protoplasmic and fibroblastic). They are primarily responsible for brain homeostasis by maintaining the integrity of BBB, facilitating neuronal growth and development, encapsulating inflammatory lesions, and controlling the environment by regulating pH, ion balance, oxidative stress, and blood flow. They play a pivotal role during inflammation favouring the recruitment of monocytes/macrophages, T cells and other glial cells (Figure 1.1).<sup>6</sup>

Microglia are the most abundant resident myeloid cell type in the CNS, around 15-20% of total, but displaying regional differences in density. They have fundamental role in CNS-synapses development and maintenance of trophic support, but, overall, they are considered as the immune-cell resident population of the brain, constituting a constant surveillance of the surrounding microenvironment.<sup>7</sup> Furthermore, CNS also contains non-microglia resident myeloid cells including perivascular, choroid plexus and meningeal macrophages and dendritic cells with mainly microglia-related duties.<sup>8</sup>

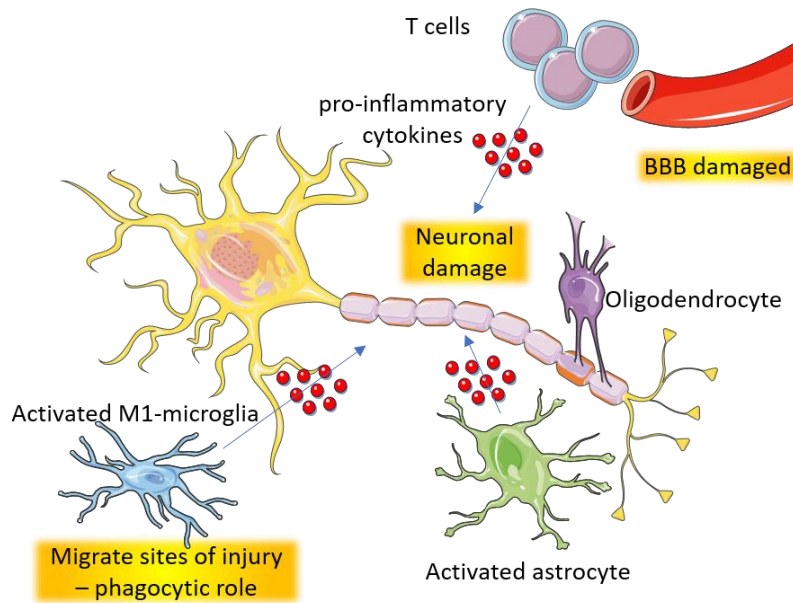


**Figure 1.1.** Schematic representation of neuroinflammatory conditions with invading T cells and loss of BBB integrity. Activated microglia and astrocytes concertedly secrete proinflammatory cytokines which fuel inflammatory cascade and neuronal damage. Modified from <sup>9</sup>.

Microglia release both proinflammatory and antiinflammatory molecules in response to the microenvironment insult and assault. Microglia are considered brain-resident macrophages, besides being the largest source of central inflammatory mediators (Figure 1.1). Their tailoring activities are represented by the ability to modify phenotype depending on the surrounding stimuli.<sup>10</sup> Based on function and morphology, different microglia states have been classified, whose activation represents a very highly regulated process depending on various endogenous/exogenous factors. The “resting” microglia phenotype (called M1-like), with high-ramified form, handles with several essential functions, spanning from synaptic plasticity and maturation, programmed cell-death control, and support to oligodendrogenesis and neurogenesis.<sup>11</sup> M1 microglia act in the forefront to protect tissues and destroy pathogens inducing proinflammatory stimuli which can setup a vicious cycle turning into neurotoxic if the injury is prolonged or becomes chronic. When challenged with proinflammatory stimuli, microglia assume amoeboid and unramified morphology (called M2-like), not to be confused with the dystrophy due to age-related deterioration, travel to the site of injury and play macrophagic properties also recruiting cells and secreting tuned cytokines and chemokines (Figure 1.2).<sup>12</sup> Normally, M2-like phenotype was induced by short-lasting low intensity neuronal damages, causing release of neurotrophic factors and blockage of inflammatory responses. Furthermore, these “alternatively activated” microglia recruit astrocytes to keep neuronal homeostasis and oligodendrocyte precursor preventing demyelination-neurodegeneration. Parallely, long-lasting and high-intensity injuries induce M1 state, causing ROS/RNS increased production and neurotoxic cytokines release (Figure 1.2).<sup>7, 11</sup>

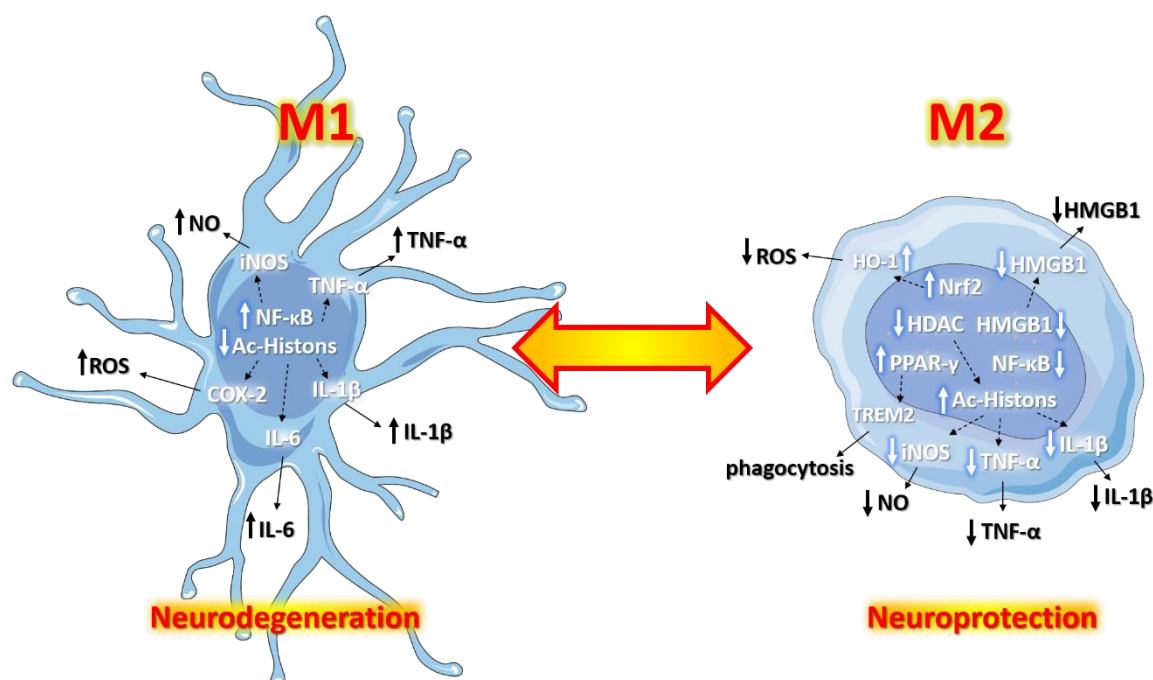


**Figure 1.2.** A schematic view of activated M1 and M2 microglia with the molecular pathways involved in both phenotypes. Modified from <sup>7</sup>.

This complex neuroimmune system develops and acts similarly to its peripheral counterpart, albeit it takes the advantage of immune privilege thanks to BBB and a nuanced contact with peripheral nervous system. Firstly, previously described CNS cells activate innate responses through pattern recognition receptors and microglia activation. Secondly, the local CNS reaction promotes recruitment of peripheral innate and adaptive immune cells.<sup>13</sup> At this step, the functional role of BBB makes the difference. It is composed of two physiological boundaries, the vascular BBB and the blood-cerebro spinal fluid. BBB, acting as sentinel barrier, can play an indirect fundamental role to counteract neuroinflammation by controlling transport of immunomodulatory agents into the brain. In fact, many neurological disorders with neuroinflammatory component are related to higher BBB permeability with a positive correlation to disease severity. Furthermore, BBB is also able to produce and secrete cytokines, playing a direct role in antiinflammatory response.<sup>14</sup>

### **1.1 The inflammation-centred network: new opportunities arise from exploring nodes and connections**

The crucial role of an inflammatory component in NDDs is a well-accepted concept.<sup>15</sup> However, even though it has passed more than twenty years since first antiinflammatory approaches against demyelinating and NDDs, a comprehensive knowledge of the etiopathological networks is not yet available.<sup>16, 17</sup> Evidence of neuroinflammatory processes in post-mortem studies has been confirmed on molecular basis. Activated microglia and increased inflammatory markers (e.g. MHC-II, CD68, IL-1β/6/8/10, TNF-α) were found in affected brain regions of Parkinson's disease (PD), Alzheimer's disease (AD) and Huntington's disease (HD)



patients, to name a few, suggesting neuroinflammation to be a feature, and not solely a consequence, of the diseases.<sup>18-20</sup>

During the '90s several epidemiological and clinical studies on chronic use of non-steroidal anti-inflammatory drugs (NSAIDs) revealed reduced risk for developing NDDs and clinical improvement in patients who already suffered from it.<sup>21-24</sup> On the wave of these results, neuroinflammation gained consideration as a potential target to treat neurodegenerative conditions. Several clinical trials investigated the effects of NSAIDs treatment on cognitive measures, mainly Alzheimer's disease-related, but all of them failed leaving unsolved the neuroinflammation-neurodegeneration paradigm.<sup>25</sup>

The failure of these approaches calls for a deeper comprehension of the exact role of neuroinflammation in the neurotoxic cascade, prompting to investigate connections between inflammatory processes and other renowned etiopathological hallmarks of neurodegenerative conditions. Misfolded proteins just like oxidative stress or neuronal loss associated to impaired neurotransmission are considered molecular alterations able to trigger inflammatory processes and microglia priming, while being in turn boosted by inflammatory events. A variety of targetable pathways can modulate these neurotoxic features, offering the view of a puzzling scenario (Figure 1.4).

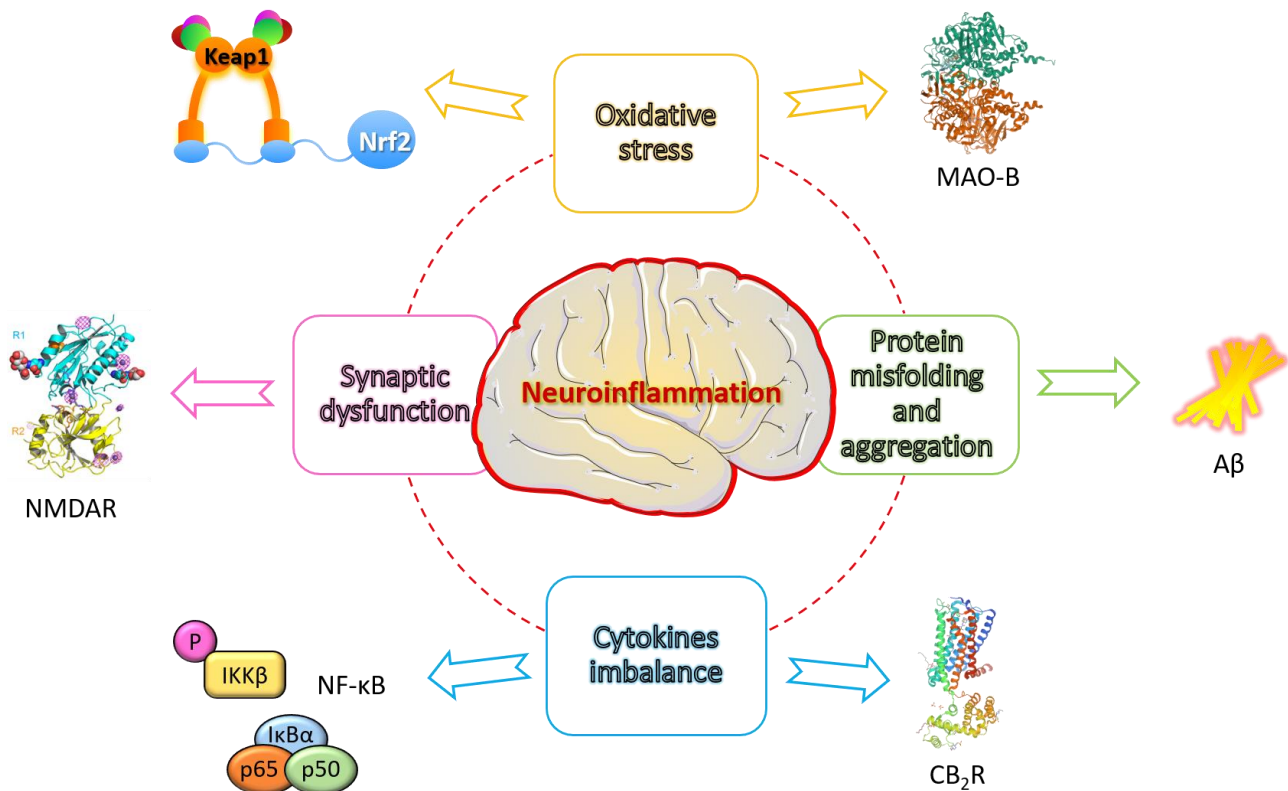


**Figure 1.4.** Overview of neuroinflammatory-related pathways characterizing neurodegenerative disorders.

In the following, I will focus on cytokine imbalance, ROS overproduction, excitotoxicity, and protein misfolding and aggregation as key pathogenic partners of neuroinflammation, dwelling on their mutual intertwined relationship. Further, I will discuss the molecular pathways and targets that we herein envisioned as a valuable opportunity to modulate the abovementioned inflammation-centred neurotoxic events.

### *1.1.1 Cytokines' imbalance: focus on NF- $\kappa$ B and CB<sub>2</sub>R as promising cellular watchmen of their release*

Cytokines are essential messengers, which provide cells with the ability to communicate among themselves. A vast array of cytokines is known in human body (more than 300), the majority of which with pleiotropic nature, indicating the complexity of cytokine's network. Most cytokines are expressed at very low levels or not expressed in CNS, while under stress conditions their expression is strongly upregulated. Depending on their functions, they are divided into different categories, ranging from growth to tumor necrosis factors (TNF), neurotrophins and colony-stimulating factors (CSF) to general interleukins (IL). Chemokines represent a subfamily of cytokines with the task to induce cell migration, fundamental for immune cells trafficking to the injured site.<sup>26</sup> Cytokines are involved in brain forming and development through growth and survival local factors. Transforming growth factor 1 $\beta$  (TGF-1 $\beta$ ) and IL-6, for instance, promote switching and differentiation of neurons, oligodendrocytes and astrocytes.<sup>27</sup> Due to their multifaceted role, some cytokines can play different roles at different cell stages. An example is represented by IL-6, a cytokine that usually promotes neuronal survival in response to neuronal damage, whereas elevated concentrations are associated with brain disorders.<sup>28</sup>

In CNS disorders with neuroinflammatory component the first proinflammatory cytokines release is carried out by peripheral invading lymphocytes and myeloid cells, fuelling the downstream cascade. In this respect, boosting actors are considered T cells with their derived multitude of specialized cytokines.<sup>29</sup>

Dysregulation of cytokine network is a major contributor to tissue injury and neurological deficit characterizing neurodegenerative conditions. Thus, counteracting cytokine imbalance is considered a forefront therapeutic approach to fight neuroinflammatory processes in neurodegeneration, with the aim to both prevent further neurotoxic boosting mechanisms and to block downstream signaling pathways.<sup>30</sup> In this respect, the nuclear factor  $\kappa$ -light-chain enhancer of activated B cells (NF- $\kappa$ B) plays a pivotal role.<sup>31</sup> The cellular NF- $\kappa$ B transcription machinery provides a pleiotropic response to a wide variety of external stimuli such as stress, cytokines and free radicals, acting as master regulator of inflammatory and immune response. This small family of inducible transcription factors can be found in almost all human cell types and its principal role lies in inflammatory response and cell survival. At basal level, NF- $\kappa$ B is usually trapped in the cytosol by inhibitor of  $\kappa$ B (I $\kappa$ B) proteins, whereas it is constitutively activated, albeit very rarely, in some immune-competent cells (e.g. T/B cells, astrocytes, monocytes).<sup>32</sup> NF- $\kappa$ B can be activated through two different pathways depending on the transduction mechanism. In the classical/canonical activation pathway

proinflammatory IL-1, TNF or lipopolysaccharide (LPS) induce I $\kappa$ B kinase (IKK) complex initiation via modulation of mutual receptors, leading to phosphorylation of I $\kappa$ B residues (e.g. Ser32-36 for I $\kappa$ B $\alpha$  and Ser19-23 for I $\kappa$ B $\beta$ ). I $\kappa$ B prevents NF- $\kappa$ B-DNA binding by masking its nuclear localization signal and the DNA binding domain. Phosphorylated I $\kappa$ B undergoes ubiquitination and degradation through 26S proteasome complex, whereas NF- $\kappa$ B becomes free to translocate into the nucleus, bind  $\kappa$ B site of promoter region in dimeric form (p50-p65/RelA subunits) and induce transcription of inflammatory agents such as inducible nitric oxide synthase (iNOS), cyclooxygenase-2 (COX-2) or cytokines like IL-1 $\beta$  and TNF- $\alpha$ .<sup>33</sup> The alternative/non-canonical pathway is activated mainly by members of TNF-receptor superfamily. At basal level TNF receptor-associated factor 3 (TRAF3) mediates recruitment of NF- $\kappa$ B inducing kinase (NIK) to TRAF2 leading to NIK ubiquitin-mediated degradation, therefore maintaining low cytosol levels of NIK and NF- $\kappa$ B trapped. Non-canonical activation promotes TRAF2 proteolysis of TRAF3, avoiding targeting of new NIK and causing its cytosol accumulation. This latter induces p100 phosphorylation by IKK $\alpha$  homodimers and partial degradation to release p52. Therefore, p52-RelB heterodimers translocate to the nucleus, inducing transcription of targeted genes. While canonical NF- $\kappa$ B activation is rapid and independent from protein synthesis, non-canonical NF- $\kappa$ B activation involves NIK synthesis and accumulation, requiring longer time of response.<sup>34</sup> Canonical and non-canonical activation pathways are strictly correlated, as they share transcriptional mediators and signaling agents such as IKK.<sup>32</sup>

Basal expression of NF- $\kappa$ B family members was found at higher levels in CNS than in peripheral tissues. Interestingly, NF- $\kappa$ B-induced neuronal response depends on differential activation of NF- $\kappa$ B-dimers. The RelA subunit paired in p50/RelA dimer and the consequent downstream signaling promote cell death and apoptosis, whereas c-Rel subunit and its post-transcriptional modification exert anti-apoptotic and neuroprotective effect.<sup>35</sup> In fact, recent genetic evidences are demonstrating important roles for NF- $\kappa$ B in physiological processes such as neurogenesis and synaptic plasticity, revealing beneficial effects like learning and memory.<sup>36</sup>

NF- $\kappa$ B activation is considered a key player in cellular response towards different injuries characterizing neurodegenerative diseases, such as oxidative stress, excitotoxicity and aggregated proteins. A first reaction involves NF- $\kappa$ B-mediated antiinflammatory effect, paired with inducing programmed cell death to remove damaged tissue. If the same neurotoxic injury persists, the constitutive activation of NF- $\kappa$ B becomes neurotoxic, fuelling neuroinflammation and contributing to neurodegeneration.<sup>37</sup> A tight and multi-layered electrophile-modulating system is taking place to manage NF- $\kappa$ B-mediated cellular response. For example, covalent adducts with Cys179 of IKK $\beta$  or Cys62 of p50 subunit proved to irreversibly alter NF- $\kappa$ B downstream cascade through different mechanisms, therefore exerting important immunomodulatory and antiinflammatory properties (Figure 1.5).<sup>38, 39</sup> Modification at Cys179 of IKK $\beta$  negatively interferes with phosphorylation of nearby Ser177 and Ser181, a key step for IKK $\beta$  activation, whereas covalent adducts with

specific cysteines in DNA-binding regions (Cys38 of p65 and Cys62 of p50) of NF- $\kappa$ B subunits prevent transcription of proinflammatory genes.<sup>40</sup>

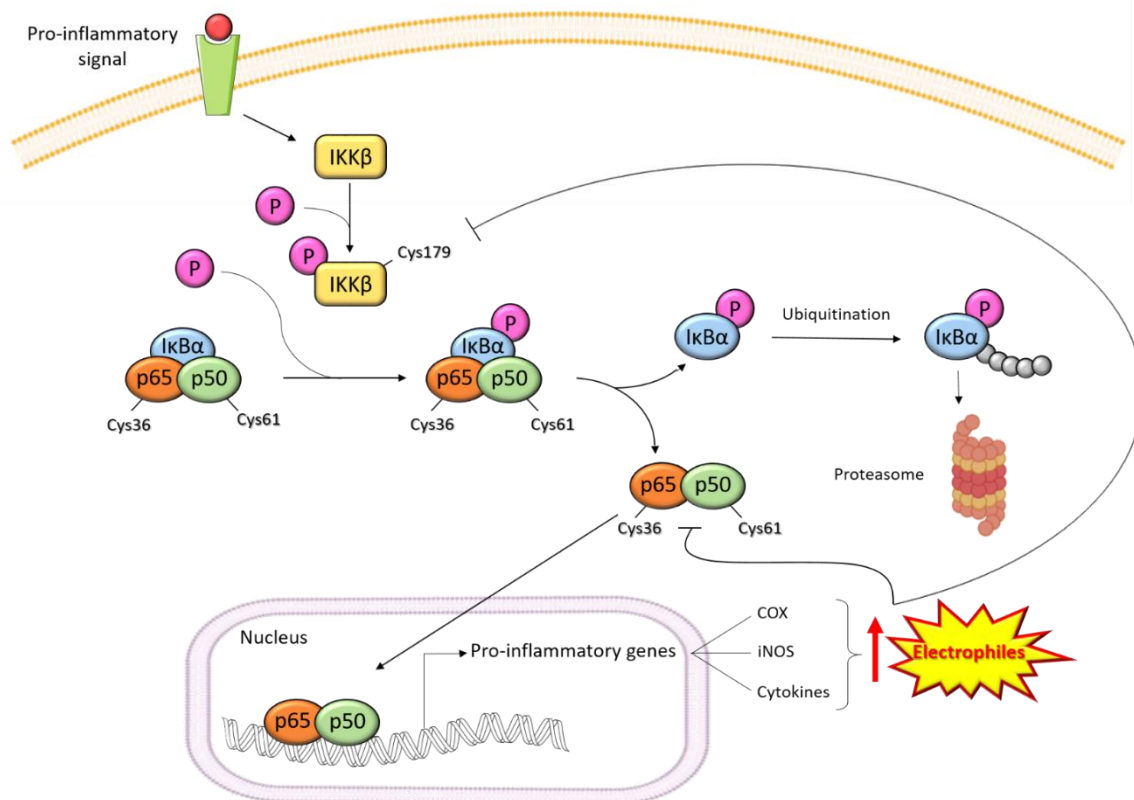


**Figure 1.5. Activation mechanism of NF- $\kappa$ B pathway.** NF- $\kappa$ B activation by proinflammatory stimuli and inhibition by electrophiles. Under basal conditions, IKK $\beta$  phosphorylates I $\kappa$ B, releasing the heterodimer p50/p65. Upon nuclear translocation, p65 activates the transcription of a variety of cytokine and inflammatory enzyme-coding genes. Addition of IKK $\beta$  by electrophiles results in its inhibition, impairing NF- $\kappa$ B activation. Moreover, direct adduction of p65 inhibits its nuclear localization by most likely interfering with the dimerization that leads to NF- $\kappa$ B dependent gene expression. Modified from <sup>41</sup>.

NF- $\kappa$ B activation in microglia and astrocytes is viewed as an important contributor in triggering local inflammatory processes.<sup>42</sup> p50-p65 activated transcription in astroglia and microglia increases ROS/RNS formation and proinflammatory cytokines (mainly IL-1 $\beta$ , IFN- $\gamma$  and TNF- $\alpha$ ) levels, which in turn cause a secondary neurotoxicity promoting cell death, increasing oxidative stress and inducing protein misfolding. Furthermore, NF- $\kappa$ B showed to affect permeability and intracellular trafficking at BBB through IL-15 production, indirectly impacting on the recruitment of peripheral inflammatory mediators.<sup>43</sup> In addition, a strict relation exists between NF- $\kappa$ B and proteinopathies. Particularly, amyloid  $\beta$  (A $\beta$ ) oligomers, amyloid protein precursor (APP),  $\alpha$ -synuclein and huntingtin directly modulate NF- $\kappa$ B expression influencing inflammatory responses.<sup>44-46</sup> In AD, A $\beta$  strongly induces IL-1 $\beta$  and IL-6 production by NF- $\kappa$ B which in turn upregulates  $\beta$ -secretase (BACE-1) and APP amyloidogenic cleavage in a vicious neurotoxic cycle. As a confirmation of NF- $\kappa$ B role in neurodegeneration, higher expression levels of relative gene or target genes were found in patients affected by neurodegenerative disorders.<sup>47, 48</sup> Based on these considerations, several inhibitors of the NF- $\kappa$ B pathway were identified and studied to further confirm *in vivo* the potential neuroprotection deriving from impairment of the downstream signaling cascade. In disease models, a variety

of inhibitors and inhibitory approaches demonstrated to strongly reduce proinflammatory cytokines expression, memory impairment and NF- $\kappa$ B-derived proteinopathies.<sup>49, 50</sup> Despite the premises, no NF- $\kappa$ B inhibitors are still marketed, neither promising clinical trials are ongoing.<sup>51</sup> One of the principal issues in exploiting NF- $\kappa$ B as target relies on its ubiquitous expression, with multiple players involved fulfilling a plethora of essential cellular duties. Nevertheless, development of selective inhibitors and their biological evaluation helped to shed light on NF- $\kappa$ B involvement in several pathologies, neuroinflammation included. Inhibition of protein kinases and DNA-binding blocking were exploited as the main strategies to alter the activation pathway. Inhibitors like ATP-analogues for kinase blocking or DNA-mimic fragments to avoid DNA binding always show selectivity problems, therefore covalent inhibition of sensible cysteines arose as a possibility to reach selective inhibitors. Blockage of nuclear translocation, proteasome inhibition or antioxidant efficacy are other pharmacological approaches exploited in preclinical trials.<sup>51</sup>

Besides the master regulator of cytokines release, novel signaling mechanisms such as cannabinoid receptors have shown to exert potential cytokines regulatory abilities with promising therapeutic translation. In particular, the endocannabinoid system (ECS) has gained increasing attention for its peculiar immunomodulatory properties at central level. Cannabinoid type-1 receptor (CB<sub>1</sub>R) is considered the class A G-protein coupled receptor (GPCR) member with the highest expression in CNS. Furthermore, tuned overexpression and unusual localization of cannabinoid type-2 receptors (CB<sub>2</sub>R) in neuroinflammatory conditions caused suspicion on its direct involvement in onset of neuroinflammation.<sup>52</sup> Besides CBRs, the ECS includes also several biological players of different nature like ionotropic cannabinoid receptors (e.g. transient receptor potential channels), nuclear hormone receptors (e.g. PPAR family) and all the catabolic/anabolic enzymes involved in EC metabolism (e.g. FAAH, MAGL), which jointly regulate essential homeostatic processes.<sup>53</sup> Since the CB<sub>2</sub>R cloning in 1993, CBRs have basically been distinguished according to their biodistribution: CB<sub>1</sub>R in the brain with neuromodulatory properties and peripherally with immunomodulatory properties, albeit this classification nowadays is overcome with CB<sub>2</sub>R spotted in microglia and CB<sub>1</sub>R in peripheral immune cells.<sup>54-56</sup> Particularly, CB<sub>2</sub>R has gained major attention as potential pharmacological target for its peculiar strong up-regulation in pathological conditions correlated with the onset of inflammatory processes such as in cancer and in neurodegenerative diseases.<sup>52, 57, 58</sup> Furthermore, CB<sub>2</sub>R activation produces the desired pharmacological effects without the unwanted psychotropic effects related to CB<sub>1</sub>R.<sup>59-61</sup> In particular, triggering CB<sub>2</sub>R-driven cascades leads to strong reduction of inflammatory processes through the switch of microglia into the M2 antiinflammatory phenotype, which promotes the release of antiinflammatory cytokines.<sup>62-64</sup> For example, it has been found in post-mortem cortical brain tissues of neuropathologically confirmed AD patients that expression of CB<sub>2</sub>Rs was 40% higher than in healthy brain and that their activation in AD animal models not only reduced inflammatory response but also seemed able to decrease amyloid-toxicity, facilitating its clearance, and improve cognitive performance.<sup>59, 65</sup> The same correlation between overexpression and beneficial effects derived from CB<sub>2</sub>R activation was found in other

neuroinflammatory disorders like PD,<sup>66</sup> HD,<sup>67</sup> ALS<sup>68</sup> or peripheral pathological conditions such as rheumatoid arthritis, inflammatory bowel disease and atherosclerosis.<sup>64</sup>

Unlike the well-characterized CB<sub>1</sub>R's signal transduction pathways, for CB<sub>2</sub>R different possible activation pathways exist, still not fully elucidated, depending on the respective tissue, agonist applied, and pathological conditions involved. For sure, we know that CB<sub>2</sub>R signaling is mediated via Gi/o proteins, thereby reducing cAMP levels, triggering kinases cascade or intracellular calcium mobilization through phospholipase C (PLC) activation and via  $\beta$ -arrestins causing receptor desensitization and internalization.<sup>69, 70</sup>

The neuroprotective potential of CB<sub>2</sub>R's ligand relies on its strategic location, and in some cases overexpression, in key glial cells. For instance, CB<sub>2</sub>R-mediated signals control BBB functions, maintaining its integrity, avoiding lymphocytes infiltration, and increasing A $\beta$  clearance. Microglial CB<sub>2</sub>R, in addition to favouring M2-phenotype shift, stimulate antiinflammatory cytokines and modulate microglia migration and infiltration in brain areas with ongoing inflammatory-degenerative processes. In astrocytes they induce chemokines and neurotrophic factors release, whereas in oligodendrocytes CB<sub>2</sub>Rs stimulate neurorepair, remyelination and neuronal differentiation (Figure 1.6).<sup>59, 71</sup>

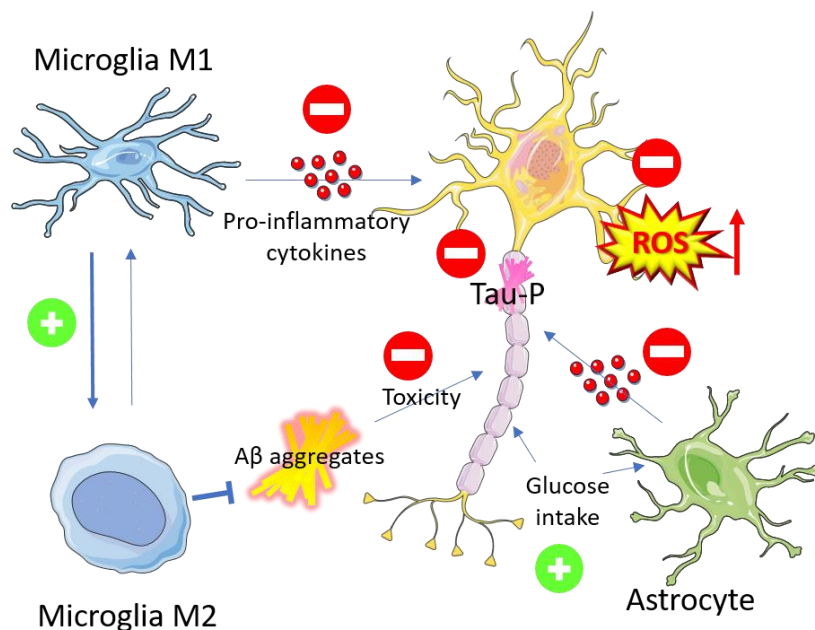


**Figure 1.6.** Main effects of CB<sub>2</sub>R activation reported in AD models. CB<sub>2</sub>R agonists reduce the release of proinflammatory molecules, facilitate A $\beta$  clearance by promoting microglia phagocytic phenotype, reduce A $\beta$ -neurotoxicity, and facilitate glucose uptake. Moreover, CB<sub>2</sub>R-mediated activity reduces oxidative stress damage produced by reactive oxidative species (ROS) and tau hyperphosphorylation. Modified from <sup>59</sup>.

CB<sub>2</sub>R agonists in AD mouse model proved to strongly reduce secretion of proinflammatory cytokines, ROS, increase A $\beta$  aggregates' phagocytosis and improve cognitive impairment.<sup>59, 72</sup> In stress-induced neuroinflammation models, selective agonists reduced expression of COX-2, iNOS and NF- $\kappa$ B, together with a decrease in TNF- $\alpha$  and MCP-1 levels.<sup>64</sup> Similar preclinical outcomes were observed in AD e PD *in vivo* models following treatment with inhibitors of endocannabinoid degradation (e.g. MAGL or FAAH inhibitors), which

determined reduced IL-1 $\beta$  and TNF- $\alpha$  release, suppression of microglial and astrocyte activation and neuroprotection (Figure 1.6). In PD, ALS and HD mouse models, CB<sub>2</sub>R agonists were shown to alter disease progression through reduction of oxidative stress-induced neuronal degeneration, as revealed by the improvement of neuroprotective markers.<sup>72, 73</sup>

Thanks to its privileged role in neuroinflammation, several CB<sub>2</sub>R selective pharmacological tools were developed to further deepen CB<sub>2</sub>R involvement in onset and progression of neurodegenerative disorders, albeit with no diagnostic agents approved so far.<sup>74</sup> Despite all the promising experimental observations listed above there is still no selective CB<sub>2</sub>R drug approved and all clinical trials involving CB<sub>2</sub>R ligands failed until now. They have been clinically evaluated in neuropathic pain, osteoarthritis, neurodegenerative diseases (e. g., AD, PD, MS, ALS, HD) resulting in generally safe drugs, but with poor therapeutic efficiencies.<sup>75, 76</sup> These failures are linked to several difficulties in targeting CBRs. First of all, the complexity and incomplete consciousness of CB<sub>2</sub>R signal transduction pathway, with many variants and bias signaling which make difficulties in obtaining a clear pharmacological evaluation of CB<sub>2</sub>R ligands.<sup>77</sup> Secondary, usual CB<sub>2</sub>R preferential ligands are too lipophilic and poorly soluble impeding suitable BBB passage and delivery at neuroinflammatory tissues. Further insights on CB<sub>2</sub>R pharmacology with different approaches are needed in the expectations to potentially translate into clinic its intriguing and multi-layered anti-inflammatory activities.

Besides CB<sub>2</sub>R and NF- $\kappa$ B, also peroxisome proliferator-activated receptors (PPAR), belonging to the superfamily of nuclear hormone receptors, regulate several anti-inflammatory and antioxidant pathways, including NF- $\kappa$ B and nuclear factor erythroid 2-related factor 2 (Nrf2). Particularly, PPAR- $\gamma$  emerged as suitable target to properly interfere with neuroinflammation processes, but yet its investigation is not part of this PhD work.<sup>78</sup>

### *1.1.2 Neuroinflammation and oxidative stress: a toxic intertwined relationship involving Nrf2 and MAO-B*

Oxidative stress and neuroinflammation are two intertwined key pathologic factors in neurodegenerative diseases. Oxidative stress consists of redox imbalance and its cytotoxic consequences. At physiological level, production of reactive species (ROS, RNS) in the body is counterbalanced by antioxidant activities of cells. Oxidative stress occurs when ROS production overwhelms antioxidant defence, thus causing altered intracellular signaling and disruption of cellular functions. The CNS is highly sensitive and susceptible to oxidative stress due to the high metabolic rate and oxygen consumption. Therefore, ROS overproduction often represents the first symptom of cellular impairment, thereby inducing proper antioxidant response.<sup>79</sup> In the CNS, microglia and astrocytes are one of the major sources of ROS as byproducts of physiological oxygen metabolism by mitochondria or intracellular peroxidase and membrane surface NADPH oxidase (NOX).<sup>80</sup> In altered conditions of inflammation, ROS are strongly overproduced, partially through the work of activated M1-phenotype. At the same time, reactive species are able to activate signaling pathways, creating a vicious cycle which maintains high levels of proinflammatory cytokines and chemokines secretion.<sup>81</sup> In

addition, aggregates of misfolded proteins are one of the featuring hallmarks of neurodegenerative disorders, which proved to be also great inducers of ROS release.<sup>82</sup> At the same time, oxidative and electrophilic stress (OES) paired with inflammatory cytokines revealed to strongly trigger misfolding processes through oxidation at specific residues, thus establishing a self-sustaining neurotoxic loop.<sup>81</sup> Microglia antioxidant defence lies with the mitochondria pool of GSH and enzymes such as catalase or superoxide dismutase (SOD), however this cellular shield to oxidative stress was found to be impaired where neuronal loss occurs. For example, in several neurodegenerative disorders, NOX-induced aberrant ROS production was found to be one of the main responsible for microglia neurotoxic activation (Figure 1.7). As a confirmation of that, pharmacological inhibition of NOX in *in vivo* models proved to strongly reduce oxidative damage as well as to exert neuroprotective efficacy.<sup>83</sup>

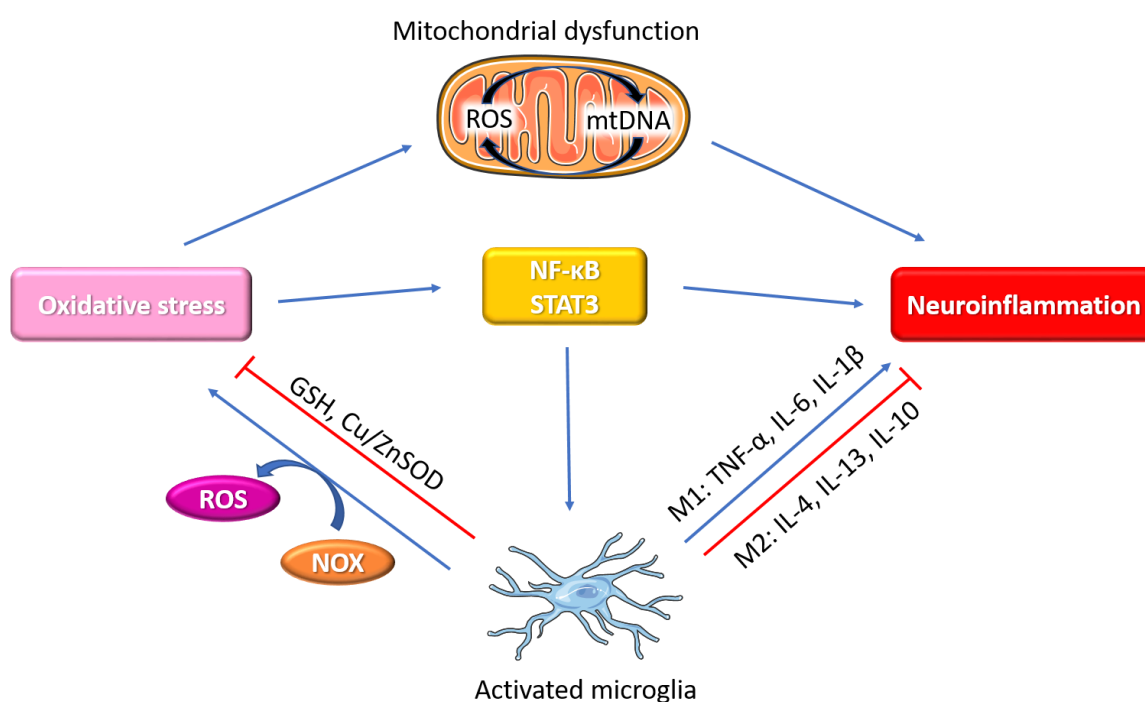


**Figure 1.7.** Crosstalk between oxidative stress and neuroinflammation in the progress of PD. Continue exposure to ROS led to mtDNA mutation which enhance ROS production, forming a positive feedback loop. On the other hand, defective mitochondria triggered an innate immune response. ROS activated NF-κB and STAT3 which mediated proinflammatory response of microglia to CNS injury. Activated microglia could be polarized to M1/M2 phenotype with proinflammatory and anti-inflammatory effects. Moreover, microglia not only induced oxidative stress through NADPH oxidase (NOX) generated ROS but also could prevent oxidative damage through high concentrations of GSH and Cu/ZnSOD. Modified from <sup>84</sup>.

A delayed and long-lasting activation of antioxidant transcription factors remains the most powerful cellular response to oxidative insults. Besides the inflammatory NF-κB pathway, Nrf2 controls both basal and inducible cellular antioxidant response transactivating cytoprotective genes through a common DNA regulatory element, called antioxidant response element (ARE), in the promoter regions of these genes.<sup>85</sup> Furthermore, Nrf2 demonstrated to play a key role in the resolution of inflammatory processes through direct down-regulation of proinflammatory cytokines levels and functional crosstalk with NF-κB, while Nrf2-deficiency induces exacerbation of inflammatory markers.<sup>86, 87</sup> At resting state, Nrf2 is trapped by its



repressor Kelch-like ECH-associated protein 1 (Keap1) and cytosolically retained to undergo ubiquitination and further proteasomal degradation. In conditions of OES, the redox sensitive Keap1 is covalently modified at specific cysteine residues, therefore altering Nrf2 binding and avoiding consequent degradation. The newly synthesized Nrf2 can now escape Keap1 binding and freely translocate into nucleus to enhance ARE-dependent transcription.<sup>88</sup> This includes a plethora of antioxidant enzymes such as NADH-quinone oxidoreductase 1 (NQO1), glutathione-S-transferase (GST), heme oxygenase-1 (HO-1). In turn, expression of these latter revealed to be deregulated in inflamed glial cells, being considered as potential targets for a concerted antioxidant reply.<sup>89</sup>

The Nrf2 repressor Keap1 possesses almost the double of cysteine residues (i.e. 27 in human) in respect to the number of average proteins. These take part to the so called “cysteine code”,<sup>88</sup> with Cys151, Cys273 and Cys288 emerging as the most susceptible to electrophilic attack. Interestingly, Cys151 in BTB domain seems to be crucial for oxidative stress-induced Nrf2 activation, whereas Cys273 and Cys288 in IVR may be essential for Nrf2 ubiquitination (Figure 1.8).<sup>90</sup> Furthermore, Cys151 covalent modification avoids Cul3 ubiquitin ligase-Nrf2 interaction.<sup>91</sup> Therefore, several Nrf2 electrophilic activators were developed, firstly, to provide biological details on Nrf2 electrophilic modulation and, secondly, to set the stage for future therapeutic applications.<sup>92, 93</sup>

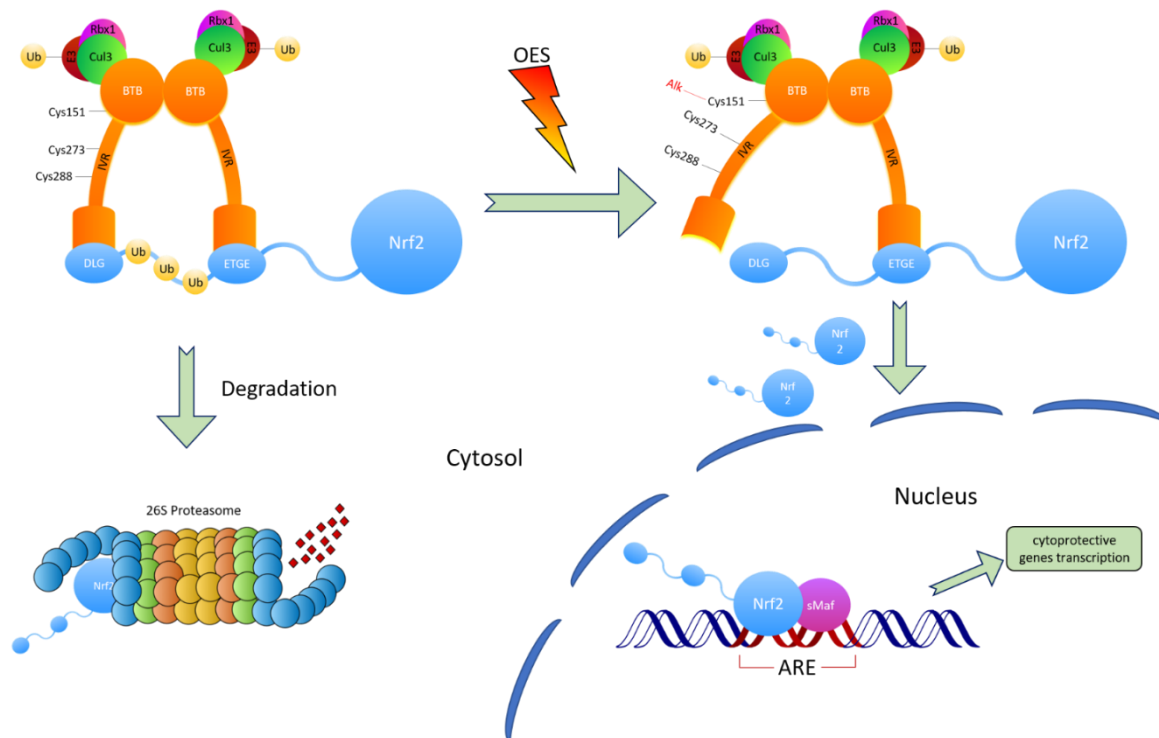


**Figure 1.8. Activation mechanism of Nrf2–ARE pathway.** In physiological/unstressed condition Keap1 dimer (in orange in the figure) traps Nrf2 in the cytosol through interaction with DLG and ETGE motifs. The following ubiquitination of several lysine residues between these two motifs from the Keap1–Cul3 E3 ligase complex is the starting point of Nrf2 degradation by 26S proteasome complex. However, under condition of oxidative or electrophilic stress, Keap1 is covalently modified at specific Cys residues in IVR/BTB region allowing stabilization of Nrf2 binding through ETGE motif. In this case, *de novo* synthesized Nrf2 immediately translocates into the nucleus and, forming heterodimers with small Maf protein (sMaf), activates cytoprotective genes transcription through binding antioxidant response elements (AREs). Modified from <sup>92</sup>.

*In vivo* models of neurodegenerative diseases confirmed the pivotal role of Nrf2-activated transcription pathways in reverting inflammatory response. Interestingly, these processes passed through activation of astrocytic and microglial Nrf2, that controlling redox homeostasis indirectly modulate and affect other inflammatory regulators such as NF- $\kappa$ B.<sup>94</sup> In AD and PD patients Nrf2 proved also to act as essential mediator of the etiopathogenetic loop between oxidative stress and aggregates of misfolded proteins-induced neurotoxicity. Particularly, Nrf2 exerted neuroprotection against  $\beta$ -amyloid toxicity, whereas it is partially sequestered in Lewy bodies with consequent impaired antioxidant efficacy.<sup>94, 95</sup> Despite the therapeutic promise of targeting Keap1-Nrf2-ARE pathway, only few compounds proved to pass BBB and therefore properly activate Nrf2 in CNS. The most famous Nrf2 activator is dimethyl fumarate (DMF), marketed as Tecfidera® and approved in 2013 from FDA for the treatment of relapsing forms of multiple sclerosis (see chapter 1.2.2 for details).

Impairment of physiological neuronal functions remains a feature of neurodegeneration. The severity grade of neurodegenerative diseases usually depends on the complexity of the alteration, ranging from distorted subcellar processes to generalized neuronal loss. The step between these two is short, especially in CNS disorders when symptoms appear at late-stage levels. A case report in this respect can be referred to pathological dysregulation of neurotransmitter catabolism leading to neurotoxic oxidative stress.<sup>96</sup> At basal level primary amines, such as dopamine (DA), serotonin (5-HT) or adrenaline (NE), are degraded by monoamine oxidases (MAOs) forming toxic byproducts (e.g. respectively aldehydes, ammonia and hydrogen peroxide) which are usually nullified by cellular antioxidant controllers, whereas in pathological conditions, they can favour the onset of oxidative damage.<sup>97</sup> MAO notable role in neurotransmitter regulation is confirmed by several marketed MAO-targeting drugs, spanning from antidepressant to anxiolytic and other neurological disorders treatment. Since selegiline approval in 1998 as MAO-B inhibitor for the treatment of PD, MAO has been repositioned as valuable target for neurodegenerative diseases.<sup>98</sup>

Two isoenzymes of MAO are present in mammalian tissues originally distinguished by substrate specificities: MAO-A with higher affinity for serotonin and noradrenaline, while MAO-B prefers phenylethylamine. Further functional-structural analysis categorized crystal structures of *h*MAO-A as a monomer while *h*MAO-B as dimer, albeit sharing around 70% of sequence identity.<sup>99</sup> They belong to the flavoenzyme family located in outer mitochondrial membrane and containing a single flavin adenine dinucleotide (FAD) cofactor per monomer, essential for catalytic process. The active site of *h*MAO-B is formed by a prolonged hydrophobic cavity, ranging from flavin isoalloxazine ring site to the protein surface nearby membrane bilayer (Figure 1.9A). A lysine residue (Lys296 in *h*MAO-B and Lys305 in *h*MAO-A) is H-bonded with flavin ring through a water molecule and it has been suggested to play an active role in enzymatic activity such as stabilize molecular oxygen during flavin reoxidation. On the other hand, Ile199 confers a dual-cavity active site in *h*MAO-B, adopting an open conformation with bulky ligand or closed position with smaller molecules which

occupy only the space close to FAD (Figure 1.9B). This bipartite nature of the cavity in *h*MAO-B and a major structural flexibility of A isoenzyme makes the difference between two isoforms, justifying substrate specificities.<sup>98</sup>

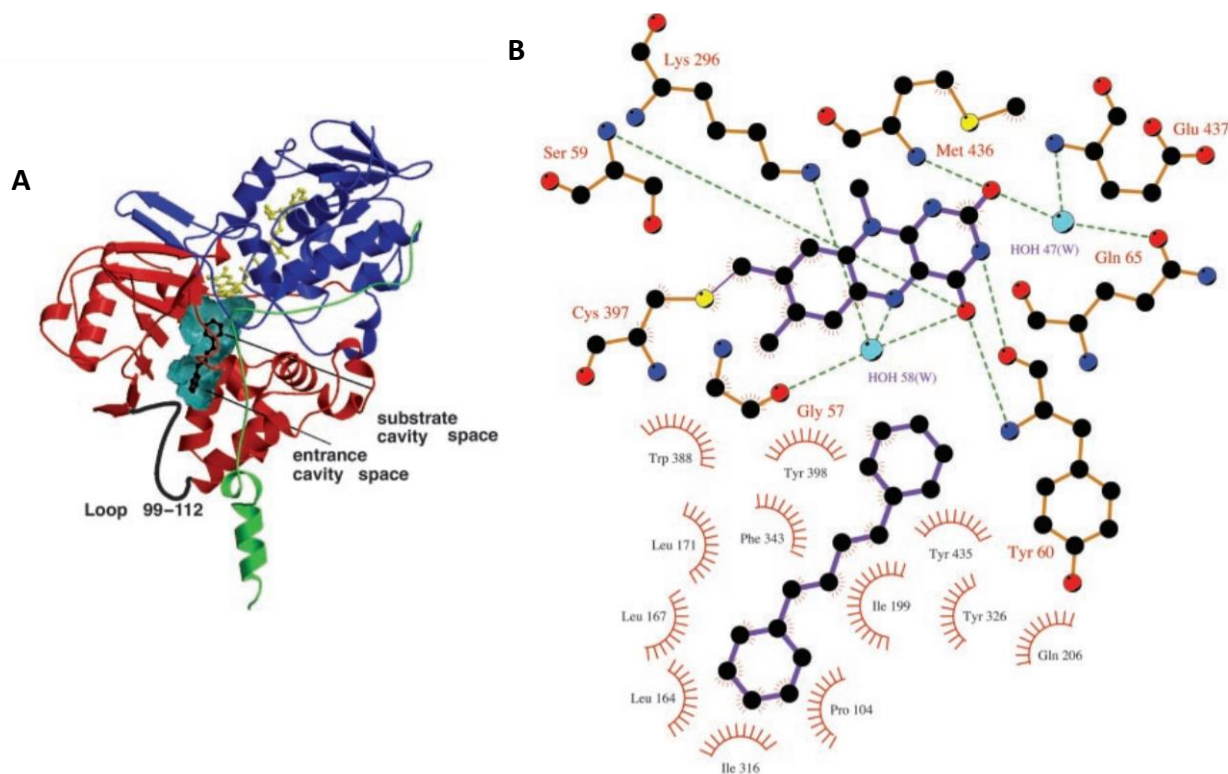


**Figure 1.9. A.** Overall three-dimensional structure of *h*MAO-B monomeric unit in complex with 1,4-diphenyl-2-butene. The FAD-binding domain is in blue, the substrate-binding domain is in red, and the C-terminal membrane-binding region is in green. The FAD cofactor and the inhibitor are shown as yellow and black ball-and-stick models, respectively. The inhibitor binds in a cavity (shown as a cyan surface) that results from the fusion of the entrance and substrate cavities. **B.** Illustration of 1,4-diphenyl-2-butene binding to MAO-B. Dashed lines indicate H-bonds. Taken from <sup>100</sup>.

Age-related increase of MAO activities in CNS paired with overexpression of MAO-B in glial cells of patients affected by neurodegenerative disorders have been considered a rational base to exploit MAO-B inhibitors to study neurodegenerative processes and potentially evaluate their clinical translation. Particularly, MAO-B has been proposed to play a pivotal role in onset of PD through inducing oxidative stress condition in astrocytes, although its first clinical outcomes referred to reduced dopamine degradation.<sup>101</sup> For example, in AD patients activated MAO-B led to cognitive dysfunctions and neuronal loss. Furthermore, increased levels of astrocytic and pyramidal MAO-B regulate A $\beta$  production modulating  $\gamma$ -secretase activity and participate in formation of neurotoxic neurofibrillary tangles (NFTs) in AD brain.<sup>101-103</sup> A correlation between MAO activity and AD progression was found, highlighting a greater enzyme activity surrounding A $\beta$  plaques and indicating MAOs' activities as potential biomarkers for AD.<sup>104</sup> Similarly, astrocytic upregulation in PD mouse model triggers ROS/RNS production which in turn activate nearby microglia therefore inducing inflammatory processes.<sup>105</sup> MAO inhibition proved to decrease microglial and partially astrocytic activation, with a beneficial reduction of IL-1 $\beta$ , IL-6 and TNF- $\alpha$  expression, as well as limited NF- $\kappa$ B nuclear translocation.<sup>106, 107</sup> Recently, a more selective MAO-B inhibition was correlated to higher astrogliosis attenuation paired with

increased cognitive markers.<sup>108</sup> To date, covalent and non-covalent MAO-B inhibitors have been approved for PD treatment, and their efficacy is under evaluation in a variety of clinical trials for treatment of other neurodegenerative diseases, mainly AD.<sup>99</sup>

Oxidative stress is a concerted cellular alteration where diverse endogenous factors play a role, thus creating a neurotoxic loop. Besides Nrf2 and MAO examples herein reported, a plethora of antioxidant strategies have been developed from researchers to counteract oxidative stress at multiple levels, ranging from direct radical scavenging activity to induced antioxidant enzyme transcription.<sup>79, 109-112</sup>

### *1.1.3 Neuroinflammation and proteinopathies: focus on $\beta$ -amyloid*

In the physiopathology and etiopathology of neurodegenerative diseases, aggregates of misfolded proteins play a pivotal role. However, the mechanism by which this happens is still unclear. Each neurodegenerative disease is characterized by a different distribution and composition of protein aggregates, although they share similar morphological characteristics and triggering events.<sup>113</sup> Since Alzheimer's findings on extracellular amyloid plaques and intracellular NFTs in post-mortem brain of AD patients, aggregates of misfolded proteins have represented the typical pathological hallmarks of almost all neurodegenerative disorders: from Lewy bodies in PD, to huntingtin deposits in HD, aggregates of SOD1 in ALS or prion proteins (PrP) in some forms of encephalopathies.<sup>114</sup> Genetic factors, such as mutations in protein primary structure, can favour destabilization of physiological conformation and induce misfolding. Parallely, environmental factors including pH, oxidative stress, dyshomeostasis of metal ions or pathological chaperones proved to be able to catalyse aggregates formation.<sup>115</sup>

In most cases, native monomeric protein is predominantly composed of  $\alpha$ -helical and unordered structure, whereas misfolded polymers are rich in  $\beta$ -sheet conformation. Kinetic studies suggested that the critical event is the formation of protein oligomers, which consequently act as seeds to propagate nucleation-dependent polymerization in similar manner to crystallization. It has been found that the probability of aggregation is directly related to increasing protein concentration, such as happens in genetic mutations which lead to local altered protein dosages. Conditions of oxidative and electrophilic stress can facilitate protein aggregation through distinctive structural changes. Beside pathological post-translational modifications, protein oxidation influences aggregates formation at different levels such as modulating proteasome capacity, chaperone activity or perturbing translational processes.<sup>116</sup> Particularly, oxidation of critical amino acids can induce changes in protein secondary structure that can differently modulate aggregation kinetic. Met46 oxidation was the primary cause of glyceraldehyde-3-phosphate dehydrogenase (GAPDH) aggregation, while Met35 oxidation hinders the rate of A $\beta$  fibril formation and alter its morphology.<sup>116, 117</sup> Some studies proposed also that intermediates of misfolded proteins at different stages exert diverse toxic effects. Misfolded oligomers could activate signaling pathways leading to apoptosis, while

bulky aggregates break down neuronal connections as well as participate in recruiting immune cells and activate inflammasomes.<sup>118</sup> If on one side we have relevant, albeit not exhaustive, information on the kinetics and mechanisms of aggregation, lot of uncertainty still exists on the plethora of putative factors occurring as starting events. Several enzyme- and non-enzyme-mediated events process primary structure of unfolded proteins into aggregation-prone oligomers. Impaired proteolytic cleavage is one of the most recurrent cause of harmful oligomers formation. In AD, APP is processed sequentially by BACE and  $\gamma$ -secretase forming neurotoxic oligomers such as  $A\beta_{40}$  or  $A\beta_{42}$ , whereas at physiological level APP undergoes cleavage by  $\alpha$ -secretase following a non-amyloidogenic pathway. Similar series of events occur in HD and PD, where enzymatically truncated huntingtin and  $\alpha$ -synuclein tend to form aggregates.<sup>113</sup> Enzymes of proteolytic cleavage constitute pivotal players which can be modulated by cellular inflammatory pathways, thus amplifying the neurotoxic cascade, but also represent possible targets to engage with pharmacological treatments.<sup>119</sup>

In the long term, misfolded protein aggregates drive to synaptic dysfunction and loss, as well as oxidative stress and neuroinflammation. Once formed, protein aggregates cause the onset of a persistent inflammatory reaction, provoking extensive astrogliosis and microglia activation, especially around protein deposits.<sup>120</sup> Among NDDs,  $\beta$ -amyloid pivotal role in AD development has been the most studied and exploited for clinical translations, albeit unsuccessful until now. Therefore, herein I will handle  $\beta$ -amyloid driven neurotoxic cascade as case study for NDDs with related proteinopathies. Evidence exists that  $A\beta$  deposition is correlated to the onset of inflammatory events through microglia activation and overproduction of inflammatory cytokines, which can in turn modulate amyloid production.<sup>121</sup> For instance, soluble  $A\beta$  oligomers and insoluble  $A\beta$  aggregates induce microglial priming and phenotype switching toward chronic level of neuroinflammation, which lead to a constant production of proinflammatory cytokines and chemokines (Figure 1.10).<sup>122</sup> Therefore, inflammatory processes and misfolded disease proteins create a neurotoxic loop where they mutually exacerbate each other.<sup>114, 123</sup> Prolonged inflammatory stimuli convert microglia into irreversible dystrophic phenotype and it is detrimental also for surrounding CNS cells such as neurons, astrocytes and oligodendrocytes, which drive to neurodegeneration.<sup>123, 124</sup>

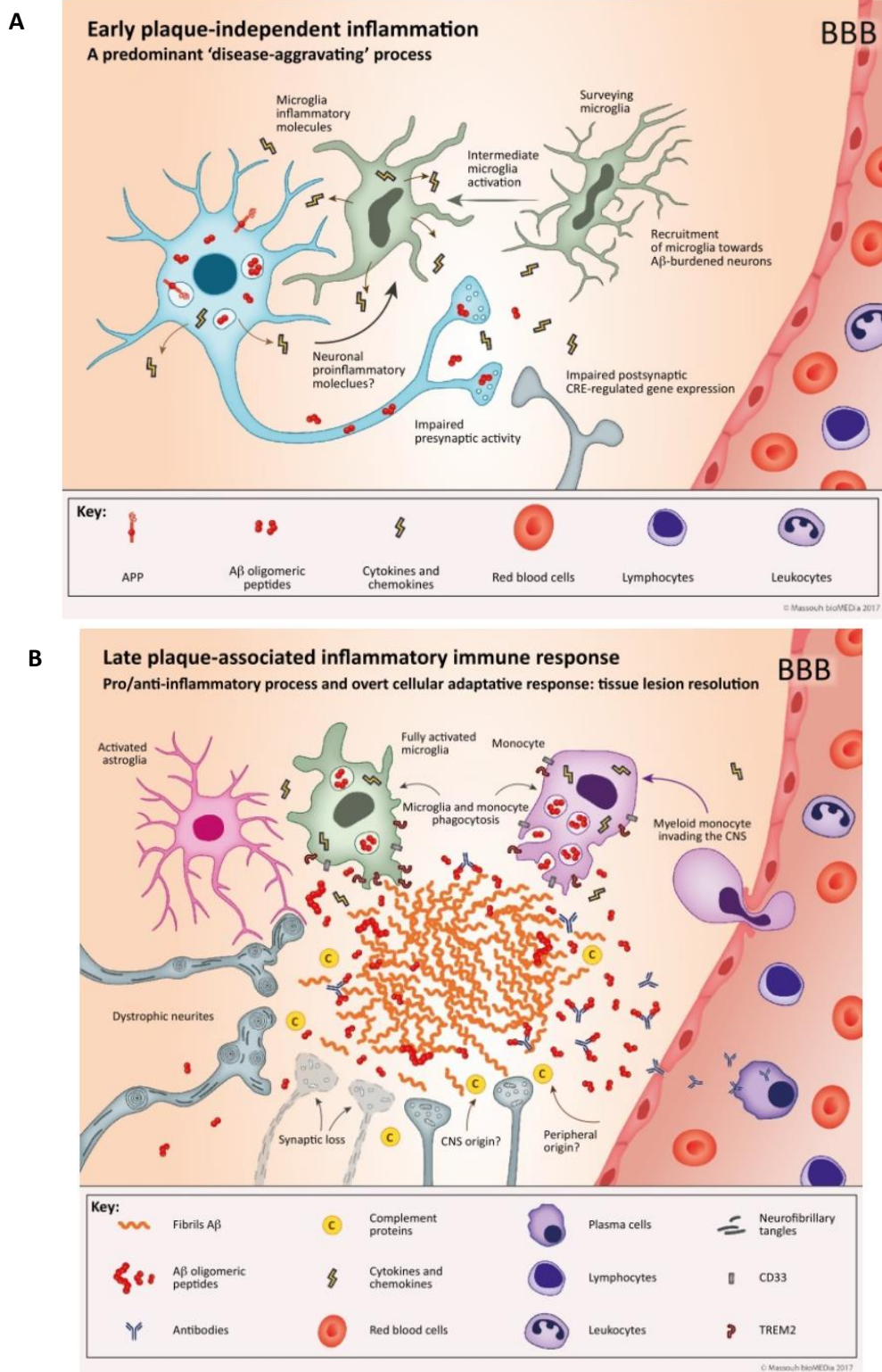


**Figure 1.10. A.** In Early AD's neuroinflammation Aβ-burdened neurons are likely to act as initiators of the inflammatory process, provoking the intermediate activation of microglia and their mobilization towards Aβ-burdened neurons. Both cell systems provoke a disease-aggravating process in which the release of proinflammatory cytokines and chemokines predominates. **B.** Late CNS Inflammation implies full microglial activation, microgliosis, and CNS invasion by peripheral monocytes. The amyloid plaque and surrounding neuropil display, in addition to cytokines and chemokines, immunoglobulins and complement-related proteins as well as activated astroglia, dystrophic neurites, and degenerating synaptic elements. Taken from <sup>125</sup>.

In detail, A $\beta$  can bind to many receptors expressed on microglial surface, such as CD14, CD36, CD47, integrins, receptor for advanced glycosylation end products (RAGE) and toll-like receptors (TLRs), resulting in subsequent increased proinflammatory cytokines and chemokines production (i.e. IL-1, IL-6, GM-CSF, IL-12, IL-23 and TNF).<sup>123</sup> Furthermore, macrophages and microglial phagocytic properties seem to be impaired in an A $\beta$ -dependent manner, thus preventing amyloid digestion/degradation.<sup>126, 127</sup>

Although the complexity of the multi-layered neurotoxic cascades, several small molecules were developed to reduce cytotoxic aggregates levels through modulation of oligomers production, inhibition of their aggregation and enhancement of the clearance (Figure 1.11).

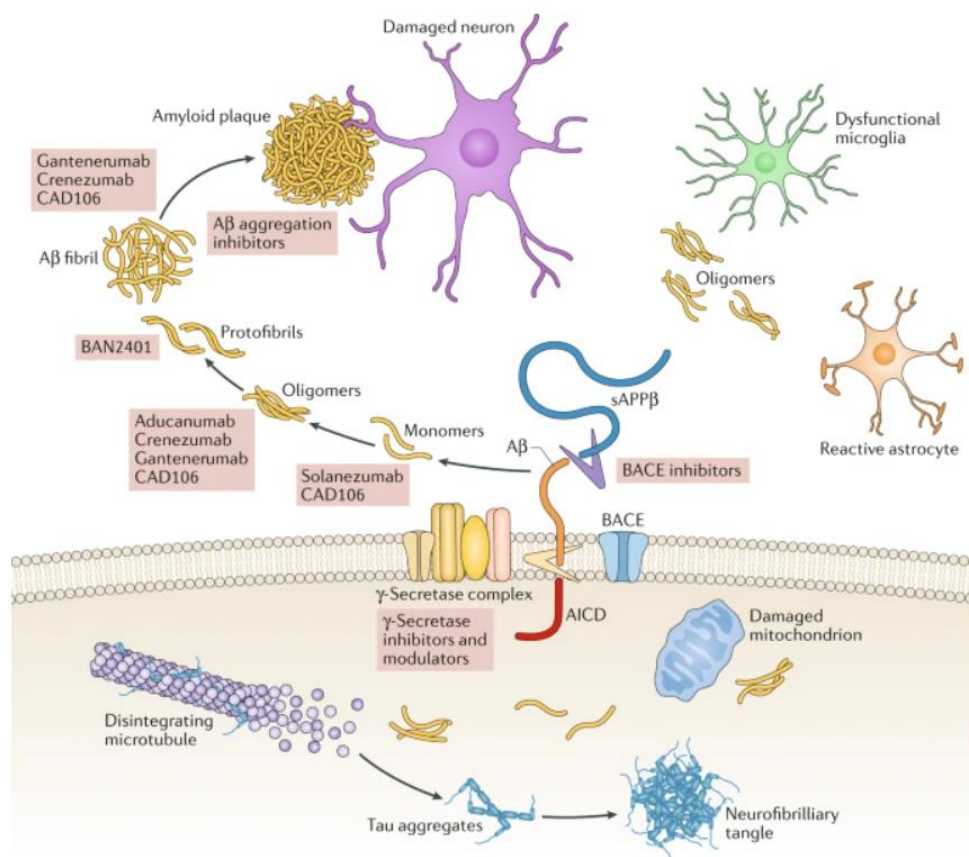


**Figure 1.11.** Mechanisms of action of the main anti-A $\beta$  drugs that are currently in clinical development for the treatment of Alzheimer disease. One of the most explored therapeutic approach regards preventing the formation of critical aggregating-prone oligomers through enzymatic cleavage modulation, such as-BACE1 and  $\gamma$ -secretase inhibitors (GSIs), thus blocking amyloidogenic pathway, or  $\alpha$ -secretase inducers which favour non-amyloidogenic cleavage. Further, enhancing A $\beta$  clearance has been evaluated as potential therapeutic strategy to decrease A $\beta$  content in the brain through the systemic infusion of monoclonal antibodies directed at A $\beta$  which was shown to prevent oligomerization and fibril formation, and to dissolve A $\beta$  aggregates, with high specificity and affinity toward the antigen. AICD, amyloid precursor protein intracellular domain; BACE,  $\beta$ -secretase; sAPP $\beta$ , soluble amyloid precursor protein- $\beta$ . Modified from <sup>128</sup>.

Unfortunately, all the A $\beta$ -targeting therapeutic approaches failed to date, underlining the limitation of disrupting only amyloid-driven pathway in such complex network and suggesting to rethink at different strategies to tackle AD neurotoxic cascade.

#### 1.1.4. *The role of excitotoxicity in neuroinflammation*

Neuronal loss and synaptic dysfunction certify advanced state of neurodegeneration. Neurotoxic network involving neuroinflammation and oxidative damage leads to impairment of neurotransmitters' signaling, thus causing irreversible neuronal deficits. Particularly, overactivity of excitatory amino acids (i.e. glutamate) which overcome astrocytic clearance or cellular uptake mechanisms results in excitotoxicity and consequent cell death. Excitotoxicity represents a common feature among NDDs, albeit it is still lacking the mechanistic comprehension of how it is involved in their pathogenesis' network.<sup>129</sup>

In NDDs injury usually occurs in consequence of prolonged neuronal exposure to glutamate and associate excessive calcium influx through N-methyl-D-aspartic acid receptors (NMDARs).<sup>129</sup> NMDAR differs from the other ionotropic glutamate receptors for the peculiar voltage-dependent activation via removal of  $Mg^{2+}$  blockage, high  $Ca^{2+}$  permeability and slow ligand-gated kinetics. These unusual features make NMDARs essential at central level, mediating the majority of excitatory neurotransmission and playing a critical role in synaptic function/plasticity as well as cellular processes that underlie learning and memory.<sup>130</sup> NMDARs are commonly composed of two glycine or *D*-serine binding GluN1 subunits, responsible for forming the ion channel, and two glutamate-binding subunits GluN2 (A-D) with regulatory role. Interestingly, different tasks depend on receptor localization. While activation of synaptic GluN2A subunit-containing NMDARs (sNMDAR) mediates neuronal survival through anti-apoptotic and antioxidant effects, activation of extrasynaptic GluN2B subunit-containing NMDARs (eNMDAR) is associated with neurotoxicity and cell death.<sup>131, 132</sup> eNMDARs overactivation can be triggered also by the onset of pro-oxidant and inflammatory stimuli characteristic of neuroinflammation. Microglial NMDARs seem to act as essential mediators to confer sensitivity for excitotoxic injury and to induce microglial activation.<sup>133</sup> In excitotoxic brain condition, increased production of ROS and proinflammatory IL-1 $\beta$  and TNF- $\alpha$  were found, which in turn promote NMDAR-mediated neuronal death and further fuel astrocytic release of extracellular glutamate or stop its uptake.<sup>134</sup> Abnormal eNMDARs stimulation leads to enhanced oxidative glutamate-mediated damage, which can foster protein misfolding and aggregating processes (Figure 1.12).<sup>135</sup>



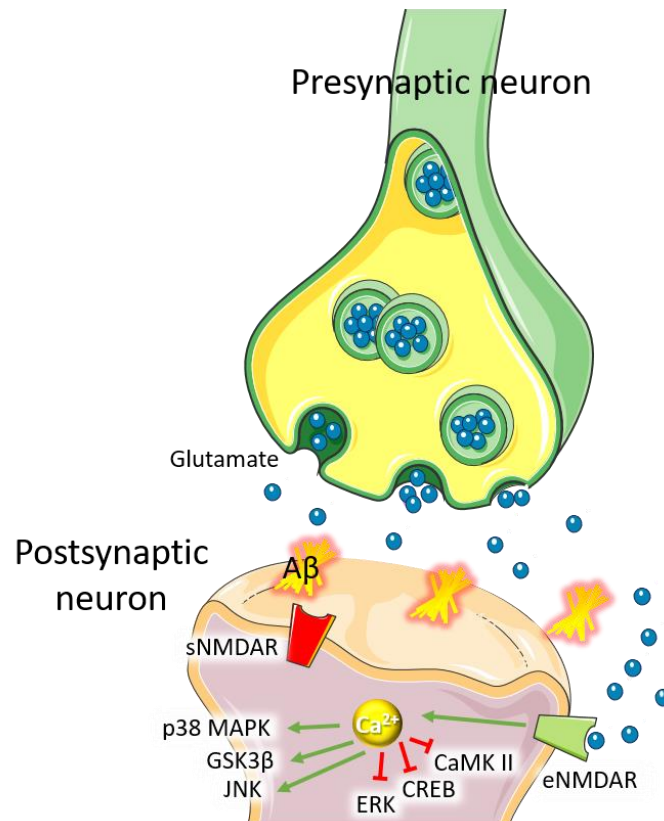


**Figure 1.12.** This figure represents the glutamate-mediated transmission at synaptic level in Alzheimer's disease. A $\beta$  oligomers interfere with NMDA signaling, inducing an internalization of postsynaptic sNMDAR. Glutamate spillover would activate eNMDARs, with increased calcium levels and activation of metabolic pathways (green path) responsible for neuronal shrinkage and synaptic loss, associated with inhibition of prosurvival pathways (red path). The more this condition persists, the more the activated pathologic pathways lead to hyperphosphorylation of cytoskeletal tau protein, with neuronal degeneration and cell death. Modified from <sup>182</sup>.

Parallely, A $\beta$  oligomers can severely disrupt the glutamatergic transmission and induce excitotoxicity through several mechanisms, including stimulation of glutamate release, inhibition of glutamate uptake, and failure of receptors' activity.<sup>136, 137</sup> GluN2B-mediated glutamatergic transmission seems to play a pivotal role in both tau- and A $\beta$ -induced neurotoxicity via Fyn pathway, a nonreceptor tyrosine kinase playing a key role in synaptic physiology. Particularly, A $\beta$  oligomers trigger Fyn activation with subsequent NMDAR and tau phosphorylation, thus disrupting cellular calcium homeostasis and inducing NFTs formation.<sup>138</sup> At the same time, Fyn-Tau interaction facilitates GluN2B phosphorylation which sensitizes NMDARs to favoured A $\beta$ -induced neurotoxicity.<sup>139</sup>

Several neuroprotective agents able to block NMDARs exist, but they are strictly related to the onset of several adverse effects. The ideal NMDAR antagonist and anti-excitotoxic therapy should block pathological NMDAR activation while not affecting physiological synaptic transmission.<sup>140</sup> This is the uncompetitive mechanism of memantine and the reason why it makes the only NMDAR-targeting drug approved for AD, whose peculiar biological profile will be dissected in chapter 2.4. Particularly, memantine (Namenda<sup>®</sup>) is marketed since 2003 for the treatment of moderate to severe forms of AD, albeit it represents only a symptomatic relief.

## 1.2 Electrophilic warheads: emerging tools in drug discovery

The concept of electrophilicity was devised by Parr et al. in 1999 as the energy lowering occurring with a maximal electron flow between a donor (nucleophile) and an acceptor (electrophile),<sup>141</sup> leading to the formation of a new covalent bond via different mechanisms (e.g. Michael addition). The tendency to seek electrons, and related molecule reactivity, relies on the chemical environment of the electrophilic fragment which determines its electronic characteristic of polarizability.<sup>142</sup> This is reflected in a wide choice of covalent binders available, ranging from reversible/transient to irreversible binding motifs.<sup>143</sup> Focusing on electrophiles chemical structure, the choice of a covalent warhead usually falls within Michael acceptors (e.g.  $\alpha,\beta$ -unsaturated carbonyls), ring-strained scaffolds (e.g. epoxide, aziridine,  $\beta$ -lactame) or carbamate, disulfide and isothiocyanate moieties.<sup>144</sup>

Due to their high reactivity, electrophilic moieties have been not well tolerated for years in drug discovery programs, albeit recent revival of covalent drugs.<sup>145</sup> Indeed, drugs acting through covalent interaction with their target have traditionally generated anxiety owing to safety concerns. However, some of the most renowned and sold medicines were discovered to act covalently after years of unknown mechanism of action. After almost a century of use it turned out that the painkiller and antiinflammatory aspirin works irreversibly inhibiting COX-1, an enzyme implicated in prostaglandin biosynthesis.<sup>146</sup> The same happens with penicillin, that was marketed as antibiotic for nearly sixty years before discovering its covalent blockage of an active site serine residue of D-Ala-D-Ala transpeptidase, tearing down bacterial cell wall biosynthesis and leading to the consequent cell lysis.<sup>147</sup>

In recent years, the historic success of non-intentionally designed covalent drugs has prompted to reconsider the power of this approach, recognizing that the combination in a single molecule of covalent and non-covalent modes, with their distinct strengths, might lead to associate carefully tuned reactivity with specific complementarity to the target.<sup>145</sup> A typical strategy is the inclusion of a reactive covalent warhead onto a potent reversible inhibitor for a particular target protein, in the expectation that selectivity will be improved by the optimized fit of the reversible moiety.<sup>148</sup> So-called “targeted covalent inhibitors” (TCIs), by specifically binding poorly conserved amino acids, now provide the basis for a multitude of industrial drug discovery programs, especially in oncology, where a variety of electrophile features are purposely exploited as key trapping instruments for target engagement.<sup>149</sup> Almost one covalent inhibitor each year has been approved ever since, thus confirming the beneficial effects of this approach deriving from careful design and balance of electrophilic properties. A deepen analysis on recent FDA-approved TCIs revealed acrylamide as one of the preferred electrophilic warheads, usually targeting Cys residues (Figure 1.13).

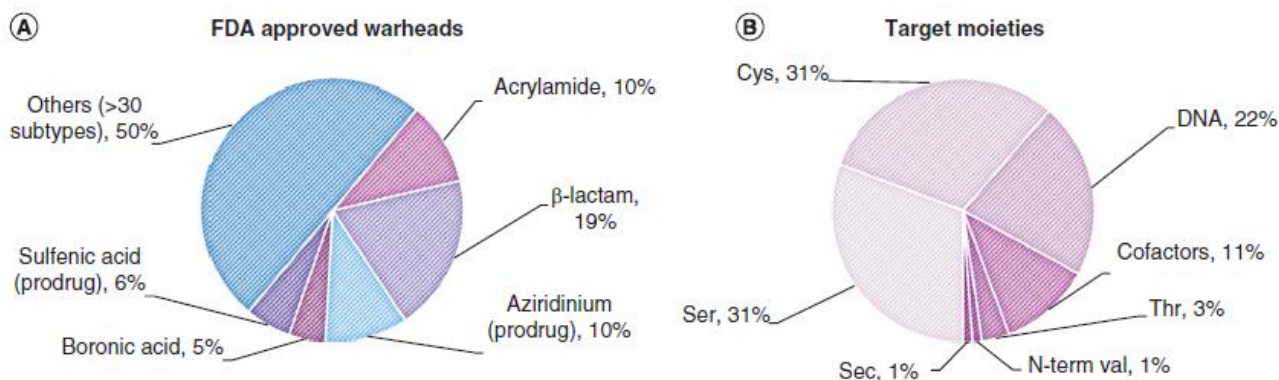


**Figure 1.13.** FDA-approved covalent inhibitors. (A) Different electrophilic warheads in FDA-approved drugs. (B) Target residues covalently bound by FDA-approved drugs.<sup>150</sup>

Several medicinal chemistry approaches were developed in order to soften and efficiently direct electrophilic reactivity, seeking to avoid loss of selectivity and related toxicity.<sup>151</sup> For example, it is gaining increasing relevance strategies aiming at efficiently direct electrophilic reactivity, such as covalently engage disease-specific cysteine mutants or precisely target non-catalytic, but biofunctional, cysteine residues.<sup>152, 153</sup>

The covalent engagement between target and drug opens horizons of hope for the resolution to several unmet questions left unsolved by following the more conventional reversible-binding approaches (Figure 1.13). Firstly, the possibility to inhibit targets previously considered undruggable due to the shallow or lack of appropriate binding pocket could be achieved.<sup>154</sup> The attachment of electrophilic agents to specific nucleophile residue could address the disruption of protein-protein interactions (PPIs), that seems so tricky to target with traditional small reversible binders, cause of their large and flat interfaces.<sup>155</sup> Selective covalent binding can also improve the biochemical efficiency related to the non-equilibrium binding. In this case, there is no competition with high concentration of endogenous ligands (e.g. ATP) with overcoming of pharmacokinetic problems like plasma concentration needed, time of substrate-target residency, dosage, and so on.<sup>149, 156</sup> To correctly focus potential benefits and hold offside effects, it is fundamental to fully know the target's machinery and its physiopathological environment. Indiscriminate action of electrophiles can be limited using pro-electrophilic molecules, which act as pro-drugs, being specifically converted to the active form where the action is needed. This happens for antiacid drugs, like omeprazole, that in acid stomach environment are converted into a tetracyclic intermediate which covalently traps a cysteine residue of gastric  $H^+/K^+$ -ATPase.<sup>157</sup> Another option to gain selectivity in covalent binding exploits the intrinsic activity of the target to activate the inhibitors known as suicide inhibitors or mechanism-based inhibitors (MBIs).<sup>145, 158</sup>

Besides the above reported strategies, aimed to tackle safety concerns related to off-target effects and excessive reactivity, careful evaluations of experimental outputs is needed in order to avoid false read-outs due to unintended reactivity. Indeed, several electrophilic moieties belong to the tricky class of “pan assay interference compounds” (PAINs), which have become a paradigm for promiscuous reactivity that might cause false readouts in biological studies. Following the original publication in 2010,<sup>159</sup> the PAINs concept has triggered a domino effect, producing a variety of selectivity filters in order to hamper progression in drug discovery campaigns of useless compounds.<sup>160</sup> To date, despite the wide acceptance of the PAINs

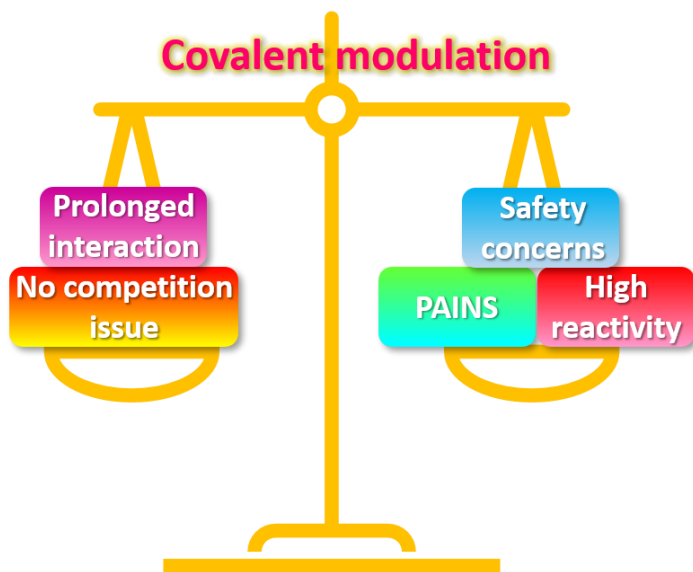


**Figure 1.14.** Pros and cons of covalent modulation of biological targets.

concept by the scientific community, it is becoming increasingly clear that a dogmatic and simplistic use of this practice might cause wrong decision-making on compounds progression, and bio-orthogonal assays and preliminary evaluations on complex cell environments are emerging as a valuable mean to avoid potential promiscuously reactive electrophiles.<sup>150</sup>

The translational relevance of electrophilic warheads in drug discovery has reinforced the value of this approach in chemical biology, where the design and optimization of chemical probes which can engage the target covalently is acquiring increasing importance.<sup>161</sup> Moreover, deepen analysis on electrophilic natural products and the mechanism by which they interact with their targets has resulted in pivotal contributions to provide both a wider selection of electrophilic warheads and strategies to covalently modulate biological binding partners.<sup>162</sup>

The innate redox cell signaling pathway represented an inspiration muse for the abovementioned electrophile-based strategies. The electrophilic tuning of cellular communications plays crucial roles in initiating signaling cascades without enzyme mediation through post-translational modification (PTM) of protein structures and functions. Furthermore, designed covalent drugs or chemical probes have to biologically interface with the endogenous electrophile signaling counterpart. Therefore, a deeper overview of the electrophile-based cellular vernacular is needed.<sup>163</sup>

### 1.2.1 Electrophilic-sensor targets as key modulators of neuroinflammatory processes

The main cellular idiom is guided by enzyme-mediated processes, where signal transduction regulates physiological cellular homeostasis or counteracts pathological disorders. Normally, a canonical external signal interacts with cellular surface, stimulating a downstream signaling pathway until to reach or deliver info to the nucleus where specific genes are up/downregulated. The signal transmission is regularly spread by small molecule messengers or small protein carriers (e.g. phosphate, acetate, ubiquitin) with enzyme-based regulation and propagation.<sup>164, 165</sup> However, there is also an emerging non-canonical mechanism of intracellular communications conveyed through reactive molecular species, mainly reactive oxidative and electrophilic species (ROS/RES). The principal difference from classical signal transduction relies in the non-enzyme assisted spread of cellular messages, which is mainly regulated by the redox status.<sup>163</sup> Notably, reactive species can be deleterious if generated or recruited without control. Therefore, precise ROS/RES-based signals are considered essential to retain physiological redox cellular homeostasis as well as illuminate previously untapped mechanisms of redox signaling networks.<sup>166</sup> Primary ROS species include radicals (e.g. superoxide and hydroxyl radical), non-radical species (e.g. hydrogen peroxide) and singlet oxygen.<sup>167, 168</sup> They are endogenously produced and tuned at physiological level as second messengers, metabolic byproducts or homeostasis sensors. Deviations from the steady-state concentration, both small and controlled changes or large perturbations, work as cellular alerts, triggering distinctive biological responses.<sup>169</sup> Reactive electrophiles can be endogenously produced, mainly by metabolic processes (e.g. lipid-derived electrophiles, fumarate and quinones), or introduced from exogenous sources like diet or pollution.<sup>163, 170</sup> RES physiological production relies on enzymatic formation, like fatty acids oxidation from cyclooxygenases, lipoxygenases and CYP450 or non-enzymatic, free radical-mediated reactions in which, under oxidizing conditions, ROS (e.g. lipid peroxidation) and reactive nitrogen species (RNS) promote electrophiles' generation. Basal RES level is maintained at very low concentrations and their proliferation is linked to pathological OES, a characterizing feature of hundreds of diseases such as cancer, diabetes and neurodegenerative disorders.<sup>163, 171</sup> Nevertheless, the cellular arsenal is full of scavenger systems able to counteract OES. A first rapid cellular detoxification and scavenging process involves a combination of antioxidant enzymes belonging to the oxidoreductase family (e.g. SOD, catalase, peroxidase). They jointly contribute to detoxify the cellular environment from abnormal levels of reactive oxidative/electrophilic species by directly inactivating them with the help of cellular free antioxidants such as glutathione (GSH).<sup>172</sup> A second more complex defence, based on electrophilic cellular sensors/mechanisms, comes into play after prolonged OES stimuli. In this case, molecular messengers consist of reactive species which mediate the DNA damage and PTM of specific residues of proteins, subsequently effecting functional changes in targeted proteins.<sup>173, 174</sup> PTM represents one of the major cellular form of adaption to metabolic and environmental stimuli, creating high proteome diversification by covalent modification of newly generated proteins (e.g. methylation, acetylation, phosphorylation).<sup>175</sup>

Redox-dependent PTMs mediated by ROS and RES act as cellular sensors of the redox status but also represent a more suited and long-lasting antioxidant response by modulating many cellular functions such as genes expression, neurotransmission, and enzyme catalysis. In case of OES, the electrophilic PTM is usually directed to the more nucleophilic protein residues. Cysteine is, by far, the conventional amino acid with the highest nucleophilicity and polarizability, acting with its thiol group as canonical junction point with soft electrophiles.<sup>176</sup> Further, also imidazole of histidine, thiomethyl of methionine, amine of lysine, hydroxyl of serine, threonine and tyrosine have the potential to be nucleophilic, but with less extent and depending on the cellular microenvironment. Therefore, they also require strong electrophilic warheads with increasing selectivity/toxicity hazards.<sup>143</sup> Nevertheless, via properly tuning electrophilic moiety with affinity-driven pharmacophore, several residues, less nucleophilic than cysteine, have been selectively targeted by drugs and chemical probes.<sup>144, 161, 177</sup>

Cysteine is underrepresented in the proteome (around 3% of frequency) but plays a crucial role in protein machinery since more than 50% of thiolate residues are solvent-faced or present in catalytic domains. Furthermore, as the most easily oxidized amino acid, cysteine also generally serves as a redox sensor for proteins.<sup>152, 178</sup> The most common example is the oxidation of thiol into sulfenic acid, mainly caused by attack of hydroxide group, which usually acts as first chemical step before final conversion to the portfolio of other cysteine oxidation (e.g. disulfide, sulfinic acid) or stable sulfenamide/sulfenylamide formation (Figure 1.15).

Sulfenamide/sulfenylamide or disulfide intermediate is also used in some proteins as a kind of temporary protection against further sulfur irreversible hyperoxidation, as far as facilitating reactivation by reducing agents such as GSH when cellular oxidative stress will be mitigated.<sup>179, 180</sup>

On the other hand, sulfenic conversion of cysteine in the active site can also completely reframe enzyme activity such as in GAPDH, where a thiol oxidation on Cys152 converts a metabolic enzyme into a pro-apoptotic

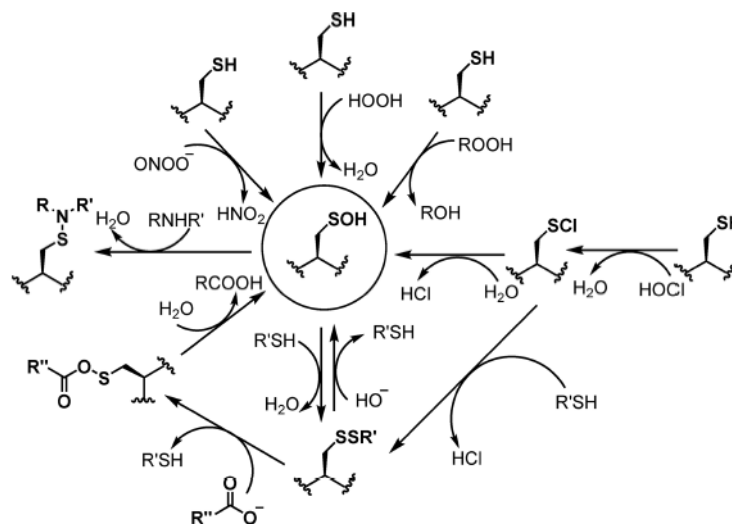


**Figure 1.15.** Oxidation of cysteine by various oxidants generates sulfenic acid, which can also act as an intermediate to other cysteine modifications including glutathionylation, disulfide bond formation, and sulfenamide species. Taken from <sup>210</sup>.

factor.<sup>181</sup> Sulfenamide or sulfenic acid formation occurs also as crucial step in marketed drugs mechanism of action, as for omeprazole and clopidogrel respectively, before covalently hijacking the target through disulfide bond formation.<sup>149</sup> A more oxidizing environment leads to cysteine conversion into irreversible sulfinic and sulfonic acids, an alteration peculiar of aging.<sup>182</sup> Besides being linked to loss of function PTM,

sulfoxide formation is also related to toxic gain of function, like triggering protein aggregation and Lewy's body formation as happens for human SOD1 after Cys111 oxidation.<sup>163, 183</sup> At the same time, targeted alkylation by RES unveils a more complex and precise dark side of electrophilic signaling.

RES-based amendments at functionally significant nucleophilic amino acids of electrophile-sensing proteins is the tuned cell response to redox altered homeostasis.<sup>41</sup> Of particular note, redox signal transductions do not operate through direct electrophilic modification of the target, but via covalent modifications of effector molecules, sensor proteins or transcription factors that in turn affect the interested cellular pathway. As discussed in chapter 1.1.2, the Keap1/Nrf2 pathway represents a crucial player in cellular antioxidant response through the regulation of cytoprotective genes transcription and the control of basal and inducible antioxidant replies.<sup>85</sup> Alongside Nrf2, NF- $\kappa$ B provides the other crucial antioxidant-ant inflammatory cellular facility activated by electrophiles. They both present key cysteine sensors whose covalent modification represents the triggering event in the activation of the protective response. A similar machinery operates for the electrophilic activation of the transcription factor heat shock factor (HSF1), which controls protein aggregation and misfolding contributing to cellular homeostasis.<sup>184</sup> Phosphorylation PTM via kinase/phosphatase activity is one of the most exploited cellular mechanisms to switch on/off targeted pathways easily and selectively. Even in the phosphate signaling pathway, the chance to covalently modify redox-responsive thiols of specific enzymes is a strategy frequently used by the cell factory. Kinases such as MAPKs, protein kinase B (PKB or Akt), in addition to the already cited IKK, show cysteine residues in active or allosteric sites which can customize enzyme activity following electrophilic conjugation. The same can be said for phosphatases like protein tyrosine phosphatases (PTPs).<sup>41, 170</sup>

What reported above is only a glimpse in the realm of endogenous electrophilic signaling mechanisms. There is a plethora, herein not discussed, of physiopathological covalent target modifications which modulate crucial cellular mechanisms, ranging from epigenetic regulation through histone deacetylases (HDACs) to antioxidant response via peroxiredoxins (Prx), or metabolism and immune reaction with PPAR- $\gamma$ .<sup>41</sup> Through the peculiar target and environment-matched modulation, electrophile signaling is still a nuanced vocabulary waiting to be deeper explored. In this view, it is of key importance to identify which protein in the proteome is sensitive to electrophilic modification and by which residue it can be covalently modulated. For this purpose, several chemical-proteomics platforms have been developed, exploiting the reactivity of chemical probes that covalently modify active/non active-site residues to interrogate the functional state of enzymes in the proteome.<sup>185, 186</sup> Activity-based protein profiling (ABPP) is only one of the approaches using small-molecule chemical probes to understand target's behaviour, including active-site mechanism or drug-target interaction. Particularly, ABPP provides a high-affinity chemical probe linked with a tag responsible of facilitating target fishing. Commonly used tags are fluorescent probes, biotin or click chemistry functional groups (e.g. alkyne/azide) which allow to easily visualize and trap the target.<sup>187</sup> Therefore, ABPP is based on

the ability of a small molecule to covalently modify targeted proteins, also enabling to identify the biological role of specific nucleophilic residues.<sup>143</sup> Bio-orthogonal chemistry approaches as well as covalent docking programs or electrophile library screening can help to evaluate the relative ligandability of specific nucleophilic residues and improve bioactive electrophile discovery campaigns.<sup>143, 188-190</sup> One last example of covalent chemical biology is targetable reactive electrophiles and oxidants (T-REX) platform that enables to live interrogate single specific redox pathways and their downstream signaling cascades after selective modification, as well as to screen redox-sensor targets.<sup>191</sup>

### 1.2.2 *Electrophiles as pharmacological tools in neuroinflammation*

Physiological ROS/RES balance and messaging in the brain is of fundamental importance, but even more crucial is to understand how to therapeutically support pathological neuroglia and glial response during the spreading of neuroinflammatory processes.<sup>192</sup> Therefore, a deeper investigation on how redox signaling works during neuroinflammation is needed, exploiting exogenous electrophilic tools to inquire endogenous responses and thus taking inspiration for potential therapeutic approaches. Through their pleiotropic and multi-layered signaling activity, exacerbated in inflammatory conditions, electrophilic compounds emerge as valuable pharmacological tools to dissect neuroinflammation-related networks.<sup>193</sup> Nrf2 and NF- $\kappa$ B represent two of the most important cellular watchmen against neuroinflammation.<sup>93</sup> With their cytosolic repressors acting as oxidative/electrophile sensors, they contribute to cell decision making in respect to antioxidant and antiinflammatory response.<sup>50</sup>

The most known Nrf2 electrophile activator is DMF (Figure 1.16), sold as Tecfidera<sup>®</sup>, approved by FDA in 2013 for the treatment of relapsing-remitting MS and, with a mixture of monoethyl fumarate salts, previously used for psoriasis. Besides the ability to shift lymphocyte to a more antiinflammatory state with a still unclear mechanism, DMF is able to covalently tie several Keap1 cysteine residues with different extent.<sup>194, 195</sup> Among all, the privileged sensor Cys151 is covalently modified at 84.3% after 3  $\mu$ g/mL DMF treatment while other residues are under 30%, confirming the pivotal role of that residue in Nrf2 activation. The correlation between covalent Keap1 modification and Nrf2 activation potencies of fumarate esters confirms the dogma of DMF-Nrf2 electrophilic activation.<sup>195</sup> Its therapeutic efficacy has been related also to antiinflammatory cascades activation, involved through T cells modulation, and GSH depletion perturbing redox homeostasis.<sup>196</sup> DMF is now in Phase 2 of clinical trials for the treatment of ALS, showing efficacy in slowing disease progression,<sup>197</sup> but also in age-related macular degeneration, pathology featured by oxidative and inflammatory conditions (NCT04292080). Monomethyl fumarate (MMF) is the primary metabolite and has been pointed as the possible metabolite responsible for DMF efficacy, given the fast metabolism of its precursor. MMF exhibits the same Nrf2 and immunomodulatory/neuroprotective effects of DMF, albeit with little less extent.<sup>198</sup> MMF derivative, ALKS-8700 (Figure 1.16), proved to exert improved bioavailability and efficacy and is now in Phase III for MS (NCT02634307).<sup>199</sup>



Several natural or nature-inspired compounds have been discovered as potent electrophilic Nrf2 activators, including sulforaphane (SFN), curcumin, resveratrol, quercetin, genistein, artemisitene and andrographolide.<sup>199</sup> Starting from promising biological properties of triterpenoid oleanolic acids several semi-synthetic compounds were developed, resulting in potent Nrf2 inducers. The most famous is bardoxolone methyl (CDDO-Me, figure 1.16) which is in clinical trial for almost a dozen of peripheral inflammatory diseases. Its demethylated analogue, CDDO, has been co-crystallized with Keap1 determining its covalent modification to Cys151 as principal mechanism of Nrf2 activation.<sup>200</sup> Within the cyanoacrylate triterpenoid family some SAR studies rebrought out the principal dogma of druglike electrophilic modulators: reactive moieties are necessary to trap the target but high-affinity moieties are essential for an efficient modulation of the downstream cascade.<sup>92, 201</sup> Particularly, triterpenoid cyanoacrylates proved to temporarily trap reactive cysteines, with the triterpenoid moiety affording shape complementarity and the cyanoenone function covalently fortifying this interaction through a dock-and-lock mechanism.<sup>202</sup> Furthermore, CDDO-Me modulates microglia activity, inhibiting proinflammatory cytokines' production and rescuing neuroinflammation.<sup>203, 204</sup> Severe cardiovascular problems have discontinued and delayed clinical trials, pushing forward necessary biological optimization. Several CDDO derivatives were developed to improve capacity to cross BBB and efficacy at central level. For instance, several CDDO-amide analogues strongly upregulated Nrf2-ARE pathway *in vivo*, exerting neuroprotective and behavioural beneficial effects in mouse models of PD and AD.<sup>205, 206</sup> Recently, a CDDO-Me derivative, RTA 408 (Figure 1.16), entered a clinical trial for Friedreich's ataxia (NCT02255435), an autosomal-recessive genetic disease characterized by impaired antioxidant defence and harsh oxidative stress condition.

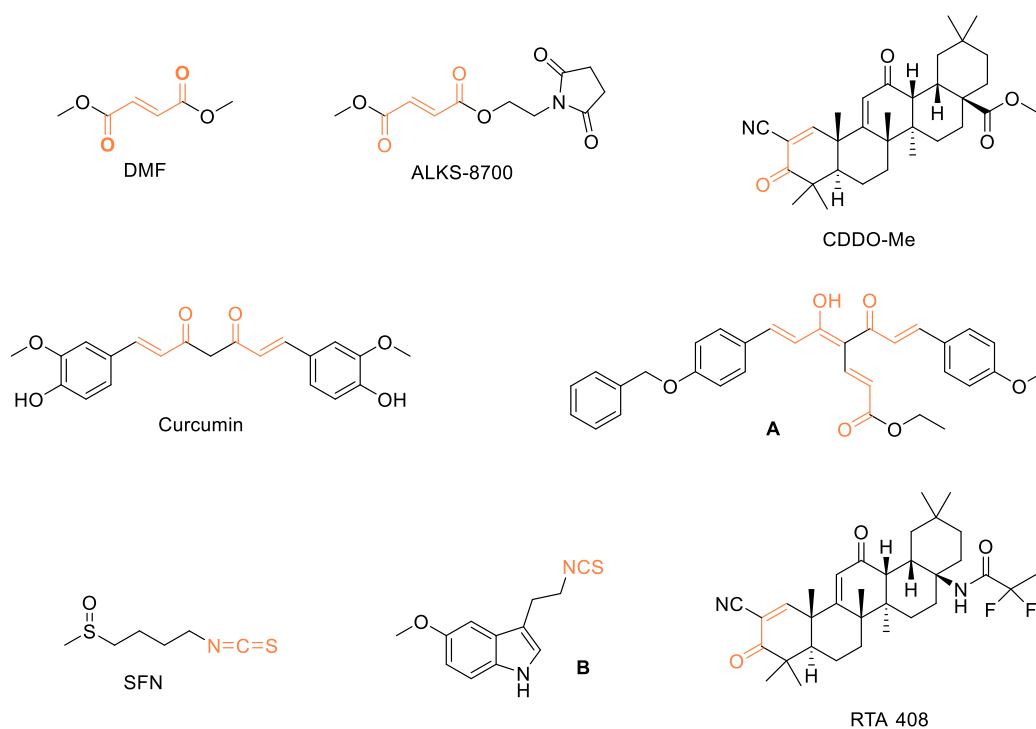


**Figure 1.16.** Electrophilic Nrf2 inducers with reactive moieties highlighted in orange.

Natural compound SFN (Figure 1.16) proved to covalently interact with several Keap1 cysteines, including functional key-residue Cys151, through its reactive isothiocyanate fragment.<sup>207</sup> SFN has been and still is studied as potential treatment for several types of cancer due to its strong antioxidant and antiinflammatory properties Nrf2-mediated combined with low side effects.<sup>208</sup> Particularly, SFN activates microglia promoting production of antiinflammatory cytokines and showed neuroprotective efficacy paired with rescue of neuronal impairment in *in vivo* models of AD, PD and HD.<sup>209</sup> Interestingly, an hybrid melatonin-SFN was developed, showing a strong neuroprotective and antioxidant effect both *in vitro* and *in vivo*, combined with unexpected antiinflammatory properties (**B**, Figure 1.16).<sup>210, 211</sup>

Curcumin (Figure 1.16) is probably one of the most explored natural electrophilic scaffolds. Covalent trapping Cys151 is the main responsible for its strong Nrf2 induction, but also other secondary pathways are involved (e.g. phosphorylation, acetylation).<sup>212</sup> Furthermore, curcumin owns a wide antioxidant and antiinflammatory profile ranging from ROS scavenger activity to impairment of proinflammatory cytokine production.<sup>213</sup> The extra gear of curcumin is represented by its intrinsic ability to tackle proteinopathies, limiting aggregates and fibrils formation both for synuclein and amyloid plaques.<sup>214, 215</sup> Due to its broad-spectrum of biological activities it is now undergoing several clinical trials spanning from AD (NCT00164749) to mild cognitive impairment (NCT01811381), but it is also used as source of inspiration for several drug discovery campaigns against complex diseases. Curcumin-fumarate hybrids have recently been proposed as Nrf2 inducers. Particularly, best derivative of the series (**A**, Figure 1.16) showed superior effects than DMF. It activated Nrf2 and the transcription of cytoprotective genes, and revealed neuroprotective profile in *in vitro* AD and PD models as well as in *C. elegans* PD model.<sup>216</sup> Curcumin scaffold, as its similar ferulic, caffeic, cinnamic derivatives, were the ground for numerous multitarget hybrids development.<sup>215, 217, 218</sup>

Recently, the pleiotropic nature of curcumin has been attributed to its potential behaviour as prodrug, which undergoes oxidative activation into reactive metabolites that covalently bind cellular protein thereby functioning as the mediators of the biological effects. Albeit possessing two reactive  $\alpha,\beta$ -unsaturated carbonyls, experimental evidences support the idea that autoxidation products (e.g. spiroepoxide and quinone methide) could provide additional electrophilic sites responsible for the biological activities (Figure 1.17).<sup>219</sup> Notably, the use of moieties with latent reactivity which can be activated in certain pathological conditions was identified for further promising Nrf2 inducers development.<sup>92</sup> Providing their protective effect selectively where it is needed, as for example by activating inducible antioxidant responses in oxidative conditions, they are thought to be safer than conventional electrophilic drugs, being inactive and harmless in physiological state.<sup>220</sup> Prototypical examples of the so called “pathologically activated therapeutics” (PAT)<sup>221</sup> lie within polyphenols, mainly catechols, which are converted to reactive quinones when redox damage occurs. Carnosic acid (CA) represents one of the most studied pro-electrophiles in the field of neuroinflammatory diseases. After oxidative activation, it triggered Nrf2 pathway by covalently binding

specific Keap1 cysteine residues, protecting neurons from oxidative stress and excitotoxicity (Figure 1.17).<sup>222</sup> Furthermore, CA exhibited promising therapeutic effects in rodent AD model decreasing astrogliosis and A $\beta$  aggregation whereas ameliorating behavioural, memory and learning markers.<sup>223</sup>

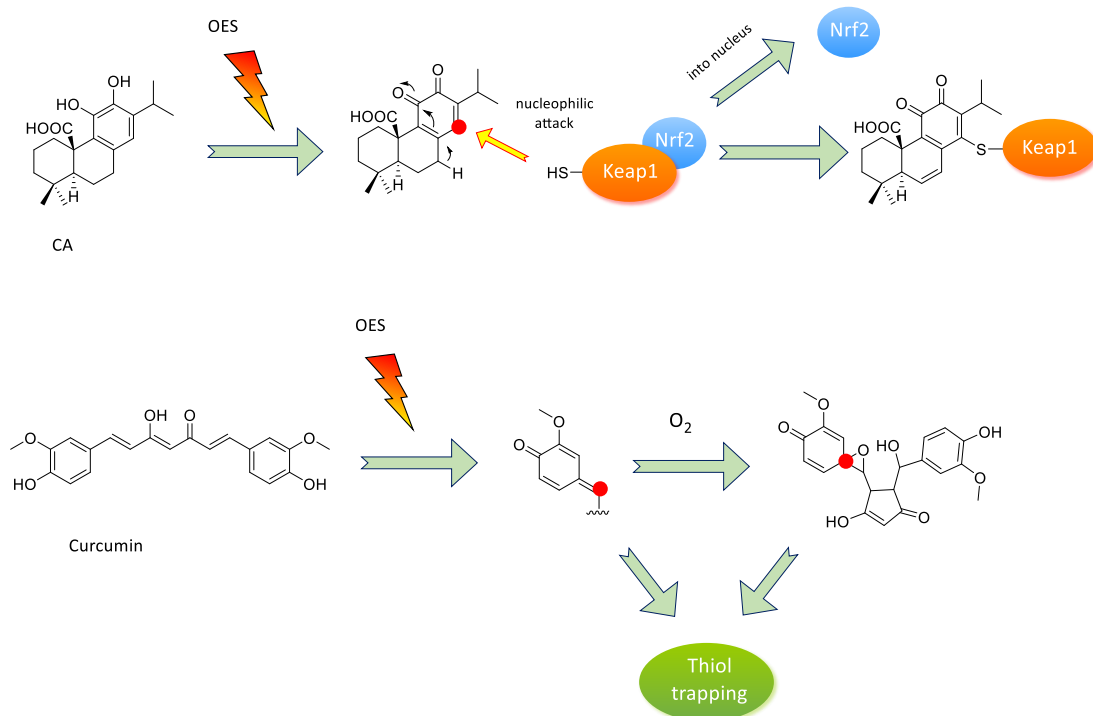


**Figure 1.17. Pro-electrophilic compounds and their mechanisms of activation.** CA, activated in the quinone form under OES conditions, can react in a particular electron deficient carbon (red bubble) with a nucleophilic Cys residue of Keap1, allowing Nrf2 translocation into the nucleus. In the same manner curcumin oxidized metabolites could be trapped by Cys in two distinct positions. Taken from <sup>92</sup>.

Several other compounds bearing activated Michael acceptors such as chalcones or nitro fatty acids and prostaglandins were proved to strongly activate Nrf2 with beneficial effects in *in vivo* models.<sup>199, 217, 224</sup>

The interplay between Nrf2 and NF- $\kappa$ B has been widely dissected for the potential treatment and study of several complex diseases.<sup>225</sup> They share similar molecular and cellular pathways in redox signaling which, consequently to exogenous stimuli, provide a joint holistic antioxidant and anti-inflammatory response. Several electrophile-sensitive cysteine residues are present in both IKK $\beta$  and NF- $\kappa$ B subunits, that were proved to be crucial for the modulation of NF- $\kappa$ B pathway. Interestingly, the same electrophile often proved to covalently activate Nrf2 pathway and exert irreversible NF- $\kappa$ B inhibition at different levels by interacting with the respective peculiar “cysteine codes”.<sup>50, 225</sup> Therefore, several natural products and derived semi-synthetic compounds bearing the above cited reactive moieties were also studied as effective modulators of the NF- $\kappa$ B pathway. For-example, the reported covalent liaison between CDDO and Nrf2 recurs also with Cys179 in the activation loop of IKK $\beta$  and the same happens for CDDO-Me.<sup>226</sup> Analogue relationship occurs between DMF and NF- $\kappa$ B, but in this case by covalently interacting with Cys38 of p65 subunit.<sup>227</sup> A special mention goes to the ubiquitous curcumin. Its renowned anti-inflammatory properties were once again directly

correlated to the bioactivation hypothesis involving oxidative transformation, as non-oxidizable analogues were less potent in this respect. This assumption was further confirmed by identifying the spiroepoxide metabolites as responsible for covalent adduct formation with Cys179 of IKK $\beta$  and thus inhibiting NF- $\kappa$ B downstream activation.<sup>228</sup> This interesting output leads to consider curcumin's NF- $\kappa$ B inhibition to be dependent on the redox status of the cell.

The diterpenoid andrographolide, sesquiterpenoids parthenolide and artemiside, characterized by reactive  $\alpha$ -methylene- $\gamma$ -lactone moiety, are potent natural antiinflammatory agents acting through NF- $\kappa$ B signaling impairment identifying Cys62 of p50 and Cys179 of IKK $\beta$ , respectively, as sites of attachment (Figure 1.18).<sup>162,</sup>

229

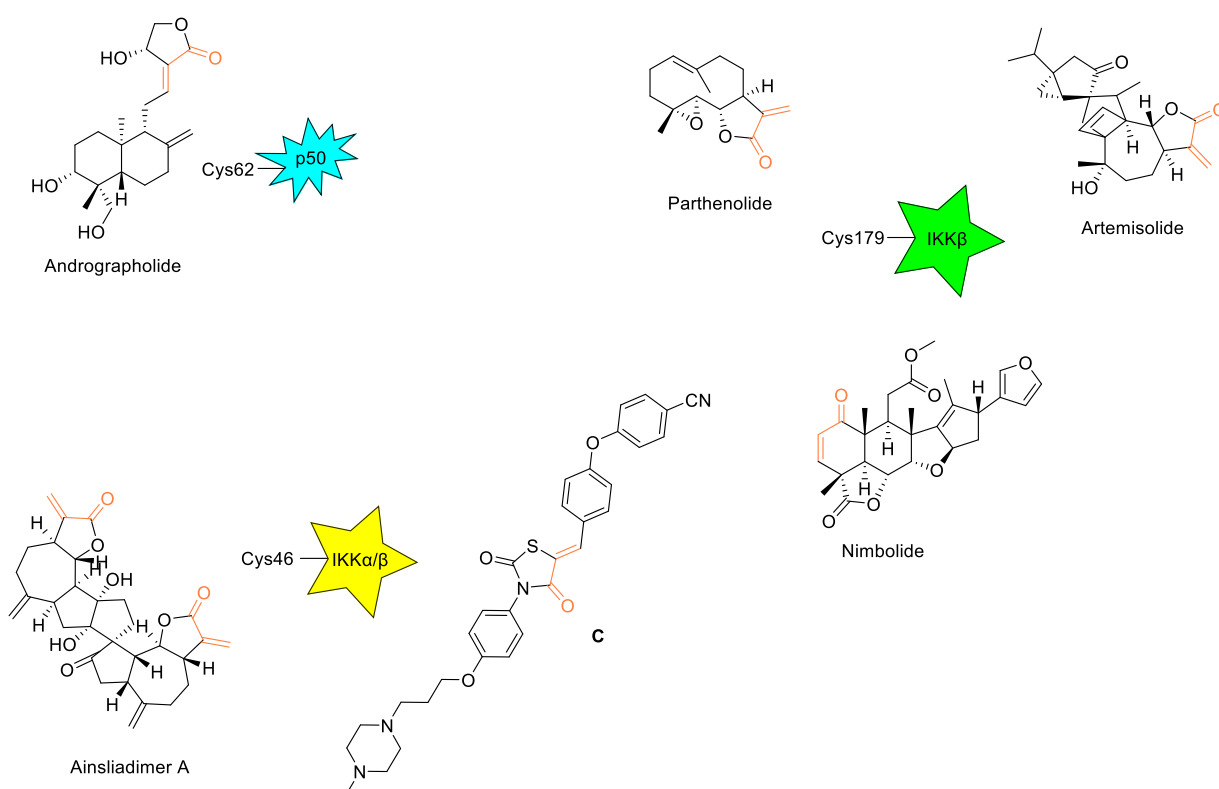


**Figure 1.18.** IKK-NF- $\kappa$ B covalent inhibitors with targeted cysteines (part 1).

Also the triterpenoid nimbolide showed inhibition of NF- $\kappa$ B by modification occurring to the usual Cys179 and thus justifying its antiinflammatory and anticarcinogenic effects.<sup>230</sup> Ainsliadimer A, a sesquiterpene lactone dimer, revealed to be the first compound able to inactivate NF- $\kappa$ B signaling by binding a peculiar cysteine residue, Cys46 in IKK (Figure 1.18). Interestingly, Cys46 is a conserved residue both in IKK $\alpha$  and IKK $\beta$  and therefore its simultaneously trapping inhibits both canonical and non-canonical NF- $\kappa$ B activation pathways. Interaction with Cys46 brought out a new allosteric site that in consequence of covalent adduct formation interferes with ATP-binding and solvent access to Trp58 residue, accompanying inhibition of kinase activity. Besides pioneering results about IKK-NF- $\kappa$ B pathway, ainsliadimer A showed promising potential for

anticancer and antiinflammatory effects in an *in vivo* mice model.<sup>231</sup> Following a structure-based virtual screening on a chemical library, an electrophilic thiazolidinedione derivative came out as potential IKK $\beta$  inhibitor, albeit with a high IC<sub>50</sub>.<sup>232</sup> Further SAR and optimization studies brought out a series of thiazolidinediones with a time-dependent IKK $\beta$  inhibition, likely owing to a covalent interaction with allosteric residue Cys46.<sup>233, 234</sup> *In vivo* evaluation of compound **C** (Figure 1.18) in animal model of LPS-induced septic shock revealed increase of 80% survival rate at 36 h post-injection.<sup>234</sup>

In the search of electrophilic compounds that could selectively recognize the intended redox-sensor protein, dual selective cysteine trapping is emerging as a valuable approach. Particularly, this assumes that anchoring of a second cysteine once the first one is trapped should result in a kinetically and thermodynamically favoured intramolecular process, thus allowing exploitation of milder electrophilic fragments. Bis-electrophile approach was first proposed toward Nrf2-Keap1 pathway, where bis-Michael

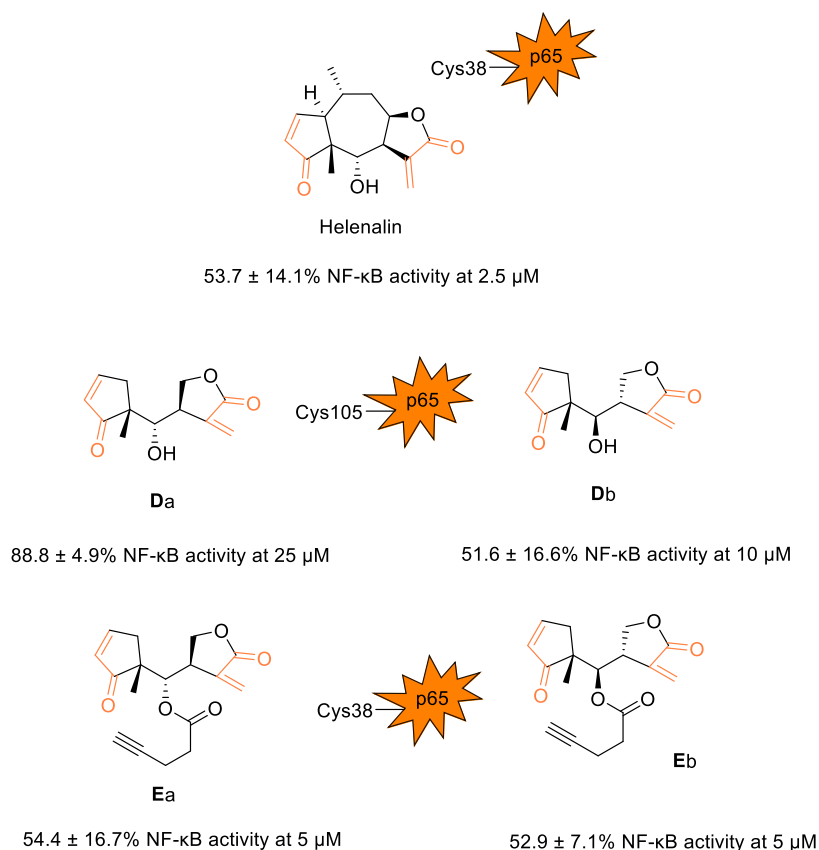


**Figure 1.19.** Helenalin and its derivative with NF-κB inhibitory activity.<sup>291</sup>

acceptors boosted expression of ARE genes.<sup>235</sup> Due to the peculiar multicysteine profile at NF-κB subunits, Harki and coworkers reposed a bis-electrophile strategy inspired by antiinflammatory helenalin, which naturally bears two  $\alpha,\beta$ -unsaturated carbonyls (Figure 1.19).<sup>236</sup> Helenalin is a sesquiterpene lactone which exerts antiinflammatory activity by covalently modifying a newly identified Cys38 of p65 subunit with Michael-type addition.<sup>237, 238</sup> Helenalin-simplified derivatives bearing bis-Michael acceptors were developed to further explore target engagement strategies in view of the large presence of electrophilic-sensitive cysteines among NF-κB cascade. Interestingly, the simplified analogues **Da-Db**, which mimic parent compound, form adducts with Cys105 residue without known biological significance, whereas do not engage with Cys38. On the other side, bis-electrophile derivatives bearing an alkyne handle (**Ea-b**) target Cys38 of p65, therefore inhibiting induced canonical NF-κB signaling with low micromolar efficiencies (Figure 1.19).<sup>236</sup>

In addition to the usual  $\alpha,\beta$ -unsaturated carbonyl, also several other electrophilic fragments were exploited to achieve NF- $\kappa$ B covalent inhibition. One example refers to epoxyquinone derivatives which were proved to react through an epoxide ring-opening and consequent covalent adduct to Cys38 of p65 subunit (Figure 1.21).<sup>239, 240</sup> Furthermore, organoselenocyanates proved to covalently interact with Cys62 of p50 through a selenium-sulphur bond formation and therefore inhibiting NF- $\kappa$ B activation justifying their antiproliferative and antiinflammatory properties.<sup>241</sup> Same biological profiles of dithiolethiones occurred to pass through covalent inhibition of p50 and p65 subunits instead of H<sub>2</sub>S release or protein phosphatase 2A activation (Figure 1.20).<sup>242</sup>

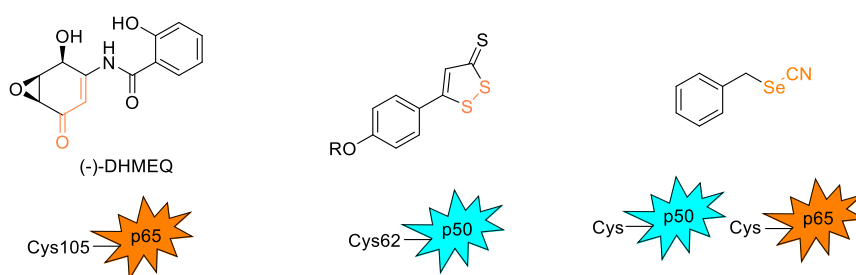


**Figure 1.20.** IKK-NF- $\kappa$ B covalent inhibitors with targeted cysteines (part 2).

Protein misfolding and aggregation are both causes and consequences of neuroinflammatory processes, representing pivotal players in neurodegeneration. Covalent inhibition of protein aggregation is not a new idea, but therapeutic approaches in this respect are still lacking, underlining that a deeper comprehension of this complex pathway is needed. Interestingly, mainly lysines play a crucial role as electrophile sensitive residues in amyloid- $\beta$  peptide. Several natural and nature-derived polyphenols proved to inhibit protein aggregation.<sup>243</sup> Their structure is generally associated to a wealth of biological properties, ranging from antioxidant, antiinflammatory and anticancer activities. Some of these are in clinical trials for neurodegenerative disease treatment (e.g. curcumin, resveratrol, epigallocatechin-3-gallate).<sup>244</sup> Regarding inhibition of A $\beta$  aggregation, polyphenols demonstrated to prevent oligomer cytotoxicity and aggregation, but the mechanism of action has still to be clarified. For example, curcumin showed to prevent oligomerization, reshape toxic into nontoxic oligomers, disaggregate preformed fibrils, resulting in reduced A $\beta$  toxicity.<sup>245, 246</sup> Mechanism of action behind these activities has to be elucidated, but seems to be driven by stacking interactions between curcumin's aromatic rings and aromatic residues of the peptide. Conversely, many other polyphenols demonstrated to inhibit protein aggregation with different mechanisms of action based on their electrophilic characters. In figure 1.21 three examples are represented of flavonoids carrying a proelectrophilic catechol feature (highlighted in green) which plays a crucial role in amyloid binding and subsequent fibrils remodelling. Particularly, (-)-epigallocatechin-3-gallate (EGCG, Figure 1.21) strongly prevents oligomers formation, quite likely by covalently binding amyloid fibrils. Indeed, EGCG was proved to covalently bind amyloidogenic protein at specific functional residues via Schiff base formation upon previous

oxidation into quinone form, thus preventing toxic oligomers formation.<sup>247</sup> The same covalent-targeting approach involving lysine residues was further confirmed with EGCG and other polyphenols for several aggregating-prone proteins.<sup>248-250</sup>

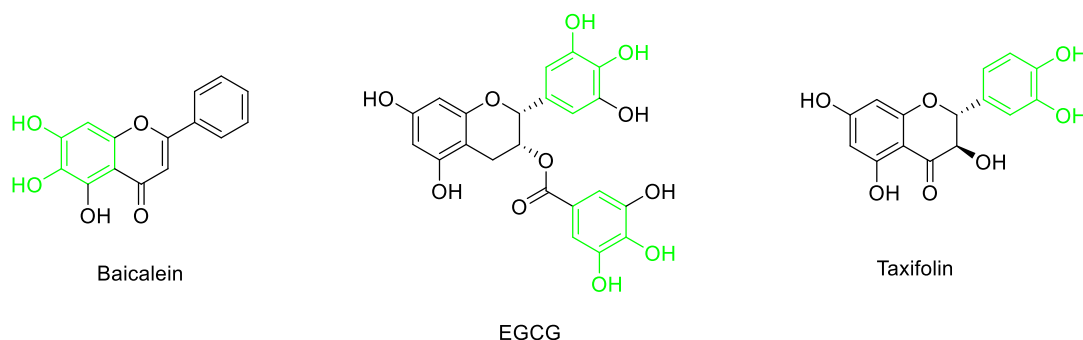


**Figure 1.21.** Covalent inhibitors of protein aggregation.

Taxifolin is another catechol-bearing flavonoid which inhibits A $\beta_{42}$  aggregation. Upon autoxidation to *o*-quinone, oxidized taxifolin covalently binds amyloid Lys16 and Lys28 through Michael addition (Figure 1.22). Because Lys16 and Lys28 are situated in the intermolecular  $\beta$ -sheet region, A $\beta_{42}$  aggregates would be destabilized by the adduct formation thus limiting plaques deposition.<sup>251</sup>

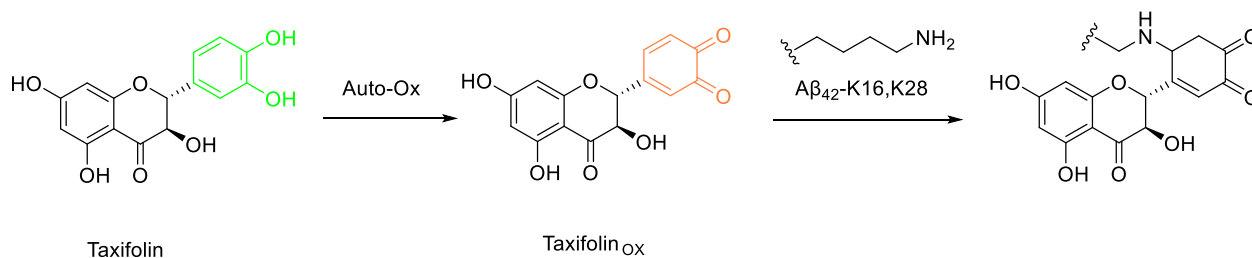


**Figure 1.22.** Inhibitory mechanism of A $\beta$  aggregation by taxifolin. Taken from <sup>251</sup>.

Some covalent inhibitors for the treatment of NDDs are already marketed and widely used for many years, thus proving the potential of covalent modulation if properly tuned. For example, MAO-B inhibitors selegiline and related rasagiline (FDA-approved in 1989 and 2006 for PD, respectively) are irreversible inhibitors that form a *N*(5)-flavocyanine covalent adduct through their terminal alkyne function (Figure 1.23).<sup>99</sup> Regarding CB<sub>2</sub>R<sub>s</sub>, several irreversible ligands were developed, but all with the aim to define structural aspects of ligand recognition and resulting pharmacological properties without any claims for clinical translations. In this respect, tetrahydrocannabinol (THC) core was mainly exploited as high-affinity CBR<sub>s</sub> pharmacophore, where isothiocyanate appendages were attached in different positions to explore ligand binding site. AM841 (Figure 1.23) represented the first selective *h*CB<sub>2</sub>R<sub>s</sub> ligand forming covalent adduct with Cys257, which proved to activate WT-*h*CB<sub>2</sub>R<sub>s</sub> with exceptional potency (IC<sub>50</sub> = 0.079 nM).<sup>74</sup> On the other hand, concerning NMDAR<sub>s</sub>, the peculiar biological profile of memantine was optimized achieving nitromemantine (Figure 1.23). It maintained blockage of excessive eNMDAR activity while sparing synaptic activity combined with nitrosylation of a redox-sensitive cysteine in GluN1, which allosterically modulates receptor activity. This two-

step mechanism enables nitromemantine to be better tolerated and possess increased efficacy than memantine in several animal models.<sup>252, 253</sup>

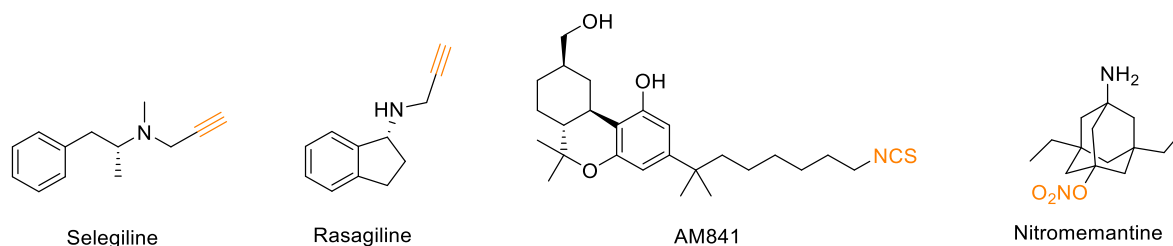


**Figure 1.23.** Covalent modulators of MAO-B, CB<sub>2</sub>R and NMDAR with electrophile moieties highlighted in orange.

Several cellular players other than the abovementioned can be covalently modified to trigger the response against neuroinflammation.<sup>254, 255</sup> Electrophile signaling is a world only partially explored and a strategy only partially considered in therapeutic approaches. Its complex regulatory role at physiological level, which is further complicated in pathological conditions, calls for a deepen overall vision, for which the design of covalent pharmacological probes could represent a powerful instrument. Targets which can be covalently and finely modulated to gain beneficial effects are uncountable, but, on the other hand, a deeper investigation on electrophile-sensitive cellular pathways is needed before their potential will be fully discovered.



## CHAPTER 2

### AIM OF THE THESIS

Most common forms of neurodegenerative disorders afflicting our aging societies share important inflammatory and oxidative components, which are accompanied by common misfolding processes. A vicious cycle of inflammation occurs between amyloid accumulation, activated microglia, and microglial inflammatory mediators, which in turn boost amyloid burden and neuroinflammation. Excitotoxicity as well as ROS-mediated events are other crucial nodes of the inflammation-driven network; these mechanisms have clearly been shown to coexist, affecting each other at multiple levels. A better understanding of neuroinflammatory dynamics emerges as a prodromal step in the discovery of effective cures, as the identification of key links in positive neurotoxic feedback loops could contribute to identify new targets for a most successful approach.

In this context, natural compounds, due to their pleiotropic activity profile, emerge as valuable molecular instruments to investigate a variety of pathologic hallmarks. In particular, polyphenols have shown to target multiple inflammatory components, as well as exert anti-amyloid and antioxidant effects.<sup>256</sup> These biological activities can be generally ascribed to (pro)electrophilic features, which play a crucial role in the modulation of both redox-sensitive transcriptional pathways and amyloid binding in a variety of diseases. In this context, taking inspiration from the structure of natural polyphenolic compounds and allyl disulfides, the research group I joined during the three years of my PhD had previously synthesized a set of hybrid molecules which afforded the catechol derivative **I** (Figure 2.1), joining remarkable antiaggregating effect to the activation of inducible Nrf2-mediated cytoprotective responses. Notably, different molecular features were responsible for the regulation of Nrf2 and  $\beta$ -amyloid activities, offering prospects of finely and separately tune the two pathways.

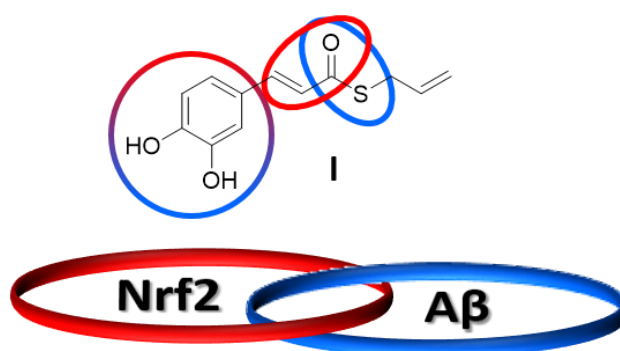


**Figure 2.1.** Compound I with highlighted functional moieties responsible of inhibition of  $\beta$ -amyloid aggregation (blue) or Nrf2 activation (red).

Based on these results, we herein envisioned the peculiar ability of (pro)electrophilic features to switch on/off biological activities as a powerful tool for investigating the complex scenario driven by inflammation in neurodegenerative diseases. On this basis, we wanted to dissect the functional role of (pro)electrophilic

moieties of **I** at a molecular level, to identify crucial structural features which could interfere with amyloid aggregation or modulate inducible cytoprotective responses, moving from Nrf2 induction to NF- $\kappa$ B inhibition.

Then, we systematically modified the identified bioactive cores to reach additional targets which could jointly contribute to the inflammatory process (Figure 2.2), as the simultaneous observation of multiple components is increasingly being perceived as a more adequate way for addressing the pluralism of causes and effects driven by neuroinflammation.

Following this workflow, during my PhD I developed four main projects, that are briefly introduced and depicted below.

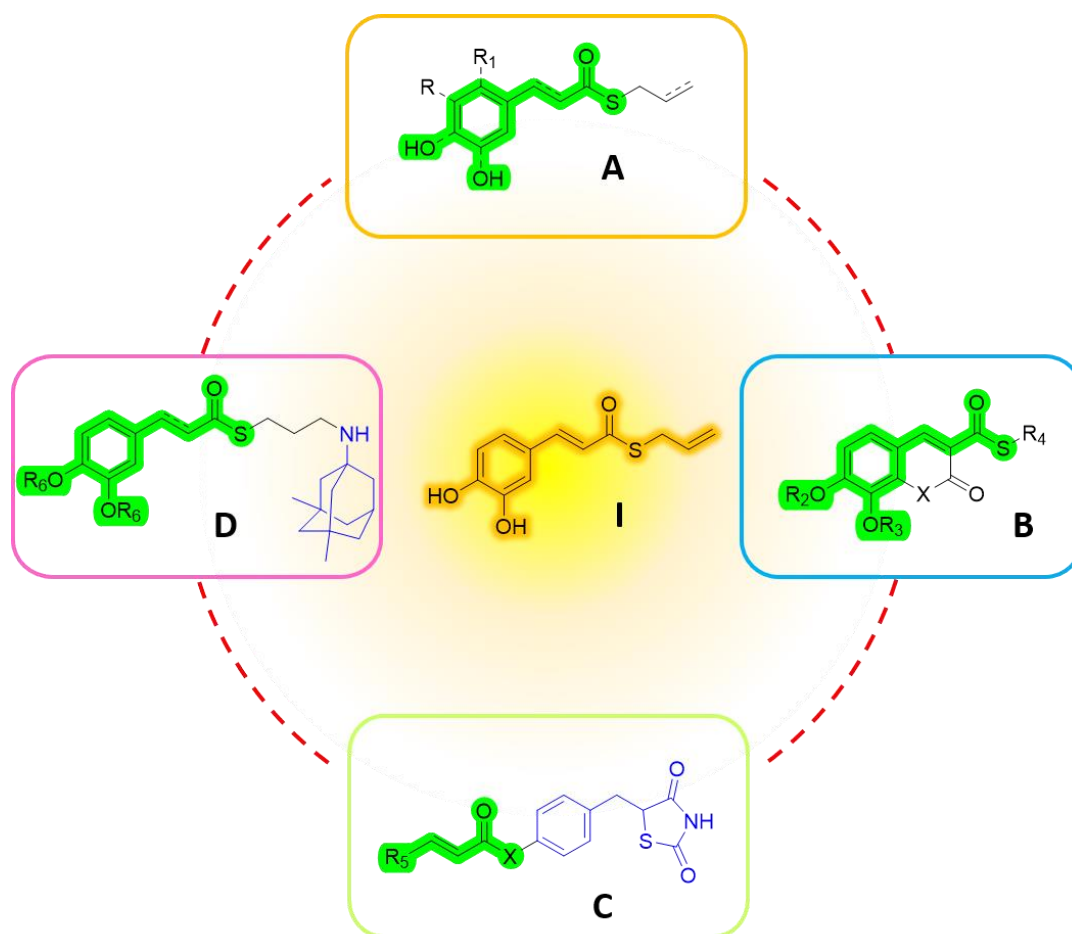


**Figure 2.2.** Bioactive (pro)electrophilic features of **I** as a common driving motif of drug design strategies **A-D**.

- A. The mechanistic underpinnings involved in catechol's inhibitory activity toward A $\beta$  aggregation were investigated through the synthesis of new dihydroxy derivatives of **I**.
- B. The identified antiaggregating nucleus was incorporated into more constrained bicyclic rings to contrast neuroinflammation also through the modulation of CB<sub>2</sub>Rs.
- C. Previously defined Nrf2 structural requirements were merged with the pharmacophoric structure of pioglitazone, an antidiabetic drug endowed with MAO-B inhibitory properties, aiming to gain a two-hit neuroprotective approach.

- D. Following a prodromal investigation on the hydroxycinnamic core, which allowed to split between Nrf2 and NF- $\kappa$ B properties, Nrf2 or NF- $\kappa$ B antiinflammatory frames were respectively conjugated with memantine, which notably contrasts excitotoxicity, to investigate connections between NMDAR overactivation and the two inflammatory-related transcriptional pathways.

All projects, which reached different stages of developments, are presented in the following paragraphs, where drug design approaches are depicted together with synthetic methods and biological evaluation assays of the new compounds.

## 2.1. Inhibition of $\beta$ -amyloid aggregation: the key role of pro-electrophilic warheads

AD is the most frequent protein misfolding disease, for which the amyloidogenic pathway represents a prominent feature. Amyloid aggregation is a critical step of  $A\beta$  toxicity, as it switches soluble nontoxic monomers into insoluble deposits through intermediate stages of oligomerization and amyloid fibril formation. These latter forms, rather than the end product of the amyloid cascade, are viewed as the main responsible for amyloid toxicity,<sup>257, 258</sup> with soluble oligomers emerging as potent mediators of synaptotoxicity.<sup>259</sup>

The prooxidant environment induced by  $A\beta$  in AD pathology is well established, and several lines of evidence indicate that  $A\beta$  accelerates ROS production, which in turn exacerbates amyloid toxicity in a vicious circle.<sup>260</sup> It has been shown that  $A\beta$  can be easily modified by ROS at specific aminoacidic residues, and the change of their redox state can alter the biological behaviour and the oligomerization process of the peptide.<sup>261</sup>

In this context, a variety of natural compounds endowed with antioxidant properties have attracted the attention of the scientific community for their ability to intervene into the protein misfolding cascade, and much effort has been dedicated to the comprehension of their mode of action at a molecular level. Thus, structure-dependent categorization of phenolic compounds has been performed suggesting both non-covalent and covalent inhibition mechanisms.<sup>251</sup>

Antiaggregating properties of the catechol derivative **I** (Figure 2.3) represent a crucial feature of its pleiotropic profile. Its ability to inhibit amyloid aggregation was shown by a thioflavin T (ThT)-based fluorometric assay, giving an  $IC_{50}$  of  $12.5 \pm 0.9 \mu M$ , and confirmed by a mass spectrometry assay, which consented to detect and quantitate the monomeric form of  $A\beta_{42}$ .<sup>262</sup> Coherently with the observed inhibitory potency, at a concentration of  $10 \mu M$  compound **I** exerted a strong protective effect against  $A\beta_{42}$ -mediated cytotoxicity in SH-SY5Y cells in a MTT assay, being more active than natural curcumin (Figure 2.3).

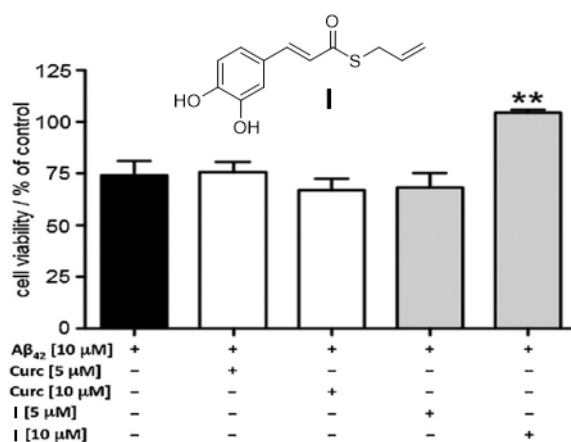


**Figure 2.3.** Effect of compound **I** on  $A\beta_{42}$ -mediated cytotoxicity in neuroblastoma cells compared to curcumin. Adapted from <sup>262</sup>.

Interestingly, the biological profile of compound **I** was driven by the catechol function, which offers a peculiar “on– off” pattern of control of the antiaggregating effect. Indeed, the removal or masking into a methoxy- or ethoxy-function of one or both the hydroxyl substituents of **I** resulted in a complete loss of the antiaggregating effect. Based on the crucial role of this feature, a small set of (bio)isosteres was previously designed, by replacing the catechol ring with a 2-(hydroxymethyl)phenol group or an indazole fragment, respectively functionalized in 5' or 6'. Note of worthy is the finding that also these structural modifications lead to a complete loss of efficacy, as all three compounds presented % inhibition of amyloid aggregation less than 10% at compound concentration of 50  $\mu$ M in ThT assay (Figure 2.4).

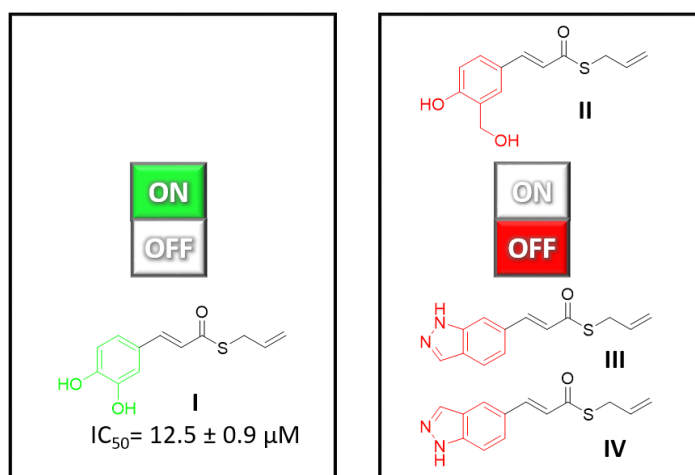


**Figure 2.4.** Compound **I** and its bioisosteres with no ability to inhibit  $\beta$ -amyloid aggregation.

Besides the determinant role of the catechol moiety, other components in the side chain have shown to contribute to the overall antiaggregating effect. In particular, the thioester moiety offered significant advantages with respect to the ester and amide analogues, revealing the catechol group to be necessary but not per se sufficient to guarantee **I**'s efficacy. Further, while the cinnamoyl double bond could be saturated with no impact on antiaggregating effect, by replacing the terminal allyl moiety with an alkyl function a 3-fold increase in potency was observed (compounds **V** and **VI**, figure 2.5), which also resulted into major neuroprotective efficacy in neuroblastoma cells.<sup>263</sup>

Albeit diverse molecular features of compound **I** were shown to drive antiaggregating and antioxidant properties (further details about chemical requirements associated to Nrf2-induction will be discussed thereafter in the dedicated session 2.3) offering the chance to separately and finely tune the two pathways, the catechol moiety emerged as a common crucial motif. However, differently from what happens for the activation of the inducible antioxidant defense system, for which variations in the catechol group of **I** are tolerable, any change in the catechol structure resulted in a complete drop of antiaggregating properties, calling for a deeper comprehension of its mechanistic underpinnings.

Despite the conspicuous quantity of data that support the anti-aggregating activity of catechol-based compounds, information about the molecular mechanisms of inhibition implicated in this process is not completely clear yet. The crucial role of the vicinal hydroxyl groups of polyphenols, such as for baicalein, epigallocatechin and (+)-taxifolin, was verified for the inhibition of a variety of protein amyloidosis, involving amylin,  $\alpha$ -synuclein and  $A\beta_{42}$  fibrilization. It was proposed that catechol-like flavonoids can be autoxidized to *ortho*-quinone intermediates and in turn undergo conjugation with amine aminoacidic residues in the peptide via a Schiff base mechanism or by means of aza-Michael adduct formation,<sup>250</sup> albeit additional mechanisms of non-covalent inhibition were not ruled out.<sup>264, 265</sup>

In this context, to dissect the role of the two hydroxyl functions of compound **I** and investigate its mode of action at molecular level, we selected prototype **I** and more active catechol-bearing antiaggregating ligands **V** and **VI**, and synthesized a new set of derivatives where the hydroxyl function in position 4 was systematically moved to position 5 or 6, affording the corresponding *meta*- and *para*-derivatives (Figure 2.5).

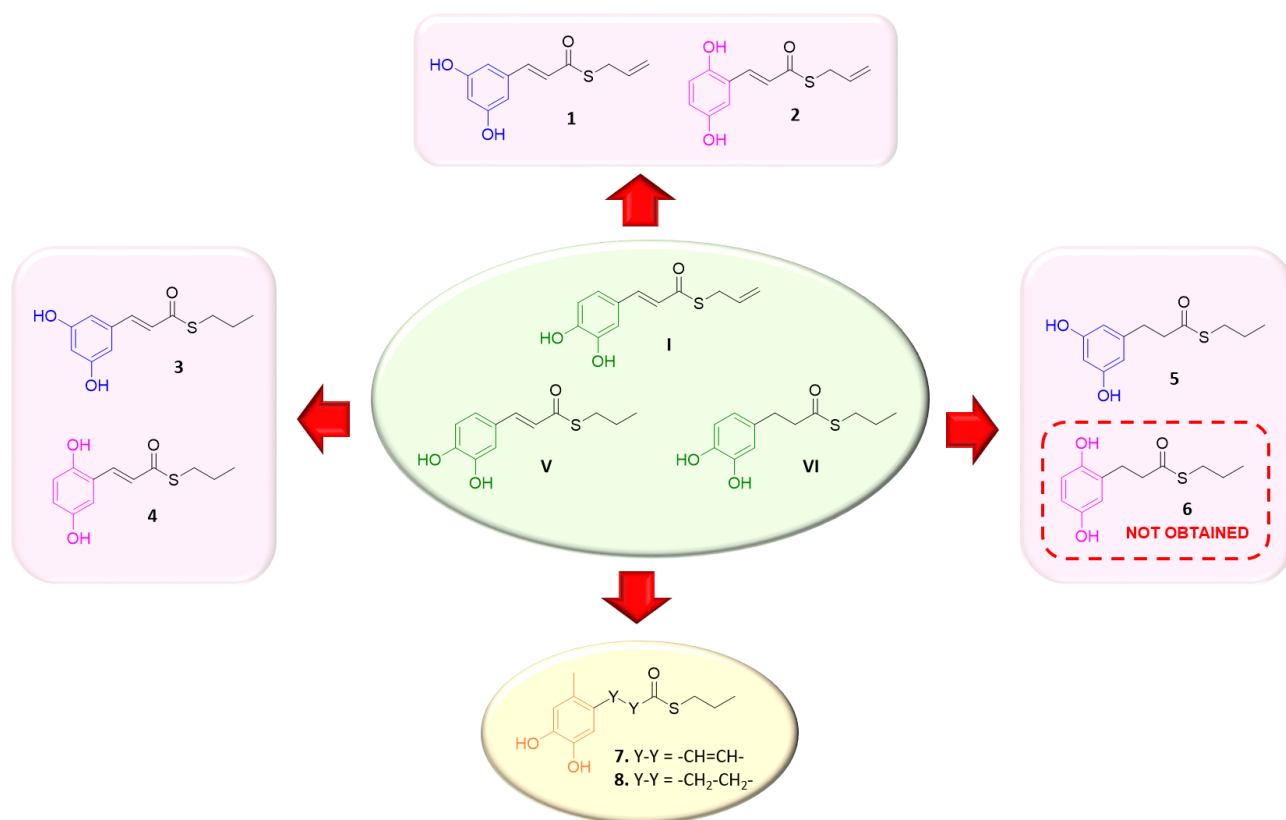


**Figure 2.5.** Design of dihydroxy-substituted catechol isomers **1-8**.

The synthesized compounds were first tested *in vitro* to assess their anti-aggregating properties toward  $A\beta_{42}$ . Then, for a selection of isomers, the oxidation potential was analyzed, and the possibility of a covalent mode of inhibition was investigated by means of both mass studies and the synthesis of the new derivatives **7** and **8** (Figure 2.5).

### 2.1.1 METHODS

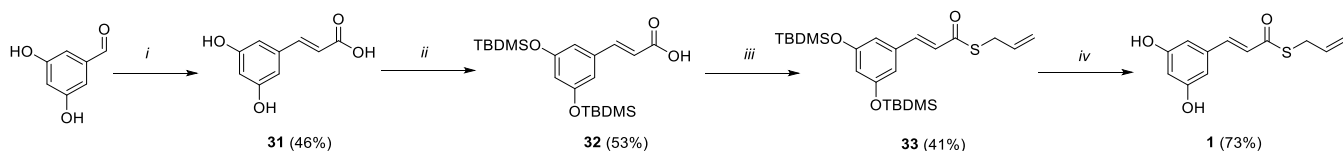
#### Chemistry

Compounds **1-8** were synthesized as outlined in Schemes 1-3.

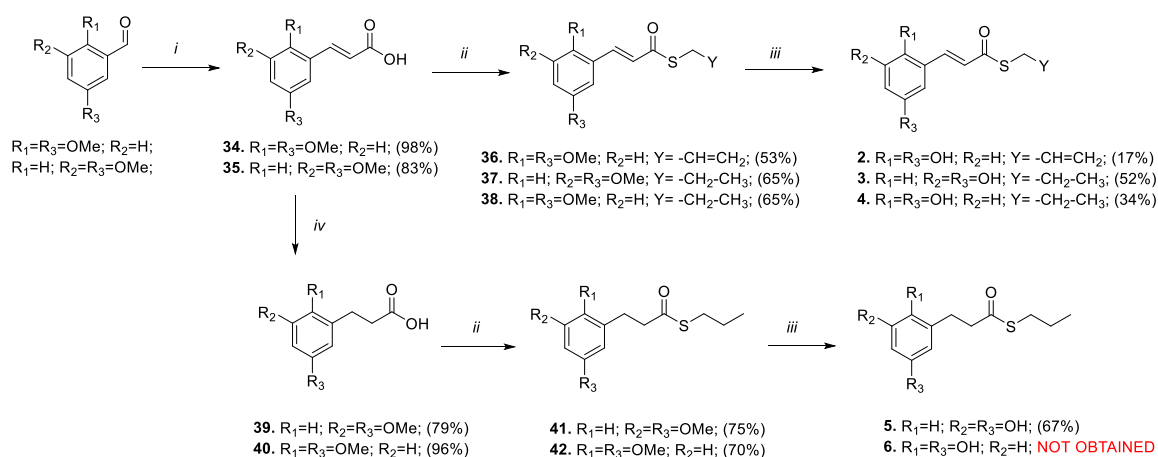
Synthetic strategy exploited to obtain derivative **1** is reported in Scheme 1. Starting from Knoevenagel condensation with 3,5-dihydroxybenzaldehyde and malonic acid, the acidic intermediate **31** was obtained. Its two hydroxy functions were protected through conversion into silyl ethers as result of reaction with *tert*-butyldimethylsilyl chloride. Therefore, acidic function of **32** was activated with DCC for the consequent coupling with allyl mercaptan. Finally, protecting groups were cleaved using a quaternary ammonium salt (TBAF) and releasing dihydroxy compound **1**. For the synthesis of other analogues, the just described procedure was further optimized at two steps, starting with commercial benzaldehyde bearing hydroxy groups protected under methoxy functions, which were deprotected at the last step. In this case, the protecting reaction is avoided, increasing overall yield and reducing steps needed. Furthermore, HOBt and EDC were later used as activating agents during coupling reaction instead of DCC and DMAP because of the easier work-up.

Compounds **2-6** were achieved, except for **6**, as indicated in Scheme 2. Selected dimethoxy benzaldehydes underwent the same Knoevenagel condensation reported above with malonic acid to obtain the derived  $\alpha,\beta$ -unsaturated carboxylic acids. In order to achieve even the corresponding saturated analogues, intermediates **34** and **35** were reduced quantitatively under basic conditions using palladium (II) chloride as catalyst and formic acid as hydrogen donor. Both saturated **39**, **40** and unsaturated **34**, **35** carboxylic acids were coupled with selected thiols (1-propanethiol or allyl mercaptan) using HOBt and EDC as activating agents. Final deprotection of methoxy groups into aromatic hydroxy functions occurred through cold reaction with boron tribromide. Compound **6** was not possible to obtain because of its intrinsic reactivity issues as reported in Scheme 3. Particularly, during demethylation step we observed both unmasking of hydroxy groups and the cleavage of thioester with the consequent removal of 1-propanethiol tail. Indeed, the hydroxyl in position 2 was able to compete and displace thiol, thus allowing intramolecular substitution and consequent closure of a chroman-2-one cycle (compound **6a**, Scheme 3). This hypothesis was further corroborated by similar behaviour reported in literature for this scaffold<sup>266</sup> and subsequent reaction with protecting group (i.e. TBDMS-Cl), revealing only one hydroxy function free to react (compound **6b**, Scheme 3). Therefore, unlike other geometric isomers, where aromatic hydroxy functions are too far away to compete with thiol and favorite ring closure, in case of compound **6** the proximity between 2-hydroxyl and carbonyl paired to the mobility of saturated side chain allowed the preferred 6-ring closing and prevented formation of the desired compound **6**.

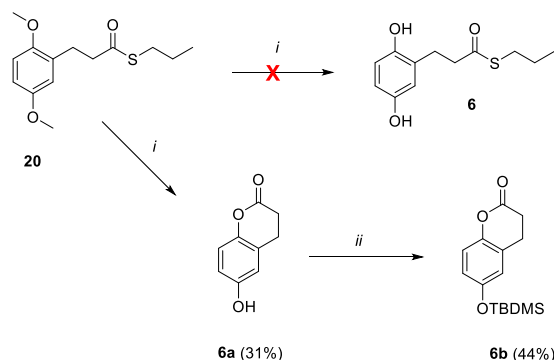
Final compounds **7** and **8** were synthesized following procedures reported in Scheme 4. An initial formylating step from 3,4-dimethoxytoluene occurred to obtain the related benzaldehyde through a Vilsmeier-Haack reaction using phosphorus oxychloride and dimethylformamide, following a reported procedure.<sup>267</sup> Therefore, intermediate **44** was obtained via condensation between **43** and malonic acid. From compound **44**, the reducing step with formic acid and PdCl<sub>2</sub> was carried out to achieve derivative **46**. This latter and its saturated analogue **44** underwent the same previously reported procedure involving coupling with 1-propanethiol and final demethylation step to obtain catechol compounds **7** and **8**.



**Scheme 1.** Reagents and conditions: (i) malonic acid, pyridine, aniline, toluene, reflux, 4h; (ii) TBDMS-Cl, imidazole, DMF, N<sub>2</sub>, rt, o/n; (iii) DCC, DMAP, DCM, N<sub>2</sub>, 0°C-rt, o/n; (iv) TBAF, THF, N<sub>2</sub>, rt, 30'.

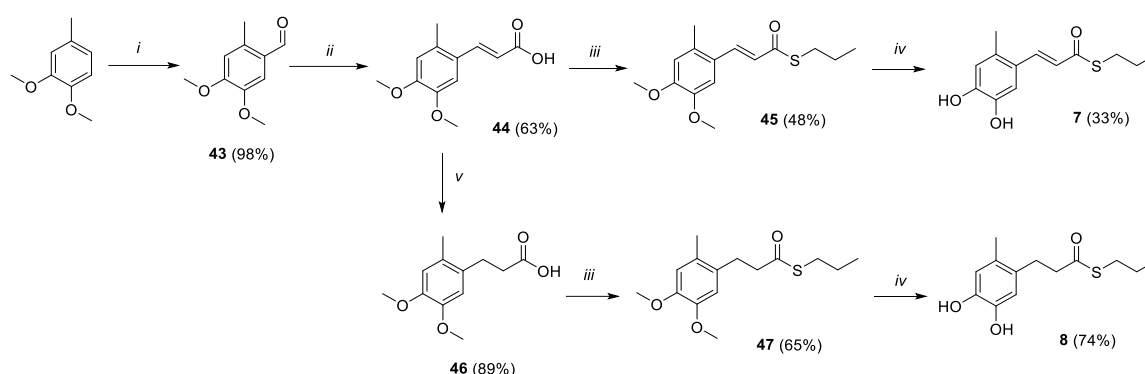


**Scheme 2.** Reagents and conditions: (i) malonic acid, pyridine, aniline, toluene, reflux, 4h; (ii) HOBt, EDC, 1-propanethiol/allyl mercaptan, DCM, rt, o/n; (iii) BBr<sub>3</sub> 1M in DCM, DCM, 0°C-rt, 2h; (iv) PdCl<sub>2</sub>, formic acid, NaOH 2.5M, 60°C, 24h.



**Scheme 3.** Reagents and conditions: (i) BBr<sub>3</sub> 1M in DCM, DCM, 0°C-rt, 2h; (ii) TBDMS-Cl, imidazole, DMF, N<sub>2</sub>, rt, o/n.





**Scheme 4.** Reagents and conditions: (i) POCl<sub>3</sub>, DMF, 80-95°C, 4h; (ii) malonic acid, pyridine, aniline, toluene, reflux, 4h; (iii) HOBt, EDC, 1-propanethiol, DCM, rt, o/n; (iv) BBr<sub>3</sub> 1M in DCM, DCM, 0°C-rt, 2h; (v) PdCl<sub>2</sub>, formic acid, NaOH 2.5M, 60°C, 24h.

<sup>1</sup>H NMR spectra indicate that compounds **1-4** and **7**, featuring a carbon-carbon double bond between the catechol ring and the carbonyl function, have an *E* configuration as revealed by the large spin coupling constants (around 15-16 Hz) of  $\alpha$ -H and  $\beta$ -H on double bonds.

## Biology

Firstly, synthesized compounds were studied to assess their potential anti-aggregating properties by means of a thioflavin T (ThT)-based fluorometric assay, generally used to monitor A $\beta$  fibrillization and its inhibition. A selected series of geometric isomers were analyzed by cyclic voltammetry to evaluate if a relation between oxidation potential and antiaggregating activity exists. In the end, deepen mass spectrometry studies were conducted to elucidate mechanism of action underlying the antiaggregating properties of selected hybrids.

### 2.1.2 RESULTS AND DISCUSSION

#### Inhibition of A $\beta$ <sub>42</sub> self-aggregation (ThT-based assay)

Following investigation with ThT assay, it clearly emerged that the reciprocal position of the two hydroxyl functions is a crucial feature, which acts as a powerful key for the on/off switch of the antiaggregating effect. In particular, we found that *para*-hydroquinones **2** and **4** were able, as for the corresponding *ortho*-analogues **I** and **V**, to effectively reduce amyloid fibrillization, while the *meta*-derivatives **1** and **3** were very low or not effective inhibitors of amyloid aggregation (Table 2.1). As we could not achieve compound **6**, the corresponding *meta*-derivative **5** was not studied in ThT-assay. The finding that *ortho*- and *para*-isomers, but not the *meta*-isomers, exert remarkable antiaggregating properties suggested that the oxidative ability of these compounds might be determinant for activity.

**Table 2.1.** Antiaggregating activity of tested compounds in ThT assay. See Figure 2.5 for structures.

**Inhibition of A $\beta$ <sub>42</sub> self-aggregation<sup>a</sup>**

Cpd.	% inhibition ThT [I]=50 $\mu$ M	IC <sub>50</sub> $\pm$ SEM ( $\mu$ M)
I <sup>263</sup>	>90	12.5 $\pm$ 0.9
V <sup>263</sup>	>90	3.99 $\pm$ 0.39
VI <sup>263</sup>	>90	3.80 $\pm$ 0.44
<b>1</b>	17.9 $\pm$ 5.9	n.d.
<b>2</b>	>90	n.d.
<b>3</b>	<10	n.d.
<b>4</b>	>90	10.2 $\pm$ 1.3

<sup>a</sup>Inhibition of A $\beta$ <sub>42</sub> 50  $\mu$ M self-aggregation by [I] = 50  $\mu$ M. The A $\beta$ <sub>42</sub>/ inhibitor ratio was equal to 1/1. For compounds showing a % inhibition higher than 50% when screened at 50  $\mu$ M the IC<sub>50</sub> value was determined. Values are the mean of two independent experiments each performed in duplicate. n.d. stands for not determined. SEM =standard error of the mean.

### Cyclic voltammetry study

It is known that *ortho*- and *para*-derivatives can be oxidized to semiquinone radicals and quinones while oxygen is reduced to hydrogen peroxide; instead *meta*-analogues can convert to radical semiquinone but not to quinones.<sup>220</sup> Thus, to investigate the role of oxidative properties in compounds antiaggregating effect, the oxidation potential of a set of the three isomers (compounds **3**, **4** and **V**) was analyzed by performing cyclic voltammetry experiments and the results were compared with functional biological activity. Cyclic voltammetry has been extensively applied to depict the redox characteristics of catechols.<sup>268</sup> With potential scanned positively, catechols are transformed into the corresponding *ortho*-benzoquinones, producing a characteristic anodic peak. On the reverse scan, the counterpart cathodic peak represents the re-conversion of *ortho*-benzoquinones back to catechols. This is verified for the *ortho*- and *para*-derivatives, although affected by some degree of side reactivity following up the electron transfer (whose investigation is out of the scope of this study), while a different behaviour was observed for the *meta*-analogue **3** which shows a completely chemical irreversible behaviour in agreement with previous reports on analogue *meta*-di-hydroxylated derivatives (Figure 2.6).<sup>220</sup>

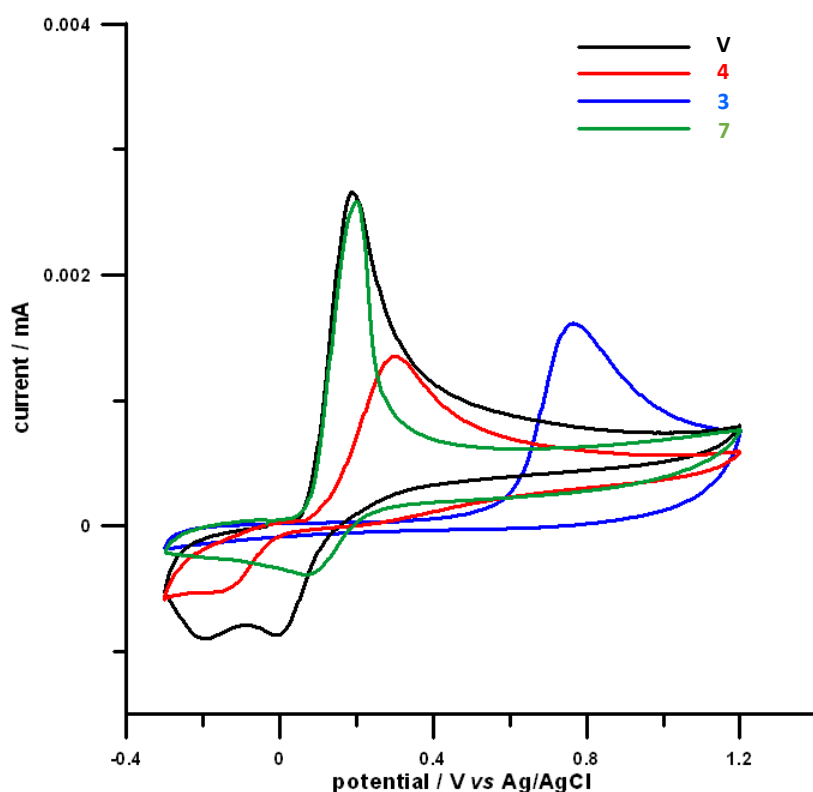


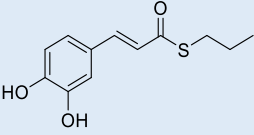
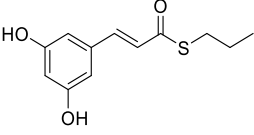
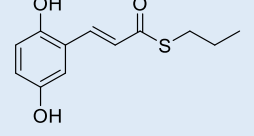
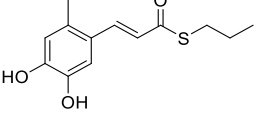
**Figure 2.6.** Cyclic voltammetric curves of **V** (black line), **3** (blue line), **4** (red line) and **7** (green line) recorded in phosphate buffer 2M electrolyte solution at a glassy carbon (GC) electrode and scan rate of 100 mV/s.

Further, by comparing antiaggregating abilities of the compounds with their anodic peak values ( $E_p^{an}$ ), which correspond for smaller values to a higher propensity to oxidation, a correlation was found, suggesting a redox-controlled conversion to the active quinone form to be plausibly involved in the inhibition of amyloid aggregation. It is worth to note that the same trend can be observed also looking at the standard redox potentials (the experimental  $E_{1/2}$  values), instead of the peak potentials (Table 2.2).

The inhibitory capability of quinones towards A $\beta$  assembly is well documented. Both covalent and non-covalent mechanisms of action have been proposed. Quinones are electrophilic species that can undergo nucleophilic addition from nucleophiles in proteins. However, the asymmetric dipole of the quinonic ring has been shown to play a crucial role in establishing a favorable dipole interaction between the central electron-poor quinone ring and the electron-rich peptidic carbonyls as well as aromatic recognition sites within the amyloidogenic proteins.<sup>269, 270</sup>

Thus, to gain information about the binding mode of pro-electrophilic compounds **V** and **4**, we focused on most active **V**, and we designed and synthesized a new compound (**7**), where the position usually attacked by amine nucleophiles is blocked by the insertion of a methyl substituent.<sup>271</sup> Interestingly, as verified by cyclic voltammetry, this structural modification did not alter the redox properties of the molecule with respect to parent compound **V** (oxidative potential of **7** = +0.20 V, Table 2.2), suggesting an analogous conversion to the corresponding quinone form before amyloid interaction (Figure 2.5).

**Table 2.2.** Antiaggregating potency of compounds **V**, **3**, **4** and **7** compared with corresponding anodic peak ( $E_p^{an}$ ) and standard redox potentials ( $E_{1/2}$ ).

Cpd.	Structure	Inhibition of $A\beta_{42}$ self-aggregation % inhibition ThT [ $I$ ]=50 $\mu$ M ( $IC_{50} \pm SEM / \mu$ M)	$E_p(ox) / V$	$E_{1/2}(ox)^a / V$
<b>V</b>		>90 ( $3.99 \pm 0.39$ ) <sup>263</sup>	0.19	0.10
<b>3</b>		<10	0.76	0.66
<b>4</b>		>90 ( $10.2 \pm 1.3$ )	0.32	0.10
<b>7</b>		> 90	0.20	0.14

<sup>a</sup> Halfwave ( $E_{1/2}$ ) values estimated by digital simulation of the experimental voltammetric curves.

With the aim to verify the impact of this structural modification on compound activity, a ThT-based assay was performed, revealing that compound **7**, as well as **V**, strongly inhibited amyloid aggregation (inhibition > 90 % for 50  $\mu$ M of **7**, Table 2.2). This preliminary result, albeit not excluding possible involvement of covalent bond formation, suggests that amyloid addition should not represent the exclusive driver of antiaggregating properties of **V**. Further, notwithstanding the lack of efficacy observed for the *meta*-derivative **3** suggests no role for the  $\alpha,\beta$ -unsaturated carbonyl moiety of the lateral chain, to exclude its possible involvement in amyloid covalent binding the saturated analogue **8** was also synthesized, and its antiaggregating activity is under evaluation.

### Mass spectrometry study

To gain a conclusive answer on the possibility that quinone transformation is or not followed by covalent interaction with amyloid peptide, active compounds **V** and **4** have been studied by means of mass spectrometry;  $A\beta_{42}$  samples were incubated under the assay conditions used for the ThT assay, with and without **4** and **V** at 50  $\mu$ M (compound/ $A\beta_{42}$  = 1/1).

In line with our previous findings, no covalent adduct has been detected between  $A\beta$  and **V**, strengthening the value of non-covalent interactions, or at least transient covalent binding, in triggering the biological response. Conversely, concerning compound **4**, a covalent adduct between  $A\beta_{42}$  and the compound has been

detected. In particular, the deconvoluted MS spectrum of A $\beta$ <sub>42</sub> analyzed immediately after addition of **4** (co-incubated sample at t=0, Figure 2.7a) showed an intense signal at 4514 Da, which corresponds to the molecular weight of the monomeric form of the peptide. Minor signals corresponding to the oxidized form of A $\beta$ <sub>42</sub> and to its adduct with potassium ions were also detected. Co-incubation of A $\beta$ <sub>42</sub> with **4** at equimolar concentration for 6 and 24 hours lead to the appearance of new species at higher molecular weights (Figures 2.7b and 2.7c). In detail, species characterized by a mass increment of 232 and 250 Da (signals at 4748 and 4764) were detected upon 6h-incubation, while a further signal at 4782 (mass increment of 268) was observed upon 24 h.

A kinetic evaluation of adduct formation, performed to monitor formation of most abundant adducts A232 and A250 in a 6h-time course experiment, revealed that the amount of both adducts increased with time, with A232 forming rapidly (detectable within 1h) while formation of A250 appeared to occur only after a lag phase (data not shown). This might lead to hypothesize that A250 is formed upon rearrangement of A232.

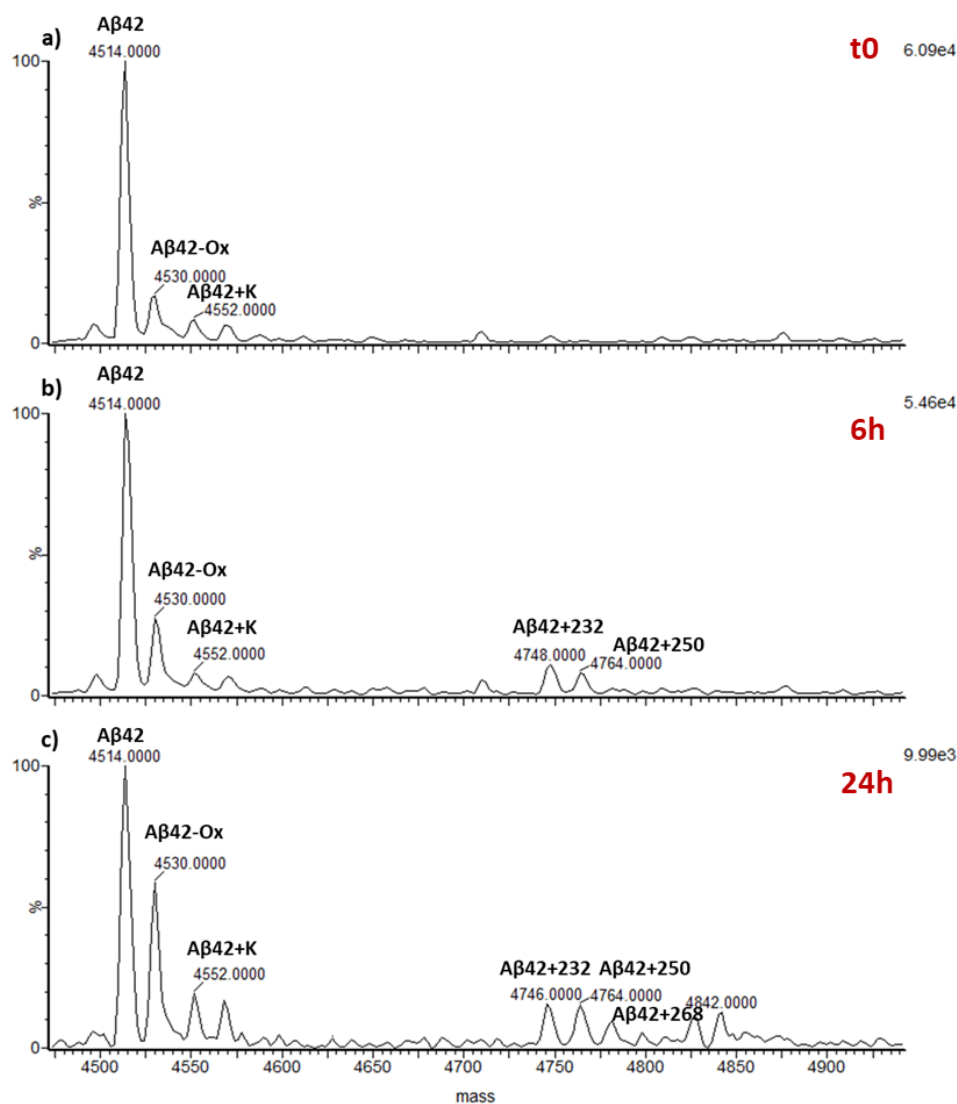


**Figure 2.7.** Deconvoluted mass spectra of A $\beta$ <sub>42</sub> before (a) and after incubation for 6 h (b) and 24 h (c) with compound **4**.

To determine the amino acid residue targeted by **4** and involved in the formation of the covalent adduct, a bottom-up MS analysis was performed. In detail,  $\text{A}\beta_{42}$  was incubated in the presence of **4** for 6 h and digested overnight by trypsin. The tryptic peptides were subsequently analyzed by LC-ESI-MSMS. The study highlighted covalent modifications only occurred at peptide 6-28 which could carry either the modification characterized by a mass increment of 232 Da or that characterized by a mass shift of 250 Da. MS/MS analysis of peptide 6-28 allowed identification of residue Lys16 as the amino acid residue involved in the formation of both covalent adducts (Figures 2.8a and 2.8b). This might further support that the two most abundant adducts are related and that A250 may generate by rearrangement of A232.

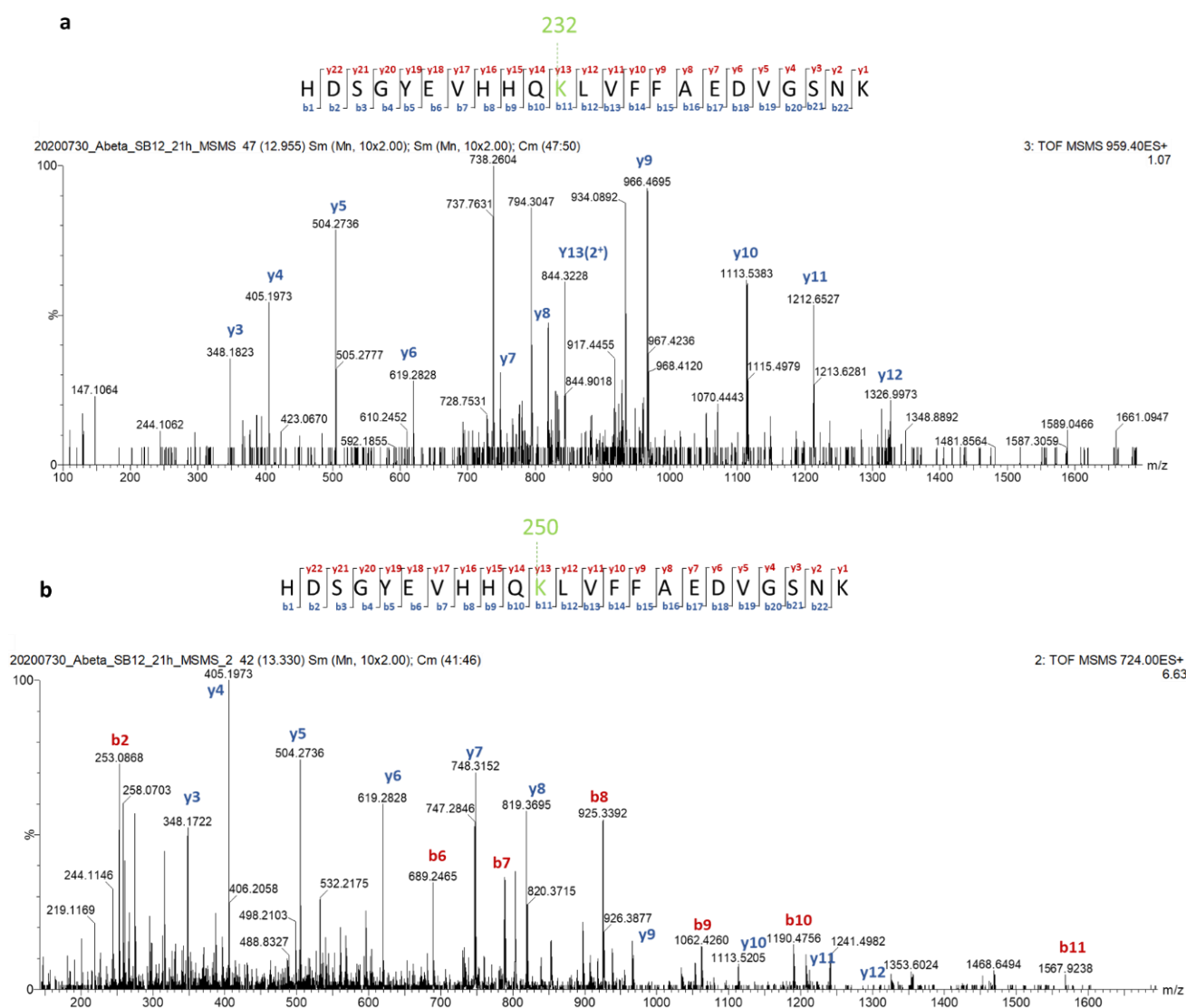


**Figure 2.8.** Bottom up analysis of  $\text{A}\beta_{42}$ . MSMS spectrum of peptide 6-28 carrying a modification characterized by a mass increment of 232 (a) and 250 Da (b) at the level of  $\text{A}\beta_{42}$  Lys16. In the mass spectra the identified fragments are labeled with the letter y or b, depending on the type of fragment, and with a number indicating the position of the fragmentation on the peptide sequence.

To justify the molecular weight of A232 adduct, based on compound **4** (MW=238 Da), we hypothesized a double attack from nucleophilic lysine 16 to the oxidized form of **4** (MW = 236 Da). This possibility should involve the double bond of the lateral chain, affording a cyclic structure. The removal of two H for each attack

might be determined by subsequent oxidation steps, or by water-assisted proton transfer, as previously reported for other similar structures.<sup>271</sup> A draft of the proposed mechanism of adduct formation, which is definitely speculative, is reported in Figure 2.9.

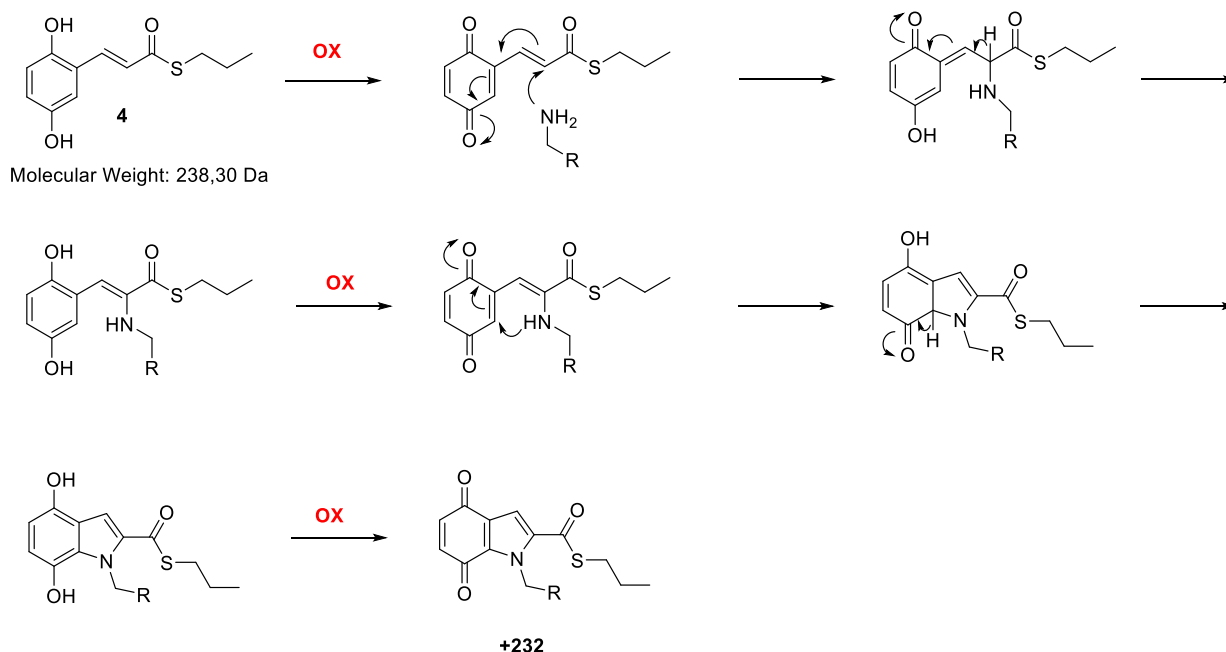


**Figure 2.9.** Proposed mechanism of covalent adduct formation between compound **4** and A $\beta$ <sub>42</sub>.

The corresponding saturated analogue of **4**, compound **6**, could have been of help in corroborating the value of the unsaturated lateral chain in amyloid binding. Unfortunately, as the synthesis failed, we could not count on this further indication. However, albeit the reason why the *ortho*-derivative **V** does not undergo nucleophilic addition as revealed by mass spectrometry assay deserves further investigation, the consideration that no difference in activity occurs between the *ortho*-derivatives **V** and **VI**, carrying respectively the unsaturated and saturated chain, is in line with the lack of covalent adduct formation found for **V**.

It is well-known that polyphenols can act as either antioxidant or pro-oxidant agents.<sup>272</sup> Prototypical example is the pro-oxidant effect exerted by the natural polyphenol myricetin toward A $\beta$ <sub>42</sub> peptide.<sup>273</sup> The oxidized form of A $\beta$ <sub>42</sub> (A $\beta$ <sub>42</sub> Ox) was shown to be less prone to aggregate than the native one (A $\beta$ <sub>42</sub> Native), accounting for its slower aggregation rate.<sup>117</sup> On this basis, we sought to verify whether pro-electrophiles **4** and **V** could partially exert their inhibitory activity through an oxidation-based mechanism. Because of their different molecular weights, both the native and oxidized forms of A $\beta$ <sub>42</sub> can be detected by MS analysis. To estimate whether **4** or **V** may favor amyloid oxidation, the content of oxidized A $\beta$ <sub>42</sub> was quantified in the same time frame and compared with values obtained in the absence of compound (Figure 2.10).

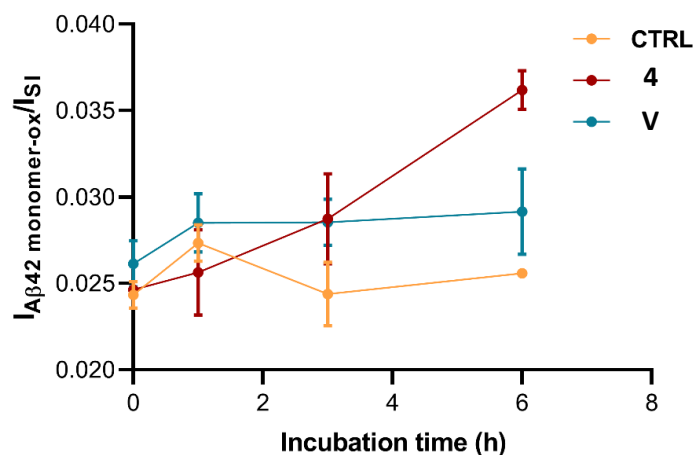


**Figure 2.10.** Evaluation of the oxidized form of  $A\beta_{42}$  in the absence and in the presence of **4** or **V** at equimolar concentration. The analysis was performed by deriving, from the ESI mass spectrum, the ratio between the intensity of the most intense signal of the oxidized form of  $A\beta_{42}$  and the intensity of the internal standard (reserpine).

As shown in figure 2.10, the  $A\beta_{42}$  degree of oxidation increased over time when amyloid was co-incubated with **4**, while no significant variations in the amount of oxidized  $A\beta_{42}$  were detected with **V**, as well as in the absence of inhibitor, thus revealing an additional difference in the inhibitory mode of action of the two compounds. Indeed, albeit the extent of **4**-induced amyloid oxidation suggests that this process would not represent the pivotal antiaggregating mechanism, it may contribute to the polyhedric mode of action of the compound.

### 2.1.3 CONCLUSIONS

We investigated the molecular mechanisms underpinning the antiaggregating activity of previously synthesized catechol-based compounds through the development of the corresponding *meta*- and *para*-dihydroxy derivatives, and the study of their antiaggregating properties. Obtained results indicate the pro-electrophilic character of the compounds as a prerequisite for activity. Indeed, the *ortho*- and *para*-derivatives, which can convert to the corresponding quinones, strongly inhibit amyloid aggregation, while the *meta*-analogues are devoid of any relevant efficacy. Mass spectrometry assays revealed differences in the mode of action of the compounds **4** and **V**, suggesting only for the former a variety of processes involved in the play, including covalent adduct formation with Lys16 of  $A\beta_{42}$ , and an oxidation-based mechanism. These processes presumably contribute to the overall antiaggregating activity of the molecule running aside with non-covalent interactions, which seem to represent the driving motif in the antiaggregating mode of **V**. Interestingly, this study highlights the concept that (pro)electrophilic features are not per se sufficient to generate covalent adduct formation with a protein target, and minimal structural modifications can generate alternative mechanisms of action at a molecular level.



## 2.2 Merging dihydroxy-cinnamic core into a coumarine nucleus to enclose CB<sub>2</sub>R modulatory properties

In NDDs, protein misfolding processes are strongly surrounded by inflammatory condition, which represents a major actor of the play. The uncontrolled spreading of proinflammatory cytokines can irreversibly damage glial and neuronal cells as well as foster detrimental oxidative damage and support protein misfolding.<sup>79, 123</sup> In this respect, ECS is assuming particular emphasis thanks to its immunomodulatory properties in CNS and its peculiar and inducible functional role in neuroinflammation.<sup>52</sup> Particular role have CB<sub>2</sub>Rs; they are present in CNS at very low spotted levels, whereas they were found to be strongly upregulated in microglial cells surrounding amyloid plaques in AD brains and their expression was correlated with A $\beta$ <sub>42</sub> levels and plaque deposition.<sup>59</sup> CB<sub>2</sub>R activation promoted microglial switch into M2 phenotype, therefore reducing proinflammatory cytokines expression (i.e. IL-1 $\beta$ , IL-6, TNF- $\alpha$  and IFN- $\gamma$ ) and ROS/RNS production as well as modulating macrophages-microglia migration.<sup>62, 63</sup> Furthermore, CB<sub>2</sub>R agonists in *in vivo* AD models reduced levels of pre-existing amyloid plaques as well as their formation, along with restoring synaptic plasticity, cognition and memory.<sup>274</sup> All of these experimental outcomes indicate selective CB<sub>2</sub>R modulators, which are devoid of psychotropic effects CB<sub>1</sub>R-related, as interesting pharmacologic tools or potential therapeutics to tackle AD neurotoxic cascade. Notably, given the multifactorial nature of AD, CB<sub>2</sub>R activation has already been combined with other validated anti-AD activities in several multitarget approaches, which intend to simultaneously contrast the disease on multiple fronts, opening new prospects for disease-modifying AD treatments.<sup>275, 276</sup>

3-carboxy bicyclic scaffolds such as coumarine and oxoquinoline are considered privileged pharmacophores for the development of selective CB<sub>2</sub>R ligands.<sup>277</sup> A high degree of structural analogy can be noticed between these heterocyclic compounds (**F**, Figure 2.11) and the thioesteric derivatives previously described (**I** reported as lead compound, Figure 2.11). Particularly, the bone of hydroxycinnamic acid is masked in the bicyclic structure of the CB<sub>2</sub>R ligands. Therefore, we envisioned the combination of antiaggregating abilities of **I** with antiinflammatory properties deriving from CB<sub>2</sub>R activation as an interesting strategy to tackle and investigate multi-layered AD etiopathology. In the search of new pharmacologic tools which could allow to deepen insights in the study of the cellular liaison A $\beta$ /inflammation also through the modulation of CB<sub>2</sub>Rs, we herein developed new compounds of general structure **G**, merging the thioesteric cinnamates' core of compounds **I** into bicyclic scaffolds of known CB<sub>2</sub>R ligands.

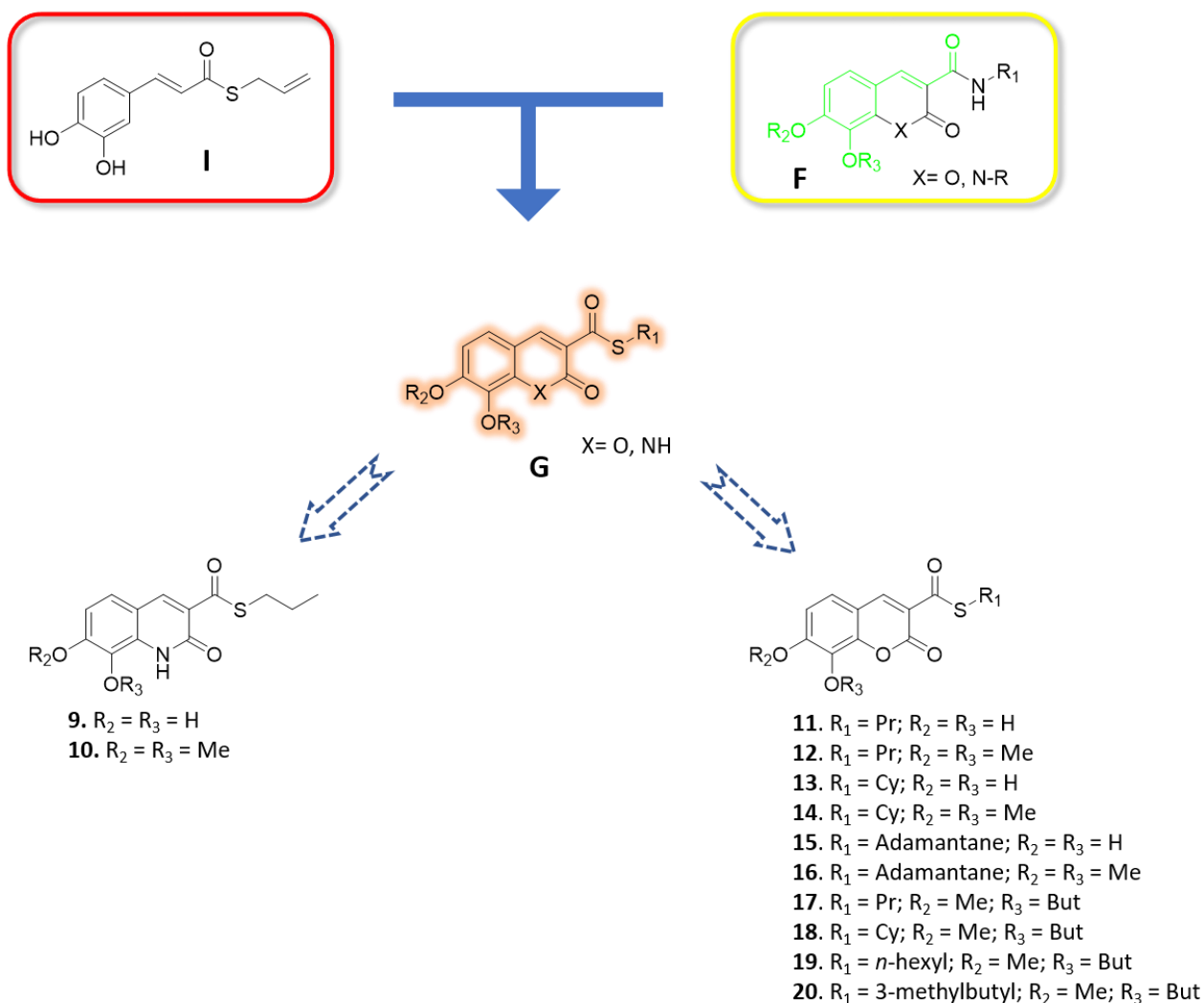


**Figure 2.11.** Drug design of newly synthesized thioesteric oxoquinoline and coumarine derivatives **9-20**.

First, oxoquinoline and coumarine cores have been exploited in compounds **9** and **11**, which maintain the antiaggregating features of compounds **I** (i.e. the catechol moiety and the thioester group), to verify if the molecular stiffening could preserve antiaggregating properties of our lead catechol-bearing compounds. To check whether oxoquinoline or coumarine moieties, for which antiaggregating properties were previously reported,<sup>278, 279</sup> might contribute in this respect, the corresponding dimethoxy-analogues **10** and **12** were included in the study with the intention to switch off putative catechol-driven effect. Preliminary evaluation of antiaggregating ability of oxoquinoline **9** by ThT assay showed solubility issues in the experimental conditions used, thus impeding a proper biological evaluation. Therefore, we herein focused on the 3-carboxy coumarine scaffold as the base for the development of multitarget compounds which could derive new value from additional CB<sub>2</sub>R activity. Based on previous literature on coumarine CB<sub>2</sub>R ligands,<sup>280</sup> we systematically modified the structure of **11** and **12** by introducing bulky and lipophilic substituents as thioester functions in position 3, replacing the propyl moiety with cyclohexyl or adamantane groups (**13-16**, Figure 2.11). Parallely, more lipophilic derivatives bearing methoxy group in 7 and butoxy in 8 position were developed evaluating different linear, branched or cyclic thioesteric substitutions, ranging from the propyl and cyclohexyl to hexyl

and 3-methylbutyl groups (**17-20**, Figure 2.11). Derivative bearing all three more lipophilic substitutions (i.e. 7-methoxy, 8-butoxy and 3-adamantanethioester) was not achieved because of low-reactivity issues met along the synthesis.

Parent compound **VI** (Figure 2.12) was included in the study for comparison.

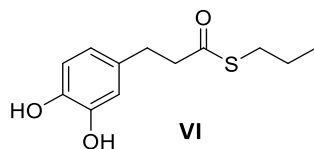


**Figure 2.12.** Structure of compound **VI**.

### 2.2.1 METHODS

#### Chemistry

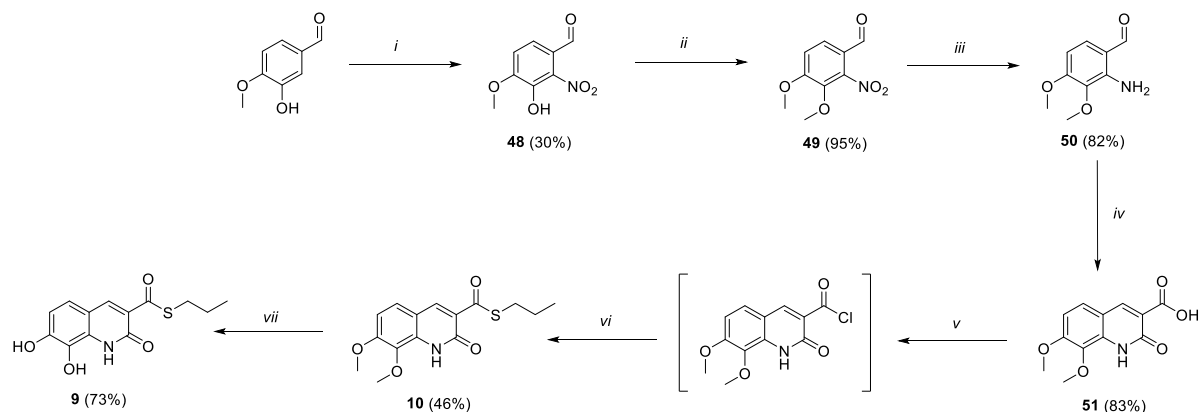
Syntheses of compounds **9-20** were performed as outlined in Schemes 5-7.

Oxoquinolines **9** and **10** were obtained as depicted in Scheme 5, with minor modifications of literature procedure referred to 2-oxoquinoline derivatives.<sup>280</sup> Commercial 3-hydroxy-4-methoxybenzaldehyde was *o*-nitrated with nitric acid and the free hydroxy group in position 3 further protected quantitatively in a methoxy function. Once reduced the nitro group of intermediate **49** to give **50**, using iron and acidic conditions, it underwent Knoevenagel condensation with Meldrum's acid to obtain key 3-carboxy-2-oxo-quinoline intermediate **51**. The carboxy function of this latter was activated as non-isolable acyl chloride with thionyl chloride for the subsequent nucleophilic substitution with 1-propanethiol using triethylamine as base to give **10**. Final demethylation step with boron tribromide at 0°C afforded catechol derivative **9**.

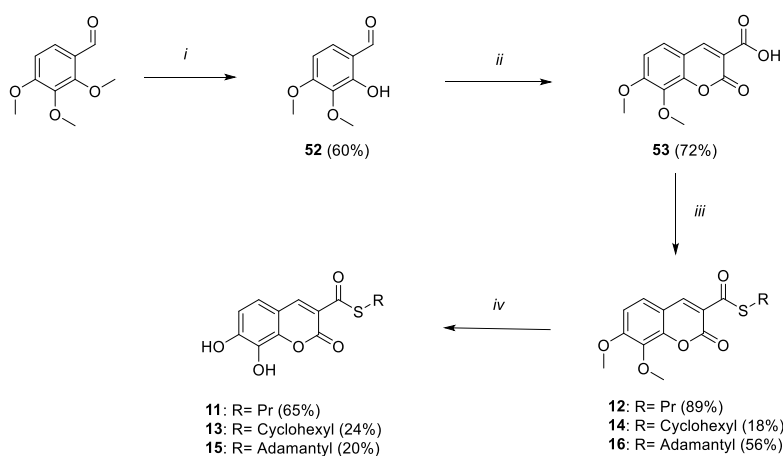
Derivatives **11-16** were achieved through the synthetic strategy reported in Scheme 6. First, *o*-demethylation of 2,3,4-trimethoxybenzaldehyde with aluminium trichloride unmasked vicinal hydroxy group, essential for the subsequent condensation to close the coumarine cycle, affording **53**. In this case, the coupling step with selected thiols, to give compounds **12**, **14** and **16**, could be carried out with a milder procedure, using hydroxy benzotriazole and 1-ethyl-3-(3-dimethylaminopropyl)carbodiimide (i.e. HOBt and EDC) as activating agents instead of thionyl chloride. Catechol analogues **11**, **13** and **15** were obtained following previously described demethylation process with boron tribromide.

In Scheme 7 is reported the synthetic strategy carried out to afford derivatives **17-20** according to a modified literature procedure.<sup>281</sup> In this case, the initial aluminium chloride-mediated demethylation was conducted in dichloromethane with twice amount of equivalent, in order to demethylate both *ortho*- and *meta*-hydroxy functions (compound **54**). From **54** we tried different strategies reported in literature to selectively alkylate the hydroxy group in meta position; unfortunately, only disubstituted or *ortho*-substituted derivatives were obtained because of higher acidity of *ortho*-hydroxy function. Therefore, we proceeded with a direct condensation with Meldrum's acid and subsequent coupling with selected branched, linear or cyclic thiols

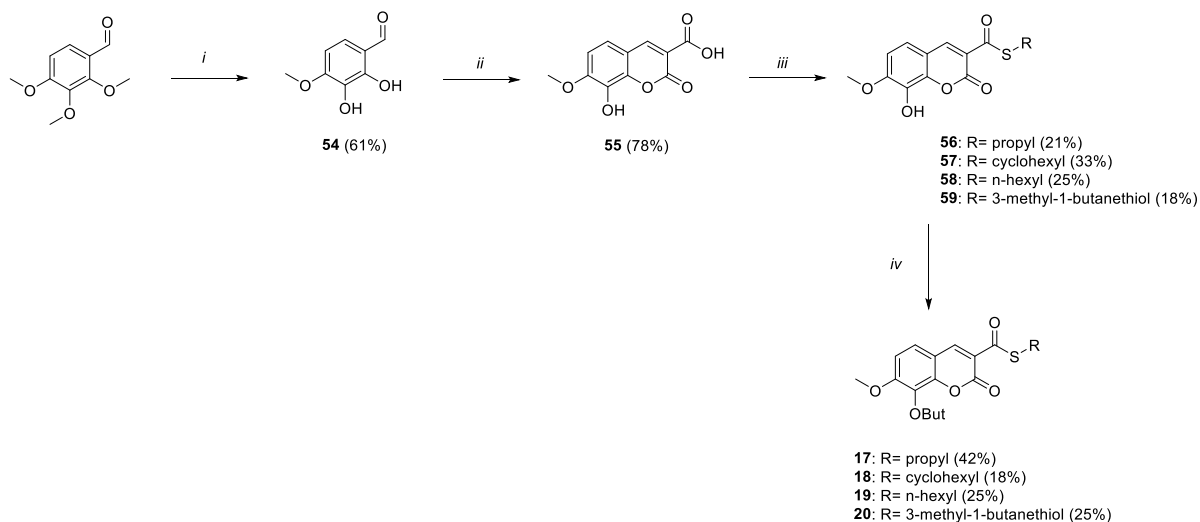
affording intermediates **56-59**. Lastly, through a nucleophilic substitution with sodium hydride as base of choice and bromobutane as hanging nucleophile we attached butyl chain to free hydroxy function in position 8, obtaining final compounds **17-20**.



**Scheme 5.** Reagent and conditions: (i) HNO<sub>3</sub>, EtOAc, N<sub>2</sub>, 0°C-rt, 24h; (ii) MeI, K<sub>2</sub>CO<sub>3</sub>, DMF, N<sub>2</sub>, 70°C, 1h; (iii) Fe/HCl, EtOAc, AcOH, H<sub>2</sub>O, reflux-rt, 1h; (iv) Meldrum's acid, piperidinium acetate, EtOH, 60°C, 48h; (v) SOCl<sub>2</sub>, toluene, reflux, 3h; (vi) R-SH, Et<sub>3</sub>N, DCM, N<sub>2</sub>, 0°C-rt, 48h; (vii) BBr<sub>3</sub> 1M in DCM, DCM, N<sub>2</sub>, 0°C-rt, 30min.



**Scheme 6.** Reagents and conditions: (i) AlCl<sub>3</sub>, toluene, 80°C, 6h; (ii) Meldrum's acid, piperidinium acetate, EtOH, 60°C, 24h; (iii) R-SH, HOBT, EDC, DCM, N<sub>2</sub>, 0°C-rt, o/n; (iv) BBr<sub>3</sub> 1M in DCM, DCM, N<sub>2</sub>, 0°C-rt, 6h.



**Scheme 7.** Reagents and conditions: (i)  $\text{AlCl}_3$ , DCM, reflux, 8h; (ii) Meldrum's acid, piperidinium acetate, EtOH,  $60^\circ\text{C}$ , 6h; (iii) R-SH, HOBT, EDC, DCM,  $\text{N}_2$ ,  $0^\circ\text{C}$ -rt, o/n; (iv) NaH 60% in mineral oil, bromobutane, DMF,  $\text{N}_2$ ,  $0^\circ\text{C}$ -rt, o/n.

## Biology

Preliminary evaluation on selected compounds was carried out to analyse ability to inhibit  $\text{A}\beta_{42}$  self-aggregation and further insights are still in progress. Parallely, synthesized compounds were screened for their  $h\text{CB}_2\text{R}$  affinity-selectivity in HEK cells and CHO cells/rat brain homogenate for  $\text{CB}_1\text{R}$  through a radioligand binding assay with  $[^3\text{H}]\text{CP 55,940}$ , whereas efficacy assays are ongoing. Chemical stability of  $h\text{CB}_2\text{R}$ -active compounds was also assessed in experimental conditions used to determinate binding affinity. For more potent  $\text{CB}_2\text{R}$  compounds neurotoxicity and immunomodulatory properties were investigated in CGNs and in immortalized murine microglia, respectively.

### 2.2.2 RESULTS AND DISCUSSION

#### Inhibition of $\text{A}\beta_{42}$ Self-Aggregation

To verify if the ability of parent compound **VI** to inhibit  $\text{A}\beta_{42}$  aggregation ( $\text{IC}_{50}$  of  $3.80 \pm 0.44 \mu\text{M}$ )<sup>263</sup> was retained by the constrained derivatives **9** and **11**, a preliminary evaluation of antiaggregating properties was performed by ThT assay. In this experimental setting, the oxoquinoline derivative **9** showed solubility issues, precluding proper biological evaluation. Conversely, compound **11** at  $50 \mu\text{M}$  concentration exerted significant inhibition of amyloid aggregation, albeit an optical interference around 20% was observed, as verified by the analysis of blanks containing inhibitor and ThT, which were prepared and evaluated to account for quenching and fluorescence properties. Altogether, these findings directed our efforts to the design and synthesis of coumarin-based derivatives as multitarget agents and indicated electrospray ionization ion trap mass spectrometry (ESI-IT-MS) in flow injection mode, which allows the monomeric form of  $\text{A}\beta_{42}$  to be detected and quantitated, as the proper mean to investigate the antiaggregating abilities of the new molecules.

Thus, to gain information on how the catechol feature, the coumarine scaffold or lipophilic substituents that seem to be fundamental to reach *hCB<sub>2</sub>R* affinity can possibly tune antiaggregating properties, compounds **11**, **12** and **17** were selected as prototypical set of compounds, and their evaluation by mass spectrometry assay is ongoing. Based on the obtained results, further compounds will be studied in relation to their antiaggregating properties in the next steps of the project.

### Radioligand binding assay to determine CBR affinity

The modulation of *CB<sub>2</sub>R* is gaining increasing interest as elected target to tackle neurodegenerative diseases with neuroinflammatory component. Particularly, the existence of an intertwined and toxic relation between amyloid deposition and *CB<sub>2</sub>R*s overexpression in damaged brain regions is now well established.<sup>71</sup> Furthermore, the activation of *CB<sub>2</sub>R*s in pathological neuroinflammation proved to exert several beneficial effects, ranging from activation of antiinflammatory pathways to a strong reduction of amyloid aggregates and related toxicity.<sup>59</sup> From these outputs, the chance to modulate both inflammatory cascades and protein aggregation mechanisms emerged as promising strategy to deepen insights into neurodegenerative disorders machinery. The thioesteric coumarine derivatives were tested to evaluate *hCB<sub>2</sub>R* and *CB<sub>1</sub>R* binding in HEK and CHO cells/rat brain homogenate, respectively, through a radioligand binding assay with [<sup>3</sup>H]CP 55,940 as non-selective high-affinity ligand (Table 2.3).<sup>276</sup> Derivative **VI**, belonging to parent antiaggregating compounds, was also included in this assay for comparison.

**Table 2.3.** CBRs affinity values for compounds **11-20** and **VI**. See figure 2.10 for structures.

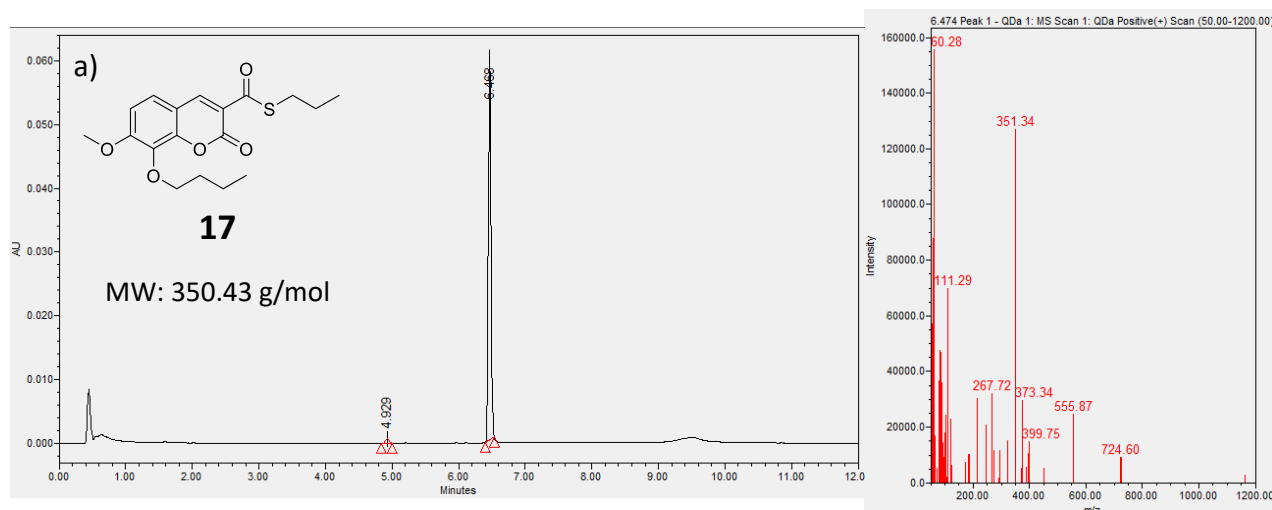
Cpd.	<i>K<sub>i</sub></i> ± SD or [ <sup>3</sup> H]CP 55,940 displ. @10μM	
	<i>hCB<sub>2</sub>R</i> <sup>a</sup>	<i>CB<sub>1</sub>R</i> <sup>b</sup>
<b>Rimonabant</b>	n.d.	100%
<b>MN-I-97</b> <sup>282</sup>	38 ± 8 μM**	n.d.
<b>VI</b>	15.6%	25.2% <sup>#</sup>
<b>11</b>	37.5%	36.9% <sup>#</sup>
<b>12</b>	5.9%	11.0% <sup>#</sup>
<b>13</b>	3.4%	n.d.
<b>14</b>	0.8%	n.d.
<b>15</b>	20.6%	23.8% <sup>§</sup>
<b>16</b>	27%	6.5% <sup>§</sup>
<b>17</b>	1.01 μM*	n.d.
<b>18</b>	330 ± 22 nM**	59.5% <sup>§</sup>
<b>19</b>	4.5 μM*	n.d.
<b>20</b>	4.1 μM*	26.2% <sup>§</sup>

<sup>a</sup> Screened on membranes of HEK cells stably expressing *hCB<sub>2</sub>R* using 10  $\mu$ M of the compound; <sup>b</sup> Screened on membranes of CHO cells stably expressing *hCB<sub>1</sub>R* (<sup>#</sup>) or rat brain homogenate stably expressing *rCB<sub>1</sub>R* (<sup>§</sup>) using 10  $\mu$ M of the compound; n.d., not determined. \* values are derived from a single experiment performed in triplicate. \*\* values are mean values from two independent experiments, each performed in triplicate.

All derivatives carrying two hydroxy or methoxy substituents on the aromatic ring resulted in no CBR affinity, independently from the lipophilicity and steric hindrance of the thioester fragment. Conversely, by introducing a butoxy chain in 8 position, *hCB<sub>2</sub>R* affinity immediately increases. Keeping fixed methoxy in 7 and butoxy in 8 positions, *hCB<sub>2</sub>R* seems to prefer bulkier and shorter (**17** and **18**) than linear and longer substituents (**19** and **20**) attached to thioester function. These data were in agreement with those already reported in literature for similar structures.<sup>281</sup> Preliminary evaluation regarding *CB<sub>1</sub>R* affinity showed no *CB<sub>1</sub>R*-affinity for tested compounds, except for **18**, whose *K<sub>i</sub>* determination is ongoing together with evaluation of *CB<sub>1</sub>R* affinity for not yet tested compounds.

### Stability study

The chemical stability of compounds which revealed *hCB<sub>2</sub>R* affinity (**17-20**) was investigated in experimental conditions used for the assay. Compounds **17-20** were analyzed by UHPLC-MS experiments at *t<sub>0</sub>* in DMSO stock solution and at *t<sub>3.5h</sub>* after incubation in assay medium at room temperature. In the figure below are reported chromatograms registered at 365 nm after 3.5h incubation (same time of radioligand binding assay) in binding buffer (50mM Tris-HCl, pH 7.4; 5 mM MgCl<sub>2</sub>·6H<sub>2</sub>O; 2.5mM EDTA) paired with mass spectra taken from peak compound (Figure 2.13).



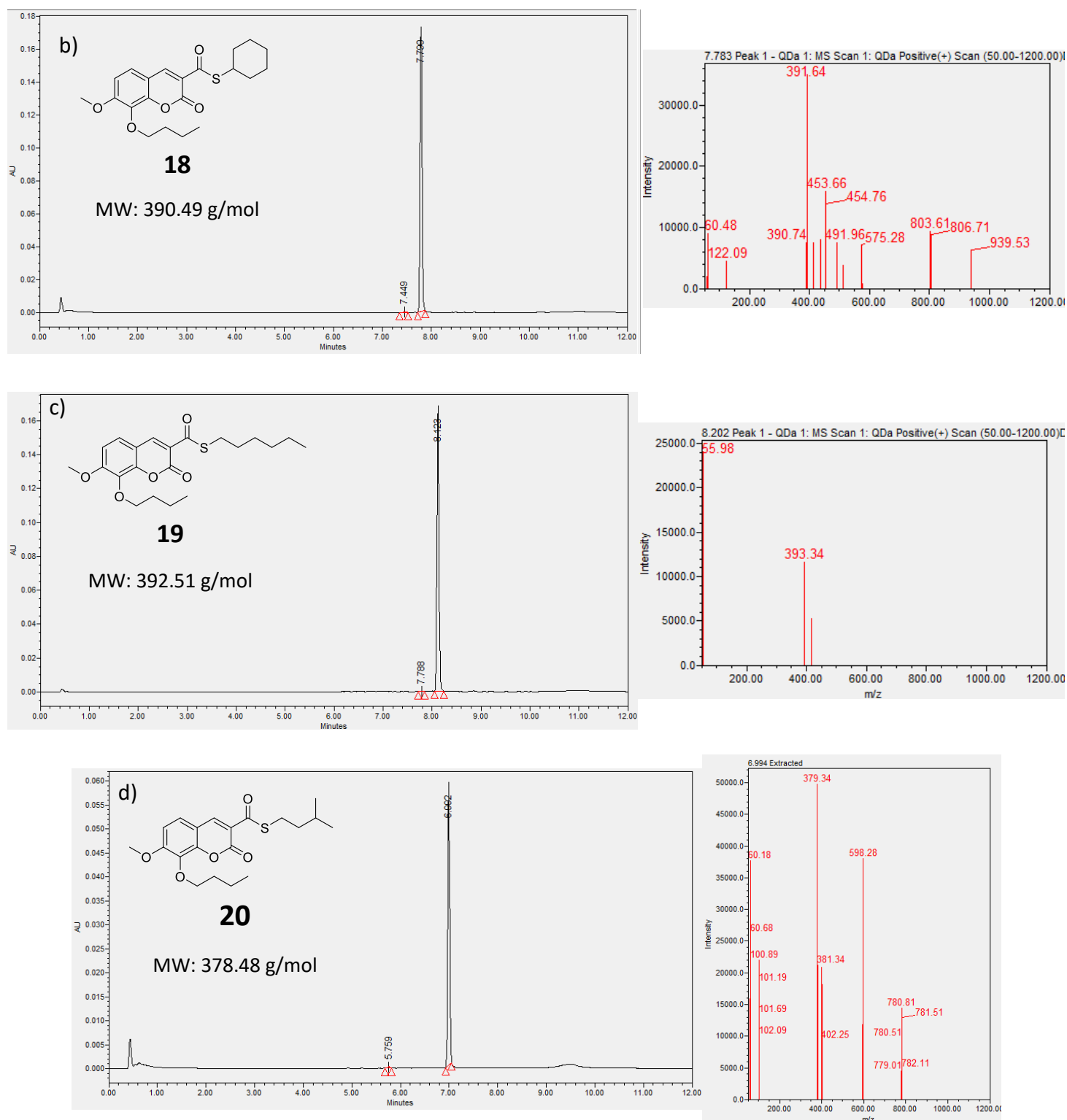


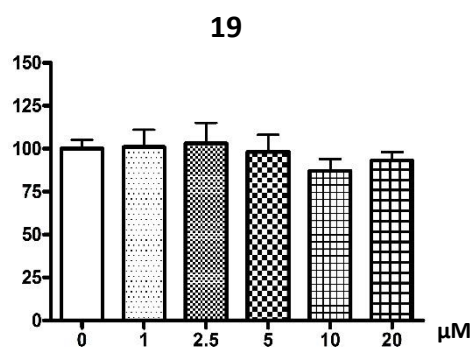
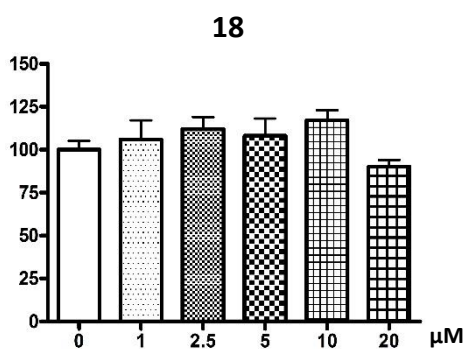
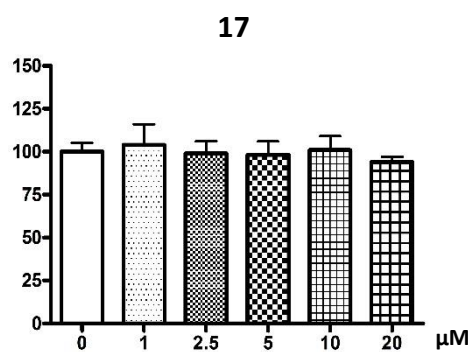
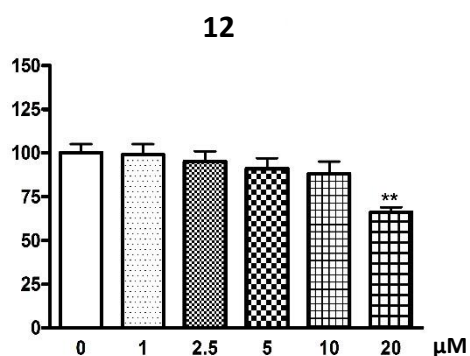
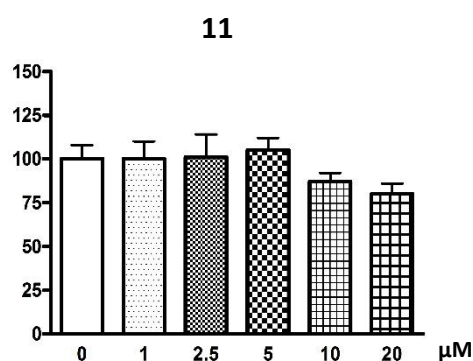
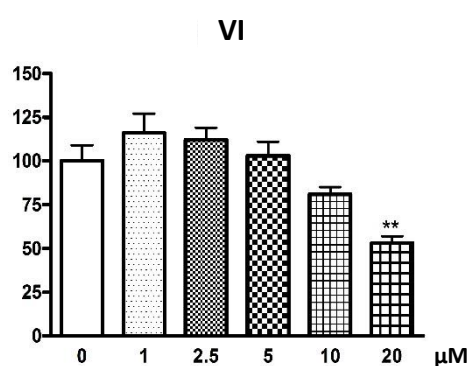
**Figure 2.13.** Chromatograms of UHPLC run paired with mass spectra registered at moment of compound elution for compounds **17** (a), **18** (b), **19** (c) and **20** (d).

Besides pure compound elution, no detection of the respective acid was observed, corroborating the chemical stability of the thioester function in the used experimental conditions.



## Neurotoxicity evaluation

With the aim to verify biological potential of selected compounds in neuronal cells, the neurotoxicity of parent compound **A**, its coumarine congeners **11**, **12** and more  $hCB_2R$ -active **17-20** was evaluated on primary rat cerebellar granule neurons (CGNs). Primary cells provide higher-quality models as well as they are more sensitive to drug treatment than immortalized cell lines, as they form synapses and incorporate significant neuromodulatory and trophic inputs. Particularly, CGNs are considered a reliable model for studying cellular and molecular mechanisms of survival/apoptosis and neurodegeneration/neuroprotection.<sup>283</sup> CGNs viability was assessed after 24 h treatment of **A**, **11**, **12** and **17-20** at clinically relevant concentrations varying from 0 to 20  $\mu\text{M}$  (i.e. 1, 2.5, 5, 10, 20  $\mu\text{M}$ ) using MTT assay (Figure 2.14).



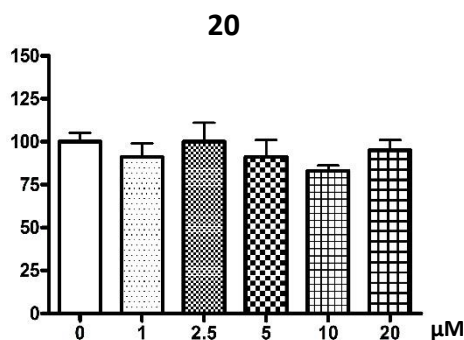


**Figure 2.14.** Toxicity of compounds **VI**, **11**, **12** and **17-20** to differentiated primary rat cerebellar granule neurons (CGNs) after 24 h treatment. CGNs were exposed to the compounds **VI**, **11**, **12** and **17-20** for 24 h at concentrations ranging from 0 to 20  $\mu$ M and cell viability measured by MTT assay. Results are expressed as percentage of controls and are the mean  $\pm$  SE of at least 3 different experiments, each run in triplicate. \*\* $p < 0,01$ ; \* $p < 0,05$  compared to control conditions (0  $\mu$ M). Analysis for data statistical significance was performed through one-way ANOVA followed by Dunnett's post-hoc comparison test by using GraphPad Prism 4.0.

All tested compounds showed safety profile until 5  $\mu$ M. At 10  $\mu$ M only **VI**, **19**, **20** and **12** slightly affect neuronal viability, but in a still tolerable manner (CGNs viability  $>80\%$ ). This trend worsens at 20  $\mu$ M for **11** and **12**, whereas **17** and **18** revealed no signs of toxicity at all tested concentrations. Based on these data, 5  $\mu$ M was the concentration selected to evaluate antiinflammatory/immunomodulatory properties of **VI**, **11**, **12** and **17-20** in immortalized murine microglia lines.

### Immunomodulation study

Microglia, considered as immune cells of the brain, are main mediators of neuroinflammatory processes and present different activated phenotypes. M1-like is activated by inflammatory stimuli and further fuel inflammatory cascade by increasing proinflammatory molecules such as iNOS. Conversely, M2-like phenotype increases neuroprotective functions through production of antiinflammatory cytokines and phagocytosis' markers.<sup>7</sup> Because of the spreading neuroinflammatory processes in pathological conditions, immunomodulation strategies triggering M1/M2 microglial shift or reducing M1 activation emerged as promising approach to counteract neurodegenerative disorders.<sup>284</sup> The experimental findings that *hCB<sub>2</sub>R* are overexpressed in microglial cells surrounding amyloid plaques, with consequent beneficial effects derived from their modulation,<sup>59</sup> prompted us to evaluate the antiinflammatory/immunomodulatory properties of the newly synthesized molecules. To this end, compounds **VI**, **11**, **12** and **17-20** at 5  $\mu$ M were tested in immortalized murine microglia N9, cell line sensitive to *CB<sub>2</sub>R* modulation.<sup>285</sup> Particularly, iNOS as M1 marker and triggering receptor expressed on myeloid cells 2 (TREM2), as M2 marker, expression upon inflammatory stimuli with LPS (100ng/mL) were analysed (Figure 2.15).

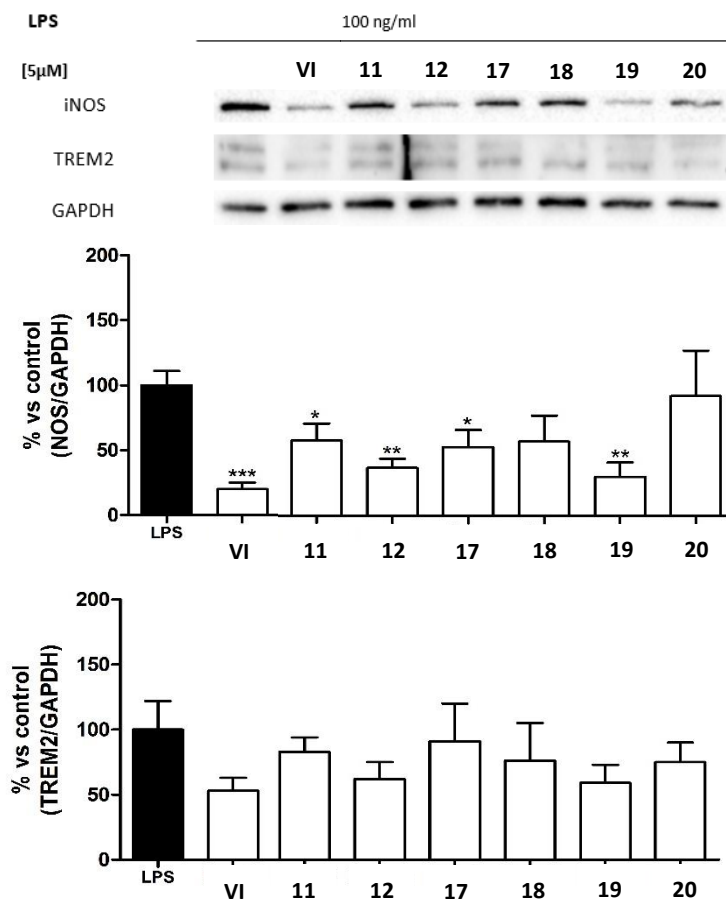


**Figure 2.15.** Mouse N9-microglial cells were treated with 5  $\mu\text{M}$  of compounds in presence or absence of LPS (100 ng/mL) for 24 h. Immunomodulatory effects of compounds were evaluated through Western blot analysis of microglial polarization markers expression. 20  $\mu\text{g}$  of protein extract were loaded into 12,5% sodium dodecyl sulfate-polyacrylamide gels (SDS-PAGE). Membranes were incubated overnight at 4°C with primary antibodies against iNOS, TREM2; GAPDH was used as loading control. Labeled proteins were detected by using the enhanced chemiluminescence method (ECL; BioRAD) with a Chemidoc (BioRad) chemiluminescence detector. Densitometric analysis was performed by using Image Lab 5.1 software. Densitometric results are expressed as percentage of LPS only and are the mean  $\pm$  SE of 3 different experiments. \*\*\* $p < 0,001$  \*\* $p < 0,01$ ; \* $p < 0,05$  compared to LPS condition. Analysis for data statistical significance was performed through T-test by using GraphPad Prism 4.0.

The tested compounds, albeit with different extent, generally lead to a decrease of proinflammatory iNOS as marker of M1 phenotype. These data underline the potential of these compounds to modulate glial inflammation and potentially revert proinflammatory phenotype. Parallely, no significative variations of M2-marker occurred, highlighting a possible immunomodulatory profile for tested compounds. Altogether, these experimental outputs suggest the ability to modulate neuroinflammation by interfering with the microglial M1/M2 switch, rather than totally repressing microglia reactivity. Albeit the common trend, differences emerge among compounds, deserving further investigations to evaluate dose-response relation and kinetic in the modulation of microglia activation to gain more conclusive results on their antiinflammatory/immunomodulatory behaviour.

### 2.2.3 CONCLUSIONS

With the aim to investigate the molecular underpinnings involved in the A $\beta$ -neuroinflammation loop, we developed a small library of thioesteric coumarines merging hydrocinnamic moiety of **1**, with proved antiaggregating efficacy, to substituted coumarine scaffolds endowed with *hCB<sub>2</sub>R* activity, possibly able to modulate neuroinflammatory processes. Radioligand binding assays revealed low micromolar *hCB<sub>2</sub>R* affinity for bulkier and more lipophilic compounds **17-20**. Particularly, compound **18** with cyclohexyl thioester fragment emerged as the best *hCB<sub>2</sub>R* ligand with sub-micromolar affinity ( $K_i=330\pm 22\text{nM}$ ). The stability of more active compounds **17-20** in medium assay was assessed using UHPLC-MS analyses. Further evaluation of *CB<sub>1</sub>R* affinity and *hCB<sub>2</sub>R* efficacy studies are still ongoing and will help to clearly delineate the ability of synthesized compounds to modulate CBRs pathway. Parallely, preliminary analysis of inhibition of cytotoxic A $\beta_{42}$  aggregation with ThT assay showed promising results but paired with optical interference of tested compounds. Therefore, deeper evaluations on the capability to inhibit amyloid aggregation are in progress with mass spectrometry assay. For selected compounds cell viability in primary culture of CGNs was firstly evaluated to further analyse their immunomodulatory properties in immortalized murine microglia. At a concentration of 5  $\mu\text{M}$  compounds **11**, **12** and **17-20** revealed a general reduction of iNOS, neurotoxic M1 marker, while no significant modifications were observed for TREM2 expression, revealing the phagocytic M2 profile to be possibly maintained. These preliminary results deserve further investigations to corroborate the hypothesis that compounds **11**, **12** and **17-20** might exert an immunomodulatory profile by means of microglia M1/M2 switch. Altogether, the obtained experimental findings confirm coumarine moiety as privileged scaffold, where small modification can drive the inhibition of A $\beta_{42}$  aggregation or trigger antiinflammatory processes. The chance to selectively and alternatively activate different neuroprotective pathways with minimal structural modifications emerged as a promising tool to shed lights on cellular mechanisms involved in the complex neuroinflammatory cascade.

### 2.3 Double attack to the neurodegenerative cascade: MAO-B and Nrf2 as elected targets

Pioglitazone (Figure 2.16a) is an insulin sensitizer belonging to the thiazolidinediones family approved since 1999 for the treatment of type-2 diabetes. Particularly, it acts as agonist of PPAR- $\gamma$ , PPAR's isoform mainly present in adipose tissue and macrophages. Furthermore, PPAR- $\gamma$  activation plays a pivotal role in inflammatory response, attenuating proinflammatory cytokines release and inhibiting NF- $\kappa$ B signaling, whereas at central level counteracts neuroinflammation also through modulation of protein misfolding.<sup>78, 255</sup> Due to the spreading of neuroinflammation in neurodegenerative conditions and its ability to penetrate BBB in therapeutic concentrations,<sup>286</sup> pioglitazone has been evaluated as therapeutic tool to tackle neurodegeneration. It exerted promising neuroprotective effects in PD animal models, showing reduction of glial activation and preventing dopaminergic neuronal loss.<sup>287</sup> These *in vivo* efficacies proved to be related more to cellular mechanisms involving MAO-B inhibition rather than PPAR- $\gamma$ -mediated antiinflammatory effects.<sup>288</sup> MAO-B, member of mono amine oxidase family, is a flavin-dependent mitochondrial enzyme responsible of catalyse oxidative degradation of amine-containing neurotransmitters. Interestingly, its CNS activity and expression were shown to increase in elderly people affected by neurological disorders, thus contributing to neurodegenerative oxidative damage.<sup>98, 289</sup>

*In vitro* studies revealed pioglitazone, the best among other glitazones, as selective submicromolar inhibitor of hMAO-B. The high-resolution crystal structure of hMAO-B with pioglitazone showed no covalent engagement, differently from most common marketed MAO-B inhibitors, highlighting a competitive mechanism of inhibition. Thiazolidinedione head drives interactions and spatial arrangement within the target binding site, establishing H-bonds with conserved water molecules close to Tyr398 and Tyr435 while facing flavin ring (Figure 2.16b). Ile199 residue is arranged in order to enable the opening of bipartite structure MAO-B active site, therefore allowing stabilizing hydrophobic interactions between ethylpyridine fragment and the loop guarding the active site cavity (i.e. Phe103, Trp119 and Pro104).<sup>290</sup>

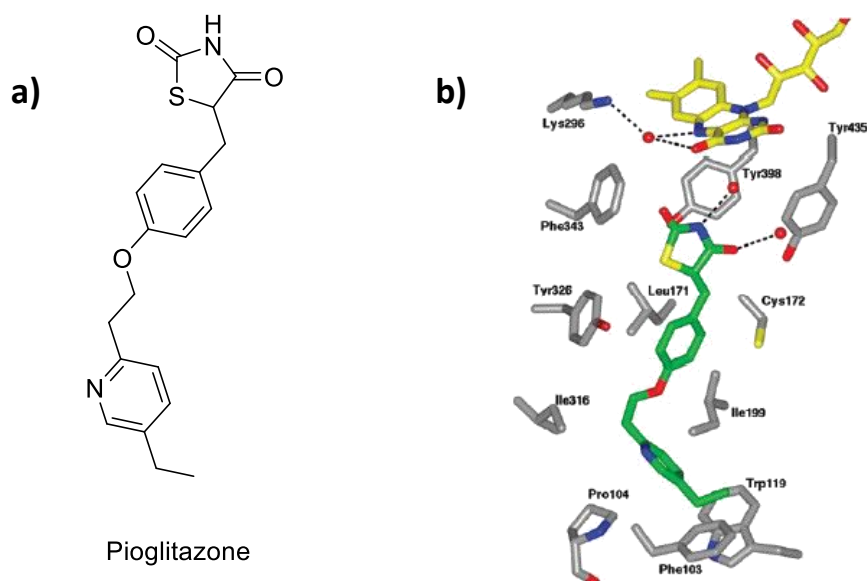


**Figure 2.16.** Structure of pioglitazone (a) and crystal structure when bound to the active site of hMAO-B (b). Taken from 290.

This repositioning as MAO-B inhibitor combined to already known PPAR- $\gamma$  agonism and corroborated by its clinical safety since marketed drug, pushed pioglitazone into several preclinical and clinical trials for the treatment of NDDs. Furthermore, pioglitazone proved to ameliorate cognitive and functional improvements as well as a reduction in detected A $\beta$  levels.<sup>291, 292</sup> Unfortunately, all clinical trials involving pioglitazone to modify progression of AD and PD registered no beneficial effects, thus highlighting need of more effective treatments. Nevertheless, thanks to its antioxidant-antiinflammatory properties in CNS, we herein sought to explore the possibility to combine the beneficial effects of pioglitazone deriving from MAO-B inhibition and PPAR- $\gamma$  activation, to the induction of cytoprotective genes transcription with the aim to possibly prevent and reduce oxidative damage and inflammation with a multi-layered strategy.

The transcription factor Nrf2 plays a pivotal role in the inducible cell defense system by coordinating a multifaced response to various forms of stress and inflammatory processes. The interaction between Nrf2 and its repressor Keap1 is a crucial point for regulating Nrf2 function. Particularly, the electrophilic modulation of Keap1 at critical cysteines represents the most common way for physiological and pharmacological Nrf2 induction. Therefore, the chance to specifically activate inducible antioxidant defense by precise electrophilic addition emerges as a valuable strategy to tackle neurodegeneration.<sup>93</sup> This has aroused significant interest in identifying Nrf2 inducers as therapeutic agents, with dimethyl fumarate representing a notable success story. In this context, previously reported thioesters of variously substituted trans-cinnamic acids allowed to identify structural requirements for electrophilic Nrf2-inducing warheads.<sup>262, 263</sup> In particular, systematic modifications had been performed on the trans-cinnamic core of prototype I and its coupling mode with the allyl function, allowing to draw a correlation between compounds structure and Nrf2 inducing properties (Figure 2.17).<sup>263</sup> To this aim, Nrf2 activity was assessed by western immunoblotting

in SH-SY5Y neuroblastoma cells in terms of up-regulation of Nrf2 expression, translocation into the nucleus and induction of the Nrf2-dependent defensive gene NQO1 (Figure 2.17b-c).

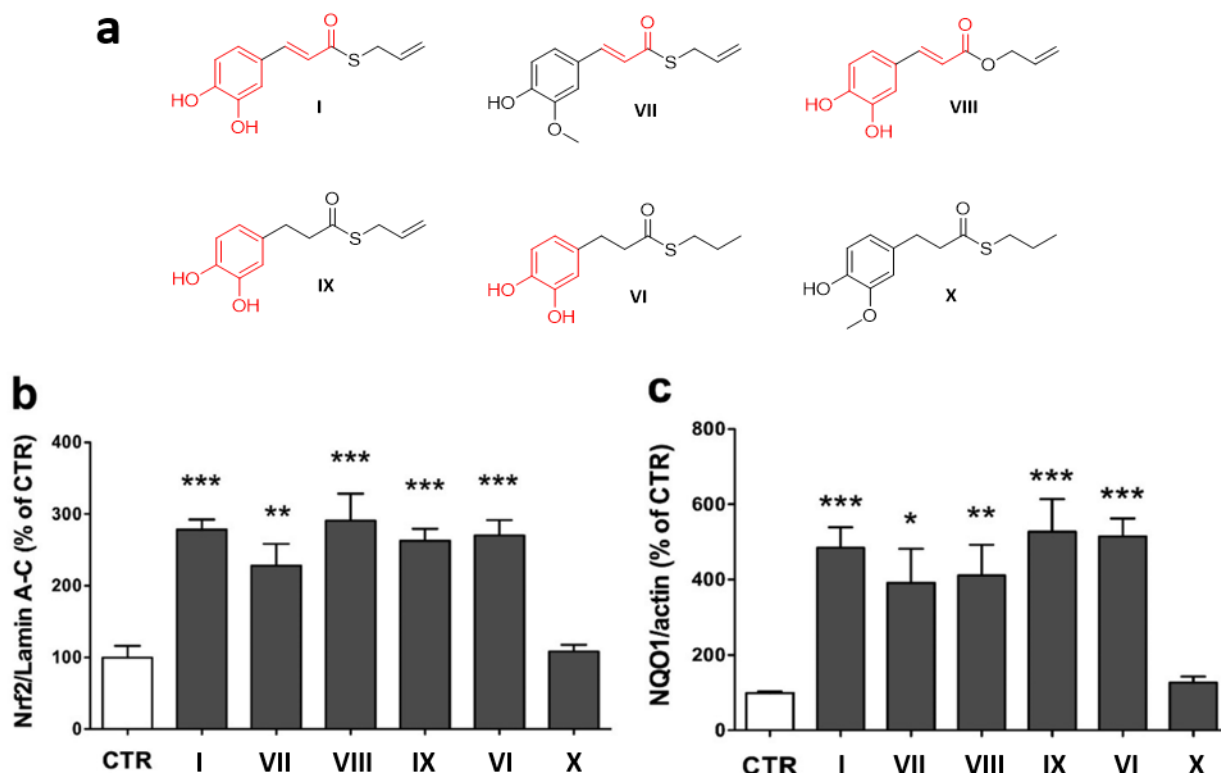


**Figure 2.17.** Activation of Nrf2-mediated phase II detoxification pathway. (a) Thioesteric hydroxycinnamic derivatives with highlighted in red (pro)electrophilic feature essential for Nrf2 activation. (b) Nuclear cellular extracts of SH-SY5Y cells were treated for 3 h with compounds **I**, **VI**, **VII**, **VIII**, **IX**, and **X** at 5  $\mu$ M concentration. Nrf2 expression was determined by Western blot. Anti-lamin A-C was used as protein loading control. Results are shown as ratio Nrf2/lamin A-C (% of CTR)  $\pm$  SEM; \*\* $p$  < 0.01 and \*\*\* $p$  < 0.001 versus CTR; Dunnett's multiple comparison test. (c) Total cellular extracts of SH-SY5Y cells treated for 24 h with 5  $\mu$ M concentration of compounds **I**, **VI**, **VII**, **VIII**, **IX**, and **X** were analyzed for NQO1 expression by Western blot. Antiactin was used as protein loading control. Results are shown as ratio NQO1/actin (% of CTR)  $\pm$  SEM; \* $p$  < 0.05, \*\* $p$  < 0.01, and \*\*\* $p$  < 0.001 versus CTR; Dunnett's multiple comparison test. Adapted from <sup>263</sup>.

The obtained results showed that one (pro)electrophilic feature in the trans-cinnamic core is sufficient to drive Nrf2 modulation, as compounds carrying the catechol group and/or the  $\alpha,\beta$ -unsaturated carbonyl moiety (Michael acceptor functionality) as possible sources for Nrf2 activation were efficient Nrf2 inducers. The lack of efficacy verified for compound **X**, which has no (pro)electrophilic features, suggests that nucleophilic addition of Keap1 cysteine residues to (pro)electrophilic portions of this set of compounds may represent the starting event of the transcriptional process. In 2020, this concept has been confirmed by evaluating the ability of the abovementioned compounds to activate the Nrf2 pathway in other biological systems, such as ARPE-19 cells and undifferentiated oligodendrocyte progenitors, and with different techniques (e.g. immunocytochemistry and real-time quantitative PCR), corroborating the solidity of the obtained data.<sup>293, 294</sup> Notably, further relevant information for properly use these electrophilic warheads in amplifying pioglitazone activity profile derives from the lack of importance of the thioester function in inducing Nrf2 activity, as revealed by the strong efficacy shown by the ester derivative **VIII**. In addition, by

comparing Nrf2 activation determined by compounds **IX** and **VI**, which only differ for the replacement of the allyl moiety with an alkyl function, the possibility emerges for further functionalization in this position as a promising multitarget drug discovery strategy.<sup>295</sup>

Structural analysis on pioglitazone scaffold underlined thiazolidinedione ring as the driving motif in MAO-B interaction, whereas different substituents at the entrance of the binding site were well tolerated.<sup>296</sup> Thus, with the aim to merge Nrf2-driven antioxidant response with neuroprotective efficacy of pioglitazone, we maintained the 5-(4-hydroxybenzyl)thiazolidine-2,4-dione moiety of pioglitazone, and exploited the hydroxyl function as attaching point for introducing electrophilic warheads with probed Nrf2 inducing capacities (Figure 2.18).

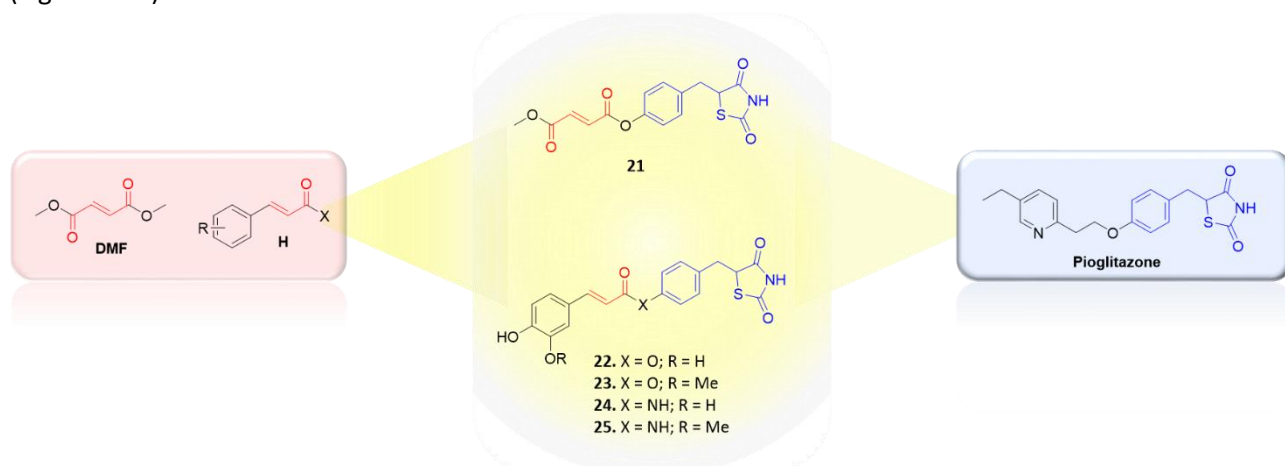


**Figure 2.18.** Drug design of pioglitazone-derived hybrids.

Particularly, based on previous results, caffeic and ferulic acids, carrying the electrophilic features of previously described hydroxycinnamic derivatives, were selected as Nrf2-inducing molecular appendages, and coupled by means ester functionality, affording compounds **22** and **23**. Monomethyl fumarate, the active metabolite of the drug dimethyl fumarate, was also used as Nrf2 pharmacophore, to give compound **21**. For most active hybrids, an alternative coupling approach was also followed, leading to the corresponding amides **24** and **25**, as this modification is generally associated to an increased chemical stability. As racemization of pioglitazone occurs reasonably rapidly,<sup>297</sup> which precludes the administration of either enantiomer to enhance therapeutic specificity as well as a more thorough analysis of their differences in binding affinities, the new compounds were synthesized and assayed in their racemic form.

### 2.3.1 METHODS

#### Chemistry

Compounds **21-25** were synthesized as reported in Schemes 8-10.

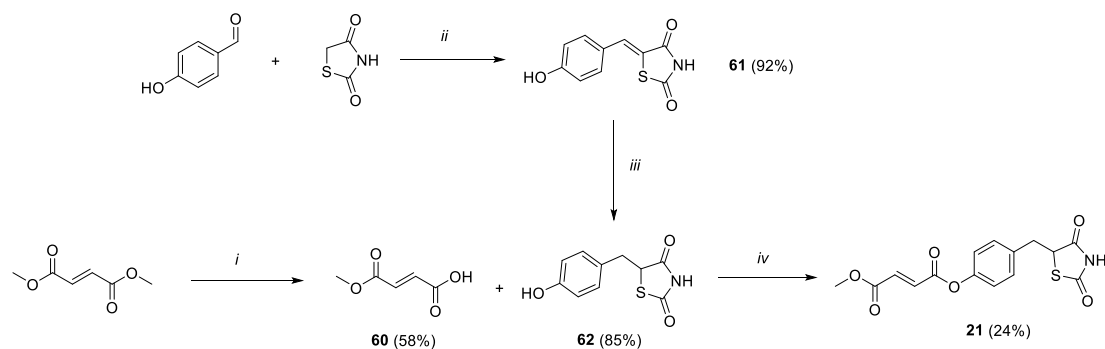
The synthetic strategy exploited to obtain compound **21** is outlined in Scheme 8. Firstly, monomethyl fumarate **60** was achieved by modifying a reported ester hydrolysis under basic conditions.<sup>298</sup> Key intermediate **62** was obtained within two-step process. 4-hydroxybenzaldehyde and thiazolidine-2,4-dione underwent a Knoevenagel condensation to give the benzylidene intermediate **61**. The double bond



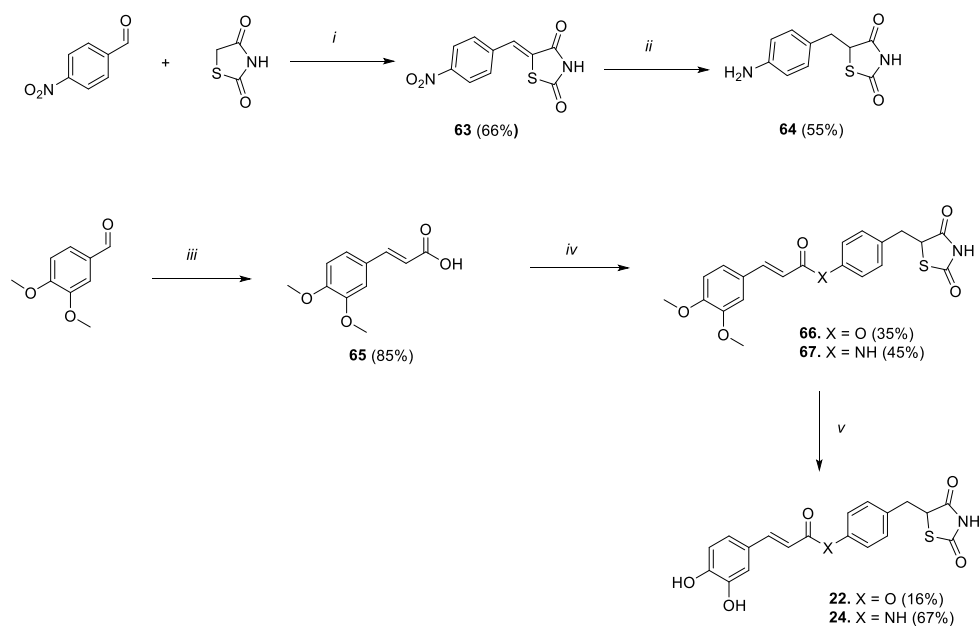
was reduced applying a reported procedure where a complex of cobalt (II) chloride and dimethylglyoxime was exploited to potentiate reducing efficacy of sodium borohydride, thus easily rip out hydride ion to reduce the highly conjugated unsaturation.<sup>299</sup> Finally, compound **21** was obtained from coupling reaction between monomethylfumarate **60** and intermediate **62** using HOBt and EDC as activating agents and adding triethylamine as base to promote coupling adduct formation.

Final compounds **22** and **24** were obtained as reported in Scheme 9. The aniline derivative **64** was prepared following the same two-step condensation-reduction procedure followed to gain the phenolic analogue **62**, albeit the reduction reaction needed a variation. In this case, a double amount of reducing agent and complex was used to reduce in a single step both benzylidene double bond and the nitro group, saving an extra step while reaching a satisfying yield (55%). Parallely, Knoevenagel condensation between 3,4-dimethoxybenzaldehyde and malonic acid allowed to obtain intermediate **65**. The carboxylic function of this latter was subsequently activated using HOBt and EDC and coupled with phenol **62** or aniline **64**, to give compounds **66** and **67**, respectively. Lastly, they were both converted into catechol analogues **22** and **24** by unmasking 3,4-dimethoxy functions using a boron tribromide-mediated demethylation procedure.

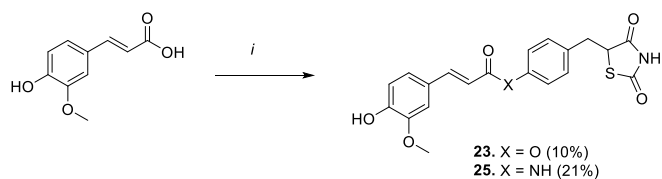
Compounds **23** and **25** were obtained starting from the commercially available ferulic acid through the reaction reported in Scheme 10. Coupling with both **62** and **64** intermediates, bearing the thiazolidine-2,4-dionic fragment, was performed following the same procedure reported above, using HOBt and EDC as activating agents and triethylamine as base.



**Scheme 8.** Reagents and conditions: (i) LiOH 1N, acetone, rt, 2h; (ii) benzoic acid, piperidine, toluene, reflux, 6h; (iii) DMG/CoCl<sub>2</sub>/DMF, NaBH<sub>4</sub>, MeOH/NaOH 1M/H<sub>2</sub>O, rt, 2h; (iv) HOBt, EDC, Et<sub>3</sub>N, DCM, 0°C-rt, 36h.



**Scheme 9.** Reagents and conditions: (i) benzoic acid, piperidine, toluene, reflux, 6h; (ii) DMG/CoCl<sub>2</sub>/DMF, NaBH<sub>4</sub>, MeOH/NaOH 1M/H<sub>2</sub>O, rt, 2h; (iii) malonic acid, pyridine, aniline, toluene, reflux, 10h; (iv) **62** or **64**, HOBT, EDC, Et<sub>3</sub>N, DMF, 0°C-rt, 36h; (v) BBr<sub>3</sub> 1M in DCM, DCM, 0°C-rt, 1h.



**Scheme 10.** Reagents and conditions: (i) **62** or **64**, HOBT, EDC, Et<sub>3</sub>N, DCM, 0°C-rt, 48h.

<sup>1</sup>H NMR spectra indicate that compounds **22-25**, featuring a carbon-carbon double bond between the catechol ring and the carbonyl function, have an *E* configuration as revealed by the large spin coupling constants (around 15-16 Hz) of  $\alpha$ -H and  $\beta$ -H on double bonds.

A critical step in these synthetic procedures was represented by the coupling reaction between acidic function of **60**, **65** and ferulic acid and phenol **62** or aniline **64** derivatives. Based on its acidity, the -NH imidic function could partially compete with the hydroxy group of **62** or the amino residue of **64** in coupling with the respective acids. With the aim to fully evaluate the occurred attaching site and therefore confirm the structures of the final compounds, deepen NMR studies were conducted on compounds **21** and **66**, taken as examples. Particularly, nuclear Overhauser effect spectroscopy (NOESY) in one dimension was exploited to highlight interaction between nuclei magnetically active through the space. Irradiating the sample at absorption frequencies specific of interacting nucleus, a responding signal is registered coming from nuclei near in space (usually within 5Å) to the irradiated one (i.e. nuclear Overhauser effect, NOE). For compound **21**, we irradiated protons 5-5' and observed a return signal from vicinal 4-4' but also from olefinic hydrogens 6-6', thus confirming proximity in space and the predicted aromatic oxygen as attaching point (Figure 2.19a).

Analogously, we studied compound **66** by irradiating H-7, and verified a return signal from H-6/6', H-7' and H-10 (Figure 2.19b). These results corroborate the predicted and intended structure of our compounds.

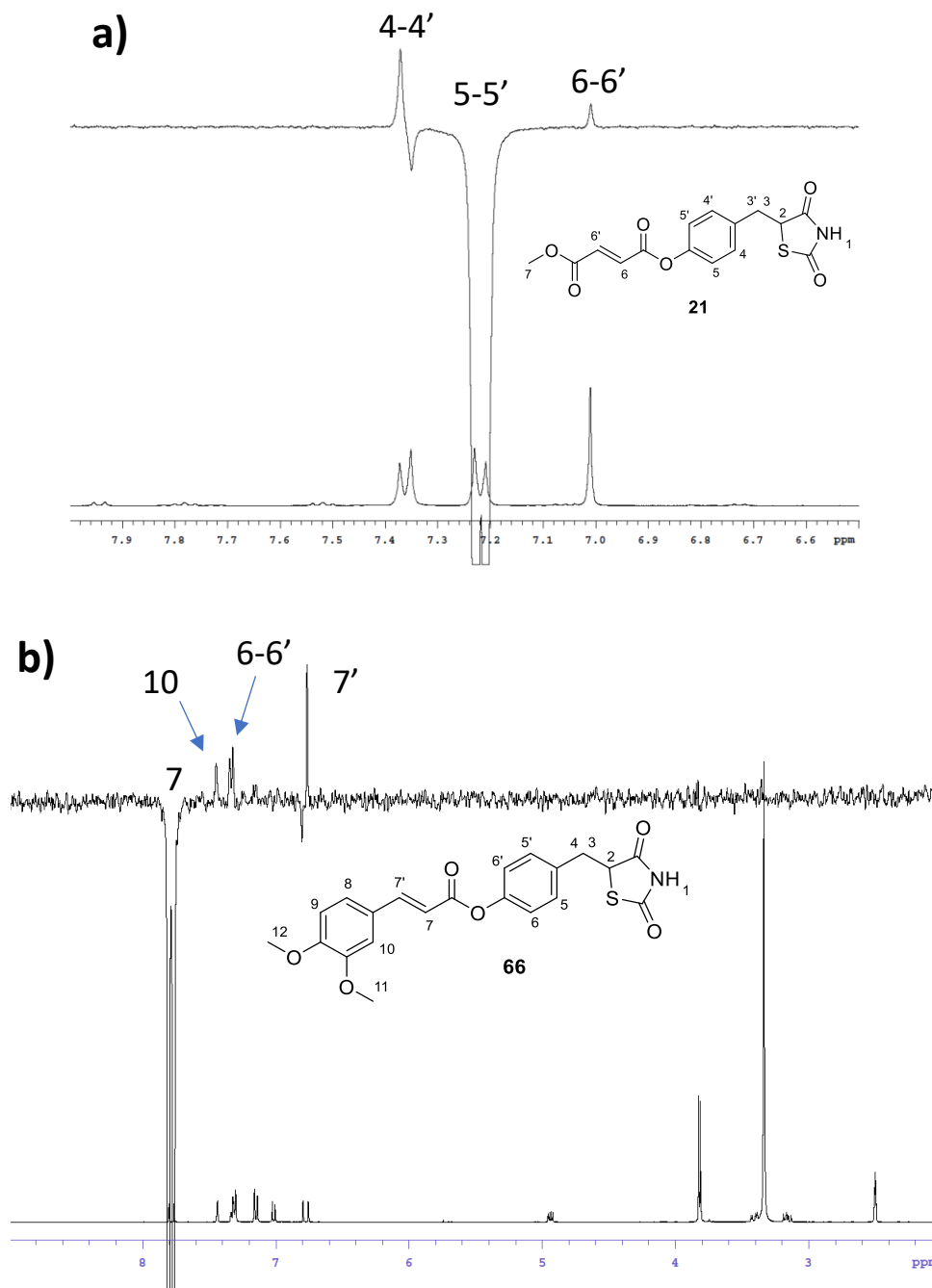


Figure 2.19. NOE spectra of compounds **21** (a) and **66** (b).

## Biology

All the hybrids were firstly evaluated *in vitro* for their ability to inhibit MAOs using kynuramine assay.<sup>300</sup> The most interesting compound for MAO-B selectivity and potency was further analysed to understand the kinetic and mechanism of inhibition. The obtained data were corroborated by computational analysis on driving interactions and spatial arrangements of obtained hybrids within MAO-B binding site. Finally, a first

series of compounds was tested for cell viability in neuroblastoma cells, using MTT assay, to determine tolerated concentrations to use for further evaluation of the ability to activate Nrf2 pathway, preliminary measured as induced Nrf2 nuclear translocation.

### 2.3.2 RESULTS AND DISCUSSION

#### Effects and kinetic characterization of compounds 21-25 on hMAOs

To evaluate hybrid's ability as potential human MAO inhibitors, they were tested *in vitro* versus both hMAO-B and hMAO-A. Stating the importance of counteracting selectively hMAO-B activation in neurodegenerative disorders, selectivity was also taken in consideration. Table 2.4 reports the inhibition constant values ( $K_i$ ) of the tested compounds and that of pioglitazone, caffeic and ferulic acid, determined under the same experimental conditions.

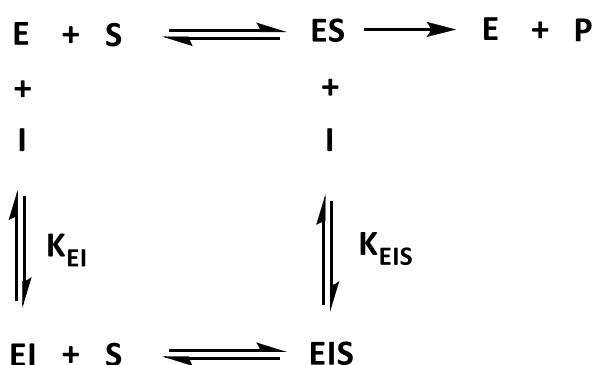
From the obtained data it clearly emerges that the linkage of the thiazolidinedione head of pioglitazone to fumaric, ferulic and caffeic fragments endowed the hybrid compounds of the capability to inhibit MAO, with hMAO-B preference, even if with lower potency than pioglitazone. Pioglitazone was confirmed to behave as selective and competitive inhibitor of hMAO-B, with  $K_i$  value about ten times lower than **22**, the best one among the hybrid compounds.<sup>290</sup> Caffeic and ferulic portions merged to pioglitazone allowed to reach hMAO-B effects that were not verified for starting compounds alone because they were not active up to 100  $\mu\text{M}$ . Fumaric moiety of compound **21** was tolerated and allowed in maintaining micromolar selective inhibition of hMAO-B, leading to a decrease of 50 times from pioglitazone. All compounds proved to inhibit hMAO-B with low micromolar efficacy and notable selectivity, being  $K_i$  for the hMAO-A isoform higher than 20  $\mu\text{M}$  for all the tested hybrids. Notably, the substitution of the ester-linker with the amide linker, performed on most active compounds **22** and **23**, decreased the inhibitory capability of the compounds by a factor of four-five (**22** vs **24**:  $K_i$  0.5 vs 2.5  $\mu\text{M}$ ; **23** vs **25**:  $K_i$  0.99 vs 3.3  $\mu\text{M}$ ).

**Table 2.4.** hMAO inhibitory activity and selectivity for compounds **21-25** and pioglitazone, caffeic and ferulic acid as reference compounds.

Cpd.	hMAO-B $K_i$ ( $\mu\text{M}$ )	hMAO-A $K_i$ ( $\mu\text{M}$ )	SI <sup>a</sup>
Pioglitazone	0.061 $\pm$ 0.018	>>100	>>1000
Caffeic acid	>100	>100	n.d.
Ferulic acid	>100	>100	n.d.
<b>21</b>	3.14 $\pm$ 0.20	25.5	8.1
<b>22</b>	0.45 $\pm$ 0.17	35 $\pm$ 4	51
<b>23</b>	0.99 $\pm$ 0.15	32 $\pm$ 2	32.3
<b>24</b>	2.5 $\pm$ 1.0	39 $\pm$ 5	15
<b>25</b>	3.3 $\pm$ 1.0	47 $\pm$ 4	14

<sup>a</sup>SI stands for selectivity index, calculated as hMAO-A  $K_i$ / hMAO-B  $K_i$ . hMAO activity assays were performed in K/Pi 0.1 M, EDTA 1mM (pH 7.4, T=37°C), in the presence and in absence of various concentration of the different compounds. The rate of reaction of hMAO ( $v$ ) was determined by the fluorimetric detection of the aldehyde produced by hMAO, using kynuramine as substrate and specific calibration curve built with the standard 4-hydroxyquinoline. Inhibition constant values ( $K_i$ ) were calculated from the plots of the ratio  $v_0/v_{-i}$  versus inhibitor concentration. All experiments were performed at least in triplicate.

For the most potent and selective *h*MAO-B inhibitor of the series, compound **22**, the mechanism of inhibition was investigated. Figure 2.20 shows the double-reciprocal plots of the rate of reaction of *h*MAO-B at different substrate concentrations, in the presence of various **22** concentrations. These plots clearly show that both  $K_m$  (the intercept on the x-axis is  $-1/K_m$ ) and  $V_{max}$  (intercept on the y-axis is  $1/V_{max}$ ) are affected by the presence of the inhibitor. In detail, apparent  $K_m$  value increases and apparent  $V_{max}$  decreases with increasing **22** concentration. This is the behaviour of a mixed inhibition mechanism, as confirmed by the global fit analysis of experimental data. It means that compound **22** is able to complex both with the free enzyme ( $K_{EI}$ ) and the enzyme-substrate complex ( $K_{EIS}$ ) with different  $K_i$ , according to the following scheme:



**Scheme 11.** Mixed inhibition model.

The following values,  $K_{EI} = 0.45 \pm 0.17 \mu\text{M}$  and  $K_{EIS} = 24 \pm 9 \mu\text{M}$ , for the mixed mode of inhibition of **22** were obtained by the global fit analysis. It is to note that the  $K_{EI}$  is more than one order of magnitude lower than  $K_{EIS}$  suggesting a much better affinity for the free enzyme than for the enzyme-substrate complex. At low concentrations of **22**, the main effect is on  $K_m$  values, suggesting a **22**-binding site inside the *h*MAO active site, in competition with the substrate entrance. Additionally, it is interesting to note that this binding is reversible, because no inactivation and no time-dependence inhibition was found for **22** vs *h*MAO-B and *h*MAO-A.

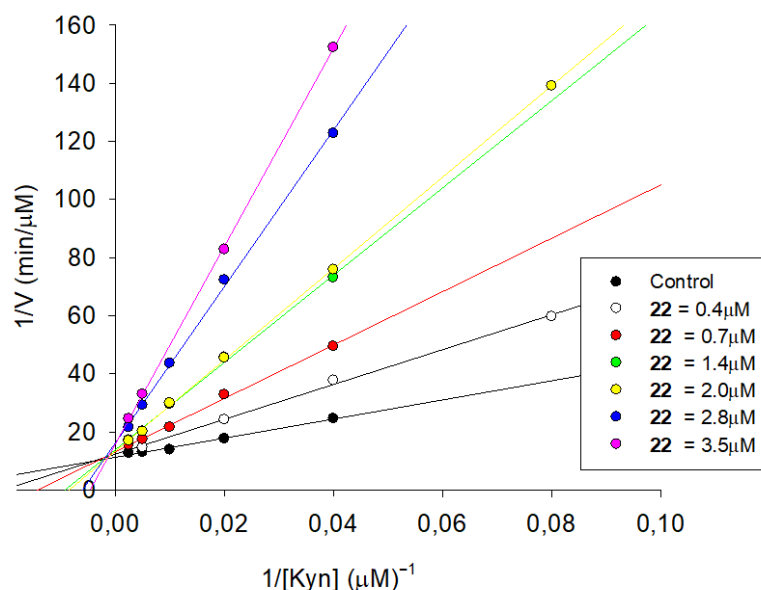


**Figure 2.20. Mixed inhibition of *h*MAO-B by compound **22**.** Double reciprocal plots of *h*MAO-B activity in the absence (●) and in the presence of different **22** concentrations (0.4-3.5  $\mu\text{M}$ ). The  $K_{EI} = 0.45 \pm 0.17 \mu\text{M}$  and  $K_{EIS} = 24 \pm 9 \mu\text{M}$  for the mixed mode of inhibition of **22**, were calculated by global fit analysis (GraphPad95.0 software). Continuous lines are the result of linear regression analysis of plotted data ( $r^2 > 0.98$ ).

This result is in line with the promising MAO inhibitory profile of pioglitazone, whose selectivity and reversibility emerged as promising source of therapeutics for neurodegeneration, avoiding adverse effect of gold-standard irreversible MAO-B inhibition (i.e. cheese effect) and onset of compensatory mechanism while maintaining beneficial outputs.<sup>108</sup> This road ahead is supported by the recent approval of the highly selective and reversible MAO-B inhibitor safinamide for the treatment of PD.

Chemical stability of derivative **22** was evaluated at the same experimental conditions exploited for determining *h*MAO-B activity, to avoid any liability in the obtained results. Compound **22** was analyzed by UHPLC-MS experiments at  $t_0$  in DMSO stock solution and at  $t_{1.5h}$  after incubation in assay medium at 37°C. In the figure below is reported chromatogram registered at 365 nm after 1.5h (same time of *h*MAO assays) incubation in K/Pi 0.1 M buffer, EDTA 1mM (pH 7.4, T=37°C) paired with mass spectra taken from peak compound (Figure 2.21).

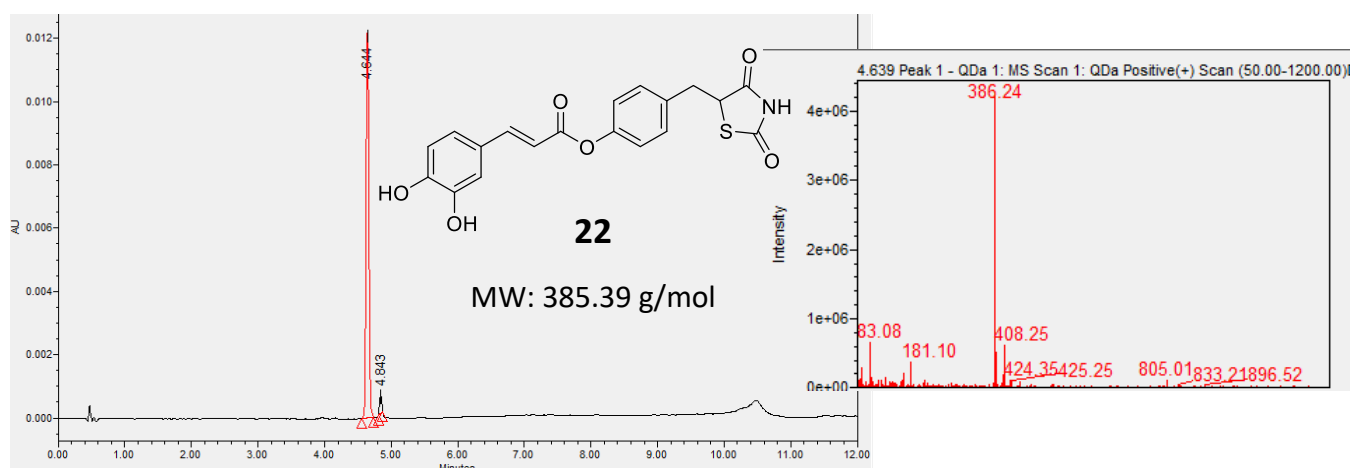


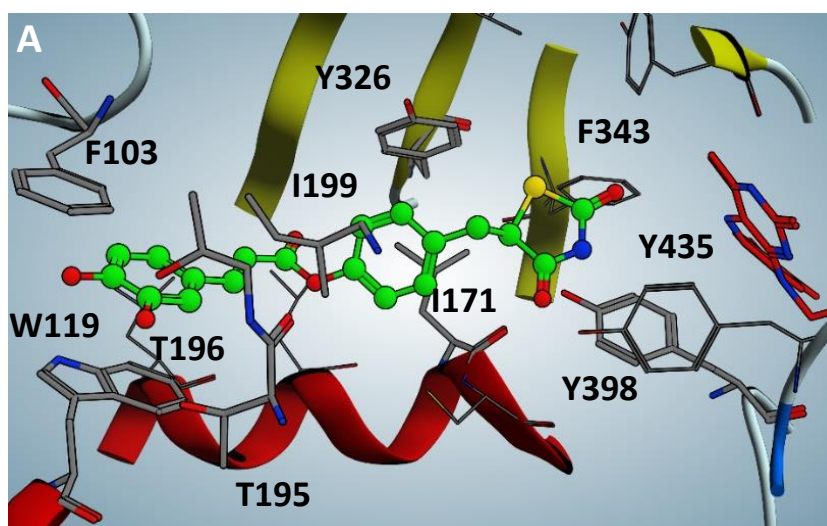
**Figure 2.21.** Chromatograms of UHPLC run paired with mass spectra registered at moment of compound elution for compounds **22**.

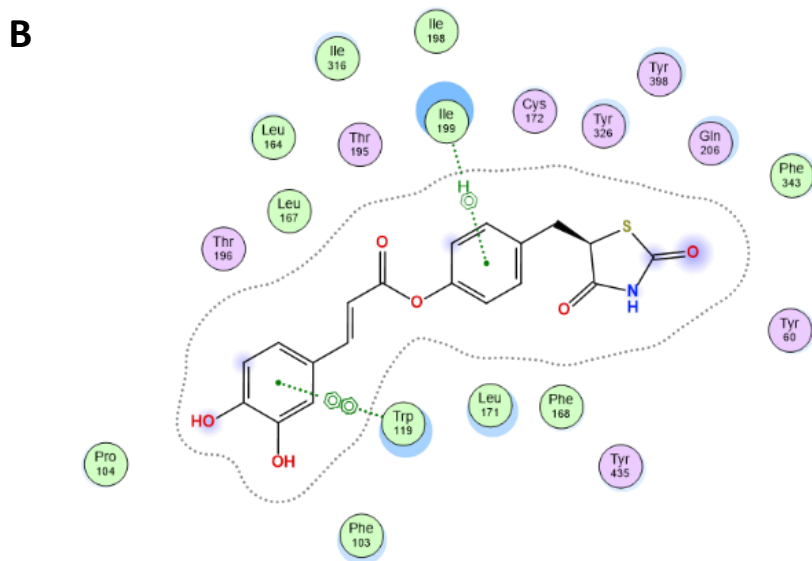
Besides pure compound elution, no detection of the respective acid was observed, corroborating the chemical stability of the ester function in the used experimental conditions.

#### Docking analysis of compounds **22-25** against *h*MAO-B

In order to study even more deeply the interaction of the new hybrids against *h*MAO-B, a series of molecular docking experiments were carried out on compounds **22-25**. Albeit the molecules have been biologically investigated in the racemic form, as previously specified, they were herein studied *in silico* with the *R*-configuration. X-ray crystallographic study conformation of *R*-pioglitazone in complex with *h*MAO-B (PDB code: 4A79) is available and, on the basis of model fitting to electron density, this enantiomer appears to preferentially bind to the enzyme.<sup>290</sup>

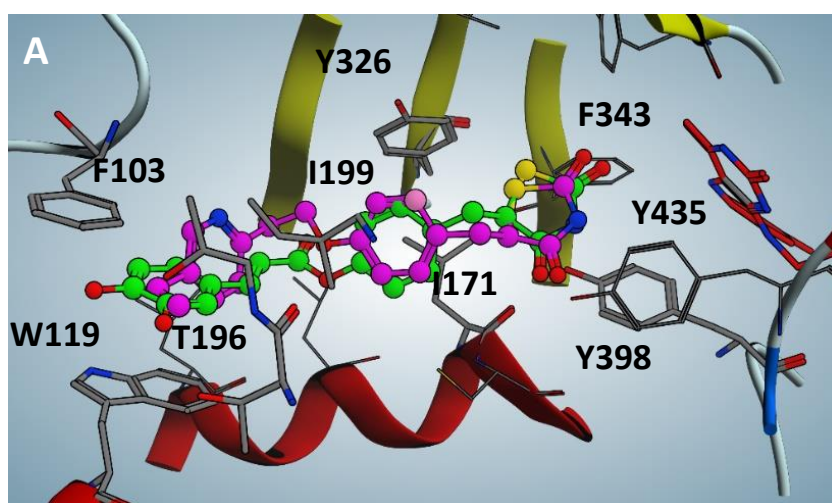
In particular, as shown in figure 2.22, best compound **22** fits inside the catalytic pocket of *h*MAO-B almost occupying the entire volume. The thiazolidinedione moiety protrudes facing FAD flavin ring, stabilized by hydrophobic interactions with Phe343, Tyr398 and Tyr435; the phenol core is sandwiched between apolar Ile171 and Ile199, accompanied by a T shaped pi-stacking with Tyr326. The catechol moiety is projected towards the entrance of the catalytic pocket and establishes efficient pi-stacking with Phe103 and Trp119. Finally, weak hydrogen bonds between the meta-hydroxy function and Thr195/196 should be noted. The estimated binding affinity, expressed as a dissociate constant of the **22**-*h*MAO-B complex (pK<sub>d</sub>, X-Score), is 7.2, thus confirming an affinity in the low micromolar range.





**Figure 2.22.** Docking pose of compound **22** against *h*MAO-B with highlighted interactions involved.

The likeliness of the **22** pose, obtained through *in silico* analysis, is confirmed by the good overlap with the X-ray crystallographic conformation of the pioglitazone in complex with *h*MAO-B (violet in figure, PDB code: 4A79; Figure 2.23A). Intriguingly, **22** is able to interact with the *h*MAO-B pocket even in the presence of the substrate kynuramine, previously docked into the catalytic site (cyan in the figure, Figure 2.23B). However, in this case, the inhibitor is forced to retreat towards the entrance of the catalytic tunnel by 2.5 Å, losing most of the efficient apolar interactions discussed previously. This results in a loss of affinity of two orders of magnitude ( $pK_d = 5.0$ ), which perfectly fits with the biochemical analysis of **22** mechanism of action, mixed-competitive at high inhibitor concentrations.





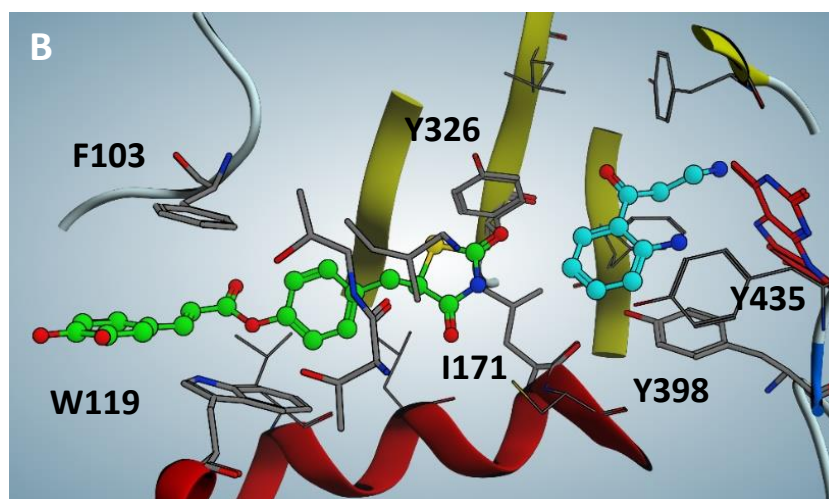


**Figure 2.23.** (A) Docking pose of compound **22** compared to pioglitazone pose (violet in figure, PDB code: 4A79) against *h*MAO-B. (B) Docking pose of **22** when substrate kynuramine (cyan in figure) is present within the active site of *h*MAO-B.

Due to the pro-oxidant environment in pathological conditions, compound **22** was also *in silico* studied in its oxidized form which presents two carbonyls at the catechol moiety with partial loss of aromaticity. However, computational studies do not reveal particular differences between the oxidized and reduced form of **22**; the interactions with the catalytic pocket are superimposable, and the pKd very similar (7.0). Indeed, the methoxy group of ferulic derivative **23** does not involve any appreciable difference in the *in vitro* activity, a result also confirmed by the docking analysis (pKd = 6.8) where the methoxyl group settles easily in an apolar region. The *in vitro* and computational data obtained with **23** suggest that the reduced conformation of **22** is the most likely to interact with *h*MAO-B catalytic pocket.

Amidic derivatives **24-25** poses are comparable to their ester analogues, albeit the amide group presents an evident distortion due to the van der Waals contact with Phe168, leading to a pKd value of 6.3-6.5, which reflect a loss of affinity of almost one order of magnitude when comparing **24** with **22**.

#### Cell toxicity assay

In order to define the range of concentration to be used in cellular experimental setting, the cytotoxicity of most active compounds **21-23** was preliminary evaluated in human neuroblastoma SH-SY5Y cells, in comparison with pioglitazone and **I** (Figure 2.24). Cells were treated with compounds at concentrations ranging from 0.5 to 50  $\mu$ M and cell viability was evaluated by MTT assay. All compounds were well tolerated at a concentration up to 50  $\mu$ M, resulting in no or very low reduction in cell viability even at the higher concentration tested, revealing an improved trend in the safety profile with respect to compound **I**. Evaluations on cell viability of amidic derivatives **24** and **25** are still ongoing.

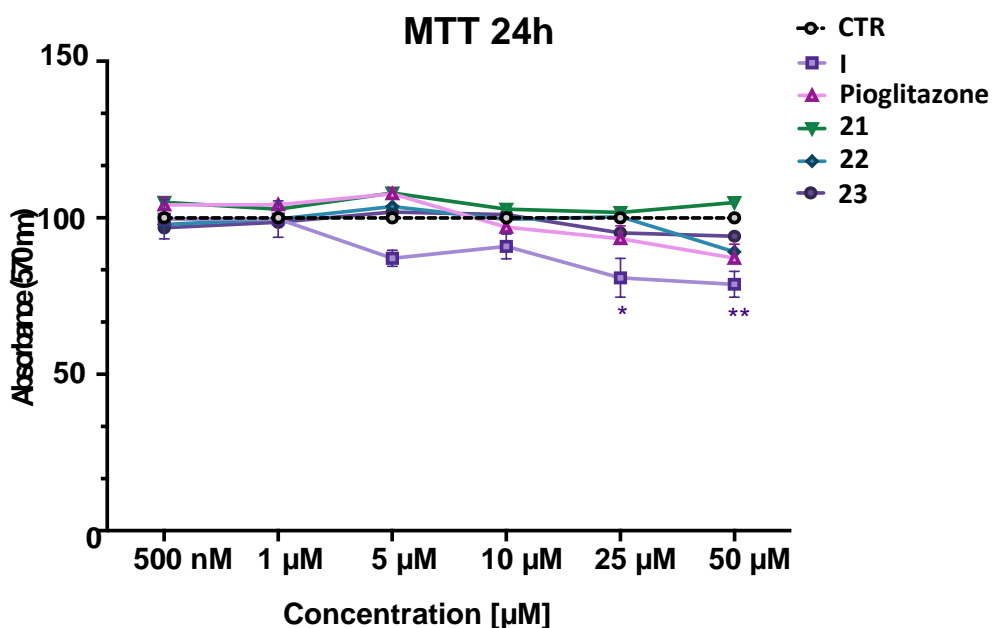


**Figure 2.24. Cell viability in SH-SY5Y cells exposed to I, pioglitazone, and compounds 21-23.** SH-SY5Y cells were treated with I, pioglitazone, and compounds 21-23 at the indicated concentrations for 24 h. Cell viability was assessed by MTT assay. Data are expressed as means of percentage of cell viability. Dunnett's multiple comparison test; \*p < 0.1; \*\*p < 0.01 versus CTR; n = 4.

#### Activation of Nrf2 pathway in neuroblastoma cells

In physiological conditions, Nrf2 is bound to its repressor Keap1 in the cytosol. Disruption of Keap1-Nrf2 interaction allows Nrf2 nuclear translocation and transcriptional activation of cytoprotective genes. Previously reported compounds I-V proved to activate Nrf2 in terms of up-regulation of Nrf2 expression, translocation into the nucleus and induction of the Nrf2-dependent defensive genes, with (pro)electrophilic features emerging as the triggering events.<sup>263</sup> Herein, to analyse the effect of the new molecules on Nrf2 downstream cascade, the ability of compounds 21-23 to increase Nrf2 nuclear translocation was preliminary evaluated as a sign of Nrf2 signaling activation (Figure 2.25). Based on MAO-B inhibitory activity and cell toxicity assay, compounds were studied at the concentration of 5 μM. Compound I was included for comparison.

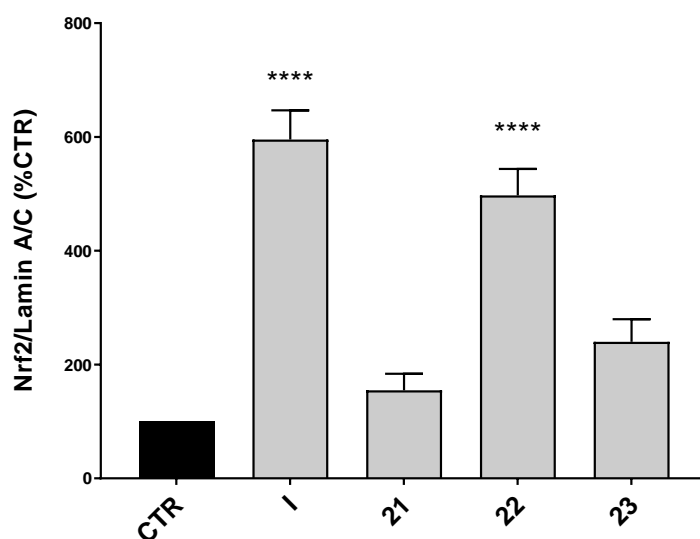


**Figure 2.25. Nrf2 nuclear translocation in SH-SY5Y cells treated with compounds 21-23.** SH-SY5Y cells were treated with compound I as reference and compounds 21-23 at the concentration of 5 μM for 3 hours. After isolation, nuclear extracts were examined by Western blot analysis and Nrf2 expression was determined using an anti-Nrf2 antibody. Anti-

lamin A/C was used as protein loading control. Results are shown as Nrf2/Lamin A/C ratio (%CTR)  $\pm$  SEM. Dunnett's multiple comparison test; \* $p < 0.05$  and \*\*\*\* $p < 0.0001$  versus CTR; n=3.

All compounds tested were able to improve Nrf2 nuclear translocation if compared to control, albeit to a different extent. Notably, pioglitazone had no effect at the concentration of 5  $\mu$ M, and minimal activation was observed at 50  $\mu$ M (data not shown). However, only the caffeic-based compound **22**, carrying two (pro)electrophilic features, exerted activity with the same magnitude of reference **1**, being significantly more potent than the ferulic derivative **23**, which can only count on the  $\alpha,\beta$ -unsaturated carbonyl group. As the two molecules only differ for a methoxy/hydroxy substituent, this may possibly be ascribed to an additive effect of the two reactive features, or to a privileged electrophilic behaviour of the catechol group. Nrf2 translocation observed for **21**, bearing the methylfumarate substituent, was increased, but not significantly, with respect to control, corroborating the idea that an electrophilic moiety in the molecule is not per se sufficient for activating redox sensor proteins. Evaluations on Nrf2 activation of amidic derivatives **24** and **25** are still ongoing.

### 2.3.3 CONCLUSIONS

In conclusion, new hybrids were synthesized with the aim to amplify the neuroprotective profile of pioglitazone. Thus, the thiazolidinedione moiety of this latter, acting as driving motif for MAO-B inhibition, was conjugated with electrophilic features which could represent a source for Nrf2 activation. From preliminary evaluation, the compounds showed promising reversible *h*MAO-B inhibition, in the low micromolar or submicromolar range, and selectivity over *h*MAO-A isoform, with compound **22** emerging as the most active. The same compound, not cytotoxic up to 50  $\mu$ M, at 5  $\mu$ M concentration was able to trigger the Nrf2 pathway in neuroblastoma cells, as revealed by its ability to strongly induce Nrf2 translocation to the nucleus. Cellular evaluation of the amidic compounds **24** and **25** is still in progress and will be accompanied by a deeper investigation of the effect of all hybrids at different levels of the Nrf2 cascade, included the downstream expression of cytoprotective genes. Based on the peculiar role of PPAR- $\gamma$  activation in inflammatory response, and its close connection with the Nrf2 pathway, the study of compounds activity at this receptor type might provide significant information on the neuroprotective/antiinflammatory power of this approach and has therefore been considered in the next steps of this project.

## 2.4 Exploiting memantine as driving-motif to build up neuroprotective hybrids

Synaptic loss is a major feature in neurodegenerative diseases. How synapses are altered in the disease progression is still unclear. The mechanistic understanding of synaptic damage represents a challenging goal and may prospect new opportunities for the prevention and cure of chronic conditions such as AD, PD, HD, HIV-associated dementia, multiple sclerosis, and amyotrophic lateral sclerosis. They are caused by different mechanisms but may share a final common pathway to neuronal injury due to the overstimulation of glutamate receptors, especially of the NMDA subtype. Defined as excessive exposure to the neurotransmitter glutamate or overstimulation of its membrane receptors, excitotoxicity is considered as one of the crucial features contributing to neuronal damage and death. Excessive activation of NMDARs and the consequent excessive  $\text{Ca}^{2+}$  influx through the receptor's associated ion channel are the main drivers of excitotoxic cell death.<sup>301</sup> However, physiological NMDARs activity is also necessary for normal neuronal function, as they are primarily involved in neuronal excitatory synaptic transmission that underlies learning and memory. Therefore, the dichotomous nature of NMDARs downstream signaling complicates the therapeutic engagement of NMDARs. It is generally accepted that these contrasting effects depend on receptor localization: activation of synaptic NMDAR (sNMDAR) may provide cell survival and plasticity, while activation of extrasynaptic NMDAR (eNMDAR) may favorably lead neuronal cells to death.<sup>131, 302</sup> Various pathologic features other than chronically elevated concentrations of glutamate, including protein misfolding, oxidative stress, and neuronal inflammation, have been associated with increased sensitivity and/or activity of the glutamatergic system.<sup>303</sup> Excitotoxicity conditions can first sensitize and then induce microglia activation, thus enhancing ROS and cytotoxic factors secretion in a neurotoxic vicious cycle. In particular, a potential detrimental link between the release of proinflammatory cytokines such as IL-1 $\beta$  and TNF- $\alpha$  and the glutamatergic system seems to contribute to increased brain excitability and excitotoxicity occurring in a variety of neurodegenerative conditions.<sup>134</sup>

Memantine (Namenda<sup>®</sup>, figure 2.29) is an anti-AD drug currently in use for the treatment of moderate-to-severe forms of the disease. It is also under investigation as a potential cure for other neurodegenerative disorders, such as ALS and epileptic encephalopathy.<sup>304</sup> Memantine is an uncompetitive/fast off-rate NMDARs antagonist. By acting as an open-channel blocker, it preferentially enters the channel when excessive and prolonged glutamate exposure occurs.<sup>305, 306</sup> Its favorable kinetics has been indicated as the key for selectively directing memantine's efficacy toward extrasynaptic/tonically-activated NMDAR over synaptic/phasicly-activated NMDAR, accounting for the safe therapeutic profile of the drug.<sup>252</sup> Interestingly, novel mechanisms far from the NMDA receptors antagonism have been proposed to contribute to the neuroprotective efficacy of memantine. Particularly, it showed neuroprotective effects against A $\beta$ -induced synaptic dysfunction and efficacy in reverting neuronal oxidative stress and the transient memory impairment caused by A $\beta$  oligomers.<sup>307</sup> Neurotrophic and neuroprotective effects of memantine seemed to

be mediated by astrocytic production of glial cell line-derived neurotrophic factor (GDNF), inhibition of microglia activation and reduction of ROS/RNS, TNF- $\alpha$  and prostaglandins' production.<sup>308</sup> Unfortunately, however, as for other available anti-AD drugs, memantine is not able to contrast the disease progression, offering only a symptomatic relief to patients.

Based on these considerations, we thought that investigating inflammatory dynamics in excitotoxicity might represent a promising strategy for in turn designing more successful therapeutic approaches. Thus, we herein sought to incorporate a bioactive payload into memantine structure, to add a second site of modulation of excitotoxicity-driven neuronal death, which could help in investigating the neurotoxic loop connecting inflammation to NMDARs overactivation.<sup>309</sup> In this context, previously reported hybrids between cinnamic acid derivatives and the allyl mercaptan moiety appeared to be a proper molecular instrument. Herein, as a prodromic step before memantine conjugation, we investigated the power of electrophilic/non-electrophilic warheads as antiinflammatory agents, focusing our attention on previously presented compounds **I**, **VI** and **X**, and compound **26**, purposely synthesized to exclude possible oxidative activation of the methoxyphenol ring of compound **X** into reactive metabolites such as quinone methide, which could provide a further electrophilic site for adduct formation (Figure 2.26).<sup>219</sup>

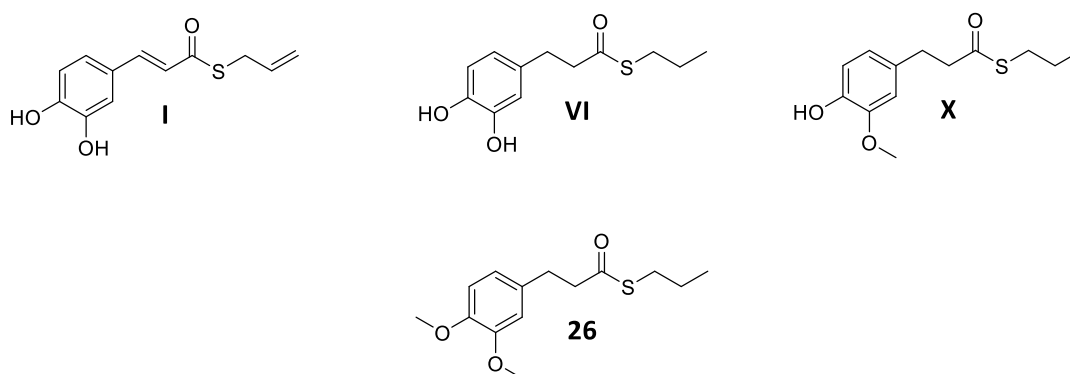


**Figure 2.26.** (Non)Electrophilic compounds developed to investigate antioxidant/antiinflammatory pathways.

First, the putative effect of Nrf2 activation by (pro)electrophilic compounds on the secretion of proinflammatory cytokines was verified. To further dissect the molecular mechanism underlying the effect on cytokine release induced by compounds **I**, **VI**, **X** and **26**, the potential interplay with other signaling cascades was studied, specifically focusing on the NF- $\kappa$ B pathway, a pivotal mediator of inflammatory responses and crucial regulator of a variety of aspects of innate and adaptive immune functions. In particular, NF- $\kappa$ B controls the transcription of genes encoding proinflammatory cytokines, such as TNF $\alpha$  and IL-1 $\beta$ , which have been shown to play a role in NMDARs mediated neurotoxicity.<sup>308</sup> In the presence of inflammatory stimuli, the phosphorylation and subsequent degradation of the inhibitor protein I $\kappa$ B allows NF- $\kappa$ B translocation into the nucleus to drive the expression of target genes. Remarkably, both NF- $\kappa$ B and Nrf2 offer peculiar patterns of thiol modifications, suggesting electrophilic signaling mediators as a valuable instrument to control their redox-sensitive transcriptional regulatory function.<sup>227</sup> A detailed description of

the pharmacological characterization of the compounds is not the main focus here. The interested reader is directed to the Ref. <sup>310</sup>, that we published in 2020. In the following, a glimpse on the correlation between compounds structure and antiinflammatory activity is provided with the aid of Figure 2.27, which summarizes the overall effects of compounds **I**, **VI**, **X** and **26**, on Nrf2 and NF- $\kappa$ B intracellular pathways.

Briefly, compounds **I**, **VI**, **X** and **26** were studied in a human immortalized monocyte-like cell line (THP-1), a well-established cell model for the immune modulation approach.<sup>311</sup> As expected, compounds **I** and **VI**, carrying a catechol moiety and/or an  $\alpha,\beta$ -unsaturated carbonyl group, significantly induced the Nrf2 pathway, while no effect was observed for compounds **X** and **26**, lacking both (pro)-electrophilic features. Conversely, all compounds, also in the absence of electrophilic moieties, significantly suppressed the LPS-evoked secretion of proinflammatory cytokines such as TNF $\alpha$  and IL-1 $\beta$ , but not of IL-8, in THP-1 cells. A similar behaviour was observed after siRNA mediated-Nrf2 knockdown, thus indicating that the reduction in cytokine secretion cannot be directly attributed to the activation of Nrf2 signaling pathway.

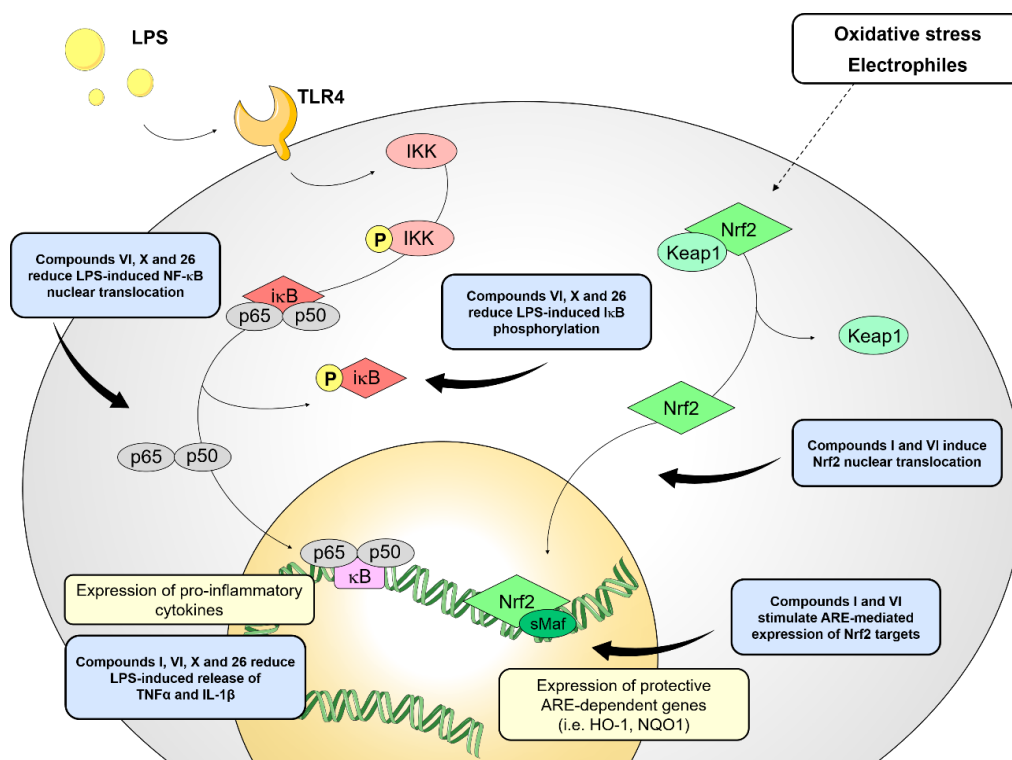


**Figure 2.27.** Schematic representation of the effects induced by **I**, **VI**, **X** and **26** on Nrf2 and NF- $\kappa$ B pathways. Modified from <sup>310</sup>.

Moreover, all compounds, with the only exception of **I**, weakened the LPS-induced activation of NF- $\kappa$ B canonical pathway, by reducing the upstream phosphorylation of I $\kappa$ B, the NF- $\kappa$ B nuclear translocation, as well as the activation of NF- $\kappa$ B promoter (Figure 2.27). As a consequence, the ability of compounds **VI**, **X**, and **26** to attenuate the activation of NF- $\kappa$ B pathway may be considered at least in part responsible for their observed effect on proinflammatory cytokine release. Conversely, the modulation of cytokine release by compound **I** might be, at some extent, related to antiinflammatory effect mediated by Nrf2 target genes, such

as HO-1. Noteworthy, while a (pro)-electrophilic feature is required for Nrf2 induction, suggesting covalent adduction as the triggering event, both (pro)-electrophile **VI** and non-electrophilic compounds **X** and **26** were able to inhibit NF- $\kappa$ B activation, suggesting a different mode of interaction (Figure 2.28).

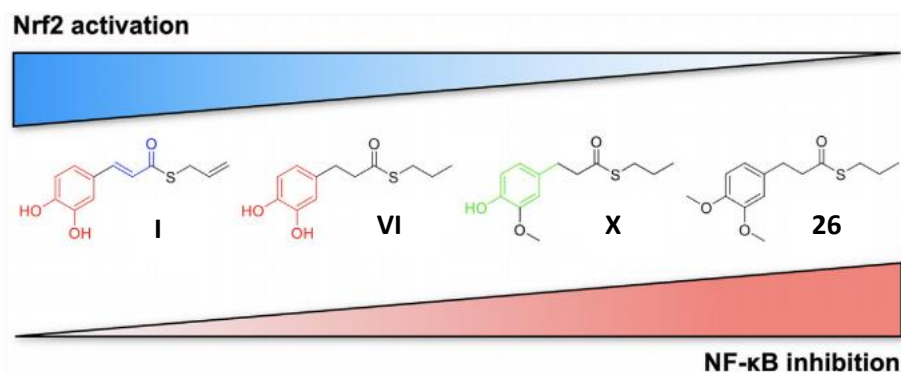


**Figure 2.28.** Differential modulation of Nrf2 and NF- $\kappa$ B intracellular signaling pathways by compounds. Electrophile **I**, carrying both the catechol moiety (red) and the  $\alpha,\beta$ -unsaturated carbonyl group (blue), is the most active Nrf2 inducer, while being devoid of activity on NF- $\kappa$ B pathway. Conversely, the non-electrophilic compound **26** is the most potent NF- $\kappa$ B inhibitor, with no impact on Nrf2 activation. Modified from <sup>310</sup>.

Altogether, the results obtained with the reported hybrids indicate that an electrophilic feature is neither necessary nor per se sufficient to guarantee inhibition of the proinflammatory transcriptional activity of NF- $\kappa$ B, with shape complementarity emerging as a possible feature of target recognition.

Albeit further mechanistic studies are necessary to comprehend the biological connection among Nrf2 activation, innate immune cytokine production, and the regulation of the NF- $\kappa$ B pathway, from this study emerged the possibility to exploit the hydroxycinnamic core to alternatively and selectively modulate different neuroprotective pathways with little structural modifications. Thus, with the aim to amplify the biological profile of memantine, which is known to specifically drive neuroprotective efficacy at damaged brain site of excitotoxicity, we linked its amantadine core with most active Nrf2 inducer (**I**) and NF- $\kappa$ B inhibitor (**26**), as well as the corresponding dimethoxy and catechol analogues (Figure 2.29). For conjugation we exploited memantine's primary amine function, whose conversion to a secondary amine has previously emerged as a feasible strategy to gain memantine-based NMDAR antagonists.<sup>312, 313</sup>

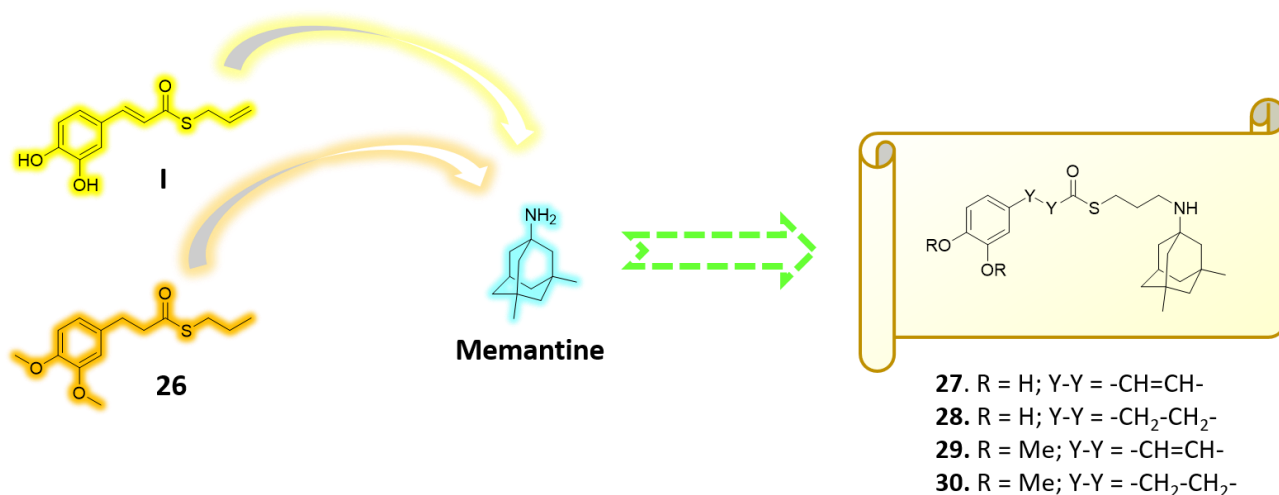


**Figure 2.29.** Design of memantine-conjugates bearing hydroxycinnamic-derived moieties (**27-30**).

#### 2.4.1 METHODS

##### Chemistry

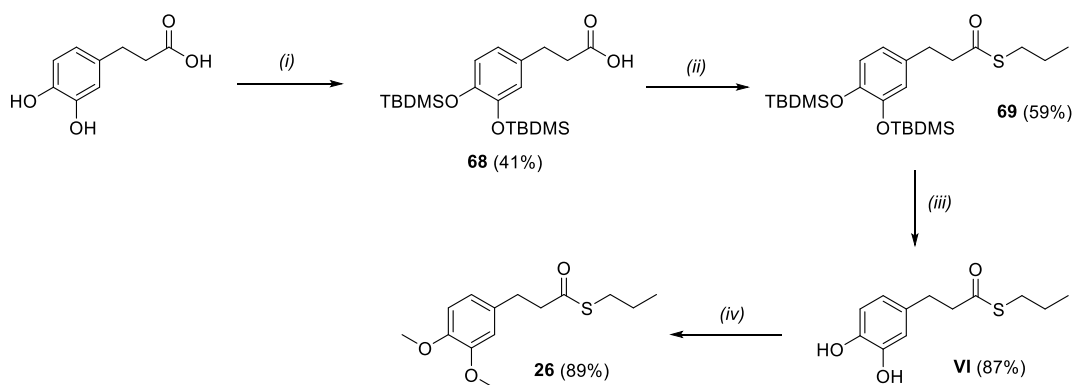
Compounds **26-30** were synthesized as reported in Schemes 12 and 13.

Synthetic procedure to obtain compound **26** is reported in Scheme 12. Particularly, **26** was achieved through a methylation step with methyl iodide of its catechol parent compound **VI**. In turn **VI** was synthesized starting from silyl ether protection of 3-(3,4-dihydroxyphenyl)propanoic acid's catechol function, coupling with 1-propane thiol and final deprotection using TBAF, according to a previously reported procedure.<sup>263</sup>

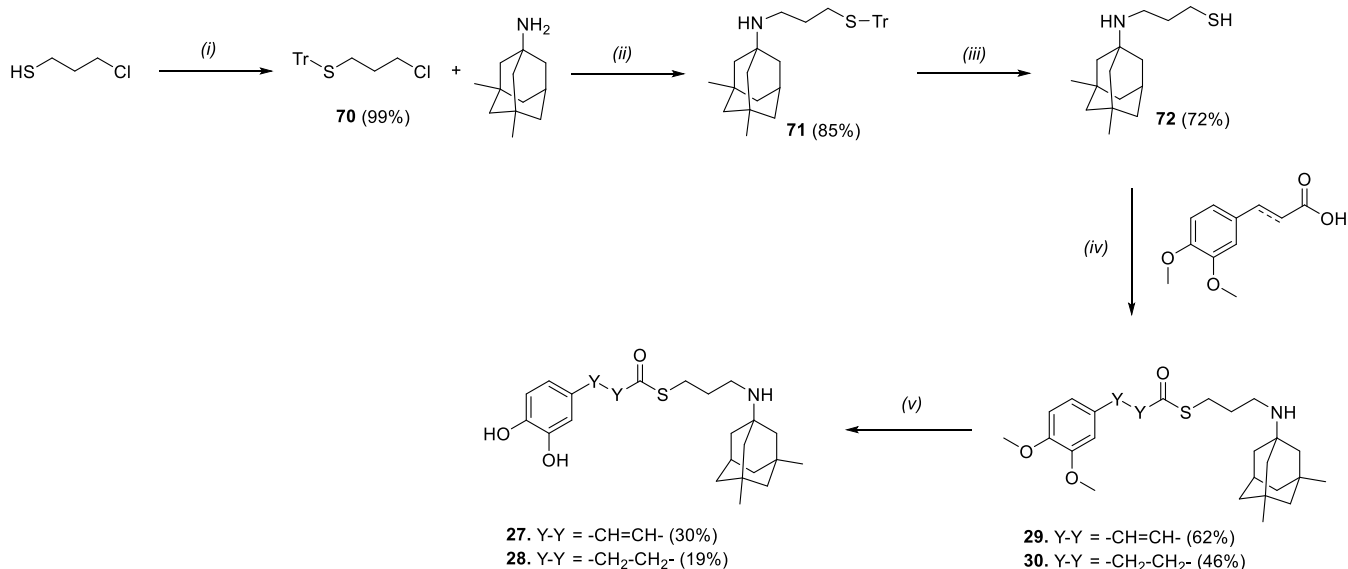
Compounds **27-30** were obtained as outlined in Scheme 13. Firstly, thiol function of 3-chloropropane-1-thiol was quantitatively protected with trityl group under microwave irradiation. The thio-protected compound **70** underwent a nucleophilic substitution with memantine free base and potassium carbonate to achieve adduct **71**, exploiting an optimized procedure microwave-assisted which allowed to selectively obtain the monosubstituted product. This latter was further treated with triethylsilane and trifluoroacetic acid at 0°C, rapidly obtaining key intermediate **72** with free thiol group. Therefore, unsaturated and saturated dimethoxycinnamic acids were coupled with compound **72** using HOBt and EDC as activating agents affording derivatives **29** and **30**, respectively. A final cold demethylation step using boron tribromide from **29** and **30** allowed to achieve compounds **27** and **28**, bearing the catechol function.

<sup>1</sup>H NMR spectra indicate that compounds **27** and **29**, featuring a carbon-carbon double bond between the catechol ring and the carbonyl function, have an *E* configuration as revealed by the large spin coupling constants (around 15-16 Hz) of  $\alpha$ -H and  $\beta$ -H on double bonds.





**Scheme 12.** Reagents and conditions: (i) TBDMS-Cl, imidazole, 1h, rt; (ii) HOBt, EDC, 1-propanethiol, 18 h, 0°C-rt; (iii) TBAF 1.0 M THF, THF, 30 min, rt; (iv) MeI, K<sub>2</sub>CO<sub>3</sub>, DMF, 18h, rt.



**Scheme 13.** Reagents and conditions: (i) TrCl, DMF, MW, 15 min, 60°C; (ii) K<sub>2</sub>CO<sub>3</sub>, KI, DMF, MW, 2.5 h, 75°C; (iii) Et<sub>3</sub>SiH, TFA, DCM, 5 min, 0°C; (iv) HOBt, EDC, 0°C-rt, 18 h; (v) BBr<sub>3</sub> 1M in DCM, DCM, 0°C-rt, 1h.

## Biology

Neurotoxicity of synthesized compounds was firstly evaluated in CGNs before analysing their immunomodulatory properties at fixed concentration in immortalized murine microglia. Parallely, preliminary patch-clamp studies regarding behaviour of compounds **27-30** toward NMDARs were carried out. Evaluation of compounds activity on Nrf2 and NF- $\kappa$ B pathways is ongoing.

### 2.4.2 RESULTS AND DISCUSSION

#### Neurotoxicity evaluation

Neurotoxicity of compounds **27-30**, in comparison with parent compound memantine, was evaluated in primary cultures of cerebellar granule neurons (CGNs) as useful *in vitro* model to study neuronal death (Figure

2.30).<sup>283</sup> 3-(4,5- Dimethylthiazol-2-yl)-2,5-diphenyltetrazolium bromide (MTT) assessment of CGNs viability after 24 h treatment revealed no toxicity for compounds **27** and **29** until 5  $\mu\text{M}$ , while they showed toxic effects at higher concentrations. Even compounds **28** and **30** confirmed a suitable profile at 5  $\mu\text{M}$  (CGNs viability > 75%), albeit slightly affecting neuronal viability. Furthermore, memantine confirmed its safety profile at all tested concentrations. Based on these data, 5  $\mu\text{M}$  was the concentration selected to evaluate immunomodulatory properties of **27-30** in immortalized murine microglia lines.

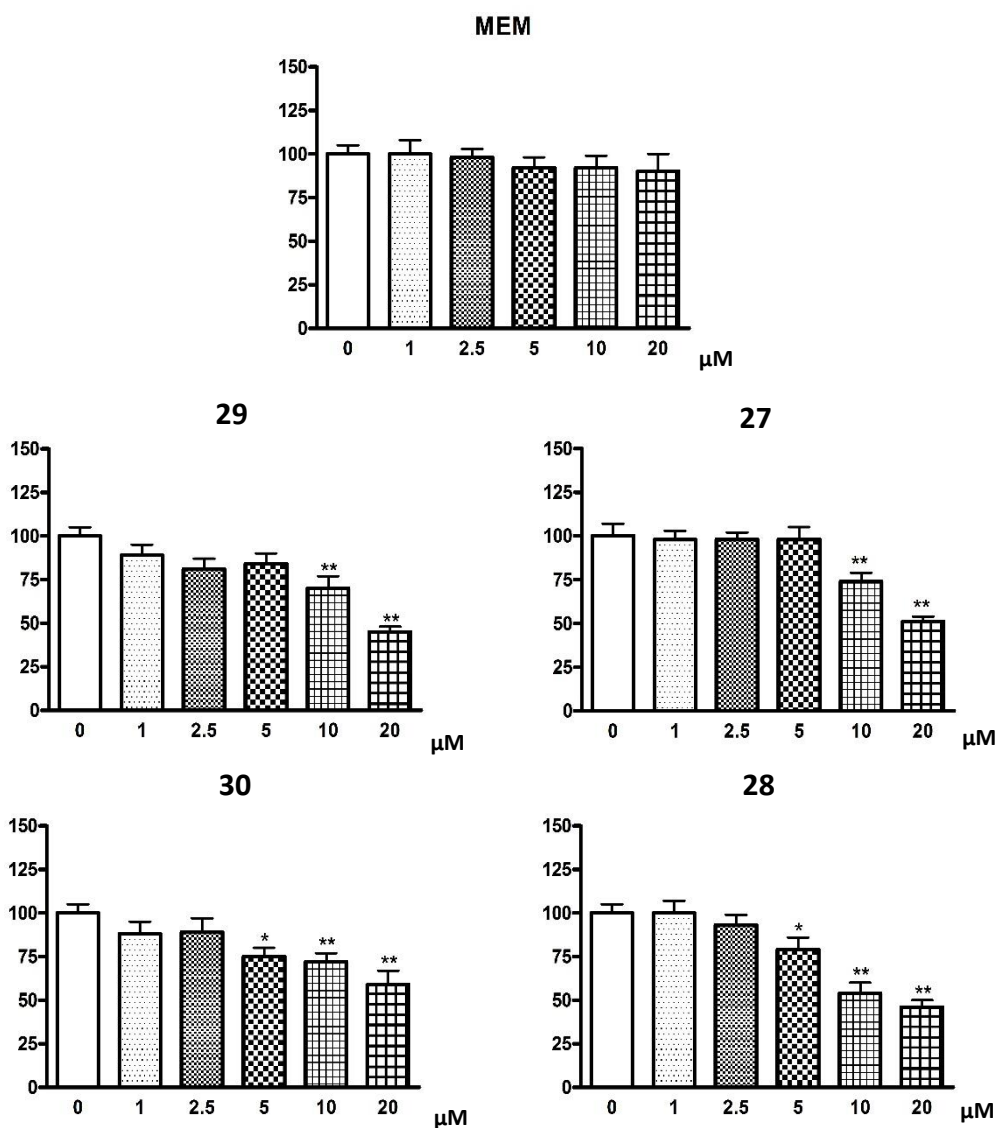


**Figure 2.30.** Toxicity of compounds **27-30** and memantine to differentiated primary rat cerebellar granule neurons (CGNs). CGNs were exposed to the compounds for 24 h at concentrations ranging from 0 to 20  $\mu\text{M}$  and cell viability measured by MTT assay. Results are expressed as percentage of controls and are the mean  $\pm$  SE of at least 3 different experiments, each run in triplicate. \*\* $p < 0,01$ ; \* $p < 0,05$  compared to control conditions (0  $\mu\text{M}$ ). Analysis for data statistical significance was performed through one-way ANOVA followed by Dunnett's post-hoc comparison test by using GraphPad Prism 4.0.

### Immunomodulation study

The crosstalk between glutamatergic and neuroinflammatory response plays a crucial role in neurotoxicity.<sup>134</sup> In this context, the chance to endow the neuroprotective efficacy of memantine with the ability of selectively

modulate antioxidant/antiinflammatory responses as for previously reported hydroxycinnamic derivatives<sup>310</sup> emerged as valuable tool to deepen insights into neuroinflammatory-neurodegenerative toxic cycle. Therefore, we evaluated the ability of compounds **27-30** to modulate the glial phenotypic switch from the proinflammatory M1 to the antiinflammatory M2 type. N9 microglial cells were treated with 100 ng/mL LPS in the presence or absence of 5  $\mu$ M of **27-30** and parent compound memantine. After treatment for 24 h, the microglial phenotype was evaluated through Western blot analysis of the M1-iNOS and M2-TREM2 markers (Figure 2.31).

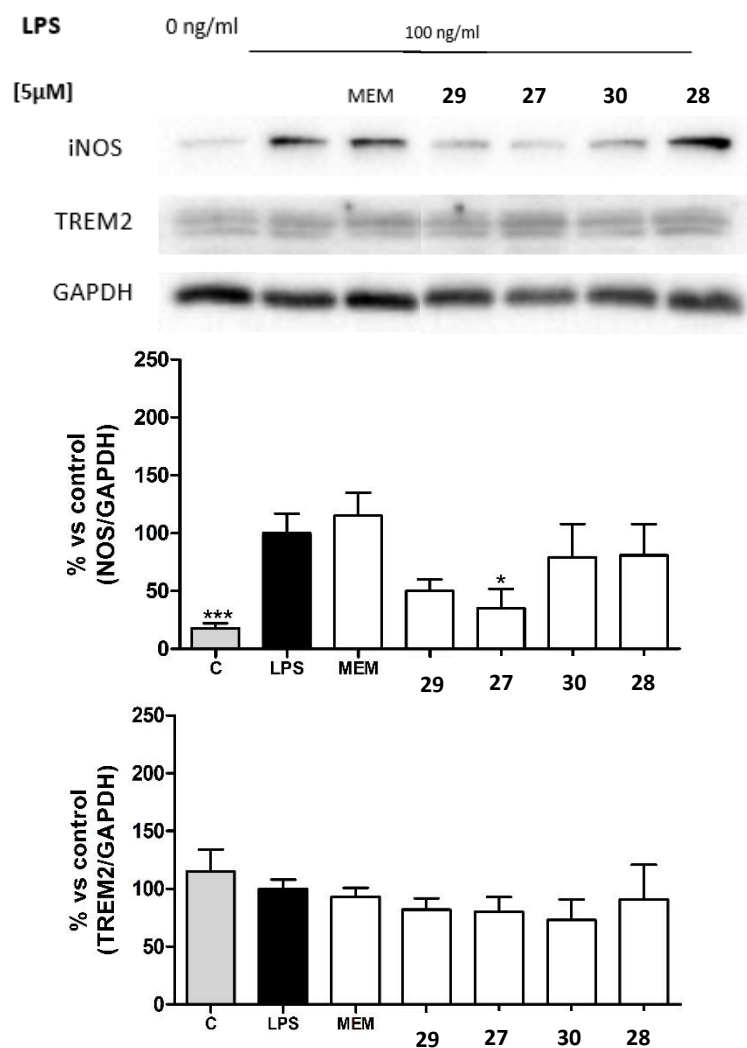


**Figure 2.31.** Mouse N9-microglial cells were treated with 5  $\mu$ M of compounds in presence or absence of LPS (100 ng/mL) for 24 h. Immunomodulatory effects of compounds were evaluated through Western blot analysis of microglial polarization markers expression. 20  $\mu$ g of protein extract were loaded into 12,5% sodium dodecyl sulfate-polyacrylamide gels (SDS-PAGE). Membranes were incubated overnight at 4°C with primary antibodies against iNOS, TREM2; GAPDH was used as loading control. Labeled proteins were detected by using the enhanced chemiluminescence method (ECL; BioRAD) with a Chemidoc (BioRad) chemiluminescence detector. Densitometric analysis was performed by using Image Lab 5.1 software. Densitometric results are expressed as percentage of LPS only and are the mean  $\pm$  SE of 4 different experiments. \*\*\* $p < 0,001$  \*\* $p < 0,01$ ; \* $p < 0,05$  compared to LPS condition. Analysis for data statistical significance was performed through T-test by using GraphPad Prism 4.0.

As reported in figure 2.31, compounds **27-30** decrease microglia production of the M1 proinflammatory marker iNOS, albeit with different extent, resulting more effective than memantine in these experimental

conditions. Furthermore, they seem to display immunomodulatory properties, as revealed by the unchanged expression of TREM2 (M2 marker). At the used concentration, no toxicity was detected in microglia.

### **NMDAR blocking activity**

Preliminary analysis was performed to assess the effect of compound **27** at NMDAR. Particularly, antagonism of response to NMDA and glycine were measured by voltage-clamp recordings on GluN2A NMDAR expressed in *Xenopus laevis* oocytes.<sup>313</sup> **27** presented a micromolar profile with the IC<sub>50</sub> obtained for the 2A subunit as 5.24 μM (95% CI, 1.30 to 22.7, n=6), whereas for parent compound memantine the IC<sub>50</sub> value at the same holding potential (-75 mV) was 1.45 μM (95% CI, 0.71 to 2.90). Further studies are ongoing to evaluate kinetic of response to NMDA and glycine on GluN2A NMDAR and behaviour toward GluN2B NMDARs for **27** and the other derivatives.

### **2.4.3 CONCLUSIONS**

Exploiting the well-known neuroprotective efficacy of memantine, we designed thioesteric memantine-conjugates **27-30** bearing different hydroxycinnamic-derived moieties which already proved to modulate alternatively and selectively different neuroprotective pathways. All tested compounds showed a suitable neuronal viability profile in CGNs until 5μM. At this concentration, they were further evaluated in immortalized murine microglia to assess their immunomodulatory properties. By reducing M1-marker iNOS without significantly affecting M2-marker TREM2, they displayed a promising immunomodulatory profile. This study is however in its infancy, and further biological characterization is needed to verify if the inclusion of bioactive payloads into memantine structure could allow to gain, as for the original moieties, modulation of innate immune cytokine release by different ways, leading to differential neuroprotective behaviours. In parallel, preliminary assay with compound **27** resulted in antagonism profile with micromolar potency at GluN2A NMDAR, but further insights are ongoing to fully evaluate the activities of all synthesized compounds regarding kinetic properties and voltage dependence in NMDAR blockage.

## CHAPTER 3

### CONCLUSIONS

Neuroinflammation is a crucial component of neurodegenerative diseases, where numerous neurotoxic pathways coexist and influence each other at multiple levels. Electrophilic compounds have been shown to interfere with several nodes of the inflammation-centred network by modulating both redox-sensitive transcriptional pathways and amyloid binding in a variety of neurodegenerative models. In this PhD work, we explored the peculiar ability of (pro)electrophilic features to selectively trigger or silence neuroprotective properties as a promising tool for investigating the neuroinflammation-centred network. To this aim, we identified a set of previously synthesized thioesters of variously substituted trans-cinnamic acids as a suitable starting point, considering that they showed to bear molecular features which, upon small structural modifications, could selectively lead to antiaggregating or Nrf2-mediated antioxidant activities. Albeit the four projects herein reported are at different stages of development, some preliminary findings could be highlighted to underline the potential of electrophilic pharmacological tools and set the stage for further biological investigations.

First, we could depict at molecular level the functional role of the catechol group in modulating A $\beta$  aggregation. The study clearly highlights that the reciprocal position of the two vicinal hydroxy functions acts as an on/off switch of antiaggregating properties, with the pro-electrophilic character of catechol or hydroquinone moieties emerging as prerequisite for activity. Notably, different mechanisms of action have been detected for the two active compounds, suggesting further opportunities for tuning the antiaggregating profile (Figure 3.1).

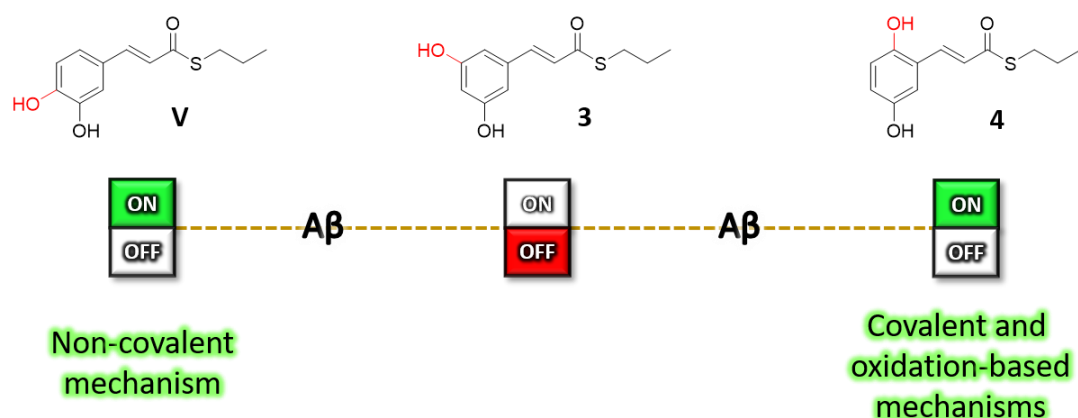


**Figure 3.1.** Catechol isomers and their antiaggregating activities with highlighted the different modes of interaction with A $\beta$ .

In parallel, we explored the same class of compounds investigating their ability to activate inducible transcriptional cytoprotective pathways. Thus, by gradually removing the (pro)electrophilic moieties responsible for Nrf2 activation, we progressively switched off this activity in favour of new-raised NF- $\kappa$ B

inhibitory properties. Thus, chemical manipulation of electrophilic fragments resulted in the intriguing opportunity to selectively and alternatively modulate inducible transcriptional responses which play a crucial role in neuroinflammation-centred diseases (Figure 3.2).

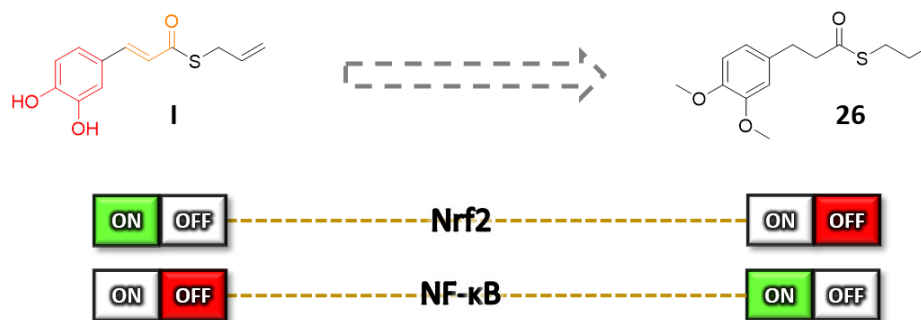


**Figure 3.2.** Molecular switchers from Nrf2- to NF-κB-mediated properties.

Encouraged by these promising results, we systematically modified the identified bioactive cores to reach additional targets which could in tandem contribute to the inflammatory process. In particular, we constrained the catechol-based antiaggregating nucleus to obtain coumarin derivatives for which is known the ability to modulate CB<sub>2</sub>Rs. In parallel, Nrf2 and/or NF-κB antiinflammatory structural requirements were combined with the neuroprotective core of pioglitazone, an antidiabetic drug endowed with MAO-B inhibitory properties, and the NMDAR antagonist memantine. Preliminary results suggest that, in the newly synthesized compounds, the activity of starting pharmacophores (e.g, CB<sub>2</sub>R affinity, MAO-B inhibition and NMDAR antagonism) could generally be maintained or slightly decreased, underlining the feasibility of the hybridization approach. In parallel, based on the obtained data, which are unfortunately not yet complete, the inclusion of electrophilic warheads is emerging as a valuable opportunity to endow the compounds with additional electrophile-based properties such as inhibition of amyloid aggregation or Nrf2 activation, which could be switched off or tuned by little structural modifications. Interestingly, the new compounds are generally well tolerated in cellular settings, offering the chance for deeper investigations. The evaluation of compounds effect on N9 microglial cells, an established cellular line to assess inflammatory-related properties, represents a first step in the direction of observing their impact on immunomodulatory/neuroinflammatory pathways.

In conclusion, we herein intended to gain small sets of compounds which could act as Swiss army knives, offering the chance to investigate connections between crucial inflammation-driven neurotoxic pathways in neurodegenerative diseases. We conducted a campaign on the characterization of electrophilic warheads, whose results were corroborated using different cellular systems and/or bio-orthogonal assays. Instead, further investigation is needed to assess the value of the electrophile-based hybridization approach, as the pharmacological characterization of the new derived hybrids is still ongoing. Thus, albeit a reliable categorization of the different approaches herein explored is not possible at this stage, we could draw the

line of a concept, suggesting the investigational potential of electrophilic regulation as a promising tool to dissect the complex cellular networks involved in neurodegenerative diseases. Notably, the nuanced and tricky profile of (pro)electrophilic fragments requires deepen and multi-layered analyses to overcome their related criticisms. In this respect, numerous tools are emerging that can help to evaluate warheads suitability as well as reactivity and accessibility of targeted nucleophiles in proteins to compose reactivity mapping toolbox. They include chemical-proteomics platform, computational programs and bio-orthogonal chemistry approaches, which could certainly contribute to unravel the power of electrophile-based approaches.

## CHAPTER 4

### EXPERIMENTAL SECTION

#### 4.1 CHEMISTRY

Chemical reagents were purchased from Merck, TCI and Fluorochem. All reactions were performed with dry glassware under a nitrogen atmosphere unless otherwise noted. Nuclear magnetic resonance spectra (NMR) were recorded at 400 MHz for  $^1\text{H}$  and 100 MHz for  $^{13}\text{C}$  on Varian VXR 400 spectrometer in  $\text{CDCl}_3$ ,  $\text{DMSO-}d_6$  or  $\text{CD}_3\text{OD}$  as solvents. Chemical shifts ( $\delta$ ) are given in ppm from tetramethylsilane (TMS) with the solvent resonance as internal standard ( $\text{CDCl}_3$ :  $\delta$  7.26,  $\text{DMSO-}d_6$ :  $\delta$  2.50,  $\text{CD}_3\text{OD}$ :  $\delta$  3.31 for  $^1\text{H}$  NMR and  $\text{CDCl}_3$ :  $\delta$  77.16,  $\text{DMSO-}d_6$ :  $\delta$  39.52,  $\text{CD}_3\text{OD}$ :  $\delta$  49.00 for  $^{13}\text{C}$  NMR). For  $^1\text{H}$  NMR, data are reported as follows: chemical shift, multiplicity (s = singlet, d = doublet, dd = double of doublets, t = triplet, q = quartet, m = multiplet, p = pentet, dt = doublet of triplets, td = triplet of doublets, tt = triplet of triplets, qd = quartet of doublets, br s = broad singlet), coupling constants (Hz) and integration. Monodimensional NOE spectra were acquired using sequence NOESY1D irradiating band of 50 Hz and using mixing time of 2 sec. Microwave assisted synthesis was performed by using CEM Discover<sup>®</sup> SP apparatus (2.45 GHz, maximum power of 300W). Chromatographic separations were performed on silica gel columns by flash or gravity column (Kieselgel 40, 0.040-0.063 mm; Merck) chromatography. Reactions were followed by thin-layer chromatography (TLC) on Merck (0.25 mm) glass-packed pre-coated silica gel plates (60 F254) that were visualized in an iodine chamber, or with a UV lamp,  $\text{KMnO}_4$ , or bromocresol green. All the names were attributed by Chem BioDraw Ultra 20.0. Final compounds mass spectra were recorded on a Waters ZQ 4000 apparatus, Waters Xevo G2-XS QToF instrument or Waters ACQUITY ARC UHPLC/MS system. All final compounds were pure >95% as determined by HPLC or UHPLC-MS analyses. HPLC analyses were performed under reversed-phase conditions on a Phenomenex Jupiter C18 (150x4.6 mm I.D.) column, using as the mobile phase a binary mixture of  $\text{H}_2\text{O}$ /acetonitrile (65/35 v/v for **1**; 50/50, v/v for **3**, **4**, **7**, **8**) with UV detection at  $\lambda = 302$  nm (for **1**, **3**, **4**, **7**) or  $\lambda = 254$  nm (for **8**) and a flow rate of 0.7 mL/min (for **1**) or 1 mL/min (for **3**, **4**, **7**, **8**). Analyses were performed on a liquid chromatograph model PU-1585 UV equipped with a 20  $\mu\text{L}$  loop valve (Jasco Europe, Italy). Final compounds **2**, **5** and **9-30** were characterized and determined pure by UHPLC-MS analysis with a purity at least > 95%. UHPLC-MS analyses were run on a Waters ACQUITY ARC UHPLC/MS system consisting of a QDa mass spectrometer equipped with an electrospray ionization interface and a 2489 UV/Vis detector. The detected wavelengths ( $\lambda$ ) were 254 nm and 365 nm. The analyses were performed on an XBridge BEH C18 column (10  $\times$  2.1 mm i.d., particle size 2.5  $\mu\text{m}$ ) with a XBridge BEH C18 VanGuard Cartridge precolumn (5 mm  $\times$  2.1 mm i.d., particle size 1.8  $\mu\text{m}$ ). The mobile phases were  $\text{H}_2\text{O}$  (0.1% formic acid) (A) and MeCN (0.1% formic acid) (B). Electrospray ionization in positive and negative mode was applied in the mass scan range 50–1200 Da. Method and gradients used were the following: Generic method. Linear gradient: 0–0.78 min,



20% B; 0.78-2.87 min, 20–95% B; 2.87-3.54 min, 95% B; 3.54-3.65 min, 95-20% B; 3.65-5.73, 20% B. Flow rate: 0.8 mL/min.

### **(E)-3-(3,5-dihydroxyphenyl)acrylic acid (31)**

Malonic acid (244 mg, 2.35 mmol) was added to a solution of aniline (0.032 mL), pyridine (0.27 mL, 3.35 mmol) and 3,5-dihydroxybenzaldehyde (300 mg, 2.17 mmol) in 2 mL of toluene and the mixture stirred at reflux for 4h. Once cooled to room temperature, HCl 3N was added until pH=1. The obtained precipitate was filtered and washed with HCl 3N. Once dried **31** was obtained as dark powder (180 mg, 46%). <sup>1</sup>H NMR (400 MHz, DMSO-*d*<sub>6</sub>) δ 9.44 (br s, 2H), 7.36 (d, *J* = 16 Hz, 1H), 6.46-6.45 (m, 2H), 6.28-6.24 (m, 2H).

### **3,5-bis((tert-butyldimethylsilyl)oxy)benzoic acid (32)**

To a solution of **31** (300 mg, 1.95 mmol) in 5 mL of dry DMF were added TBDMS-Cl (735 mg, 4.88 mmol) and imidazole (531 mg, 7.8 mmol) under nitrogen atmosphere. After leaving the reaction to room temperature overnight, the mixture was concentrated to dryness, and the residue purified by column chromatography using petroleum ether: ethyl acetate (8.5:1.5) as mobile phase. **32** was obtained as a waxy solid (360 mg, 53 %). <sup>1</sup>H NMR (400 MHz, CDCl<sub>3</sub>) δ 7.65 (d, *J* = 16 Hz, 1H), 6.65 (s, 2H), 6.38 (d, *J* = 7.2 Hz, 1H) 6.33 (s, 1H), 0.98 (s, 18H), 0.20 (s, 12H).

### **S-allyl (E)-3-(3,5-bis((tert-butyldimethylsilyl)oxy)phenyl)prop-2-enethioate (33)**

To an ice-cooled solution of **32** (360 mg, 0.88 mmol) in 4 mL of dry dichloromethane was added DCC (200 mg, 0.97 mmol) and DMAP (cat.). The reaction mixture was stirred for 10 min, followed by addition of allyl mercaptan (0.29 mL, 3.52 mmol). Stirring was then continued at room temperature overnight, and the reaction worked up by filtration and evaporation. The crude was purified by chromatography using petroleum ether: ethyl acetate (9.7:0.3) as mobile phase. **33** was obtained as pale oil (170 mg, 41%). <sup>1</sup>H NMR (400 MHz, CDCl<sub>3</sub>) δ 7.46 (d, *J* = 15.6 Hz, 1H), 6.62-6.57 (m, 3H), 6.36 (s, 1H), 5.82-5.88 (m, 1H), 5.28 (d, *J* = 17.2 Hz, 1H), 5.12 (d, *J* = 10.4 Hz, 1H), 3.66 (d, *J* = 6.8 Hz, 2H), 0.96 (s, 18H), 0.19 (s, 12H).

### **S-allyl (E)-3-(3,5-dihydroxyphenyl)prop-2-enethioate (1)**

To a solution of **33** (170 mg, 0.37 mmol) in 5 mL of THF was added TBAF (387 mg, 1.48 mmol) and stirring was continued at room temperature. After 20-30 min, the reaction was quenched by addition of saturated aqueous NH<sub>4</sub>Cl solution; the aqueous phase was extracted with ethyl acetate (3 x 10 mL) and the combined organic layer was dried over anhydrous sodium sulphate. Following evaporation of the solvent, the residue was purified by column chromatography using dichloromethane: methanol (9.5:0.5) as mobile phase. **1** was obtained as pale oil (63 mg, 73%). <sup>1</sup>H NMR (400 MHz, CD<sub>3</sub>OD) δ 7.43 (d, *J* = 15.6 Hz, 1H), 6.67 (d, *J* = 16 Hz, 1H), 6.52 (s, 2H), 6.34 (s, 1H), 5.87-5.79 (m, 1H), 5.25 (d, *J* = 16.8 Hz, 1H), 5.08 (d, *J* = 10 Hz, 1H), 3.63 (d, *J* =

6.4 Hz, 2H). <sup>13</sup>C NMR (100 MHz, CD<sub>3</sub>OD) δ 190.72, 160.04, 142.38, 137.10, 134.55, 125.38, 118.14, 107.80, 106.22, 32.40. MS [ESI+] m/z 237 [M+H]<sup>+</sup>.

#### **4,5-dimethoxy-2-methylbenzaldehyde (43)**

Phosphorus oxychloride (0.98 mL, 10.52 mmol) was added to 3,4-dimethoxytoluene (0.38 mL, 2.63 mmol) and the reaction mixture was left stirring under nitrogen atmosphere at 80°C until complete mixing. Thus, dimethylformamide (0.82 mL, 10.52 mmol) was added and the mixture stirred at 95°C for 4h. Once cooled to 40°C crushed ice was added and obtained mixture was extracted with ether (3x8mL). Ether extracts, once reunited, were washed with brine, dried with anhydrous sodium sulphate and concentrated in vacuo. **43** was obtained as yellow orange oil (470 mg, 98%). <sup>1</sup>H NMR (400 MHz, CDCl<sub>3</sub>) δ 10.13 (s, 1H), 7.26 (s, 1H), 6.62 (s, 1H), 3.87 (s, 3H), 3.83 (s, 3H), 2.55 (s, 3H). <sup>13</sup>C NMR (100 MHz, CDCl<sub>3</sub>) δ 189.93, 153.38, 147.22, 135.67, 126.76, 113.37, 110.99, 55.80, 55.73, 17.88.

#### **General procedure for the synthesis of compounds 34, 35 and 44**

Malonic acid (1.1 eq) was added to a solution of aniline (0.03-0.05 mL), pyridine (1.5 eq) and selected benzaldehyde (1 eq) in 2-4 mL of toluene and the mixture stirred at reflux for 4h. Once cooled to room temperature, HCl 3N was added until pH=1. The obtained precipitate was filtered, washed with HCl 3N and dried.

#### **(E)-3-(2,5-dimethoxyphenyl)acrylic acid (34)**

Compound **34** was synthesized from 2,5-dimethoxybenzaldehyde (400 mg, 2.41 mmol) and obtained as yellowish powder (490 mg, 98%). <sup>1</sup>H NMR (400 MHz, DMSO-d<sub>6</sub>) δ 12.27 (br s, 1H), 7.77 (d, *J* = 16 Hz, 1H), 7.22-7.21 (m, 1H), 7.00-6.94 (m, 2H), 6.52 (d, *J* = 16 Hz, 1H), 3.77 (s, 3H), 3.71 (s, 3H). <sup>13</sup>C NMR (100 MHz, DMSO-d<sub>6</sub>) δ 167.78, 153.12, 152.01, 138.37, 122.94, 119.50, 117.46, 112.94, 112.50, 56.01, 55.48.

#### **(E)-3-(3,5-dimethoxyphenyl)acrylic acid (35)**

Compound **35** was synthesized from 3,5-dimethoxybenzaldehyde (500 mg, 3.01 mmol) and obtained as white powder (520 mg, 83%). <sup>1</sup>H NMR (400 MHz, CDCl<sub>3</sub>) δ 7.69 (d, *J* = 16 Hz, 1H), 6.68-6.67 (m, 2H), 6.51-6.50 (m, 1H), 6.41 (d, *J* = 16 Hz, 1H), 3.81 (s, 6H). <sup>13</sup>C NMR (100 MHz, CDCl<sub>3</sub>) δ 171.72, 161.03 (2C), 147.06, 135.85, 117.66, 106.19 (2C), 103.01, 55.44 (2C).

#### **(E)-3-(4,5-dimethoxy-2-methylphenyl)acrylic acid (44)**

Compound **44** was synthesized from **43** (470 mg, 2.61 mmol) and obtained as yellow powder (366 mg, 63%). <sup>1</sup>H NMR (400 MHz, CDCl<sub>3</sub>) δ 8.00 (d, *J* = 15.6 Hz, 1H), 7.05 (s, 1H), 6.66 (s, 1H), 6.25 (d, *J* = 15.6 Hz, 1H), 3.87 (s, 6H), 2.39 (s, 3H). <sup>13</sup>C NMR (100 MHz, CDCl<sub>3</sub>) δ 173.21, 151.36, 147.62, 144.36, 132.41, 125.00, 115.51, 113.54, 108.94, 56.15, 56.07, 19.40.

### General procedure for the synthesis of compounds **39**, **40** and **46**

Palladium (II) chloride (0.3 eq) and formic acid (6 eq) were added to a solution of selected acid **34**, **35** or **44** (1 eq) in 13-20 mL of sodium hydroxide 2.5M and left stirring at 60°C for 24h. Once cooled to room temperature HCl 1N was added until pH=7. Reaction mixture was extracted with diethyl ether (4x10 mL). Organic phases, once reunited, were dried with anhydrous sodium sulphate and concentrated in vacuo.

#### **3-(3,5-dimethoxyphenyl)propanoic acid (39)**

Compound **39** was synthesized from **35** (490 mg, 2.35 mmol) and obtained as orange oil (390 mg, 79%). <sup>1</sup>H NMR (400 MHz, CDCl<sub>3</sub>) δ 11.67 (br s, 1H), 6.41-6.40 (m, 2H), 6.37-6.36 (m, 1H), 3.78 (s, 6H), 2.92 (t, *J* = 7.8 Hz, 2H), 2.69 (t, *J* = 7.8 Hz, 2H). <sup>13</sup>C NMR (100 MHz, CDCl<sub>3</sub>) δ 179.39, 160.99 (2C), 142.67, 106.44 (2C), 98.39, 55.24, 35.48, 30.90.

#### **3-(2,5-dimethoxyphenyl)propanoic acid (40)**

Compound **40** was synthesized from **34** (466 mg, 2.24 mmol) and obtained as yellow oil (450 mg, 96%). <sup>1</sup>H NMR (400 MHz, CDCl<sub>3</sub>) δ 6.79-6.77 (m, 2H), 6.75-6.74 (m, 1H), 3.79 (s, 3H), 3.77 (s, 3H), 2.94 (t, *J* = 7.6 Hz, 2H), 2.67 (t, *J* = 7.6 Hz, 2H). <sup>13</sup>C NMR (100 MHz, CDCl<sub>3</sub>) δ 179.75, 153.46, 151.82, 129.74, 116.44, 111.74, 111.19, 55.80, 55.75, 34.08, 26.08.

#### **3-(4,5-dimethoxy-2-methylphenyl)propanoic acid (46)**

Compound **46** was synthesized from **44** (366 mg, 1.65 mmol) and obtained as yellow powder (330 mg, 89%). <sup>1</sup>H NMR (400 MHz, CDCl<sub>3</sub>) δ 11.21 (br s, 1H), 6.67 (s, 1H), 6.63 (s, 1H), 3.79 (s, 6H), 2.85 (t, *J* = 7.8 Hz, 2H), 2.57 (t, *J* = 7.8 Hz, 2H), 2.22 (s, 3H). <sup>13</sup>C NMR (100 MHz, CDCl<sub>3</sub>) δ 178.87, 146.89, 146.65, 129.88, 127.50, 113.48, 112.13, 55.60, 55.50, 34.46, 27.52, 18.28.

### General procedure for the synthesis of compounds **36-38**, **41**, **42**, **45** and **47**

To a solution of corresponding acid **34**, **35**, **39**, **40**, **44**, **46** (1 eq) in 1.5-3.5 mL of dichloromethane at 0°C under nitrogen atmosphere, HOBT (1.3 eq) and EDC (1.3 eq) were added. Reaction mixture was left stirring at this temperature for 30 min. After confirming the complete conversion of starting material in activated complex, selected thiol (4 eq) was added and the reaction mixture left stirring overnight at room temperature. After evaporation of the solvent, the crude was purified through flash column chromatography using petroleum ether: ethyl acetate as mobile phase.

#### **S-allyl (*E*)-3-(2,5-dimethoxyphenyl)prop-2-enethioate (36)**

Compound **36** was synthesized from **34** (500 mg, 2.4 mmol) and allyl mercaptan (0.79 mL, 9.60 mmol). Compound was eluted with petroleum ether: ethyl acetate (9.2:0.8), which afforded **36** as yellowish oil (340 mg, 53%). <sup>1</sup>H NMR (400 MHz, CDCl<sub>3</sub>) δ 7.90 (d, *J* = 16 Hz, 1H), 7.00-6.99 (m, 1H), 6.89-6.86 (m, 2H), 6.81-6.73

(m, 2H), 5.87-5.79 (m, 1H), 5.25 (d,  $J = 16$  Hz, 1H), 5.09 (d,  $J = 9.6$  Hz, 1H), 3.79 (s, 3H), 3.74 (s, 3H), 3.63 (d,  $J = 6.4$  Hz, 1H).  $^{13}\text{C}$  NMR (100 MHz,  $\text{CDCl}_3$ )  $\delta$  189.37, 153.46, 153.23, 136.12, 133.28, 125.41, 123.46, 117.82, 117.53, 113.33, 112.42, 56.02, 55.73, 31.72.

#### **S-propyl (*E*)-3-(3,5-dimethoxyphenyl)prop-2-enethioate (37)**

Compound **37** was synthesized from **35** (520 mg, 2.50 mmol) and 1-propanethiol (0.91 mL, 9.99 mmol). Compound was eluted with petroleum ether: ethyl acetate (9:1), which afforded **37** as colourless oil (430 mg, 65%).  $^1\text{H}$  NMR (400 MHz,  $\text{CDCl}_3$ )  $\delta$  7.50 (d,  $J = 16$  Hz, 1H), 6.67-6.64 (m, 3H), 6.49-6.47 (m, 1H), 3.80 (s, 6H), 2.98 (t,  $J = 7.2$  Hz, 2H), 1.68-1.61 (m, 2H), 0.99 (t,  $J = 7.4$  Hz, 3H).  $^{13}\text{C}$  NMR (100 MHz,  $\text{CDCl}_3$ )  $\delta$  189.90, 161.00, 140.17, 136.03, 125.58, 106.15, 102.79, 55.44, 30.86, 22.99, 13.38.

#### **S-propyl (*E*)-3-(2,5-dimethoxyphenyl)prop-2-enethioate (38)**

Compound **38** was synthesized from **34** (300 mg, 1.44 mmol) and 1-propanethiol (0.52 mL, 5.76 mmol). Compound was eluted with petroleum ether: ethyl acetate (9.2:0.8), which afforded **38** as yellowish oil (250 mg, 65%).  $^1\text{H}$  NMR (400 MHz,  $\text{CDCl}_3$ )  $\delta$  7.89 (d,  $J = 15.8$  Hz, 1H), 7.04-7.03 (m, 1H), 6.92-6.89 (m, 1H), 6.85-6.82 (m, 1H), 6.77 (d,  $J = 15.8$  Hz, 1H), 3.83 (s, 3H), 3.78 (s, 3H), 2.98 (t,  $J = 7.2$  Hz, 2H), 1.69-1.64 (m, 2H), 1.01 (t,  $J = 7.4$  Hz, 3H).  $^{13}\text{C}$  NMR (100 MHz,  $\text{CDCl}_3$ )  $\delta$  190.42, 153.58, 153.32, 135.66, 126.01, 123.75, 117.50, 113.40, 112.54, 56.16, 55.88, 30.88, 23.14, 13.49.

#### **S-propyl 3-(3,5-dimethoxyphenyl)propanethioate (41)**

Compound **41** was synthesized from **39** (210 mg, 1 mmol) and 1-propanethiol (0.36 mL, 4 mmol). Compound was eluted with petroleum ether: ethyl acetate (9.2:0.8), which afforded **41** as colourless oil (200 mg, 75%).  $^1\text{H}$  NMR (400 MHz,  $\text{CDCl}_3$ )  $\delta$  6.33-6.30 (m, 3H), 3.74 (s, 6H), 2.90-2.83 (m, 6H), 1.60-1.55 (m, 2H), 0.94 (t,  $J = 7.4$  Hz, 3H).  $^{13}\text{C}$  NMR (100 MHz,  $\text{CDCl}_3$ )  $\delta$  198.81, 161.09 (2C), 142.72, 106.54 (2C), 98.51, 55.43 (2C), 45.56, 31.96, 31.01, 23.19, 13.53.

#### **S-propyl 3-(2,5-dimethoxyphenyl)propanethioate (42)**

Compound **42** was synthesized from **40** (190 mg, 0.90 mmol) and 1-propanethiol (0.33 mL, 3.62 mmol). Compound was eluted with petroleum ether: ethyl acetate (9.2:0.8), which afforded **42** as yellowish oil (170 mg, 70%).  $^1\text{H}$  NMR (400 MHz,  $\text{CDCl}_3$ )  $\delta$  6.75-6.67 (m, 3H), 3.76 (s, 3H), 3.72 (s, 3H), 2.95-2.91 (m, 2H), 2.86-2.80 (m, 4H), 1.60-1.55 (m, 2H), 0.95 (t,  $J = 7.4$  Hz, 3H).  $^{13}\text{C}$  NMR (100 MHz,  $\text{CDCl}_3$ )  $\delta$  198.84, 153.33, 151.61, 129.49, 116.22, 111.51, 111.01, 55.63, 55.50, 43.76, 30.63, 26.71, 22.92, 13.23.

#### **S-propyl (*E*)-3-(4,5-dimethoxy-2-methylphenyl)prop-2-enethioate (45)**

Compound **45** was synthesized from **44** (200 mg, 0.90 mmol) and 1-propanethiol (0.33 mL, 3.6 mmol). Compound was eluted with ether: ethyl acetate (8:2), which afforded **45** as yellow crystal powder (120 mg,

48%). <sup>1</sup>H NMR (400 MHz, CDCl<sub>3</sub>) δ 7.79 (d, *J* = 15.6 Hz, 1H), 6.99 (s, 1H), 6.62 (s, 1H), 6.49 (d, *J* = 15.6 Hz, 1H), 3.84 (s, 6H), 2.94 (t, *J* = 7.2 Hz, 2H), 2.34 (s, 3H), 1.65-1.60 (m, 2H), 0.96 (t, *J* = 7.6 Hz, 3H). <sup>13</sup>C NMR (100 MHz, CDCl<sub>3</sub>) δ 189.86, 151.06, 147.45, 137.46, 132.52, 124.89, 123.50, 113.46, 108.60, 56.02, 55.89, 30.86, 23.16, 19.26, 13.45.

#### **S-propyl 3-(4,5-dimethoxy-2-methylphenyl)propanethioate (47)**

Compound **47** was synthesized from **46** (330 mg, 1.47 mmol) and 1-propanethiol (0.53 mL, 5.88 mmol). Compound was eluted with petroleum ether: ethyl acetate (7:3), which afforded **47** as white solid (270 mg, 65%). <sup>1</sup>H NMR (400 MHz, CDCl<sub>3</sub>) δ 6.65 (s, 1H), 6.64 (s, 1H), 3.84 (s, 3H), 3.83 (s, 3H), 2.92-2.77 (m, 4H), 2.77-2.75 (m, 2H), 2.25 (s, 3H), 1.62-1.56 (m, 2H), 0.96 (t, *J* = 7.4 Hz, 3H). <sup>13</sup>C NMR (100 MHz, CDCl<sub>3</sub>) δ 198.85, 147.21, 147.00, 130.13, 127.77, 113.71, 112.44, 56.00, 55.88, 44.68, 30.81, 28.82, 22.93, 18.69, 13.29.

#### **General procedure for the synthesis of compounds 2-8**

A solution of dimethoxy analogues **36-38**, **41**, **42**, **45**, **47** (1 eq) in 0.2-0.6 mL of anhydrous dichloromethane was cooled at 0°C. Boron tribromide 1M in dichloromethane (2.3 eq) was added to the solution and the reaction was left stirring at the same temperature until completion. 6-10 mL of cold water were added to terminate the reaction and the mixture extracted with ethyl acetate (3 x 8 mL). Organic phases, once reunited, were dried with anhydrous sodium sulphate, concentrated in vacuo and the crude obtained purified by column chromatography using dichloromethane: methanol as mobile phase.

#### **S-allyl (E)-3-(2,5-dihydroxyphenyl)prop-2-enethioate (2)**

Compound **2** was synthesized from **36** (130 mg, 0.49 mmol). Compound was eluted with dichloromethane: methanol (9.3:0.7), which afforded **2** as yellow powder (20 mg, 17%). <sup>1</sup>H NMR (400 MHz, CD<sub>3</sub>OD) δ 7.86 (d, *J* = 16 Hz, 1H), 6.91-6.90 (m, 1H), 6.82 (d, *J* = 16 Hz, 1H), 6.74-6.68 (m, 2H), 5.91-5.81 (m, 1H), 5.26 (d, *J* = 16.8 Hz, 1H), 5.09 (d, *J* = 10.4 Hz, 1H), 3.64 (d, *J* = 7.2 Hz, 2H). <sup>13</sup>C NMR (100 MHz, CD<sub>3</sub>OD) δ 191.35, 152.09, 151.36, 138.13, 134.82, 125.15, 122.50, 120.66, 117.99 (2C), 114.87, 32.38. MS [ESI+] *m/z* 237 [M+H]<sup>+</sup>.

#### **S-propyl (E)-3-(3,5-dihydroxyphenyl)prop-2-enethioate (3)**

Compound **3** was synthesized from **37** (430 mg, 1.61 mmol). Compound was eluted with dichloromethane: methanol (9.5:0.5), which afforded **3** as yellow powder (200 mg, 52%). <sup>1</sup>H NMR (400 MHz, CD<sub>3</sub>OD) δ 7.41 (d, *J* = 15.8 Hz, 1H), 6.67 (d, *J* = 15.8 Hz, 1H), 6.51 (s, 2H), 6.33-6.32 (m, 1H), 2.95 (t, *J* = 7.2 Hz, 2H), 1.66-1.59 (m, 2H), 0.99 (t, *J* = 7.2 Hz, 3H). <sup>13</sup>C NMR (100 MHz, CD<sub>3</sub>OD) δ 191.65, 160.12 (2C), 141.97, 137.21, 125.76, 107.76 (2C), 106.16, 31.56, 24.18, 13.58. MS [ESI-] *m/z* 237 [M-H]<sup>-</sup>.

#### **S-propyl (*E*)-3-(2,5-dihydroxyphenyl)prop-2-enethioate (4)**

Compound **4** was synthesized from **38** (220 mg, 0.83 mmol). Compound was eluted with dichloromethane:methanol (9.6:0.4), which afforded **4** as yellow powder (66 mg, 34%). <sup>1</sup>H NMR (400 MHz, CD<sub>3</sub>OD) δ 7.82 (d, *J* = 16 Hz, 1H), 6.89-6.88 (m, 1H), 6.79 (d, *J* = 16 Hz, 1H), 6.69-6.68 (m, 2H), 2.94 (t, *J* = 7.4 Hz, 2H), 1.65-1.60 (m, 2H), 0.99 (t, *J* = 7.4 Hz, 3H). <sup>13</sup>C NMR (100 MHz, CD<sub>3</sub>OD) δ 190.87, 150.60, 149.93, 136.23, 124.07, 121.14, 119.10, 116.54, 113.38, 30.07, 22.84, 12.17. MS [ESI<sup>-</sup>] *m/z* 237 [M-H]<sup>-</sup>. MS [ESI<sup>+</sup>] *m/z* 261 [M+Na]<sup>+</sup>.

#### **S-propyl 3-(3,5-dihydroxyphenyl)propanethioate (5)**

Compound **5** was synthesized from **41** (170 mg, 0.63 mmol). Compound was eluted with dichloromethane:methanol (9.6:0.4), which afforded **5** as white powder (100 mg, 67%). <sup>1</sup>H NMR (400 MHz, CDCl<sub>3</sub>) δ 6.21 (s, 3H), 2.79-2.73 (m, 6H), 1.53-1.48 (m, 2H), 0.87 (t, *J* = 7.2 Hz, 3H). <sup>13</sup>C NMR (100 MHz, CDCl<sub>3</sub>) δ 201.92, 156.89 (2C), 143.10, 108.33 (2C), 101.46, 45.21, 31.58, 31.27, 22.92, 13.48. MS [ESI<sup>+</sup>] *m/z* 241 [M+H]<sup>+</sup>. MS [ESI<sup>+</sup>] *m/z* 263 [M+Na]<sup>+</sup>.

#### **6-hydroxychroman-2-one (6a)**

Compound **6a** was synthesized from **42** (250 mg, 0.97 mmol). Compound was eluted with dichloromethane:methanol (9.6:0.4), which afforded **6a** as white powder (50 mg, 31%). <sup>1</sup>H NMR (400 MHz, CDCl<sub>3</sub>) δ 6.93 (d, *J* = 12 Hz, 1H), 6.72-6.67 (m, 2H), 2.95 (t, *J* = 8 Hz, 2H), 2.76 (t, *J* = 8 Hz, 2H).

#### **S-propyl (*E*)-3-(4,5-dihydroxy-2-methylphenyl)prop-2-enethioate (7)**

Compound **7** was synthesized from **45** (100 mg, 0.36 mmol). Compound was eluted with dichloromethane:methanol (9.7:0.3) as mobile phase, which afforded **7** as yellow powder (30 mg, 33%). <sup>1</sup>H NMR (400 MHz, CD<sub>3</sub>OD) δ 7.83 (d, *J* = 15.4 Hz, 1H), 7.08 (s, 1H), 6.64 (s, 1H), 6.53 (d, *J* = 15.4 Hz, 1H), 2.97 (t, *J* = 7.2 Hz, 2H), 2.30 (s, 3H), 1.68-1.63 (m, 2H), 1.01 (t, *J* = 7.4 Hz, 3H). <sup>13</sup>C NMR (100 MHz, CD<sub>3</sub>OD) δ 191.82, 149.69, 144.90, 139.10, 132.80, 125.06, 123.01, 118.42, 113.54, 31.45, 24.22, 18.73, 13.53. MS [ESI<sup>-</sup>] *m/z* 251 [M-H]<sup>-</sup>.

#### **S-propyl 3-(4,5-dihydroxy-2-methylphenyl)propanethioate (8)**

Compound **8** was synthesized from **47** (270 mg, 0.96 mmol). Compound was eluted with dichloromethane:methanol (9.6:0.4) as mobile phase, which afforded **8** as yellow powder (180 mg, 74%). <sup>1</sup>H NMR (400 MHz, CDCl<sub>3</sub>) δ 6.65 (s, 1H), 6.63 (s, 1H), 2.87-2.84 (m, 2H), 2.80-2.77 (m, 2H), 2.73-2.71 (m, 2H), 2.13 (s, 3H), 1.61-1.56 (m, 2H), 0.95 (t, *J* = 7.4 Hz, 3H). <sup>13</sup>C NMR (100 MHz, CDCl<sub>3</sub>) δ 201.28, 142.09, 141.69, 130.53, 128.42, 117.71, 116.28, 44.70, 31.13, 28.70, 22.92, 18.55, 13.44. MS [ESI<sup>+</sup>] *m/z* 255 [M+H]<sup>+</sup>.

#### **6-((*tert*-butyldimethylsilyl)oxy)chroman-2-one (6b)**

To a solution of **6a** (50 mg, 0.28 mmol) in 0.4 mL of dry DMF were added TBDMS-Cl (85 mg, 0.56 mmol) and imidazole (48 mg, 0.7 mmol) under nitrogen atmosphere. After leaving the reaction to room temperature

overnight, the mixture was concentrated to dryness, and the residue purified by column chromatography using petroleum ether: ethyl acetate (9:1) as mobile phase. **6b** was obtained as waxy solid (50 mg, 44%). <sup>1</sup>H NMR (400 MHz, CDCl<sub>3</sub>) δ 6.88 (d, *J* = 8 Hz, 1H), 6.67 (d, *J* = 8 Hz, 1H), 6.63 (s, 1H), 2.91 (t, *J* = 8 Hz, 2H), 2.73 (t, *J* = 8 Hz, 2H), 0.96 (s, 9H), 0.17 (s, 6H). <sup>13</sup>C NMR (100 MHz, CDCl<sub>3</sub>) δ 168.72, 152.09, 146.39, 123.50, 119.39, 119.10, 117.59, 29.19, 25.67, 23.93, 18.19, -4.44.

### **3-hydroxy-4-methoxy-2-nitrobenzaldehyde (48)**

Nitric acid (0.71 mL, 15.78 mmol) was added dropwise to a solution of 3-hydroxy-4-methoxy benzaldehyde (2 g, 13.15 mmol) in 15 mL ethyl acetate at 0°C, and further left stirring under nitrogen atmosphere for 24 h at room temperature. 30 mL of ethyl acetate was added to the reaction mixture, which was subsequently washed with water (3 x 30 mL). Organic phase was dried with anhydrous sodium sulphate, concentrated in vacuo and the crude obtained purified by column chromatography using petroleum ether: ethyl acetate (6.5:3.5) as mobile phase. **X** was obtained as brown oil (770 mg, 30%). <sup>1</sup>H NMR (400 MHz, CDCl<sub>3</sub>) δ 10.09 (s, 1H), 8.82 (br s, 1H), 7.49 (d, *J* = 8.2 Hz, 1H), 7.12 (d, *J* = 8.2 Hz, 1H), 4.04 (s, 3H). <sup>13</sup>C NMR (100 MHz, CDCl<sub>3</sub>) δ 186.67, 153.17, 143.00, 123.86, 122.71, 113.56 (2C), 56.98.

### **3,4-dimethoxy-2-nitrobenzaldehyde (49)**

To a solution of **48** (250 mg, 1.27 mmol) in 5 mL of anhydrous DMF, potassium carbonate (614 mg, 4.45 mmol) and methyl iodide (0.35 mL, 4.45 mmol) were added dropwise under vigorously agitation. Reaction was left stirring for 1 h at 70°C under nitrogen atmosphere. 8 mL of water were added to the mixture that was further extracted with diethyl ether (3 x 8 mL). Organic phases, once reunited, were dried with anhydrous sodium sulphate, concentrated in vacuo and the crude obtained purified by column chromatography using petroleum ether: ethyl acetate (6:4) as mobile phase. **49** was obtained as brownish oil (255 mg, 95%). <sup>1</sup>H NMR (400 MHz, CDCl<sub>3</sub>) δ 9.76 (s, 1H), 7.63 (d, *J* = 8.4 Hz, 1H), 7.13 (d, *J* = 8.4 Hz, 1H), 4.00 (s, 3H), 3.92 (s, 3H). <sup>13</sup>C NMR (100 MHz, CDCl<sub>3</sub>) δ 186.19, 158.75, 144.93, 141.29, 128.65, 120.54, 113.21, 62.52, 56.99.

### **2-amino-3,4-dimethoxybenzaldehyde (50)**

In a mixture of ethyl acetate: acetic acid: water 2: 2: 1 (3 mL: 3 mL: 1.5 mL) and **49** (355 mg, 1.68 mmol), iron (282 mg, 5.04 mmol) and HCl 37% (0.10 mL) were added and the reaction mixture was left stirring at reflux for 15 min and at room temperature for the following hour. Water (20 mL) was added to terminate the reaction. The resulted mixture was extracted with ethyl acetate (3 x 20 mL). Organic phases, once reunited, were washed with brine (13 mL), dried with anhydrous sodium sulphate, concentrated in vacuo and the crude obtained purified by column chromatography using petroleum ether: ethyl acetate (6:4) as mobile phase. **50** was obtained as colourless oil (304 mg, 82%). <sup>1</sup>H NMR (400 MHz, CDCl<sub>3</sub>) δ 9.61 (s, 1H), 7.08 (d, *J* = 8.8 Hz, 1H), 6.25 (d, *J* = 8.8 Hz, 1H), 3.78 (s, 3H), 3.68 (s, 3H). <sup>13</sup>C NMR (100 MHz, CDCl<sub>3</sub>) δ 191.87, 156.30, 144.18, 133.44, 132.07, 114.50, 100.60, 59.23, 55.39.

### **7,8-dimethoxy-2-oxo-1,2-dihydroquinoline-3-carboxylic acid (51)**

Meldrum's acid (251 mg, 1.74 mmol), piperidine (7  $\mu$ L, 0.07 mmol) and acetic acid (4  $\mu$ L, 0.07 mmol) were added to a solution of **50** (250 mg, 1.38 mmol) in 15 mL of ethanol. The mixture was left stirring for 24h at 60°C in a pressure tube (Ace pressure tubes-Sigma Aldrich). The reaction was cooled to 0°C and the formed precipitate filtered and washed with cold ethanol. Once dried, **51** was obtained as white powder (301 mg, 83%). <sup>1</sup>H NMR (400 MHz, DMSO-*d*<sub>6</sub>)  $\delta$  12.52 (br s, 1H), 8.89 (s, 1H), 7.82 (d, *J* = 9.0 Hz, 1H), 7.27 (d, *J* = 9.0 Hz, 1H), 3.98 (s, 3H), 3.82 (s, 3H). <sup>13</sup>C NMR (100 MHz, DMSO-*d*<sub>6</sub>)  $\delta$  164.71, 164.62, 155.82, 149.78, 146.38, 144.51, 134.00, 126.72, 114.31, 110.35, 60.71, 56.42.

### **S-propyl 7,8-dimethoxy-2-oxo-1,2-dihydroquinoline-3-carbothioate (10)**

Thionyl chloride (0.12 mL) was added to a solution of **51** (120 mg, 0.48 mmol) in 9 mL of anhydrous toluene. The reaction mixture was left stirring at reflux for 3h. Once cooled at room temperature, the mixture was concentrated in vacuo. The crude obtained was directly solubilized in 5 mL of anhydrous dichloromethane. Triethylamine (0.10 mL, 0.68 mmol) and 1-propanethiol (0.16 mL, 1.8 mmol) were added to this mixture at 0°C and the reaction was left stirring at room temperature for 48h. Solvent was evaporated under vacuum and the crude purified by column chromatography using dichloromethane: methanol (9.5:0.5) as mobile phase. **10** was obtained as colourless oil (65 mg, 46%). <sup>1</sup>H NMR (400 MHz, CDCl<sub>3</sub>)  $\delta$  9.39 (br s, 1H), 8.49 (s, 1H), 7.42 (d, *J* = 9 Hz, 1H), 6.90 (d, *J* = 9 Hz, 1H), 3.98 (s, 3H), 3.97 (s, 3H), 3.00 (t, *J* = 7.4 Hz, 2H), 1.73-1.67 (m, 2H), 1.03 (t, *J* = 7.4 Hz, 3H). <sup>13</sup>C NMR (100 MHz, CDCl<sub>3</sub>)  $\delta$  189.58, 160.28, 155.26, 143.20, 134.27, 133.40, 126.37, 125.29, 113.82, 109.02, 61.32, 56.54, 31.49, 22.68, 13.90.

### **S-propyl 7,8-dihydroxy-2-oxo-1,2-dihydroquinoline-3-carbothioate (9)**

A solution of **10** (60 mg, 0.20 mmol) in 0.20 mL of anhydrous dichloromethane was cooled at 0°C. Boron tribromide 1M in dichloromethane (0.28 mL, 0.28 mmol) was added to the solution and the reaction was left stirring at the same temperature until completion. Cold water (2 mL of) was added to terminate the reaction and the mixture extracted with ethyl acetate (3 x 4 mL). Organic phases, once reunited, were dried with anhydrous sodium sulphate, concentrated in vacuo and the crude obtained purified by column chromatography using dichloromethane: methanol: acetic acid (9.2:0.8:0.05) as mobile phase. **9** was obtained as brown powder (40 mg, 73%). <sup>1</sup>H NMR (400 MHz, CD<sub>3</sub>OD)  $\delta$  8.52 (s, 1H), 7.23 (d, *J* = 8.6 Hz, 1H), 6.85 (d, *J* = 8.6 Hz, 1H), 2.96 (t, *J* = 7.2 Hz, 2H) 1.70-1.64 (m, 2H), 1.03 (t, *J* = 7.2 Hz, 3H). <sup>13</sup>C NMR (100 MHz, CD<sub>3</sub>OD)  $\delta$  190.32, 161.31, 150.33, 144.35, 131.47, 130.82, 123.66, 122.63, 113.68, 113.62, 31.26, 23.16, 13.15. MS [ESI-] *m/z* 278 [M-H]<sup>-</sup>

### **2-hydroxy-3,4-dimethoxybenzaldehyde (52)**

Aluminium trichloride (748 mg, 5.61 mmol) was added to a solution of 2,3,4-trimethoxybenzaldehyde (1 g, 5.10 mmol) in 35 mL of anhydrous toluene. The reaction mixture was left stirring at 80°C for 6h. Water (20 mL) and of HCl 37% (3.5 mL) were added to terminate the reaction and the obtained mixture was extracted with ethyl acetate (3 x 20 mL). Organic phases, once reunited, were subsequently washed with water and



brine, dried with anhydrous sodium sulphate, concentrated in vacuo and the crude obtained purified by column chromatography using petroleum ether: ethyl acetate (8:2) as mobile phase. **52** was obtained as white powder (555 mg, 60%). <sup>1</sup>H NMR (400 MHz, CDCl<sub>3</sub>) δ 11.15 (br s, 1H), 9.70 (s, 1H), 7.25 (d, *J* = 8.6 Hz, 1H), 6.57 (d, *J* = 8.6 Hz, 1H), 3.91 (s, 3H), 3.86 (s, 3H). <sup>13</sup>C NMR (100 MHz, CDCl<sub>3</sub>) δ 194.85, 159.31, 155.63, 136.05, 130.16, 116.46, 103.98, 60.65, 56.18.

#### **7,8-dimethoxy-2-oxo-2H-chromene-3-carboxylic acid (53)**

To a solution of **52** (270 mg, 1.48 mmol) in 20 mL of anhydrous ethanol, Meldrum's acid (256 mg, 1.78 mmol), piperidine (7 μL, 0.07 mmol) and acetic acid (4 μL, 0.07 mmol) were added. The reaction mixture was left stirring at 60°C for 24h. Once cooled at 0°C the formed precipitate was filtered and washed with cold EtOH. Once dried, **53** was obtained as yellow powder (267 mg, 72%). <sup>1</sup>H NMR (400 MHz, CDCl<sub>3</sub>) δ 12.20 (br s, 1H), 8.84 (s, 1H), 7.48 (d, *J* = 8.8 Hz, 1H), 7.06 (d, *J* = 8.8 Hz, 1H), 4.03 (s, 3H), 4.01 (s, 3H). <sup>13</sup>C NMR (100 MHz, CDCl<sub>3</sub>) δ 164.33, 163.17, 159.24, 151.82, 148.74, 136.55, 126.50, 113.50, 111.44, 110.70, 61.93, 56.99.

#### **General procedure for the synthesis of compounds 12, 14, 16**

To a solution of **53** (1 eq) in dichloromethane (1-2 mL) at 0°C, HOBT (1.3 eq) and EDC (1.3 eq) were added. Reaction mixture was left stirring at this temperature for 30 min. After confirming the complete conversion of starting material in activated complex, selected thiol (4 eq) was added and the reaction mixture left stirring overnight. After evaporation of the solvent, the crude was purified through column chromatography.

#### **S-propyl 7,8-dimethoxy-2-oxo-2H-chromene-3-carbothioate (12)**

Compound **12** was synthesized from **53** (100 mg, 0.40 mmol) and 1-propanethiol (0.15 mL, 1.6 mmol). Compound was eluted with petroleum ether: ethyl acetate (5:5), which afforded **12** as yellow powder (109 mg, 89%). <sup>1</sup>H NMR (400 MHz, CDCl<sub>3</sub>) δ 8.43 (s, 1H), 7.35 (d, *J* = 8.6 Hz, 1H), 6.93 (d, *J* = 8.6 Hz, 1H), 3.97 (s, 6H), 2.98 (t, *J* = 7.4 Hz, 2H), 1.71-1.62 (m, 2H), 1.01 (t, *J* = 7.4 Hz, 3H). <sup>13</sup>C NMR (100 MHz, CDCl<sub>3</sub>) δ 188.04, 157.95, 157.84, 148.72, 146.11, 135.90, 125.80, 119.98, 112.89, 109.39, 61.47, 56.54, 31.32, 22.34, 13.49.

#### **S-cyclohexyl 7,8-dimethoxy-2-oxo-2H-chromene-3-carbothioate (14)**

Compound **14** was synthesized from **53** (200 mg, 0.80 mmol) and cyclohexanethiol (0.56 mL, 3.20 mmol). Compound was eluted with petroleum ether: ethyl acetate (7.5:2.5), which afforded **14** as yellow powder (50 mg, 18%). <sup>1</sup>H NMR (400 MHz, CDCl<sub>3</sub>) δ 8.39 (s, 1H), 7.33 (d, *J* = 8.6 Hz, 1H), 6.91 (d, *J* = 8.6 Hz, 1H), 3.94 (s, 6H), 3.64-3.62 (m, 1H), 1.96-1.94 (m, 2H), 1.72-1.70 (m, 2H), 1.56 (m, 1H), 1.46-1.42 (m, 4H), 1.23-1.21 (m, 1H). <sup>13</sup>C NMR (100 MHz, CDCl<sub>3</sub>) δ 187.67, 158.00, 157.86, 148.77, 146.17, 135.91, 125.90, 120.33, 112.99, 109.46, 61.58, 56.66, 42.55, 32.77, 26.10, 25.67.

#### **S-(adamantan-1-yl) 7,8-dimethoxy-2-oxo-2H-chromene-3-carbothioate (16)**

Compound **16** was synthesized from **53** (200 mg, 0.8 mmol) and 1-adamantanethiol (538 mg, 3.2 mmol). Compound was eluted with dichloromethane: methanol (9.8:0.2), which afforded **16** as yellow powder (180 mg, 56%). <sup>1</sup>H NMR (400 MHz, CDCl<sub>3</sub>) δ 8.27 (s, 1H), 7.28 (d, *J* = 8 Hz, 1H), 6.89 (d, *J* = 8 Hz, 1H), 3.93 (s, 3H), 3.91 (s, 3H), 2.19-2.17 (m, 6H), 2.02-2.00 (m, 2H), 1.75-1.66 (m, 6H). <sup>13</sup>C NMR (100 MHz, CDCl<sub>3</sub>) δ 187.94,

157.68, 157.32, 148.54, 145.52, 135.74, 125.53, 121.47, 112.81, 109.27, 61.42, 56.53, 51.49, 47.50, 43.02, 41.53, 36.31, 36.06, 35.73, 30.04, 29.97, 29.78.

#### **General procedure for the synthesis of compounds 11, 13, 15**

A solution of **12**, **14** or **16** (1 eq) in 0.15-0.25 mL of anhydrous dichloromethane was cooled at 0°C. Boron tribromide 1M in dichloromethane (2.5 eq) was added to the solution and the reaction was left stirring at the same temperature until completion. Cold water (5 mL) was added to terminate the reaction and the mixture extracted with ethyl acetate (3 x 4 mL). Organic phases, once reunited, were dried with anhydrous sodium sulphate, concentrated in vacuo and the crude obtained purified by column chromatography using dichloromethane: methanol as mobile phase.

#### **S-propyl 7,8-dihydroxy-2-oxo-2H-chromene-3-carbothioate (11)**

Compound **11** was synthesized from **12** (95 mg, 0.31 mmol). Compound was eluted with dichloromethane: methanol (9.7:0.3), which afforded **11** as yellow powder (57 mg, 65%). <sup>1</sup>H NMR (400 MHz, DMSO-*d*<sub>6</sub>) δ 8.57 (s, 1H), 7.31-7.30 (m, 1H), 6.88-6.86 (m, 1H), 2.91 (t, *J* = 8 Hz, 2H), 1.62-1.57 (m, 2H), 0.96 (t, *J* = 8 Hz, 3H). <sup>13</sup>C NMR (100 MHz, DMSO-*d*<sub>6</sub>) δ 188.10, 158.67, 147.41, 146.52, 144.42, 131.85, 122.11, 117.81, 113.35, 111.64, 30.61, 22.33, 12.38. MS [ESI+] *m/z* 281 [M+H]<sup>+</sup>, 303 [M+Na]<sup>+</sup>

#### **S-cyclohexyl 7,8-dihydroxy-2-oxo-2H-chromene-3-carbothioate (13)**

Compound **13** was synthesized from **14** (80 mg, 0.23 mmol). Compound was eluted with dichloromethane: methanol (9.4:0.4), which afforded **13** as yellow powder (18 mg, 24%). <sup>1</sup>H NMR (400 MHz, CD<sub>3</sub>OD) δ 8.53 (s, 1H), 7.20 (d, *J* = 8.4 Hz, 1H), 6.86 (d, *J* = 8.4 Hz, 1H), 3.63-3.61 (m, 1H), 2.00-1.97 (m, 2H), 1.77-1.76 (m, 2H), 1.66-1.59 (m, 1H), 1.52-1.43 (m, 4H). <sup>13</sup>C NMR (100 MHz, CD<sub>3</sub>OD) δ 189.27, 160.17, 154.84, 148.89, 145.95, 133.49, 123.64, 119.48, 115.00, 113.10, 43.57, 34.06, 27.25, 26.87. MS [ESI+] *m/z* 343 [M+H]<sup>+</sup>

#### **S-(adamantan-1-yl) 7,8-dihydroxy-2-oxo-2H-chromene-3-carbothioate (15)**

Compound **15** was synthesized from **16** (180 mg, 0.45 mmol). Compound was eluted with dichloromethane: methanol (9.6:0.4), which afforded **15** as yellow powder (34 mg, 20%). <sup>1</sup>H NMR (400 MHz, DMSO-*d*<sub>6</sub>) δ 8.50 (s, 1H), 7.28 (d, *J* = 8Hz, 1H), 6.85 (d, *J* = 8Hz, 1H), 2.15-2.13 (m, 6H), 2.03-2.02 (m, 2H), 1.74-1.66 (m, 6H). <sup>13</sup>C NMR (100 MHz, DMSO-*d*<sub>6</sub>) δ 187.96, 157.93, 153.72, 147.41, 144.82, 132.30, 122.75, 118.94, 114.07, 111.57, 50.80, 49.02, 41.59, 36.27, 29.58. MS [ESI+] *m/z* 373 [M+H]<sup>+</sup>

#### **2,3-dihydroxy-4-methoxybenzaldehyde (54)**

A solution of 2,3,4-trimethoxybenzaldehyde (1.5 g, 7.65 mmol) in anhydrous dichloromethane (8 mL) was added to a suspension of aluminium chloride (2.55 g, 19.13 mmol) in anhydrous dichloromethane (30 mL). The reaction mixture was left stirring for 8h at reflux. Cold water (25 mL) and HCl 37% (8 mL) were added to quench the reaction. Organic phase was separated and the aqueous phase was further extracted with dichloromethane (4x15mL). All organic phases, once reunited, were dried with anhydrous sodium sulphate, concentrated in vacuo and the crude obtained was purified with chromatography using dichloromethane: methanol: acetic acid (9.5:0.5:0.05) as mobile phase. **54** was obtained as yellowish solid (787 mg, 61%). <sup>1</sup>H

NMR (400 MHz, CDCl<sub>3</sub>)  $\delta$  11.06 (s, 1H), 9.68 (s, 1H), 7.08 (d,  $J$  = 8.8 Hz, 1H), 6.56 (d,  $J$  = 8.8 Hz, 1H), 3.92 (s, 3H). <sup>13</sup>C NMR (100 MHz, CDCl<sub>3</sub>)  $\delta$  195.48, 153.31, 149.17, 133.11, 126.32, 116.15, 103.80, 56.48.

#### **8-hydroxy-7-methoxy-2-oxo-2H-chromene-3-carboxylic acid (55)**

To a solution of **54** (280 mg, 1.67 mmol) in 16 mL of ethanol, Meldrum's acid (288 mg, 2.00 mmol), piperidine (8  $\mu$ L, 0.08 mmol) and acetic acid (4  $\mu$ L, 0.08 mmol) were added and the reaction mixture was left stirring at 60°C for 24 h. Once the reaction mixture was cooled until 0°C, the obtained precipitate was filtered and washed with cold ethanol. Once dried in the oven, **55** was obtained as a yellow powder (309 mg, 78%). <sup>1</sup>H NMR (400 MHz, DMSO-*d*<sub>6</sub>)  $\delta$  8.60 (s, 1H), 7.36 (d,  $J$  = 8.6 Hz, 1H), 7.09 (d,  $J$  = 8.6 Hz, 1H), 3.91 (s, 3H). <sup>13</sup>C NMR (100 MHz, DMSO-*d*<sub>6</sub>)  $\delta$  164.40, 162.67, 152.69, 148.78, 143.47, 132.95, 120.74, 114.98, 112.64, 109.03, 56.39.

#### **General procedure for the synthesis of compounds 56–59**

To a solution of **55** (eq) in dimethylformamide (1-2 mL) at 0°C, HOBt (1.3 eq) and EDC (1.3 eq) were added. Reaction mixture was left stirring at this temperature for 30 min. After confirming the complete conversion of starting material in activated complex, selected thiol (4 eq) was added and the reaction mixture left stirring overnight. After evaporation of the solvent, the crude was purified by column chromatography.

#### **S-propyl 8-hydroxy-7-methoxy-2-oxo-2H-chromene-3-carbothioate (56)**

Compound **56** was synthesized from **55** (155 mg, 0.66 mmol) and 1-propanethiol (0.24 mL, 2.64 mmol). Compound was eluted with dichloromethane: methanol (9.8:0.2), which afforded **56** as yellow powder (40 mg, 21%). <sup>1</sup>H NMR (400 MHz, CDCl<sub>3</sub>)  $\delta$  8.48 (s, 1H), 7.25 (d,  $J$  = 8.8 Hz, 1H), 6.93 (d,  $J$  = 8.8 Hz, 1H), 4.02 (s, 3H), 3.01 (t,  $J$  = 7.3 Hz, 2H), 1.72 – 1.67 (m, 2H), 1.03 (t,  $J$  = 7.3 Hz, 3H). <sup>13</sup>C NMR (100 MHz, CDCl<sub>3</sub>)  $\delta$  188.11, 157.78, 151.97, 146.44, 142.59, 132.56, 121.92, 119.94, 112.63, 108.49, 56.67, 31.32, 22.29, 13.49.

#### **S-cyclohexyl 8-hydroxy-7-methoxy-2-oxo-2H-chromene-3-carbothioate (57)**

Compound **57** was synthesized from **55** (550 mg, 2.33 mmol) and cyclohexanethiol (1.14 mL, 9.32 mmol). Compound was eluted with dichloromethane: methanol: acetic acid (9.8:0.2:0.01), which afforded **57** as yellow powder (260 mg, 33%). <sup>1</sup>H NMR (400 MHz, CDCl<sub>3</sub>)  $\delta$  8.42 (s, 1H), 7.19 (d,  $J$  = 8.4 Hz, 1H), 6.90 (d,  $J$  = 8.4 Hz, 1H), 3.99 (s, 3H), 3.66-3.65 (m, 1H), 1.98 – 1.96 (m, 2H), 1.74 – 1.72 (m, 2H), 1.61 – 1.58 (m, 1H), 1.38 – 1.28 (m, 4H), 1.17 – 1.15 (m, 1H). <sup>13</sup>C NMR (100 MHz, CDCl<sub>3</sub>)  $\delta$  187.78, 157.80, 152.01, 146.51, 142.72, 132.65, 122.01, 120.41, 112.81, 108.59, 56.82, 42.60, 32.77, 26.11, 25.68.

#### **S-hexyl 8-hydroxy-7-methoxy-2-oxo-2H-chromene-3-carbothioate (58)**

Compound **58** was synthesized from **55** (290 mg, 1.23 mmol) and 1-hexanethiol (0.70 mL, 4.92 mmol). Compound was eluted with dichloromethane: methanol (9.8:0.2), which afforded **58** as yellow orange powder (104 mg, 25%). <sup>1</sup>H NMR (400 MHz, CDCl<sub>3</sub>)  $\delta$  8.43 (s, 1H), 7.18 (d,  $J$  = 8.4 Hz, 1H), 6.90 (d,  $J$  = 8.4 Hz, 1H), 3.99 (s, 3H), 2.98 (t,  $J$  = 7 Hz, 2H), 1.66-1.59 (m, 2H), 1.39-1.22 (m, 6H), 0.85-0.84 (m, 3H). <sup>13</sup>C NMR (100 MHz, CDCl<sub>3</sub>)  $\delta$  188.12, 157.81, 152.06, 146.46, 142.66, 132.63, 121.88, 119.89, 112.63, 108.52, 56.67, 31.26, 29.45, 28.80, 28.62, 22.41, 13.93.

### **S-isopentyl 8-hydroxy-7-methoxy-2-oxo-2H-chromene-3-carbothioate (59)**

Compound **59** was synthesized from **55** (309 mg, 1.31 mmol) and 3-methyl-1-butanethiol (0.65 mL, 5.24 mmol). Compound was eluted with dichloromethane: methanol (9.9:0.1), which afforded **59** as yellow orange powder (76 mg, 18%). <sup>1</sup>H NMR (400 MHz, CDCl<sub>3</sub>) δ 8.46 (s, 1H), 7.20 (d, *J* = 8.8 Hz, 1H), 6.91 (d, *J* = 8.8 Hz, 1H), 4.00 (s, 3H), 3.01 (t, *J* = 7.8 Hz, 2H), 1.75-1.65 (m, 1H), 1.54-1.52 (m, 2H), 0.93-0.92 (m, 6H). <sup>13</sup>C NMR (100 MHz, CDCl<sub>3</sub>) δ 188.18, 157.81, 151.96, 146.44, 142.68, 132.63, 121.96, 120.12, 112.75, 108.52, 56.72, 40.12, 37.70, 27.65, 22.27, 22.20.

### **General procedure for the synthesis of compounds 17 – 20**

To a suspension of NaH 60% in mineral oil (1 eq) in 0.2-0.6 mL of DMF, a solution of selected thiol (1 eq) in DMF (0.4-1 mL) was added dropwise. The reaction mixture was left stirring at this temperature for 1h. Then, 1-bromobutane (2 eq) was added and the mixture was left stirring overnight. The reaction was terminated adding ice (5 mL) and acidifying until pH=1. Organic phase was separated and the aqueous phase was further extracted with dichloromethane (3x5mL). All organic phases, once reunited, were dried with anhydrous sodium sulphate, concentrated in vacuo and the crude obtained was purified by column chromatography.

### **S-propyl 8-butoxy-7-methoxy-2-oxo-2H-chromene-3-carbothioate (17)**

Compound **17** was synthesized from **56** (40 mg, 0.45 mmol). Compound was eluted with petroleum ether: ethyl acetate (7:3), which afforded **17** as white powder (20 mg, 42%). <sup>1</sup>H NMR (400 MHz, CDCl<sub>3</sub>) δ 8.46 (s, 1H), 7.35 (d, *J* = 8.8 Hz, 1H), 6.93 (d, *J* = 8.8 Hz, 1H), 4.13 (t, *J* = 6.4 Hz, 2H), 3.97 (s, 3H), 3.00 (t, *J* = 7.3 Hz, 2H), 1.81 – 1.76 (m, 2H), 1.72 – 1.67 (m, 2H), 1.57 – 1.51 (m, 2H), 1.05 – 0.96 (m, 6H). <sup>13</sup>C NMR (100 MHz, CDCl<sub>3</sub>) δ 188.12, 158.29, 158.00, 148.96, 146.24, 135.17, 125.73, 119.84, 112.86, 109.36, 73.99, 56.51, 32.05, 31.31, 22.38, 18.93, 13.79, 13.55. MS [ESI+] *m/z* 351 [M+H]<sup>+</sup>, 373 [M+Na]<sup>+</sup>

### **S-cyclohexyl 8-butoxy-7-methoxy-2-oxo-2H-chromene-3-carbothioate (18)**

Compound **18** was synthesized from **57** (120 mg, 0.36 mmol). Compound was eluted with dichloromethane: methanol (9.9:0.1), which afforded **18** as yellow powder (25 mg, 18%). <sup>1</sup>H NMR (400 MHz, CDCl<sub>3</sub>) δ 8.41 (s, 1H), 7.33 (d, *J* = 8.6 Hz, 1H), 6.91 (d, *J* = 8.6 Hz, 1H), 4.11 (t, *J* = 6.6 Hz, 2H), 3.96 (s, 3H), 3.67-3.66 (m, 1H), 2.00 - 1.97 (m, 2H), 1.79 – 1.74 (m, 4H), 1.60 - 1.59 (m, 1H), 1.56 – 1.43 (m, 6H), 1.34 – 1.24 (m, 1H), 0.96 (t, *J* = 7.4 Hz, 3H). <sup>13</sup>C NMR (100 MHz, CDCl<sub>3</sub>) δ 187.86, 158.33, 157.98, 149.13, 146.18, 135.41, 125.67, 120.46, 113.10, 109.46, 74.18, 56.64, 42.59, 32.84, 32.20, 26.15, 25.75, 19.06, 13.90. MS [ESI+] *m/z* 391 [M+H]<sup>+</sup>, 413 [M+Na]<sup>+</sup>

### **S-hexyl 8-butoxy-7-methoxy-2-oxo-2H-chromene-3-carbothioate (19)**

Compound **19** was synthesized from **58** (200 mg, 0.59 mmol). Compound was eluted with dichloromethane: methanol (9.9:0.1), which afforded **19** as reddish powder (60 mg, 25%). <sup>1</sup>H NMR (400 MHz, CDCl<sub>3</sub>) δ 8.43 (s, 1H), 7.33 (d, *J* = 8.6 Hz, 1H), 6.91 (d, *J* = 8.6 Hz, 1H), 4.10 (t, *J* = 6.4 Hz, 2H), 3.95 (s, 3H), 2.98 (t, *J* = 7.4 Hz, 2H), 1.78-1.75 (m, 2H), 1.65-1.61 (m, 2H), 1.55-1.49 (m, 2H), 1.42-1.39 (m, 2H), 1.30-1.23 (m, 4H), 0.95 (t, *J* = 7.6 Hz, 3H), 0.86 (t, *J* = 6.6 Hz, 3H). <sup>13</sup>C NMR (100 MHz, CDCl<sub>3</sub>) δ 188.20, 158.26, 158.02, 148.98, 146.20, 135.20,

125.68, 119.88, 112.89, 109.33, 74.02, 56.49, 32.05, 31.31, 29.45, 28.87, 28.66, 22.47, 18.92, 13.97, 13.78.  
MS [ESI+] m/z 393 [M+H]<sup>+</sup>, 415 [M+Na]<sup>+</sup>

#### **S-isopentyl 8-butoxy-7-methoxy-2-oxo-2H-chromene-3-carbothioate (20)**

Compound **20** was synthesized from **59** (100 mg, 0.31 mmol). Compound was eluted with dichloromethane:methanol (9.8:0.2), which afforded **20** as yellow powder (29 mg, 25%). <sup>1</sup>H NMR (400 MHz, CDCl<sub>3</sub>) δ 8.45 (s, 1H), 7.35 (d, *J* = 8.4 Hz, 1H), 6.92 (d, *J* = 8.4 Hz, 1H), 4.12 (t, *J* = 6.6 Hz, 2H), 3.96 (s, 3H), 3.01 (t, *J* = 7.6 Hz, 2H), 1.80-1.71 (m, 3H), 1.56-1.51 (m, 4H), 0.99-0.92 (m, 9H). <sup>13</sup>C NMR (100 MHz, CDCl<sub>3</sub>) δ 188.25, 158.28, 158.03, 149.02, 146.19, 135.26, 125.66, 119.93, 112.94, 109.34, 74.06, 56.51, 37.73, 32.06, 29.66, 27.66, 27.59, 22.21, 18.93, 13.79. MS [ESI+] m/z 379 [M+H]<sup>+</sup>, 401 [M+Na]<sup>+</sup>

#### **(E)-4-methoxy-4-oxobut-2-enoic acid (60)**

To a solution of dimethyl fumarate (1 g, 6.94 mmol) in 45 mL of acetone, lithium hydroxide 1N (7 mL) was added dropwise by using a dropping funnel. The reaction mixture was left stirring at room temperature for 1h. To terminate the reaction, 60 mL of HCl 2N were added. Organic phase was separated and the aqueous phase was further extracted with ethyl acetate (3 x 40 mL). Organic phases, once reunited, were dried with anhydrous sodium sulphate, concentrated in vacuo and the crude obtained purified by column chromatography using ethyl acetate as mobile phase. **60** was obtained as white solid (520 mg, 58%). <sup>1</sup>H NMR (400 MHz, CD<sub>3</sub>OD) δ 6.48 (s, 2H), 3.49 (s, 3H). <sup>13</sup>C NMR (100 MHz, CD<sub>3</sub>OD) δ 168.09, 167.26, 135.74, 134.38, 53.06.

#### **(Z)-5-(4-hydroxybenzylidene)thiazolidine-2,4-dione (61)**

Thiazolidine-2,4-dione (625 mg, 5.12 mmol), piperidine (0.13 mL, 1.28 mmol) and benzoic acid (156 mg, 1.28 mmol) were added to a solution of 4-hydroxybenzaldehyde (600 mg, 5.12 mmol) in 25 mL of toluene. The reaction mixture was left stirring at reflux for 6h. Once cooled to room temperature, the obtained precipitate was filtered and washed with water and toluene. The precipitate was dried, to give **61** as yellow powder (1.04 g, 92%). <sup>1</sup>H NMR (400 MHz, DMSO-*d*<sub>6</sub>) δ 12.38 (br s, 1H), 10.23 (br s, 1H), 7.70 (s, 1H), 7.45 (d, *J* = 8.4 Hz, 2H), 6.91 (d, *J* = 8.4 Hz, 2H). <sup>13</sup>C NMR (100 MHz, DMSO-*d*<sub>6</sub>) δ 181.18, 175.80, 159.08, 132.18 (2C), 131.30 (2C), 127.49, 125.51, 117.00.

#### **5-(4-hydroxybenzyl)thiazolidine-2,4-dione (62)**

2.5 mL of cobalt (II) chloride-dimethylglyoxime complex solution (42 mg CoCl<sub>2</sub>·6H<sub>2</sub>O, 250 mg DMG in 5.0 mL DMF) was added to a suspension of **61** (1.51 g, 6.83 mmol) in water (7.26 mL), methanol (5.1 mL) and NaOH 1M (5.79 mL) and this mixture was left stirring at room temperature for 15 min. Sodium borohydride (646 g, 17.08 mmol) under nitrogen atmosphere was added. Subsequently, HCl 6N was added until reach pH=7 and the reaction mixture left stirring at room temperature for 3h. HCl 10% was further added to terminate the reaction and the formed precipitate was filtered and washed with water. Once dried, **62** was obtained as white solid (820 mg, 54%). <sup>1</sup>H NMR (400 MHz, DMSO-*d*<sub>6</sub>) δ 11.97 (br s, 1H), 9.32 (br s, 1H), 7.02 (d, *J* = 8.4 Hz,

2H), 6.68 (d,  $J = 8.4$  Hz, 2H), 4.84 – 4.80 (m, 1H), 3.27 – 3.23 (m, 1H), 3.02 – 2.96 (m, 1H).  $^{13}\text{C}$  NMR (100 MHz, DMSO- $d_6$ )  $\delta$  176.63, 172.62, 157.27, 131.14 (2C), 127.66, 116.07 (2C), 54.14, 37.33.

#### **4-((2,4-dioxothiazolidin-5-yl)methyl)phenyl methyl fumarate (21)**

To a solution of **60** (100 mg, 0.77 mmol) in 1.2 mL of acetonitrile at 0°C under nitrogen atmosphere, HOBT (135 mg, 1.00 mmol) and EDC (191 mg, 1.00 mmol) were added. Reaction mixture was left stirring at this temperature for 30 min. After confirming the complete conversion of starting material in activated complex, intermediate **62** (240 mg, 1.08 mmol) was added and the reaction mixture left stirring overnight at room temperature. After evaporation of the solvent, the crude was purified through column chromatography using dichloromethane: methanol (9.75:0.25). **21** was obtained as white crystal powder (62 mg, 24%).  $^1\text{H}$  NMR (400 MHz,  $\text{CDCl}_3$ )  $\delta$  8.32 (br s, 1H), 7.23 (d,  $J = 4.6$  Hz, 2H), 7.11 (d,  $J = 4.6$  Hz, 1H), 7.01 (s, 2H), 4.51-4.48 (m, 1H), 3.82 (s, 3H), 3.52-3.48 (m, 1H), 3.17-3.11 (m, 1H).  $^{13}\text{C}$  NMR (100 MHz,  $\text{CDCl}_3$ )  $\delta$  173.81, 170.70, 165.23, 163.36, 149.89, 135.14, 133.83, 132.97, 130.54, 121.86, 53.24, 52.63, 38.12. MS [ESI-]  $m/z$  334 [M-H] $^-$

#### **(Z)-5-(4-nitrobenzylidene)thiazolidine-2,4-dione (63)**

Thiazolidine-2,4-dione (773 mg, 6.60 mmol), piperidine (0.16 mL, 1.65 mmol) and benzoic acid (201 mg, 1.65 mmol) were added to a solution of 4-nitrobenzaldehyde (1 g, 6.60 mmol) in 37 mL of toluene. The reaction mixture was left stirring at reflux for 6h. Once cooled to room temperature, the obtained precipitate was filtered and washed with water and toluene. The precipitate was dried, giving **63** as yellow powder (1.09 g, 66%).  $^1\text{H}$  NMR (400 MHz, DMSO- $d_6$ )  $\delta$  12.78 (br s, 1H), 8.32 (d,  $J = 11.2$  Hz, 2H), 7.88 (s, 1H), 7.84 (d,  $J = 11.2$  Hz, 2H).  $^{13}\text{C}$  NMR (100 MHz, DMSO- $d_6$ )  $\delta$  167.15, 167.15, 147.59, 139.52, 131.03 (2C), 129.20, 128.18, 124.38 (2C).

#### **5-(4-aminobenzyl)thiazolidine-2,4-dione (64)**

2.50 mL of cobalt (II) chloride-dimethylglyoxime complex solution (42 mg  $\text{CoCl}_2 \cdot 6\text{H}_2\text{O}$ , 250 mg DMG in 5.0 mL DMF) were added to a suspension of **63** (1.07 g, 4.26 mmol) in water (4.5 mL), methanol (3.2 mL) and NaOH 1M (3.6 mL) and this mixture was left stirring at room temperature for 15 min. Sodium borohydride (726 mg, 19.19 mmol) under nitrogen atmosphere was added. Subsequently, HCl 6N was added until reach pH=7 and the reaction mixture left stirring at room temperature for 3h. HCl 10% was further added to terminate the reaction and the formed precipitate was filtered and washed with water. Once dried, **64** was obtained as yellow powder (524 mg, 55%).  $^1\text{H}$  NMR (400 MHz, DMSO- $d_6$ )  $\delta$  6.89 (d,  $J = 8$  Hz, 2H), 6.51 (d,  $J = 8$  Hz, 2H) 4.78 – 4.76 (m, 1H), 3.21 – 3.17 (m, 1H), 2.94 – 2.89 (m, 1H).  $^{13}\text{C}$  NMR (100 MHz, DMSO- $d_6$ )  $\delta$  175.67, 171.72, 146.89, 129.62 (2C), 123.72, 114.06 (2C), 53.41, 36.48.

#### **(E)-3-(3,4-dimethoxyphenyl)acrylic acid (65)**

3,4-dimethoxybenzaldehyde (500 mg, 3.00 mmol) and malonic acid (338 mg, 3.25 mmol) were added to a solution of aniline (0.05 mL) and pyridine (0.37 mL, 4.63 mmol) in 2 mL of toluene. The reaction mixture was

left stirring at reflux for 3h. Thus, HCl 3N was added until pH=1 to terminate the reaction and the precipitate formed was filtered and washed with HCl 3N. Once dried, **65** was obtained as yellowish powder (530 mg, 85%). <sup>1</sup>H NMR (400 MHz, CDCl<sub>3</sub>) δ 10.09 (br s, 1H), 7.97 (d, *J* = 16 Hz, 1H), 7.37 – 7.22 (m, 2H), 7.12 (s, 1H), 6.56 (d, *J* = 16 Hz, 1H), 4.15 (s, 6H). <sup>13</sup>C NMR (100 MHz, CDCl<sub>3</sub>) δ 172.58, 151.50, 149.24, 146.93, 127.02, 123.09, 114.91, 111.03, 109.79, 55.96, 55.88.

#### General procedure for the synthesis of compounds **66** and **67**

To a solution of **65** (1 eq) in dimethylformamide (1-2 mL) at 0°C, HOBT (1.3 eq) and EDC (1.3 eq) were added. Reaction mixture was left stirring at this temperature for 30 min. After confirming the complete conversion of starting material in activated complex, triethylamine (1.3 eq) and **62** or **64** (1.3 eq) were added and the reaction mixture left stirring for 36h. After evaporation of the solvent, the crude was purified through column chromatography.

#### **4-((2,4-dioxothiazolidin-5-yl)methyl)phenyl (E)-3-(3,4-dimethoxyphenyl)acrylate (66)**

Compound **66** was synthesized from **65** (460 mg, 2.24 mmol) and **62** (650 mg, 2.91 mmol). Compound was eluted with dichloromethane: methanol (9.8:0.2), which afforded **66** as white solid (230 mg, 25%). <sup>1</sup>H NMR (400 MHz, DMSO-*d*<sub>6</sub>) δ 12.08 (br s, 1H), 7.77 (d, *J* = 15.8 Hz, 1H), 7.44 (s, 1H), 7.33 – 7.29 (m, 3H), 7.14 (d, *J* = 6.8 Hz, 1H), 7.01 (d, *J* = 8 Hz, 1H), 6.78 (d, *J* = 15.8 Hz, 1H), 4.95 – 4.92 (m, 1H), 3.81 (s, 3H), 3.80 (s, 3H), 3.41 – 3.33 (m, 1H), 3.18 – 3.15 (m, 1H). <sup>13</sup>C NMR (100 MHz, DMSO-*d*<sub>6</sub>) δ 175.84, 171.74, 165.35, 151.60, 149.81, 149.26, 146.89, 134.44, 130.47 (2C), 126.91, 123.66, 121.96 (2C), 114.72, 111.81, 110.86, 55.89, 55.82, 52.78, 36.73.

#### **(E)-3-(3,4-dimethoxyphenyl)-N-(4-((2,4-dioxothiazolidin-5-yl)methyl)phenyl)acrylamide (67)**

Compound **67** was synthesized from **65** (145 mg, 0.70 mmol) and **64** (201 mg, 0.91 mmol). Compound was eluted with dichloromethane: methanol (9.8:0.2), which afforded **67** as yellowish powder (130 mg, 45%). <sup>1</sup>H NMR (400 MHz, DMSO-*d*<sub>6</sub>) δ 10.09 (br s, 1H), 7.60 (d, *J* = 8.4 Hz, 2H), 7.49 (d, *J* = 15.4 Hz, 1H), 7.17 – 7.14 (m, 4H), 6.97 (d, *J* = 8.4 Hz, 1H), 6.66 (d, *J* = 15.4, 1H), 4.86 – 4.83 (m, 1H), 3.79 (s, 3H), 3.76 (s, 3H), 3.33 – 3.29 (m, 1H), 3.07 – 3.05 (m, 1H). <sup>13</sup>C NMR (100 MHz, DMSO-*d*<sub>6</sub>) δ 175.81, 171.71, 163.67, 150.25, 148.79, 140.13, 138.24, 131.37, 129.48 (2C), 127.33, 121.66, 119.67, 118.95 (2C), 111.62, 109.84, 55.44, 55.28, 52.86, 36.59.

#### General procedure for the synthesis of compounds **22** and **24**

A solution of **66** or **67** (1 eq) in 0.15-0.20 mL of anhydrous dichloromethane was cooled at 0°C. Boron tribromide 1M in dichloromethane (2.5 eq) was added to the solution and the reaction was left stirring at the same temperature until completion. 5 mL of cold water were added to terminate the reaction and the mixture extracted with ethyl acetate (3 x 4 mL). Organic phases, once reunited, were dried with anhydrous sodium sulphate, concentrated in vacuo and the crude obtained purified by column chromatography using dichloromethane: methanol as mobile phase.

#### **4-((2,4-dioxothiazolidin-5-yl)methyl)phenyl (E)-3-(3,4-dihydroxyphenyl)acrylate (22)**

Compound **22** was synthesized from **66** (110 mg, 0.27 mmol). Compound was eluted with dichloromethane: methanol (9.7:0.3), which afforded **22** as white solid (16 mg, 16%). <sup>1</sup>H NMR (400 MHz, CD<sub>3</sub>OD) δ 7.71 (d, *J* = 16 Hz, 1H), 7.31 (d, *J* = 8 Hz, 2H), 7.11 – 7.08 (m, 3H), 7.00 (d, *J* = 10 Hz 1H), 6.79 (d, *J* = 8.4, 1H), 6.44 (d, *J* = 16 Hz, 1H), 4.75 – 4.72 (m, 1H), 3.45 – 3.44 (m, 1H), 3.19 – 3.16 (m, 1H). <sup>13</sup>C NMR (100 MHz, CD<sub>3</sub>OD) δ 177.89, 173.92, 168.07, 152.17, 150.55, 149.26, 147.42, 135.95, 131.99 (2C), 128.06, 123.89, 123.41 (2C), 117.07, 115.86, 114.65, 54.99, 39.10. MS [ESI+] *m/z* 408 [M+Na]<sup>+</sup>. MS [ESI-] *m/z* 384 [M-H]<sup>-</sup>

#### **(E)-3-(3,4-dihydroxyphenyl)-N-(4-((2,4-dioxothiazolidin-5-yl)methyl)phenyl)acrylamide (24)**

Compound **24** was synthesized from **67** (88 mg, 0.21 mmol). Compound was eluted with dichloromethane: methanol (9.5:0.5), which afforded **24** as yellow powder (55 mg, 67%). <sup>1</sup>H NMR (400 MHz, CD<sub>3</sub>OD) δ 7.56 (d, *J* = 8.6 Hz, 2H), 7.47 (d, *J* = 15.6 Hz, 1H), 7.18 (d, *J* = 8.6 Hz, 2H), 7.02 (s, 1H), 6.91 (d, *J* = 8.5 Hz, 1H), 6.75 (d, *J* = 8.5 Hz, 1H), 6.50 (d, *J* = 15.6 Hz, 1H), 4.69 – 4.65 (m, 1H), 3.40 – 3.35 (m, 1H), 3.11 – 3.05 (m, 1H). <sup>13</sup>C NMR (100 MHz, CD<sub>3</sub>OD) δ 177.30, 173.37, 167.22, 148.90, 146.63, 143.34, 139.20, 133.39, 130.78 (2C), 128.11, 122.29, 121.11, 118.51, 116.36 (2C), 115.03, 54.48, 38.51. MS [ESI+] *m/z* 385 [M+H]<sup>+</sup>

#### **General procedure for the synthesis of compounds 23 and 25**

To a solution of ferulic acid (1 eq) in dimethylformamide (1-2 mL) at 0°C, HOBt (1.3 eq) and EDC (1.3 eq) were added. Reaction mixture was left stirring at this temperature for 30 min. After confirming the complete conversion of starting material in activated complex, triethylamine (1.3 eq) and **62** or **64** (1.3 eq) was added and the reaction mixture left stirring for 48h. After evaporation of the solvent, the crude was purified through column chromatography.

#### **4-((2,4-dioxothiazolidin-5-yl)methyl)phenyl (E)-3-(4-hydroxy-3-methoxyphenyl)acrylate (23)**

Compound **23** was synthesized from ferulic acid (100 mg, 0.52 mmol) and **62** (151 mg, 0.68 mmol). Compound was eluted with dichloromethane: methanol (9.9:0.1), which afforded **23** as white crystal powder (21 mg, 10%). <sup>1</sup>H NMR (400 MHz, DMSO-*d*<sub>6</sub>) δ 12.02 (br s, 1H), 9.66 (br s, 1H), 7.71 (d, *J* = 15.6 Hz, 1H), 7.38 (s, 1H), 7.27 (d, *J* = 8 Hz, 2H), 7.14 (d, *J* = 9 Hz, 1H), 7.11 (d, *J* = 8 Hz, 2H), 6.79 (d, *J* = 9 Hz, 1H), 6.66 (d, *J* = 15.6 Hz, 1H), 4.91 – 4.89 (m, 1H), 3.80 (s, 3H), 3.40 – 3.36 (m, 1H), 3.16 – 3.13 (m, 1H). <sup>13</sup>C NMR (100 MHz, DMSO-*d*<sub>6</sub>) δ 176.07, 171.99, 165.71, 150.26, 150.08, 148.44, 147.50, 134.14, 130.70 (2C), 125.88, 124.10, 122.23 (2C), 116.01, 113.82, 111.94, 56.18, 53.04, 36.96. MS [ESI+] *m/z* 422 [M+Na]<sup>+</sup>

#### **(E)-N-(4-((2,4-dioxothiazolidin-5-yl)methyl)phenyl)-3-(4-hydroxy-3-methoxyphenyl)acrylamide (25)**

Compound **25** was synthesized from ferulic acid (350 mg, 1.80 mmol) and **64** (520 mg, 2.34 mmol). Compound was eluted with dichloromethane: methanol (9.7:0.3), which afforded **25** as yellow orange powder (150 mg, 21%). <sup>1</sup>H NMR (400 MHz, CD<sub>3</sub>OD) δ 7.62 – 7.56 (m, 3H), 7.24 (d, *J* = 8.4 Hz, 2H), 7.17 (s, 1H), 7.09 (d, *J* = 8 Hz, 1H), 6.82 (d, *J* = 8 Hz, 1H), 6.61 (d, *J* = 15.6, 1H), 4.74 – 4.71 (m, 1H), 3.90 (s, 3H), 3.45 – 3.41 (m, 1H), 3.17 –



3.11 (m, 1H). <sup>13</sup>C NMR (100 MHz, CD<sub>3</sub>OD) δ 177.45, 173.46, 167.25, 150.15, 149.34, 143.30, 139.35, 133.58, 130.94 (2C), 128.22, 123.45, 121.23, 119.02, 116.56 (2C), 111.72, 56.41, 54.61, 38.66. MS [ESI-] m/z 397.04 [M-H]<sup>-</sup>

### **3-(3,4-bis((tert-butyldimethylsilyl)oxy)phenyl)propanoic acid (68)**

To a solution of 3-(3,4-dihydroxyphenyl)propanoic acid (400 mg, 2.20 mmol) in DMF (1.6 mL), TBDMS-Cl (1.3 g, 8.8 mmol) and imidazole (750 mg, 11 mmol) were added and the solution stirred for 1h at room temperature. Solvent was evaporated in vacuo and crude obtained was purified through column chromatography using petroleum ether: ethyl acetate (8:2). **68** was obtained as colourless oil (370 mg, 41%). <sup>1</sup>H NMR (400 MHz, CDCl<sub>3</sub>) δ 6.76 (d, *J* = 8 Hz, 1H), 6.69 (s, 1H), 6.65 (d, *J* = 8 Hz, 1H), 2.86–2.84 (m, 2H), 2.66–2.63 (m, 2H), 1.00 (s, 18H), 0.20 (s, 12H).

### **S-Propyl 3-(3,4-Bis((tert-butyldimethylsilyl)oxy)phenyl)-propanethioate (69)**

To an ice-cooled solution of **68** (370 mg, 0.9 mmol) in dry dichloromethane (2 mL) HOBt (158 mg, 1.17 mmol) and EDC (224 mg, 1.17 mmol) were added. The reaction mixture was stirred for 10 min, followed by addition of 1-propanethiol (0.33 mL, 3.6 mmol). Stirring was then continued at room temperature overnight, and the reaction worked up by filtration and evaporation. The crude was purified by column chromatography using petroleum ether: ethyl acetate (9.7:0.3) as mobile phase. **69** was obtained as orange oil (250 mg, 59%). <sup>1</sup>H NMR (400 MHz, CDCl<sub>3</sub>) δ 6.72 (d, *J* = 8 Hz, 1H), 6.64 (s, 1H), 6.61 (d, *J* = 8 Hz, 1H), 2.86–2.79 (m, 6H), 1.60–1.55 (m, 2H), 0.99–0.93 (m, 18H + 3H), 0.18 (s, 12H). <sup>13</sup>C NMR (100 MHz, CDCl<sub>3</sub>) δ 198.86, 146.74, 145.35, 133.35, 121.33, 121.25, 121.06, 45.91, 30.94, 30.87, 26.07 (6C), 23.07, 18.54 (2 C), 13.45, –3.98 (4 C).

### **S-Propyl 3-(3,4-Dihydroxyphenyl)propanethioate (VI)**

To a solution of **69** (250 mg, 0.53 mmol) in THF (2 mL) was added TBAF 1.0 M in THF (2.65 mL, 2.65 mmol) and stirring was continued at room temperature. After 20–30 min, the reaction was quenched by addition of saturated aqueous NH<sub>4</sub>Cl solution; the aqueous phase was extracted with EtOAc (3 × 10 mL), and the combined organic layer was dried over Na<sub>2</sub>SO<sub>4</sub>. Following evaporation of the solvent, the residue was purified by column chromatography using petroleum ether: ethyl acetate (5.5:4.5) as mobile phase. **II** was obtained as a waxy oil (110 mg, 87%). <sup>1</sup>H NMR (400 MHz, CDCl<sub>3</sub>) δ 6.76 (d, *J* = 8.4 Hz, 1H), 6.68 (d, *J* = 2 Hz 1H), 6.59 (dd, <sup>1</sup>*J* = 8.4, <sup>2</sup>*J* = 2 Hz 1H), 2.86–2.81 (m, 6H), 1.58–1.57 (m, 2H), 0.94 (t, *J* = 7.2 Hz, 3H). <sup>13</sup>C NMR (100 MHz, CDCl<sub>3</sub>) δ 200.23, 143.60, 142.07, 132.89, 120.61, 115.44, 115.39, 45.71, 30.92, 30.88, 22.82, 13.27. MS [ESI+] m/z 263 [M + Na]<sup>+</sup>.

### **S-Propyl 3-(3,4-Dimethoxyphenyl) propanethioate (26)**

To a solution of compound **VI** (110 mg, 0.46 mmol) in DMF (1.80 mL), potassium carbonate (222.5 mg, 1.61 mmol) and methyl iodide dropwise (0.10 mL, 1.61 mmol) were added. The reaction mixture was left stirring at room temperature overnight. The reaction was quenched by adding 3 mL of water and the mixture obtained was further extracted with diethyl ether (2 x 5 mL). Organic phases were collected, reunited, dried

with anhydrous sodium sulphate and solvent was evaporated under vacuum. The crude oil was purified by column chromatography on silica gel using petroleum ether/ethyl acetate (8/2) as mobile phase. **26** was obtained as colourless oil (110 mg, 89%). <sup>1</sup>H NMR (400 MHz, CDCl<sub>3</sub>) δ 6.74 (d, *J* = 8 Hz, 1H), 6.69–6.67 (m, 2H), 3.82 (s, 3H), 3.80 (s, 3H), 2.89 (t, *J* = 8 Hz, 2H), 2.83–2.77 (m, 4H), 1.59–1.50 (m, 2H), 0.91 (t, *J* = 8 Hz, 3H). <sup>13</sup>C NMR (100 MHz, CDCl<sub>3</sub>) δ 198.79, 148.98, 147.61, 132.83, 120.27, 111.77, 111.41, 55.98, 55.89, 45.88, 31.23, 30.87, 23.06, 13.39. MS [ESI+] *m/z* 291 [M+Na]<sup>+</sup>.

### **(3-chloropropyl)(trityl)sulfane (70)**

A mixture of trityl chloride (1.51 g, 5.42 mmol) and 3-chloropropane-1-thiol (0.26 mL, 2.71 mmol) in 2 mL of DMF was placed in a microwave (60°C, 250 psi, 100W) for 15 min. The solvent was removed under reduced pressure and the product obtained was purified by column chromatography using petroleum ether: ethyl acetate (9.5:0.5) as mobile phase. **70** was obtained as white solid (947 mg, 99%). <sup>1</sup>H NMR (400 Hz, CDCl<sub>3</sub>) δ 7.42 (d, *J* = 8 Hz, 6H), 7.28 (d, *J* = 8 Hz, 6H), 7.24–7.19 (m, 3H) 3.46 (t, *J* = 6 Hz, 2H), 2.33 (t, *J* = 6 Hz, 2H), 1.77–1.70 (m, 2H). <sup>13</sup>C NMR (100 Hz, CDCl<sub>3</sub>) δ 144.84 (3C), 129.69 (6C), 128.03 (6C), 126.80 (3C), 66.81, 43.80, 31.63, 29.17.

### **3,5-dimethyl-*N*-(3-(tritylthio)propyl)adamantan-1-amine (71)**

To a solution of memantine free base (402 mg, 2.24 mmol) in 4 mL of DMF, potassium carbonate (705 mg, 5.10 mmol), **70** (720 mg, 2.04 mmol) and potassium iodide (cat.) were added and the reaction placed in a microwave for 2.5 h (75°C, 250 psi, 80W). The solvent was removed under reduced pressure and the product obtained was purified by column chromatography using dichloromethane: methanol: aqueous ammonia solution 30% (9.5:0.5:0.015) as mobile phase. **71** was obtained as yellowish oil (940 mg, 85%). <sup>1</sup>H NMR (400 Hz, CDCl<sub>3</sub>) δ 7.39 (d, *J* = 8 Hz, 6H), 7.26 (t, *J* = 8 Hz, 6H), 7.20–7.16 (m, 3H), 2.52 (t, *J* = 6 Hz, 2H), 2.18 (t, *J* = 6 Hz, 2H), 2.11–2.10 (m, 1H), 1.67–1.63 (m, 2H), 1.48 (s, 2H), 1.31–1.22 (m, 8H), 1.12–1.05 (m, 2H), 0.82 (s, 6H). <sup>13</sup>C NMR (100 Hz, CDCl<sub>3</sub>) δ 144.91 (3C), 129.58 (6C), 127.81 (6C), 126.53 (3C), 50.90, 48.73, 48.69, 42.96 (2C), 41.01, 39.77, 32.35, 30.30 (4C), 30.22 (2C), 29.93.

### **3-((3,5-dimethyladamantan-1-yl)amino)propane-1-thiol (72)**

Trifluoroacetic acid (4.8 mL) and triethyl silane (0.17 mL, 1.09 mmol) were added to a solution of **71** (270 mg, 0.55 mmol) in 13 mL of dichloromethane at 0°C and stirred for 5 min at this temperature. The solvent was then evaporated under reduced pressure and the product obtained was purified by column chromatography using dichloromethane: methanol: aqueous ammonia solution 30% (9.5:0.5:0.04) as mobile phase. **72** was obtained as yellowish oil (100 mg, 72%). <sup>1</sup>H NMR (400 Hz, CDCl<sub>3</sub>) δ 2.66 (t, *J* = 7.2 Hz, 2H), 2.60 (t, *J* = 7.2 Hz, 2H), 2.04–2.03 (m, 1H), 1.79–1.73 (m, 2H), 1.41 (s, 2H), 1.24–1.15 (m, 8H), 1.03–1.00 (m, 2H), 0.75 (s, 6H). <sup>13</sup>C NMR (100 Hz, CDCl<sub>3</sub>) δ 52.70, 50.83, 48.60, 42.88, 40.90, 39.17, 39.02, 36.86, 32.31 (2C), 30.25 (4C), 30.13.

### General procedure for synthesis of compound 29 and 30

To a solution of **65** or 3-(3,4-dimethoxyphenyl)propanoic acid (1 eq) in dichloromethane (1-2 ml) at 0°C, HOBT (1.3 eq) and EDC (1.3 eq) were added. Reaction mixture was left stirring at this temperature for 30 min. After confirming the complete conversion of starting material in activated complex, **72** (1.3 eq) was added and the reaction mixture left stirring for 18h. After evaporation of the solvent, the crude was purified through column chromatography.

#### **S-(3-((3,5-dimethyladamantan-1-yl)amino)propyl) (E)-3-(3,4-dimethoxyphenyl)prop-2-enethioate (29)**

Compound **29** was synthesized from **72** (109 mg, 0.43 mmol) and **65** (69 mg, 0.33 mmol). Compound was eluted with dichloromethane: methanol: aqueous ammonia solution 30% (9.5:0.5:0.045), which afforded **28** as colourless oil (90 mg, 62%). <sup>1</sup>H NMR (400 Hz, CDCl<sub>3</sub>) δ 7.53 (d, *J* = 15.6 Hz, 2H), 7.10 (d, *J* = 8 Hz, 2H), 7.03 (s, 1H), 6.84 (d, *J* = 8 Hz, 2H), 6.57 (d, *J* = 15.6 Hz, 2H), 3.89 (s, 6H), 3.06 (t, *J* = 7.2 Hz, 2H), 2.66 (t, *J* = 7.2 Hz, 2H), 2.11-2.10 (m, 1H), 1.83-1.77 (m, 2H), 1.46 (s, 2H), 1.30-1.21 (m, 8H), 1.10-1.06 (m, 2H), 0.81 (s, 6H). <sup>13</sup>C NMR (100 Hz, CDCl<sub>3</sub>) δ 189.66, 151.37, 149.23, 140.39, 127.01, 123.19, 122.90, 111.06, 109.70, 55.94, 55.88, 52.62, 50.89, 48.69, 42.94 (2C), 40.98, 39.30, 32.35 (2C), 30.84, 30.27, 30.22 (2C), 29.65, 26.73. MS [ESI+] *m/z* 444 [M+H]<sup>+</sup>.

#### **S-(3-((3,5-dimethyladamantan-1-yl)amino)propyl) 3-(3,4-dimethoxyphenyl)propanethioate (30)**

Compound **30** was synthesized from **72** (150 mg, 0.59 mmol) and 3-(3,4-dimethoxyphenyl)propanoic acid (95 mg, 0.45 mmol). Compound was eluted with dichloromethane: methanol: aqueous ammonia solution 30% (9.5:0.5:0.045), which afforded **30** as colourless oil (92 mg, 46%). <sup>1</sup>H NMR (400 Hz, CDCl<sub>3</sub>) δ 6.77 (d, *J* = 8 Hz, 1H), 6.71-6.69 (m, 2H), 3.84 (s, 3H), 3.83 (s, 3H), 2.92-2.88 (m, 4H), 2.84-2.80 (m, 2H), 2.64-2.61 (m, 2H), 2.12-2.11 (m, 1H), 1.75-1.72 (m, 2H), 1.47 (s, 2H), 1.28-1.23 (m, 8H), 1.11-1.08 (m, 2H), 0.82 (s, 6H). <sup>13</sup>C NMR (100 Hz, CDCl<sub>3</sub>) δ 198.92, 148.98, 147.62, 132.74, 120.24, 111.72, 111.40, 56.00, 55.94, 53.04, 50.96, 48.65, 45.87, 43.02 (2C), 40.95, 39.37, 32.50 (2C), 31.23, 30.71, 30.38, 30.32 (3C), 26.86. MS [ESI+] *m/z* 446 [M+H]<sup>+</sup>.

### General procedure for synthesis of compound 27 and 28

A solution of **29** or **30** (1 eq) in 0.15-0.20 mL of anhydrous dichloromethane was cooled at 0°C. Boron tribromide 1M in dichloromethane (2.5 eq) was added to the solution and the reaction was left stirring at the same temperature until completion. Cold water (5 mL) was added to terminate the reaction and the mixture extracted with ethyl acetate (3 x 4 mL). Organic phases, once reunited, were dried with anhydrous sodium sulphate, concentrated in vacuo and the crude obtained purified by column chromatography using dichloromethane: methanol as mobile phase.

#### **S-(3-((3,5-dimethyladamantan-1-yl)amino)propyl) (E)-3-(3,4-dihydroxyphenyl)prop-2-enethioate (27)**

Compound **27** was synthesized from **29** (110 mg, 0.27 mmol). Compound was eluted with dichloromethane: methanol: aqueous ammonia solution 30% (9.2:0.8:0.05), which afforded **27** as yellow powder (16 mg, 30%).

<sup>1</sup>H NMR (400 Hz, CD<sub>3</sub>OD) δ 7.50 (d, *J* = 15.6 Hz, 1H), 7.05 (s, 1H), 6.98 (d, *J* = 8 Hz, 1H), 6.78 (d, *J* = 8 Hz, 1H), 6.61 (d, *J* = 15.6 Hz, 1H), 3.10-3.02 (m, 4H), 2.26-2.24 (m, 1H), 2.04- 1.97 (m, 2H), 1.76 (s, 2H), 1.59-1.50 (m, 4H), 1.42-1.38 (m, 4H), 1.22-1.19 (m, 2H), 0.90 (s, 6H). <sup>13</sup>C NMR (100 Hz, CD<sub>3</sub>OD) δ 191.27, 150.19, 146.93, 143.30, 127.15, 123.75, 122.18, 116.64, 115.43, 60.23, 50.78, 45.29, 42.82 (2C), 39.72, 37.99, 33.63 (4C), 31.22, 30.12, 28.43, 26.35. MS [ESI+] *m/z* 416 [M+H]<sup>+</sup>.

### **S-(3-((3,5-dimethyladamantan-1-yl)amino)propyl) 3-(3,4-dihydroxyphenyl)propanethioate (28)**

Compound **28** was synthesized from **30** (70 mg, 0.16 mmol). Compound was eluted with dichloromethane: methanol: aqueous ammonia solution 30% (9.2:0.8:0.05), which afforded **28** as dark yellow powder (13 mg, 19%). <sup>1</sup>H NMR (400 Hz, CDCl<sub>3</sub>) δ 6.83 (d, *J* = 8 Hz, 1H), 6.59-6.56 (m, 2H), 2.96-2.88 (m, 4H), 2.78 (t, *J* = 8 Hz, 4H), 2.22-2.21 (m, 1H), 1.77- 1.74 (m, 1H), 1.63 (s, 2H), 1.35-1.26 (m, 8H), 1.21-1.14 (m, 2H), 0.88 (s, 6H). <sup>13</sup>C NMR (100 Hz, CDCl<sub>3</sub>) δ 199.30, 144.42, 119.73, 116.29, 115.64, 115.48, 115.01, 60.47, 58.51, 50.68, 47.57, 47.39, 46.24, 42.78, 42.73, 39.86, 39.20, 36.73, 32.57 (2C), 30.22 (2C), 30.17, 26.85. MS [ESI+] *m/z* 418 [M+H]<sup>+</sup>.

### **Cyclic voltammetry study**

Electrochemical experiments were carried out in an airtight single-compartment glass cell described elsewhere<sup>314</sup> by using glassy carbon (GC) as working electrode, a platinum spiral as counter electrode and a silver spiral surface modified by silver chloride as a reference electrode. For the measurements in aqueous solutions a 2M phosphate buffer was used as electrolyte solution. All the *E*<sub>1/2</sub> potentials have been directly obtained from CV curves as averages of the cathodic and anodic peak potentials for one-electron reversible peaks and by digital simulation for those processes either closely spaced in multielectron voltammetric peaks or for the irreversible electron transfers. The *E*<sub>1/2</sub> values are referred to an Ag/AgCl. The GC working electrode was a 3 mm diameter disk that was mechanically polished by an alumina slurry in water. Voltammograms were recorded with a Biologic potentiostat model SP-300. Digital simulations of the cyclic voltammetric curves were carried out either by Antigona or DigiSim 3.0.

## **4.2 BIOLOGY**

### **Sample preparation for Aβ<sub>42</sub> self-aggregation**

1,1,1,3,3,3- Hexafluoro-2-propanol (HFIP)-pretreated Aβ<sub>42</sub> samples (Bachem AG, Switzerland) were resolubilized with a CH<sub>3</sub>CN/0.3 mM Na<sub>2</sub>CO<sub>3</sub>/250 mM NaOH (48.4:48.4:3.2) mixture to have a stable stock solution ([Aβ<sub>42</sub>] = 500 μM).<sup>315, 316</sup> Tested inhibitors were dissolved in MeOH and diluted in the assay buffer. Experiments were performed by incubating the peptide diluted in 10 mM phosphate buffer (pH 8.0) containing 10 mM NaCl at 30 °C (Thermomixer Comfort, Eppendorf, Italy) for 24 h (final Aβ concentration = 50 μM) with and without inhibitor.

### **Inhibition of A $\beta$ <sub>42</sub> self-aggregation by ThT**

Inhibition studies were performed by incubating A $\beta$ <sub>42</sub> samples in the assay conditions reported above, with and without tested inhibitors. Inhibitors were first screened at 50  $\mu$ M in a 1:1 ratio with A $\beta$ <sub>42</sub>. To quantify amyloid fibril formation, the ThT fluorescence method was used.<sup>317</sup> After incubation, samples were diluted to a final volume of 2.0 mL with 50 mM glycine-NaOH buffer (pH = 8.5) containing 1.5  $\mu$ M ThT. A 300 s-time scan of fluorescence intensity was carried out ( $\lambda_{exc}$  = 446 nm;  $\lambda_{em}$  = 490 nm), and values at plateau were averaged after subtracting the background fluorescence of 1.5  $\mu$ M ThT solution. Blanks containing inhibitor and ThT were also prepared and evaluated to account for quenching and fluorescence properties. The fluorescence intensities were compared and the % inhibition was calculated. For selected compounds the IC<sub>50</sub> value was also determined. To this aim four increasing concentrations were tested. IC<sub>50</sub> value was obtained from the % inhibition vs log[inhibitor] plot.

### **Mass spectrometry study**

**Sample preparation.** Studies were performed by incubating A $\beta$ <sub>42</sub> samples under the assay conditions used for the ThT assay, with and without **4** at 50  $\mu$ M (**4**/A $\beta$ <sub>42</sub> = 1/1). Samples were incubated at 30°C for 24h. At selected time points (0, 1, 3, 6 and 24 h) 5  $\mu$ L-aliquots of mixture were collected, diluted to 25  $\mu$ L with reserpine 20  $\mu$ g/mL (IS) in H<sub>2</sub>O/MeOH (50/50; v/v) and subjected to LC-MS analysis. Experiments were performed in duplicate.

**LC-MS analysis.** LC-MS analyses were performed by an Agilent 1200 Series (Walbronn, Germany) coupled with an ESI-Q-ToF mass spectrometer equipped with a Z-spray ion source (Micromass, Manchester, UK). Flow injection analyses were performed by employing H<sub>2</sub>O/AcCN/FA (70/30/ 0.1; v/v/v) as the mobile phase at the flow rate of 0.1 mL/min. The injection volume was 5  $\mu$ L. The capillary voltage was set at 3000 V, the cone voltage was 35 V, the capillary temperature was 120°C, while the desolvation temperature was 300°C. Mass spectra were recorded in total ion current (TIC), within 1000 and 2000 m/z, in positive polarity. The A $\beta$ <sub>42</sub> baseline subtracted spectrum (m/z 650–1700) was deconvoluted onto a true mass scale using the maximum entropy (MaxEnt1)-based software supplied with MassLynx 4.1 software. The output parameters were mass range: 4000–5000 Da and resolution: 2 Da/channel. The uniform Gaussian model was used, with 0.65 Da width at half height.

**Bottom up analysis of A $\beta$ <sub>42</sub> upon incubation with compound 4.** A $\beta$ <sub>42</sub> 50  $\mu$ M alone and co-incubated with **4** 50  $\mu$ M were incubated for 6h and digested overnight at 37°C upon dilution 1:2 with a solution of trypsin in ammonium bicarbonate 20 mM, pH 8; the final A $\beta$ <sub>42</sub>/trypsin ratio was 100/1 (w/w). A $\beta$ <sub>42</sub> tryptic digest (10  $\mu$ L) was analyzed by an Agilent 1100 Series HPLC system (Walbronn, Germany) coupled with a Q-ToF mass spectrometer (Micromass, Manchester, UK) equipped with a Z-spray ion source. Analyses were performed on a C18 column (Aeris peptide XB-C18; 150  $\times$  2.1 mm; 3.5  $\mu$ m; Phenomenex). Mobile phases A

[water/acetonitrile/FA (99/1/0.1, v/v/v)] and B [water/acetonitrile/FA (1/99/0.1, v/v/v)] were used to develop a gradient. The solvent gradient was set as follows: A–B from (98:8, v/v) to (40:60, v/v) in 20 min; (40:60, v/v) for 2 min. The column was equilibrated with the mobile phase composition of the starting conditions for 10 min before the next injection. The ESI-Q-ToF source temperature was set at 100°C, the capillary voltage at 3.0 kV, and the cone voltage at 35 V. Peptide ions within a  $m/z$  400–1700 survey scan mass range were analyzed for subsequent fragmentation. 2+, 3+, and 4+ charged ions exceeding a threshold abundance (TIC value: 10 counts/s) were selected for MS/MS analyses. From a single survey scan, 4 ions were selected for subsequent fragmentation. Scan returns to mass survey mode when the ion intensity falls below 5 counts/s or after 8 s. Scan time was 1 s for the parent ion and 1 s for the MS/MS ions. The collision energy was selected using charge state recognition.

### **Radioligand binding studies on CB<sub>1</sub>R and hCB<sub>2</sub>R**

Cells expressing hCB<sub>1</sub>R or hCB<sub>2</sub>R were grown, treated and membranes prepared as described in Scheiner et al.<sup>276</sup> The rCB<sub>1</sub>R membranes derived from homogenate of brains' female rats and were prepared according to the protocol described in Catani and Gasperi.<sup>318</sup> Radioligand binding assay started with saturation assays similar to Murkherjee et al.<sup>319</sup> to determine the  $K_D$  value of the membrane samples. Saturation assays were carried out using eight concentrations of [<sup>3</sup>H]CP 55,940, ranging from 0.088 to 4.4 nM. Reactions were started by adding 8 µg membrane per well of a 96 well Multiscreen filter plate (Millipore) containing the radioligand in assay buffer (50mM Tris-HCl, pH 7.4; 5mM MgCl<sub>2</sub>·6H<sub>2</sub>O; 2.5mM EDTA; 2 mg/mL BSA). After incubating for 3 h at RT, the reaction was stopped by vacuum filtration, and each well was washed four times with 100 µL of cold binding buffer (50mM Tris-HCl, pH 7.4; 5 mM MgCl<sub>2</sub>·6H<sub>2</sub>O; 2.5mM EDTA). The filter plate was dried at 40 °C. The activity was measured in a Microbeta Trilux counter (Wallac) using an IRGA Safe plus-scintillation cocktail (PerkinElmer). Competition assays were performed with 5–11 concentrations of replacing ligands (0.1 nM–0.4 mM) and 0.44 nM [<sup>3</sup>H]CP 55,940. Nonspecific binding was determined using 10 µM MN-I-79<sup>282, 320</sup> for hCB<sub>2</sub>R and 10 µM rimonabant for hCB<sub>1</sub>R. To determine the IC<sub>50</sub> values, statistical evaluations and sigmoidal dose–response curve fittings were performed using GraphPad Prism 5 software applying nonlinear regression and one site fit logIC<sub>50</sub> as curve fitting functions.  $K_i$  values were determined according to the Cheng–Prusoff equation when the displacement of [<sup>3</sup>H]CP 55,940 was higher than 50% at 10 µM test compound concentration.

### **Stability study**

For compounds **17-20**: stock solutions (4 mM) were prepared by dissolving the compounds in DMSO. For determination of the starting point  $t_0$ , the stock solution was diluted to 2 mM with DMSO and 30 µL were injected in LC-MS. For determination of the stability at  $t_{3.5h}$ , the stock solution was diluted to 100 µM with the binding buffer (50 mM TRIS, 5 mM MgCl<sub>2</sub>·6 H<sub>2</sub>O, 2.5 mM EDTA, pH = 7.4) used in the assay and incubated for 3.5 h at room temperature before 30 µL were injected UHPLC-MS.

For compounds **22**: stock solutions (1 mM) were prepared by dissolving the compounds in DMSO. For determination of the starting point  $t_0$ , 30  $\mu\text{L}$  of stock solution were injected in LC-MS. For determination of the stability at  $t_{1.5\text{h}}$ , the stock solution was diluted to 100  $\mu\text{M}$  with potassium phosphate buffer used in the assay (0.1 M, pH 7.4, 0.1 mM EDTA) and incubated for 1.5 h at 37°C before 30  $\mu\text{L}$  were injected UHPLC-MS.

UHPLC–MS analyses were run on a Waters ACQUITY ARC UHPLC/MS system consisting of a QDa mass spectrometer equipped with an electrospray ionization interface and a 2489 UV/Vis detector. The analyses were performed on an XBridge BEH C18 column (10  $\times$  2.1 mm i.d., particle size 2.5  $\mu\text{m}$ ) with a XBridge BEH C18 VanGuard Cartridge precolumn (5 mm  $\times$  2.1 mm i.d., particle size 1.8  $\mu\text{m}$ ). As mobile phase a gradient of water / acetonitrile (phase A / phase B), both containing 0.1% formic acid, was used. Compounds were analyzed using the following parameters and method: flow rate: 0.6 mL/min; UV-Detection: 365 nm; Scan range: 50 – 1200 m/z. Gradient: A: H<sub>2</sub>O (0.1% formic acid); B: MeCN (0.1% formic acid) 0-1.50 20 % B, 1.50-6.50 min 20 %  $\rightarrow$  90 % B, 6.50-8.50 min 90% B, 8.50-10 min 90%  $\rightarrow$  20% B, 10-12 min 20% B. Each analysis was performed in two independent experiments.

### **Neurotoxicity evaluation**

Cerebellar granule neurons (CGNs) were prepared from 7-day-old pups of Wistar rat strain, as elsewhere described.<sup>321</sup> All animal experiments were authorized by the University of Bologna bioethical committee (protocol no. 17–72-1212) and performed according to Italian and European Community laws on the use of animals for experimental purposes. Cells were dissociated from cerebella and plated on 96-well plates, previously coated with 10  $\mu\text{g}/\text{mL}$  poly-L-lysine, at a density of  $1.2 \times 10^5$  cells/0.2 mL medium/well in BME supplemented with 100 mL/L heat-inactivated FBS (Aurogene), 2 mmol/L glutamine, 100  $\mu\text{mol}/\text{L}$  gentamicin sulphate and 25 mmol/L KCl (all from Sigma–Aldrich). 16 h later, 10  $\mu\text{M}$  cytosine arabino-furanoside (Sigma–Aldrich) was added to avoid glial proliferation. After 7 days *in vitro*, differentiated neurons were shifted to serum free BME medium containing 25 mmol/L KCl and treated with increasing concentrations of the compounds (0, 1, 2.5, 5, 10 and 20  $\mu\text{M}$ ) for 24 h. After 24 h of treatment, the viability of CGNs was evaluated through the MTT assay.

### **Immunomodulation study**

Mouse N9-microglial cells were cultured in Dulbecco Modified Eagle Medium (DMEM) supplemented with 10% heat inactivated Foetal Bovine Serum (FBS), 1% Penicillin/Streptomycin and 2mM Glutamine (all cell cultures' reagents were from Aurogene). At confluence, after a short wash with sterile PBS, microglia were trypsinized for 5 minutes at 37 ° C and trypsin was inactivated with complete DMEM medium. Detached cells were then collected, centrifuged for 5 minutes at 300x g and resuspended to be counted. For the experiments, microglial cells were plated at the density of  $2.5 \times 10^5$  in 35 mm dish and exposed to 100ng/ml LPS, in presence or absence of 5  $\mu\text{M}$  of the compounds to be tested. After treatment for 24 h, microglial cells

were lysed in icecold lysis buffer (50 mM Tris-HCl pH 7.4, 1% SDS, 0.05% protease inhibitor cocktail; all from Sigma-Aldrich), protein content was determined by using the Lowry method and samples were loaded for western blot analysis of iNOS (M1 microglia marker), TREM2 (M2 microglia marker) and GAPDH (loading control) expression.

### **Cell viability in SH-SY5Y cells**

The mitochondrial dehydrogenase activity that reduces 3-(4,5-dimethylthiazol-2-yl)-2,5-diphenyl-tetrazolium bromide (MTT, Sigma, St Louis, MO) was used to determine cellular viability, in a quantitative colorimetric assay. At day 0, SH-SY5Y cells were plated at a density of  $2.5 \times 10^4$  viable cells per well in 96-well plates. After treatment, according to the experimental setting, cells were exposed to an MTT solution in serum free medium (1 mg/mL). Following 4 h incubation with MTT and treatment with SDS for 24 h, cell viability reduction was quantified by using a Synergy HT multidetection microplate reader (Bio-Tek).

### **Nrf2 nuclear translocation**

SH-SY5Y cells ( $5 \times 10^6$ ) were seeded in 100 mm<sup>2</sup> dishes and treated for 3 h with 5  $\mu$ M compounds; afterward the medium was removed, and cells were washed twice with ice-cold PBS. Cells were subsequently homogenized 15 times using a glass-glass dounce homogenizer in 0.32 M sucrose buffered with 20 mM Tris-HCl (pH 7.4) containing 2 mM EDTA, 0.5 mM EGTA, 50 mM  $\beta$ -mercaptoethanol, and 20  $\mu$ g/mL leupeptin, aprotinin, and pepstatin. The homogenate was centrifuged at 300g for 5 min to obtain the nuclear fraction. An aliquot of the nuclear fraction was used for protein assay by the Bradford method, whereas the remaining was boiled for 5 min after dilution with sample buffer and subjected to polyacrylamide gel electrophoresis and immunoblotting as described.

### **hMAOs activity assays**

Human recombinant MAO-A and MAO-B expressed in Baculovirus infected BT1 cells (5 mg/ml) and horseradish peroxidases were purchased from Fluka-Sigma-Aldrich s.r.l. (Italy). A Cary-Eclipse fluorimeter (Varian Inc., Palo Alto, CA, USA) was used for fluorescence measurements. The stock solutions of compounds and pioglitazone were prepared in dimethyl sulfoxide. Monoamine oxidase activity was determined according to the kynuramine assay.<sup>300</sup>

To study the mechanism of inhibition, the steady-state kinetic parameters ( $V_{max}$  and  $K_m$ ) of MAO-A and MAO-B were determined by performing experiment at different substrate concentration and in absence and presence of different concentrations of the tested compound.  $V_{max}$  and  $K_m$  were calculated by fitting the Michaelis-Menten equation to the experimental data (initial rate of reactions vs substrate concentrations), with Sigma Plot software, version 9.0 (Jandel Scientific, San Rafael, CA, USA). The mode of inhibition was determined by global fit analysis (GraphPad 9.0 software, GraphPad Software, San Diego, CA, USA) of the initial rate of reaction vs substrate concentration plots, in the presence and absence of inhibitor, to fit



equations for competitive, mixed, non-competitive and uncompetitive inhibition models; the fit giving the highest  $r^2$  value was selected for the calculation of inhibition constants. The results are presented as double reciprocal Lineweaver-Burk plots ( $1/v$  vs  $1/S$ ) to show the mixed mode of inhibition of the tested compounds.  $K_i$  values are expressed as mean  $\pm$  S.D. All experiments were performed at least in triplicate.

*Time-dependent inhibition studies.* The time dependence inactivation by **3** was performed as previously reported.<sup>322</sup> In details, recombinant MAO-B and MAO-A, were pre-incubated in the K/Pi buffer for periods from 0 to about 20 minutes, at 37 °C in the absence (control sample) and in presence of compound **3** (20 and 50  $\mu$ M). After various time intervals of pre-incubation (at least 5 times after mixing of enzyme and inhibitor), the residual MAOs enzyme activity of samples was determined: an aliquot of sample was withdrawn and diluted in the assay buffer (50-fold dilution) and, then substrate was added under “saturating” condition, ( $K_{yn}=300\mu$ M).

### **Docking analysis at hMAO-B**

The crystal structure of human MAO-B was retrieved from the Protein Data Bank (PDB code: [4A79](#)) and processed in order to remove ligands and water molecules. Hydrogen atoms were added to the protein structure using standard geometries with the MOE program (2020.09). To minimize contacts between hydrogens, the structure was subjected to Amber99 force-field minimization until the rms (root mean square) of conjugate gradient was  $<0.1 \text{ kcal}\cdot\text{mol}^{-1}\cdot\text{\AA}^{-1}$  ( $1 \text{ \AA} = 0.1 \text{ nm}$ ) keeping the heavy atoms fixed at their crystallographic positions. Selected compounds, were built using MOE, considering the molecules in both oxidized and reduced states; Gasteiger partial charges (MOE Suite) were added.<sup>322</sup> Docking procedure was performed using Dock (Moe suite) triangle matcher with London dG as placement score. The receptor was subjected to induced fit protocol. The binding score was performed using X-Score, an empirical scoring functions which estimate the binding affinity of a given protein-ligand complex, including terms accounting for van der Waals interaction, hydrogen bonding, deformation penalty, and hydrophobic effect. The estimated binding affinity is expressed as a dissociate constant of the protein-ligand complex in negative logarithm (pKd), in which for example a pKd equal to 9 represent a binding affinity in the nanomolar range, while a pKd equal to 6 in the micromolar range.

## ABBREVIATIONS AND ACRONYMS

5-HT, serotonin; A $\beta$ , amyloid  $\beta$ ; ABPP, activity-based protein profiling; AD, Alzheimer's disease; AICD, amyloid precursor protein intracellular domain; ALS, amyotrophic lateral sclerosis; ANOVA, analysis of variance; APP, amyloid protein precursor; ARE, antioxidant response element; BACE,  $\beta$ -secretase; BBB, blood-brain barrier; CA, carnosis acid; CaMK II (Ca<sup>2+</sup>/calmodulin-dependent protein kinase II); CB<sub>1</sub>R, cannabinoid type-1 receptor; CB<sub>2</sub>R, cannabinoid type-2 receptor; CD, cluster of differentiation; CDDO-Me, bardoloxone methyl; CGN, cerebellar granule neuron; CHO, chinese hamster ovary; CNS, central nervous system; COX, cyclooxygenase; CREB, cAMP response element-binding protein; CSF, colony-stimulating factors; CYP450, cytochrome P450; DA, dopamine; DCC, N,N'-dicyclohexylcarbodiimide; DCM, dichloromethane; DMAP, dimethylaminopyridine; DMEM, Dulbecco Modified Eagle Medium; DMF, dimethyl fumarate or dimethylformamide; DMSO, dimethyl sulfoxide; EC, endocannabinoid; ECS, endocannabinoid system; EDC, 1-ethyl-3-(3-dimethylaminopropyl)carbodiimide; EDTA, ethylenediaminetetraacetic acid; EGCG, (-)-epigallocatechin-3-gallate; eNMDAR, extrasynaptic NMDAR; ERK, extracellular signal-regulated kinase; ESI, electrospray ionization; FA, formic acid; FAAH, fatty acid amide hydrolase; FAD, flavin adenine dinucleotide; FBS, foetal bovine serum; GAPDH, glyceraldehyde-3-phosphate dehydrogenase; GDNF, glial cell line-derived neurotrophic factor; GM-CSF, granulocyte-macrophage colony-stimulating factor; GPCR, G-protein coupled receptor; GSK-3 $\beta$ , glycogen synthase kinase 3 $\beta$ ; GSH, glutathione; GSI,  $\gamma$ -secretase inhibitors; GST, glutathione-S-transferase; HD, Huntington's disease; HDAC, histone deacetylase; HEK, human embryonic kidney; HPLC, high performance liquid chromatography; HO-1, heme oxygenase-1; HOBt, hydroxy benzotriazole; HSF, heat shock factor; IFN, interferon; I $\kappa$ B, inhibitor of  $\kappa$ B; IKK, I $\kappa$ B kinase; IL, interleukin; iNOS, inducible nitric oxide synthase; JNK, c-Jun N-terminal kinase; Keap1, Kelch-like ECH-associated protein 1; LPS, lipopolysaccharide; MAGL, monoacylglycerol lipase; MAO, monoamine oxidase; MAPK, mitogen-activated protein kinase; MBI, mechanism-based inhibitor; MCP-1, monocyte chemoattractant protein-1; MHC, major histocompatibility complex; MMF, monomethyl fumarate; MS, multiple sclerosis or mass spectrometry; MTT, 3-(4,5-Dimethylthiazol-2-yl)-2,5-diphenyltetrazolium bromide; NDD, neurodegenerative disease; NE, adrenaline or norepinephrine; NF- $\kappa$ B, nuclear factor  $\kappa$ -light-chain enhancer of activated B cells; NFT, neurofibrillary tangles; NIK, NF- $\kappa$ B inducing kinase; NMDAR, N-methyl-D-aspartic acid receptors; NMR, nuclear magnetic resonance; NOE, nuclear Overhauser effect; NOESY, nuclear Overhauser effect spectroscopy; NQO1, NADH-quinone oxidoreductase 1; Nrf2, nuclear factor erythroid 2-related factor 2; NSAID, non-steroidal antiinflammatory drug; NOX, NADPH oxidase; OES, oxidative and electrophilic stress; o/n, overnight; PAIN, pan assay interference compound; PAT, pathologically activated therapeutics; PCR, polymerase chain reaction; PD, Parkinson's disease; PKB, protein kinase B; PLC, phospholipase C; PPAR, peroxisome proliferator-activated receptors; PPI, protein-protein interaction; PrP; prion protein; Prx, peroxiredoxins; PTM, post-translational modification; PTP, phosphatase; RAGE, receptor for advanced glycosylation end products; RES, reactive electrophilic species; RNS, reactive nitrogen species; ROS, reactive

oxygen species; rt, room temperature; sNMDAR, synaptic NMDAR; SFN, sulforaphane; siRNA, short-interfering RNA; SAR, structure-activity relationship; SOD, superoxide dismutase; STAT, signal transducer and activator of transcription; TBAF, tetra-n-butylammonium fluoride; TBDMS-Cl, tert-butyldimethylsilyl chloride; TCI, targeted covalent inhibitors; TGF, transforming growth factor; THC, tetrahydrocannabinol; THF, tetrahydrofuran; ThT, thioflavin T; TLC, thin layer chromatography; TLR, toll-like receptor; TMS, tetramethylsilane; TNF, tumor necrosis factor; TRAF, TNF receptor-associated factor; TREM2, triggering receptor expressed on myeloid cells 2; T-REX, targetable reactive electrophiles and oxidants; UHPLC, ultra high performance liquid chromatography; UV, ultraviolet.

## BIBLIOGRAPHY

1. Deuschl, G.; Beghi, E.; Fazekas, F.; Varga, T.; Christoforidi, K. A.; Sipido, E.; Bassetti, C. L.; Vos, T.; Feigin, V. L., The burden of neurological diseases in Europe: an analysis for the Global Burden of Disease Study 2017. *Lancet Public Health* **2020**, *5* (10), e551-e567.
2. Amor, S.; Puentes, F.; Baker, D.; van der Valk, P., Inflammation in neurodegenerative diseases. *Immunology* **2010**, *129* (2), 154-169.
3. Michaud, M.; Balardy, L.; Moulis, G.; Gaudin, C.; Peyrot, C.; Vellas, B.; Cesari, M.; Nourhashemi, F., Proinflammatory cytokines, aging, and age-related diseases. *J. Am. Med. Dir. Assoc.* **2013**, *14* (12), 877-882.
4. Rivest, S., Regulation of innate immune responses in the brain. *Nat. Rev. Immunol.* **2009**, *9* (6), 429-439.
5. Domingues, H. S.; Portugal, C. C.; Socodato, R.; Relvas, J. B., Oligodendrocyte, Astrocyte, and Microglia Crosstalk in Myelin Development, Damage, and Repair. *Front. Cell. Dev. Biol.* **2016**, *4*, 71.
6. Giovannoni, F.; Quintana, F. J., The Role of Astrocytes in CNS Inflammation. *Trends Immunol.* **2020**, *41* (9), 805-819.
7. Peña-Altamira, E.; Prati, F.; Massenzio, F.; Virgili, M.; Contestabile, A.; Bolognesi, M. L.; Monti, B., Changing paradigm to target microglia in neurodegenerative diseases: from anti-inflammatory strategy to active immunomodulation. *Expert Opin. Ther. Targets* **2016**, *20* (5), 627-640.
8. Ousman, S. S.; Kubes, P., Immune surveillance in the central nervous system. *Nat. Neurosci.* **2012**, *15* (8), 1096-1101.
9. Becher, B.; Spath, S.; Goverman, J., Cytokine networks in neuroinflammation. *Nat. Rev. Immunol.* **2017**, *17* (1), 49-59.
10. Dubbelaar, M. L.; Kracht, L.; Eggen, B. J. L.; Boddeke, E. W. G. M., The Kaleidoscope of Microglial Phenotypes. *Front Immunol.* **2018**, *9*, 1753.
11. Salter, M. W.; Beggs, S., Sublime microglia: expanding roles for the guardians of the CNS. *Cell* **2014**, *158* (1), 15-24.
12. Cherry, J. D.; Olschowka, J. A.; O'Banion, M. K., Neuroinflammation and M2 microglia: the good, the bad, and the inflamed. *J. Neuroinflammation* **2014**, *11*, 98.
13. Erickson, M. A.; Banks, W. A., Neuroimmune Axes of the Blood-Brain Barriers and Blood-Brain Interfaces: Bases for Physiological Regulation, Disease States, and Pharmacological Interventions. *Pharmacol. Rev.* **2018**, *70* (2), 278-314.
14. Kennedy, R. H.; Silver, R., Neuroimmune Signaling: Cytokines and the CNS. In *Neuroscience in the 21st Century*, Pfaff, D. W.; Volkow, N. D., Eds. Springer Science: New York, 2015.
15. Chitnis, T.; Weiner, H. L., CNS inflammation and neurodegeneration. *J. Clin. Invest.* **2017**, *127* (10), 3577-3587.
16. McGeer, P. L.; Rogers, J., Anti-inflammatory agents as a therapeutic approach to Alzheimer's disease. *Neurology* **1992**, *42* (2), 447-449.
17. Martino, G.; Adorini, L.; Rieckmann, P.; Hillert, J.; Kallmann, B.; Comi, G.; Filippi, M., Inflammation in multiple sclerosis: the good, the bad, and the complex. *Lancet Neurol.* **2002**, *1* (8), 499-509.
18. Hopperton, K. E.; Mohammad, D.; Trépanier, M. O.; Giuliano, V.; Bazinet, R. P., Markers of microglia in post-mortem brain samples from patients with Alzheimer's disease: a systematic review. *Mol. Psychiatry* **2018**, *23* (2), 177-198.
19. Hirsch, E. C.; Hunot, S., Neuroinflammation in Parkinson's disease: a target for neuroprotection? *Lancet Neurol.* **2009**, *8* (4), 382-397.
20. Silvestroni, A.; Faull, R. L.; Strand, A. D.; Möller, T., Distinct neuroinflammatory profile in post-mortem human Huntington's disease. *Neuroreport* **2009**, *20* (12), 1098-1103.
21. McGeer, P. L.; Schulzer, M.; McGeer, E. G., Arthritis and anti-inflammatory agents as possible protective factors for Alzheimer's disease: a review of 17 epidemiologic studies. *Neurology* **1996**, *47* (2), 425-432.
22. Bergamaschi, R.; Versino, M.; Raiola, E.; Citterio, A.; Cosi, V., High-dose methylprednisolone infusions in relapsing and in chronic progressive multiple sclerosis patients. One year follow-up. *Acta Neurol. (Napoli)* **1993**, *15* (1), 33-43.
23. Chen, H.; Zhang, S. M.; Hernán, M. A.; Schwarzschild, M. A.; Willett, W. C.; Colditz, G. A.; Speizer, F. E.; Ascherio, A., Nonsteroidal anti-inflammatory drugs and the risk of Parkinson disease. *Arch. Neurol.* **2003**, *60* (8), 1059-1064.
24. in t' Veld, B. A.; Ruitenber, A.; Hofman, A.; Launer, L. J.; van Duijn, C. M.; Stijnen, T.; Breteler, M. M.; Stricker, B. H., Nonsteroidal anti-inflammatory drugs and the risk of Alzheimer's disease. *N. Engl. J. Med.* **2001**, *345* (21), 1515-1521.

25. Moore, A. H.; Bigbee, M. J.; Boynton, G. E.; Wakeham, C. M.; Rosenheim, H. M.; Staral, C. J.; Morrissey, J. L.; Hund, A. K., Non-Steroidal Anti-Inflammatory Drugs in Alzheimer's Disease and Parkinson's Disease: Reconsidering the Role of Neuroinflammation. *Pharmaceuticals (Basel)* **2010**, *3* (6), 1812-1841.
26. *The Cytokine Handbook*. 4th Edition ed.; Academic Press: San Diego, California, USA, 2003.
27. Deverman, B. E.; Patterson, P. H., Cytokines and CNS development. *Neuron* **2009**, *64* (1), 61-78.
28. Erta, M.; Quintana, A.; Hidalgo, J., Interleukin-6, a major cytokine in the central nervous system. *Int. J. Biol. Sci.* **2012**, *8* (9), 1254-1266.
29. Schetters, S. T. T.; Gomez-Nicola, D.; Garcia-Vallejo, J. J.; Van Kooyk, Y., Neuroinflammation: Microglia and T Cells Get Ready to Tango. *Front. Immunol.* **2017**, *8*, 1905.
30. Ramesh, G.; MacLean, A. G.; Philipp, M. T., Cytokines and chemokines at the crossroads of neuroinflammation, neurodegeneration, and neuropathic pain. *Mediators Inflamm.* **2013**, *2013*, 480739.
31. Liu, T.; Zhang, L.; Joo, D.; Sun, S. C., NF- $\kappa$ B signaling in inflammation. *Signal Transduct. Target. Ther.* **2017**, *2*.
32. Lawrence, T., The nuclear factor NF-kappaB pathway in inflammation. *Cold Spring Harb. Perspect. Biol.* **2009**, *1* (6), a001651.
33. Vallabhapurapu, S.; Karin, M., Regulation and function of NF-kappaB transcription factors in the immune system. *Annu. Rev. Immunol.* **2009**, *27*, 693-733.
34. Sun, S. C., The noncanonical NF- $\kappa$ B pathway. *Immunol. Rev.* **2012**, *246* (1), 125-140.
35. Shih, R. H.; Wang, C. Y.; Yang, C. M., NF-kappaB Signaling Pathways in Neurological Inflammation: A Mini Review. *Front. Mol. Neurosci.* **2015**, *8*, 77.
36. Kaltschmidt, B.; Kaltschmidt, C., NF-KappaB in Long-Term Memory and Structural Plasticity in the Adult Mammalian Brain. *Front. Mol. Neurosci.* **2015**, *8*, 69.
37. Yang, L.; Tao, L. Y.; Chen, X. P., Roles of NF-kappaB in central nervous system damage and repair. *Neurosci. Bull.* **2007**, *23* (5), 307-313.
38. Heyninck, K.; Lahtela-Kakkonen, M.; Van der Veken, P.; Haegeman, G.; Vanden Berghe, W., Withaferin A inhibits NF-kappaB activation by targeting cysteine 179 in IKK $\beta$ . *Biochem. Pharmacol.* **2014**, *91* (4), 501-509.
39. Xia, Y. F.; Ye, B. Q.; Li, Y. D.; Wang, J. G.; He, X. J.; Lin, X.; Yao, X.; Ma, D.; Slungaard, A.; Hebbel, R. P.; Key, N. S.; Geng, J. G., Andrographolide attenuates inflammation by inhibition of NF-kappa B activation through covalent modification of reduced cysteine 62 of p50. *J. Immunol.* **2004**, *173* (6), 4207-4217.
40. Gilmore, T. D.; Herscovitch, M., Inhibitors of NF-kappaB signaling: 785 and counting. *Oncogene* **2006**, *25* (51), 6887-6899.
41. Schopfer, F. J.; Cipollina, C.; Freeman, B. A., Formation and signaling actions of electrophilic lipids. *Chem. Rev.* **2011**, *111* (10), 5997-6021.
42. Dresselhaus, E. C.; Meffert, M. K., Cellular Specificity of NF- $\kappa$ B Function in the Nervous System. *Front. Immunol.* **2019**, *10*, 1043.
43. Stone, K. P.; Kastin, A. J.; Pan, W., NF $\kappa$ B is an unexpected major mediator of interleukin-15 signaling in cerebral endothelia. *Cell Physiol. Biochem.* **2011**, *28* (1), 115-124.
44. Reijonen, S.; Kukkonen, J. P.; Hyrskyluoto, A.; Kivinen, J.; Kairisalo, M.; Takei, N.; Lindholm, D.; Korhonen, L., Downregulation of NF-kappaB signaling by mutant huntingtin proteins induces oxidative stress and cell death. *Cell Mol. Life Sci.* **2010**, *67* (11), 1929-1941.
45. Bellucci, A.; Bubacco, L.; Longhena, F.; Parrella, E.; Faustini, G.; Porrini, V.; Bono, F.; Missale, C.; Pizzi, M., Nuclear Factor- $\kappa$ B Dysregulation and  $\alpha$ -Synuclein Pathology: Critical Interplay in the Pathogenesis of Parkinson's Disease. *Front. Aging Neurosci.* **2020**, *12*, 68.
46. Snow, W. M.; Albeni, B. C., Neuronal Gene Targets of NF- $\kappa$ B and Their Dysregulation in Alzheimer's Disease. *Front. Mol. Neurosci.* **2016**, *9*, 118.
47. Hunot, S.; Brugg, B.; Ricard, D.; Michel, P. P.; Muriel, M. P.; Ruberg, M.; Faucheux, B. A.; Agid, Y.; Hirsch, E. C., Nuclear translocation of NF-kappaB is increased in dopaminergic neurons of patients with parkinson disease. *Proc. Natl. Acad. Sci. USA* **1997**, *94* (14), 7531-7536.
48. Srinivasan, M.; Lahiri, D. K., Significance of NF- $\kappa$ B as a pivotal therapeutic target in the neurodegenerative pathologies of Alzheimer's disease and multiple sclerosis. *Expert Opin. Ther. Targets* **2015**, *19* (4), 471-487.
49. Hwang, C. J.; Choi, D. Y.; Park, M. H.; Hong, J. T., NF- $\kappa$ B as a Key Mediator of Barin Inflammation in Alzheimer's Disease. *CNS & Neurological Disorders - Drug Targets* **2019**, *18* (1), 3-10.
50. Sivandzade, F.; Prasad, S.; Bhalariao, A.; Cucullo, L., NRF2 and NF- $\kappa$ B interplay in cerebrovascular and neurodegenerative disorders: Molecular mechanisms and possible therapeutic approaches. *Redox Biol.* **2019**, *21*, 101059.
51. Ramadass, V.; Vaiyapuri, T.; Tergaonkar, V., Small Molecule NF- $\kappa$ B Pathway Inhibitors in Clinic. *Int. J. Mol. Sci.* **2020**, *21* (14).
52. Benito, C.; Tolon, R.; Pazos, M.; Nunez, E.; Castillo, A.; Romero, J., Cannabinoid CB2 receptors in human brain inflammation. *Br. J. Pharmacol.* **2008**, *153* (2), 277-285.

53. Kendall, D.; Alexander, S., *Cannabinoid Pharmacology*. Academic Press: Cambridge, 2017; Vol. 80.
54. Munro, S.; Thomas, K.; Abushaar, M., Molecular Characterization of a Peripheral Receptors for Cannabinoids. *Nature* **1993**, *365* (6441), 61-65.
55. Van Sickle, M. D.; Duncan, M.; Kingsley, P. J.; Mouihate, A.; Urbani, P.; Mackie, K.; Stella, N.; Makriyannis, A.; Piomelli, D.; Davison, J. S.; Marnett, L. J.; Di Marzo, V.; Pittman, Q. J.; Patel, K. D.; Sharkey, K. A., Identification and functional characterization of brainstem cannabinoid CB2 receptors. *Science* **2005**, *310* (5746), 329-332.
56. Howlett, A. C.; Barth, F.; Bonner, T. I.; Cabral, G.; Casellas, P.; Devane, W. A.; Felder, C. C.; Herkenham, M.; Mackie, K.; Martin, B. R.; Mechoulam, R.; Pertwee, R. G., International Union of Pharmacology. XXVII. Classification of cannabinoid receptors. *Pharmacol. Rev.* **2002**, *54* (2), 161-202.
57. Perez-Gomez, E.; Andradas, C.; Blasco-Benito, S.; Caffarel, M.; Garcia-Taboada, E.; Villa-Morales, M.; Moreno, E.; Hamann, S.; Martin-Villar, E.; Flores, J.; Wenners, A.; Alkatout, I.; Klapper, W.; Rocken, C.; Bronsert, P.; Stickeler, E.; Staebler, A.; Bauer, M.; Arnold, N.; Soriano, J.; Perez-Martinez, M.; Megias, D.; Moreno-Bueno, G.; Ortega-Gutierrez, S.; Artola, M.; Vazquez-Villa, H.; Quintanilla, M.; Fernandez-Piqueras, J.; Canela, E.; McCormick, P.; Guzman, M.; Sanchez, C., Role of Cannabinoid Receptor CB2 in HER2 Pro-oncogenic Signaling in Breast Cancer. *J. Natl. Cancer Inst.* **2015**, *107* (6).
58. Xu, S.; Ma, H.; Bo, Y.; Shao, M., The oncogenic role of CB2 in the progression of non-small-cell lung cancer. *Biomed. Pharmacother.* **2019**, *117*.
59. Aso, E.; Ferrer, I., CB2 Cannabinoid Receptor As Potential Target against Alzheimer's Disease. *Front. Neurosci.* **2016**, *10*, 243.
60. Javed, H.; Azimullah, S.; Haque, M. E.; Ojha, S. K., Cannabinoid Type 2 (CB2) Receptors Activation Protects against Oxidative Stress and Neuroinflammation Associated Dopaminergic Neurodegeneration in Rotenone Model of Parkinson's Disease. *Front. Neurosci.* **2016**, *10*, 321.
61. Bouchard, J.; Truong, J.; Bouchard, K.; Dunkelberger, D.; Desrayaud, S.; Moussaoui, S.; Tabrizi, S. J.; Stella, N.; Muchowski, P. J., Cannabinoid receptor 2 signaling in peripheral immune cells modulates disease onset and severity in mouse models of Huntington's disease. *J. Neurosci.* **2012**, *32* (50), 18259-18268.
62. Mecha, M.; Feliú, A.; Carrillo-Salinas, F. J.; Rueda-Zubiaurre, A.; Ortega-Gutiérrez, S.; de Sola, R. G.; Guaza, C., Endocannabinoids drive the acquisition of an alternative phenotype in microglia. *Brain Behav. Immun.* **2015**, *49*, 233-245.
63. Mecha, M.; Carrillo-Salinas, F. J.; Feliú, A.; Mestre, L.; Guaza, C., Microglia activation states and cannabinoid system: Therapeutic implications. *Pharmacol. Ther.* **2016**, *166*, 40-55.
64. Turcotte, C.; Blanchet, M. R.; Laviolette, M.; Flamand, N., The CB<sub>2</sub> receptor and its role as a regulator of inflammation. *Cell Mol. Life Sci.* **2016**, *73* (23), 4449-4470.
65. Solas, M.; Francis, P. T.; Franco, R.; Ramirez, M. J., CB2 receptor and amyloid pathology in frontal cortex of Alzheimer's disease patients. *Neurobiol. Aging* **2013**, *34* (3), 805-808.
66. Gómez-Gálvez, Y.; Palomo-Garo, C.; Fernández-Ruiz, J.; García, C., Potential of the cannabinoid CB(2) receptor as a pharmacological target against inflammation in Parkinson's disease. *Prog. Neuropsychopharmacol. Biol. Psychiatry* **2016**, *64*, 200-208.
67. Palazuelos, J.; Aguado, T.; Pazos, M.; Julien, B.; Carrasco, C.; Resel, E.; Sagredo, O.; Benito, C.; Romero, J.; Azcoitia, I.; Fernandez-Ruiz, J.; Guzman, M.; Galve-Roperh, I., Microglial CB2 cannabinoid receptors are neuroprotective in Huntington's disease excitotoxicity. *Brain* **2009**, *132*, 3152-3164.
68. Shoemaker, J.; Seely, K.; Reed, R.; Crow, J.; Prather, P., The CB2 cannabinoid agonist AM-1241 prolongs survival in a transgenic mouse model of amyotrophic lateral sclerosis when initiated at symptom onset. *J. Neurochem.* **2007**, *101* (1), 87-98.
69. Howlett, A. C.; Abood, M. E., CB<sub>1</sub> and CB<sub>2</sub> Receptor Pharmacology. In *Cannabinoid Pharmacology*, 2017/06/12 ed.; Kendall, D.; Alexander, S., Eds. Academic Press: Cambridge, 2017; Vol. 80, pp 169-206.
70. Atwood, B.; Mackie, K., CB2: a cannabinoid receptor with an identity crisis. *Br. J. Pharmacol.* **2010**, *160* (3), 467-479.
71. Navarro, G.; Morales, P.; Rodríguez-Cueto, C.; Fernández-Ruiz, J.; Jagerovic, N.; Franco, R., Targeting Cannabinoid CB2 Receptors in the Central Nervous System. Medicinal Chemistry Approaches with Focus on Neurodegenerative Disorders. *Front. Neurosci.* **2016**, *10*, 406.
72. Chiurchiù, V.; van der Stelt, M.; Centonze, D.; Maccarrone, M., The endocannabinoid system and its therapeutic exploitation in multiple sclerosis: Clues for other neuroinflammatory diseases. *Prog. Neurobiol.* **2018**, *160*, 82-100.
73. Bisogno, T.; Oddi, S.; Piccoli, A.; Fazio, D.; Maccarrone, M., Type-2 cannabinoid receptors in neurodegeneration. *Pharmacol. Res.* **2016**, *111*, 721-730.
74. Basagni, F.; Rosini, M.; Decker, M., Functionalized Cannabinoid Subtype 2 Receptor Ligands: Fluorescent, PET, Photochromic and Covalent Molecular Probes. *ChemMedChem* **2020**, *15* (15), 1374-1389.

75. Morales, P.; Hernandez-Folgado, L.; Goya, P.; Jagerovic, N., Cannabinoid receptor 2 (CB2) agonists and antagonists: a patent update. *Expert Opin. Ther. Pat.* **2016**, *26* (7), 843-856.
76. Fernández-Ruiz, J.; Moro, M. A.; Martínez-Orgado, J., Cannabinoids in Neurodegenerative Disorders and Stroke/Brain Trauma: From Preclinical Models to Clinical Applications. *Neurotherapeutics* **2015**, *12* (4), 793-806.
77. Dhopeswarkar, A.; Mackie, K., CB2 Cannabinoid receptors as a therapeutic target-what does the future hold? *Mol. Pharmacol.* **2014**, *86* (4), 430-437.
78. Zolezzi, J. M.; Santos, M. J.; Bastías-Candia, S.; Pinto, C.; Godoy, J. A.; Inestrosa, N. C., PPARs in the central nervous system: roles in neurodegeneration and neuroinflammation. *Biol. Rev. Camb. Philos. Soc.* **2017**, *92* (4), 2046-2069.
79. Simpson, D. S. A.; Oliver, P. L., ROS Generation in Microglia: Understanding Oxidative Stress and Inflammation in Neurodegenerative Disease. *Antioxidants (Basel)* **2020**, *9* (8), 743.
80. Hsieh, H. L.; Yang, C. M., Role of redox signaling in neuroinflammation and neurodegenerative diseases. *Biomed. Res. Int.* **2013**, *2013*, 484613.
81. Solleiro-Villavicencio, H.; Rivas-Arancibia, S., Effect of Chronic Oxidative Stress on Neuroinflammatory Response Mediated by CD4. *Front. Cell Neurosci.* **2018**, *12*, 114.
82. Gregersen, N.; Bross, P., Protein misfolding and cellular stress: an overview. *Methods Mol. Biol.* **2010**, *648*, 3-23.
83. Gao, H. M.; Zhou, H.; Hong, J. S., Oxidative Stress, Neuroinflammation, and Neurodegeneration. In *Neuroinflammation and Neurodegeneration*, Peterson, P. K.; Toborek, M., Eds. Springer Science + Business Media: New York, 2014.
84. He, J.; Zhu, G.; Wang, G.; Zhang, F., Oxidative Stress and Neuroinflammation Potentiate Each Other to Promote Progression of Dopamine Neurodegeneration. *Oxid. Med. Cell Longev.* **2020**, *2020*, 6137521.
85. Hayes, J. D.; Dinkova-Kostova, A. T., The Nrf2 regulatory network provides an interface between redox and intermediary metabolism. *Trends Biochem. Sci.* **2014**, *39* (4), 199-218.
86. Kobayashi, E. H.; Suzuki, T.; Funayama, R.; Nagashima, T.; Hayashi, M.; Sekine, H.; Tanaka, N.; Moriguchi, T.; Motohashi, H.; Nakayama, K.; Yamamoto, M., Nrf2 suppresses macrophage inflammatory response by blocking proinflammatory cytokine transcription. *Nat. Commun.* **2016**, *7*, 11624.
87. Innamorato, N. G.; Rojo, A. I.; García-Yagüe, A. J.; Yamamoto, M.; de Ceballos, M. L.; Cuadrado, A., The transcription factor Nrf2 is a therapeutic target against brain inflammation. *J. Immunol.* **2008**, *181* (1), 680-689.
88. Dinkova-Kostova, A. T.; Kostov, R. V.; Canning, P., Keap1, the cysteine-based mammalian intracellular sensor for electrophiles and oxidants. *Arch. Biochem. Biophys.* **2017**, *617*, 84-93.
89. Syapin, P. J., Regulation of haeme oxygenase-1 for treatment of neuroinflammation and brain disorders. *Br. J. Pharmacol.* **2008**, *155* (5), 623-640.
90. Zhang, D. D.; Hannink, M., Distinct cysteine residues in Keap1 are required for Keap1-dependent ubiquitination of Nrf2 and for stabilization of Nrf2 by chemopreventive agents and oxidative stress. *Mol. Cell. Biol.* **2003**, *23* (22), 8137-8151.
91. Rachakonda, G.; Xiong, Y.; Sekhar, K. R.; Stamer, S. L.; Liebler, D. C.; Freeman, M. L., Covalent modification at Cys151 dissociates the electrophile sensor Keap1 from the ubiquitin ligase CUL3. *Chem. Res. Toxicol.* **2008**, *21* (3), 705-10.
92. Basagni, F.; Lanni, C.; Minarini, A.; Rosini, M., Lights and shadows of electrophile signaling: focus on the Nrf2-Keap1 pathway. *Future Med. Chem.* **2019**, *11* (7), 707-721.
93. Dinkova-Kostova, A. T.; Kostov, R. V.; Kazantsev, A. G., The role of Nrf2 signaling in counteracting neurodegenerative diseases. *FEBS J.* **2018**, *285* (19), 3576-3590.
94. Cuadrado, A., NRF2 in neurodegenerative diseases. *Curr. Opin. Toxicol.* **2016**, *1*, 46-43.
95. Osama, A.; Zhang, J.; Yao, J.; Yao, X.; Fang, J., Nrf2: a dark horse in Alzheimer's disease treatment. *Ageing Res. Rev.* **2020**, *64*, 101206.
96. Copley, J. N.; Fiorello, M. L.; Bailey, D. M., 13 reasons why the brain is susceptible to oxidative stress. *Redox Biol.* **2018**, *15*, 490-503.
97. Edmondson, D. E.; Binda, C.; Wang, J.; Upadhyay, A. K.; Mattevi, A., Molecular and mechanistic properties of the membrane-bound mitochondrial monoamine oxidases. *Biochemistry* **2009**, *48* (20), 4220-4230.
98. Edmondson, D. E.; Binda, C., Monoamine Oxidases. In *Membrane Protein Complexes: Structure and Function*, Harris, J. R.; Boekema, E. J., Eds. Springer Nature: Singapore, 2018; pp 117-140.
99. Youdim, M. B.; Edmondson, D.; Tipton, K. F., The therapeutic potential of monoamine oxidase inhibitors. *Nat. Rev. Neurosci.* **2006**, *7* (4), 295-309.
100. Binda, C.; Li, M.; Hubalek, F.; Restelli, N.; Edmondson, D. E.; Mattevi, A., Insights into the mode of inhibition of human mitochondrial monoamine oxidase B from high-resolution crystal structures. *Proc. Natl. Acad. Sci USA* **2003**, *100* (17), 9750-9755.

101. Naoi, M.; Maruyama, W.; Inaba-Hasegawa, K., Type A and B monoamine oxidase in age-related neurodegenerative disorders: their distinct roles in neuronal death and survival. *Curr. Top. Med. Chem.* **2012**, *12* (20), 2177-2188.
102. Schedin-Weiss, S.; Inoue, M.; Hromadkova, L.; Teranishi, Y.; Yamamoto, N. G.; Wiehager, B.; Bogdanovic, N.; Winblad, B.; Sandebring-Matton, A.; Frykman, S.; Tjernberg, L. O., Monoamine oxidase B is elevated in Alzheimer disease neurons, is associated with  $\gamma$ -secretase and regulates neuronal amyloid  $\beta$ -peptide levels. *Alzheimers Res. Ther.* **2017**, *9* (1), 57.
103. Cai, Z., Monoamine oxidase inhibitors: promising therapeutic agents for Alzheimer's disease (Review). *Mol. Med. Rep.* **2014**, *9* (5), 1533-1541.
104. Kim, D.; Baik, S. H.; Kang, S.; Cho, S. W.; Bae, J.; Cha, M. Y.; Sailor, M. J.; Mook-Jung, I.; Ahn, K. H., Close Correlation of Monoamine Oxidase Activity with Progress of Alzheimer's Disease in Mice, Observed by in Vivo Two-Photon Imaging. *ACS Cent. Sci.* **2016**, *2* (12), 967-975.
105. Mallajosyula, J. K.; Kaur, D.; Chinta, S. J.; Rajagopalan, S.; Rane, A.; Nicholls, D. G.; Di Monte, D. A.; Macarthur, H.; Andersen, J. K., MAO-B elevation in mouse brain astrocytes results in Parkinson's pathology. *PLoS One* **2008**, *3* (2), e1616.
106. Bielecka, A. M.; Paul-Samojedny, M.; Obuchowicz, E., Moclobemide exerts anti-inflammatory effect in lipopolysaccharide-activated primary mixed glial cell culture. *Naunyn Schmiedebergs Arch. Pharmacol.* **2010**, *382* (5-6), 409-417.
107. Park, H.; Han, K. M.; Jeon, H.; Lee, J. S.; Lee, H.; Jeon, S. G.; Park, J. H.; Kim, Y. G.; Lin, Y.; Lee, Y. H.; Jeong, Y. H.; Hoe, H. S., The MAO Inhibitor Tranylcypromine Alters LPS- and A $\beta$ -Mediated Neuroinflammatory Responses in Wild-type Mice and a Mouse Model of AD. *Cells* **2020**, *9* (9), 1982.
108. Park, J. H.; Ju, Y. H.; Choi, J. W.; Song, H. J.; Jang, B. K.; Woo, J.; Chun, H.; Kim, H. J.; Shin, S. J.; Yarishkin, O.; Jo, S.; Park, M.; Yeon, S. K.; Kim, S.; Kim, J.; Nam, M. H.; Londhe, A. M.; Cho, S. J.; Cho, S.; Lee, C.; Hwang, S. Y.; Kim, S. W.; Oh, S. J.; Cho, J.; Pae, A. N.; Lee, C. J.; Park, K. D., Newly developed reversible MAO-B inhibitor circumvents the shortcomings of irreversible inhibitors in Alzheimer's disease. *Sci Adv* **2019**, *5* (3), eaav0316.
109. Singh, A.; Kukreti, R.; Saso, L.; Kukreti, S., Oxidative Stress: A Key Modulator in Neurodegenerative Diseases. *Molecules* **2019**, *24* (8), 1583.
110. Uttara, B.; Singh, A. V.; Zamboni, P.; Mahajan, R. T., Oxidative stress and neurodegenerative diseases: a review of upstream and downstream antioxidant therapeutic options. *Curr. Neuropharmacol.* **2009**, *7* (1), 65-74.
111. Mendiola, A. S.; Ryu, J. K.; Bardehle, S.; Meyer-Franke, A.; Ang, K. K.; Wilson, C.; Baeten, K. M.; Hanspers, K.; Merlini, M.; Thomas, S.; Petersen, M. A.; Williams, A.; Thomas, R.; Rafalski, V. A.; Meza-Acevedo, R.; Tognatta, R.; Yan, Z.; Pfaff, S. J.; Machado, M. R.; Bedard, C.; Rios Coronado, P. E.; Jiang, X.; Wang, J.; Pleiss, M. A.; Green, A. J.; Zamvil, S. S.; Pico, A. R.; Bruneau, B. G.; Arkin, M. R.; Akassoglou, K., Transcriptional profiling and therapeutic targeting of oxidative stress in neuroinflammation. *Nat. Immunol.* **2020**, *21* (5), 513-524.
112. Asimwe, N.; Yeo, S. G.; Kim, M. S.; Jung, J.; Jeong, N. Y., Nitric Oxide: Exploring the Contextual Link with Alzheimer's Disease. *Oxid. Med. Cell. Longev.* **2016**, *2016*, 7205747.
113. Ross, C. A.; Poirier, M. A., Protein aggregation and neurodegenerative disease. *Nat. Med.* **2004**, *10* Suppl, S10-7.
114. Sweeney, P.; Park, H.; Baumann, M.; Dunlop, J.; Frydman, J.; Kopito, R.; McCampbell, A.; Leblanc, G.; Venkateswaran, A.; Nurmi, A.; Hodgson, R., Protein misfolding in neurodegenerative diseases: implications and strategies. *Transl. Neurodegener.* **2017**, *6*, 6.
115. Soto, C., Unfolding the role of protein misfolding in neurodegenerative diseases. *Nat. Rev. Neurosci.* **2003**, *4* (1), 49-60.
116. Lévy, E.; El Banna, N.; Baille, D.; Heneman-Masurel, A.; Truchet, S.; Rezaei, H.; Huang, M. E.; Béringue, V.; Martin, D.; Vernis, L., Causative Links between Protein Aggregation and Oxidative Stress: A Review. *Int. J. Mol. Sci.* **2019**, *20* (16).
117. Hou, L.; Kang, I.; Marchant, R. E.; Zagorski, M. G., Methionine 35 oxidation reduces fibril assembly of the amyloid abeta-(1-42) peptide of Alzheimer's disease. *J. Biol. Chem.* **2002**, *277* (43), 40173-40176.
118. Soto, C.; Estrada, L. D., Protein misfolding and neurodegeneration. *Arch Neurol* **2008**, *65* (2), 184-9.
119. Ciccocioppo, F.; Bologna, G.; Ercolino, E.; Pierdomenico, L.; Simeone, P.; Lanuti, P.; Pieragostino, D.; Del Boccio, P.; Marchisio, M.; Miscia, S., Neurodegenerative diseases as proteinopathies-driven immune disorders. *Neural. Regen. Res.* **2020**, *15* (5), 850-856.
120. Currais, A.; Fischer, W.; Maher, P.; Schubert, D., Intraneuronal protein aggregation as a trigger for inflammation and neurodegeneration in the aging brain. *FASEB J.* **2017**, *31* (1), 5-10.
121. Yankner, B. A.; Lu, T., Amyloid beta-protein toxicity and the pathogenesis of Alzheimer disease. *J. Biol. Chem.* **2009**, *284* (8), 4755-4759.
122. Golde, T. E.; Borchelt, D. R.; Giasson, B. I.; Lewis, J., Thinking laterally about neurodegenerative proteinopathies. *J. Clin. Invest.* **2013**, *123* (5), 1847-1855.



123. Heppner, F. L.; Ransohoff, R. M.; Becher, B., Immune attack: the role of inflammation in Alzheimer disease. *Nat. Rev. Neurosci.* **2015**, *16* (6), 358-372.
124. Ben Haim, L.; Carrillo-de Sauvage, M. A.; Ceyzériat, K.; Escartin, C., Elusive roles for reactive astrocytes in neurodegenerative diseases. *Front. Cell. Neurosci.* **2015**, *9*, 278.
125. Cuello, A. C., Early and Late CNS Inflammation in Alzheimer's Disease: Two Extremes of a Continuum? *Trends Pharmacol. Sci.* **2017**, *38* (11), 956-966.
126. Pan, X. D.; Zhu, Y. G.; Lin, N.; Zhang, J.; Ye, Q. Y.; Huang, H. P.; Chen, X. C., Microglial phagocytosis induced by fibrillar  $\beta$ -amyloid is attenuated by oligomeric  $\beta$ -amyloid: implications for Alzheimer's disease. *Mol. Neurodegener.* **2011**, *6*, 45.
127. Lai, A. Y.; McLaurin, J., Clearance of amyloid- $\beta$  peptides by microglia and macrophages: the issue of what, when and where. *Future Neurol.* **2012**, *7* (2), 165-176.
128. Panza, F.; Lozupone, M.; Logroscino, G.; Imbimbo, B. P., A critical appraisal of amyloid- $\beta$ -targeting therapies for Alzheimer disease. *Nat. Rev. Neurol.* **2019**, *15* (2), 73-88.
129. Dong, X. X.; Wang, Y.; Qin, Z. H., Molecular mechanisms of excitotoxicity and their relevance to pathogenesis of neurodegenerative diseases. *Acta Pharmacol. Sin.* **2009**, *30* (4), 379-387.
130. Wang, R.; Reddy, P. H., Role of Glutamate and NMDA Receptors in Alzheimer's Disease. *J. Alzheimers Dis.* **2017**, *57* (4), 1041-1048.
131. Hardingham, G. E.; Fukunaga, Y.; Bading, H., Extrasynaptic NMDARs oppose synaptic NMDARs by triggering CREB shut-off and cell death pathways. *Nat. Neurosci.* **2002**, *5* (5), 405-14.
132. Liu, Y.; Wong, T. P.; Aarts, M.; Rooyackers, A.; Liu, L.; Lai, T. W.; Wu, D. C.; Lu, J.; Tymianski, M.; Craig, A. M.; Wang, Y. T., NMDA receptor subunits have differential roles in mediating excitotoxic neuronal death both in vitro and in vivo. *J. Neurosci.* **2007**, *27* (11), 2846-2857.
133. Kaindl, A. M.; Degos, V.; Peineau, S.; Gouadon, E.; Chhor, V.; Loron, G.; Le Charpentier, T.; Josserand, J.; Ali, C.; Vivien, D.; Collingridge, G. L.; Lombet, A.; Issa, L.; Rene, F.; Loeffler, J. P.; Kavelaars, A.; Verney, C.; Mantz, J.; Gressens, P., Activation of microglial N-methyl-D-aspartate receptors triggers inflammation and neuronal cell death in the developing and mature brain. *Ann. Neurol.* **2012**, *72* (4), 536-549.
134. Viviani, B.; Boraso, M.; Marchetti, N.; Marinovich, M., Perspectives on neuroinflammation and excitotoxicity: a neurotoxic conspiracy? *Neurotoxicology* **2014**, *43*, 10-20.
135. Lipton, S. A., NMDA receptor activity regulates transcription of antioxidant pathways. *Nat. Neurosci.* **2008**, *11* (4), 381-382.
136. Tu, S.; Okamoto, S.; Lipton, S. A.; Xu, H., Oligomeric A $\beta$ -induced synaptic dysfunction in Alzheimer's disease. *Mol. Neurodegener.* **2014**, *9*, 48.
137. Esposito, Z.; Belli, L.; Toniolo, S.; Sancesario, G.; Bianconi, C.; Martorana, A., Amyloid  $\beta$ , glutamate, excitotoxicity in Alzheimer's disease: are we on the right track? *CNS Neurosci. Ther.* **2013**, *19* (8), 549-555.
138. Nygaard, H. B., Targeting Fyn Kinase in Alzheimer's Disease. *Biol. Psychiatry.* **2018**, *83* (4), 369-376.
139. Ittner, L. M.; Götz, J., Amyloid- $\beta$  and tau--a toxic pas de deux in Alzheimer's disease. *Nat. Rev. Neurosci.* **2011**, *12* (2), 65-72.
140. Olivares, D.; Deshpande, V. K.; Shi, Y.; Lahiri, D. K.; Greig, N. H.; Rogers, J. T.; Huang, X., N-methyl D-aspartate (NMDA) receptor antagonists and memantine treatment for Alzheimer's disease, vascular dementia and Parkinson's disease. *Curr. Alzheimer Res.* **2012**, *9* (6), 746-758.
141. Parr, R. G.; Szentpaly, L. v.; Liu, S., Electrophilicity Index. *J. Am. Chem. Soc.* **1999**, *121*, 1922-1924.
142. Lopachin, R. M.; Gavin, T.; Decaprio, A.; Barber, D. S., Application of the Hard and Soft, Acids and Bases (HSAB) theory to toxicant--target interactions. *Chem. Res. Toxicol.* **2012**, *25* (2), 239-251.
143. Vasudevan, A.; Argiriadi, M. A.; Baranczak, A.; Friedman, M. M.; Gavrilyuk, J.; Hobson, A. D.; Hulce, J. J.; Osman, S.; Wilson, N. S., Covalent binders in drug discovery. *Prog. Med. Chem.* **2019**, *58*, 1-62.
144. Gehring, M.; Laufer, S. A., Emerging and Re-Emerging Warheads for Targeted Covalent Inhibitors: Applications in Medicinal Chemistry and Chemical Biology. *J. Med. Chem.* **2019**, *62* (12), 5673-5724.
145. Singh, J.; Petter, R. C.; Baillie, T. A.; Whitty, A., The resurgence of covalent drugs. *Nat. Rev. Drug Discovery* **2011**, *10* (4), 307-317.
146. Roth, G. J.; Stanford, N.; Majerus, P. W., Acetylation of prostaglandin synthase by aspirin. *Proc. Natl. Acad. Sci. USA* **1975**, *72* (8), 3073-3076.
147. Yocum, R. R.; Waxman, D. J.; Rasmussen, J. R.; Strominger, J. L., Mechanism Of Penicillin Action - Penicillin And Substrate Bind Covalently To The Same Active-Site Serine In 2 Bacterial D-Alanine Carboxypeptidases. *Proceed. Natl. Acad. Sci. U. S. A.* **1979**, *76* (6), 2730-2734.
148. Voice, A.; Tresadern, G.; van Vlijmen, H.; Mulholland, A., Limitations of Ligand-Only Approaches for Predicting the Reactivity of Covalent Inhibitors. *J. Chem. Inf. Model.* **2019**, *59* (10), 4220-4227.
149. Baillie, T. A., Targeted Covalent Inhibitors for Drug Design. *Angew. Chem. Int. Ed. Engl.* **2016**, *55* (43), 13408-13421.

150. Vita, E., 10 years into the resurgence of covalent drugs. *Future Med Chem* **2021**, *13*(2), 193-210.
151. Baillie, T. A., Approaches to Mitigate the Risk of Serious Adverse Reactions in Covalent Drug Design. *Expert Opin Drug Discov* **2021**, *16*, 275-287.
152. Hallenbeck, K. K.; Turner, D. M.; Renslo, A. R.; Arkin, M. R., Targeting Non-Catalytic Cysteine Residues Through Structure-Guided Drug Discovery. *Curr. Top. Med. Chem.* **2017**, *17* (1), 4-15.
153. Visscher, M.; Arkin, M. R.; Dansen, T. B., Covalent targeting of acquired cysteines in cancer. *Curr. Opin. Chem. Biol.* **2016**, *30*, 61-67.
154. Johnson, D. S.; Weerapana, E.; Cravatt, B. F., Strategies for discovering and derisking covalent, irreversible enzyme inhibitors. *Future Med. Chem.* **2010**, *2* (6), 949-964.
155. Cheng, S. S.; Yang, G. J.; Wang, W.; Leung, C. H.; Ma, D. L., The design and development of covalent protein-protein interaction inhibitors for cancer treatment. *J. Hematol. Oncol.* **2020**, *13* (1), 26.
156. Smith, A. J.; Zhang, X.; Leach, A. G.; Houk, K. N., Beyond picomolar affinities: quantitative aspects of noncovalent and covalent binding of drugs to proteins. *J. Med. Chem.* **2009**, *52* (2), 225-233.
157. Besancon, M.; Simon, A.; Sachs, G.; Shin, J. M., Sites of reaction of the gastric H,K-ATPase with extracytoplasmic thiol reagents. *J. Biol. Chem.* **1997**, *272* (36), 22438-22446.
158. Ray, S.; Murkin, A. S., New Electrophiles and Strategies for Mechanism-Based and Targeted Covalent Inhibitor Design. *Biochemistry* **2019**, *58* (52), 5234-5244.
159. Baell, J. B.; Holloway, G. A., New substructure filters for removal of pan assay interference compounds (PAINS) from screening libraries and for their exclusion in bioassays. *J. Med. Chem.* **2010**, *53* (7), 2719-2740.
160. Baell, J. B.; Nissink, J. W. M., Seven Year Itch: Pan-Assay Interference Compounds (PAINS) in 2017-Utility and Limitations. *ACS Chem. Biol.* **2018**, *13* (1), 36-44.
161. Noe, M. C.; Gilbert, A. M., Targeted Covalent Enzyme Inhibitors. In *Annual Reports in Medicinal Chemistry*, Elsevier Inc.: 2012; pp 413-439.
162. Gersch, M.; Kreuzer, J.; Sieber, S. A., Electrophilic natural products and their biological targets. *Nat. Prod. Rep.* **2012**, *29* (6), 659-682.
163. Parvez, S.; Long, M. J. C.; Poganik, J. R.; Aye, Y., Redox Signaling by Reactive Electrophiles and Oxidants. *Chem. Rev.* **2018**, *118* (18), 8798-8888.
164. Newton, A. C.; Bootman, M. D.; Scott, J. D., Second Messengers. *Cold Spring Harb. Perspect. Biol.* **2016**, *8* (8).
165. Hershko, A.; Ciechanover, A., The ubiquitin system. *Ann. Rev. Biochem.* **1998**, *67*, 425-479.
166. Long, M. J. C.; Aye, Y., The Die Is Cast: Precision Electrophilic Modifications Contribute to Cellular Decision Making. *Chem. Res. Toxicol.* **2016**, *29* (10), 1575-1582.
167. Bindoli, A.; Rigobello, M. P., Principles in redox signaling: from chemistry to functional significance. *Antioxid. Redox Signal.* **2013**, *18* (13), 1557-1593.
168. Murphy, M. P.; Holmgren, A.; Larsson, N. G.; Halliwell, B.; Chang, C. J.; Kalyanaraman, B.; Rhee, S. G.; Thornalley, P. J.; Partridge, L.; Gems, D.; Nyström, T.; Belousov, V.; Schumacker, P. T.; Winterbourn, C. C., Unraveling the biological roles of reactive oxygen species. *Cell Metab.* **2011**, *13* (4), 361-366.
169. Schieber, M.; Chandel, N. S., ROS function in redox signaling and oxidative stress. *Curr. Biol.* **2014**, *24* (10), R453-462.
170. Kumagai, Y.; Abiko, Y., Environmental Electrophiles: Protein Adducts, Modulation of Redox Signaling, and Interaction with Persulfides/Polysulfides. *Chem. Res. Toxicol.* **2017**, *30* (1), 203-219.
171. Liguori, I.; Russo, G.; Curcio, F.; Bulli, G.; Aran, L.; Della-Morte, D.; Gargiulo, G.; Testa, G.; Cacciatore, F.; Bonaduce, D.; Abete, P., Oxidative stress, aging, and diseases. *Clin. Interv. Aging* **2018**, *13*, 757-772.
172. Ahmadinejad, F.; Geir Møller, S.; Hashemzadeh-Chaleshtori, M.; Bidkhor, G.; Jami, M. S., Molecular Mechanisms behind Free Radical Scavengers Function against Oxidative Stress. *Antioxidants (Basel)* **2017**, *6* (3), 51.
173. Rudolph, T. K.; Freeman, B. A., Transduction of redox signaling by electrophile-protein reactions. *Sci. Signal.* **2009**, *2* (90), re7.
174. Marnett, L. J.; Riggins, J. N.; West, J. D., Endogenous generation of reactive oxidants and electrophiles and their reactions with DNA and protein. *J. Clin. Invest.* **2003**, *111* (5), 583-593.
175. *Post-Translational Modifications in Health and Disease*. Springer Science: 2011; Vol. 13.
176. Long, M. J. C.; Aye, Y., Privileged Electrophile Sensors: A Resource for Covalent Drug Development. *Cell Chem. Biol.* **2017**, *24*, 787-800.
177. Shannon, D. A.; Weerapana, E., Covalent protein modification: the current landscape of residue-specific electrophiles. *Curr. Opin. Chem. Biol.* **2015**, *24*, 18-26.
178. Go, Y. M.; Chandler, J. D.; Jones, D. P., The cysteine proteome. *Free Radic. Biol. Med.* **2015**, *84*, 227-245.
179. van Montfort, R. L.; Congreve, M.; Tisi, D.; Carr, R.; Jhoti, H., Oxidation state of the active-site cysteine in protein tyrosine phosphatase 1B. *Nature* **2003**, *423* (6941), 773-777.
180. Buhrman, G.; Parker, B.; Sohn, J.; Rudolph, J.; Mattos, C., Structural mechanism of oxidative regulation of the phosphatase Cdc25B via an intramolecular disulfide bond. *Biochemistry* **2005**, *44* (14), 5307-5316.

181. Brandes, N.; Schmitt, S.; Jakob, U., Thiol-based redox switches in eukaryotic proteins. *Antioxid. Redox Signal* **2009**, *11* (5), 997-1014.
182. Friguet, B., Oxidized protein degradation and repair in ageing and oxidative stress. *FEBS Lett.* **2006**, *580* (12), 2910-2916.
183. Fujiwara, N.; Nakano, M.; Kato, S.; Yoshihara, D.; Ookawara, T.; Eguchi, H.; Taniguchi, N.; Suzuki, K., Oxidative modification to cysteine sulfonic acid of Cys111 in human copper-zinc superoxide dismutase. *J. Biol. Chem.* **2007**, *282* (49), 35933-35944.
184. Dayalan Naidu, S.; Dinkova-Kostova, A. T., Regulation of the mammalian heat shock factor 1. *FEBS J.* **2017**, *284* (11), 1606-1627.
185. Wall, S. B.; Smith, M. R.; Ricart, K.; Zhou, F.; Vayalil, P. K.; Oh, J. Y.; Landar, A., Detection of electrophile-sensitive proteins. *Biochim. Biophys. Acta* **2014**, *1840* (2), 913-922.
186. Petri, L.; Ábrányi-Balogh, P.; Imre, T.; Pálffy, G.; Perczel, A.; Knez, D.; Hrast, M.; Gobec, M.; Sosič, I.; Nyíri, K.; Vértessy, B. G.; Jänsch, N.; Desczyk, C.; Meyer-Almes, F. J.; Ogris, I.; Grdadolnik, S. G.; Iacovino, L. G.; Binda, C.; Gobec, S.; Keserű, G. M., Assessment of tractable cysteines by covalent fragments screening. *ChemBioChem* **2021**, *22*, 743-753.
187. Wang, S.; Tian, Y.; Wang, M.; Sun, G. B.; Sun, X. B., Advanced Activity-Based Protein Profiling Application Strategies for Drug Development. *Front. Pharmacol.* **2018**, *9*, 353.
188. London, N.; Miller, R. M.; Krishnan, S.; Uchida, K.; Irwin, J. J.; Eidam, O.; Gibold, L.; Cimermančič, P.; Bonnet, R.; Shoichet, B. K.; Taunton, J., Covalent docking of large libraries for the discovery of chemical probes. *Nat. Chem. Biol.* **2014**, *10* (12), 1066-1072.
189. Resnick, E.; Bradley, A.; Gan, J.; Douangamath, A.; Krojer, T.; Sethi, R.; Geurink, P. P.; Aimon, A.; Amitai, G.; Bellini, D.; Bennett, J.; Fairhead, M.; Fedorov, O.; Gabizon, R.; Guo, J.; Plotnikov, A.; Reznik, N.; Ruda, G. F.; Díaz-Sáez, L.; Straub, V. M.; Szommer, T.; Velupillai, S.; Zaidman, D.; Zhang, Y.; Coker, A. R.; Dowson, C. G.; Barr, H. M.; Wang, C.; Huber, K. V. M.; Brennan, P. E.; Ovaa, H.; von Delft, F.; London, N., Rapid Covalent-Probe Discovery by Electrophile-Fragment Screening. *J. Am. Chem. Soc.* **2019**, *141* (22), 8951-8968.
190. Keeley, A.; Petri, L.; Ábrányi-Balogh, P.; Keserű, G. M., Covalent fragment libraries in drug discovery. *Drug Discov. Today* **2020**, *25* (6), 983-996.
191. Parvez, S.; Long, M. J.; Lin, H. Y.; Zhao, Y.; Haegele, J. A.; Pham, V. N.; Lee, D. K.; Aye, Y., T-REX on-demand redox targeting in live cells. *Nat. Protoc.* **2016**, *11* (12), 2328-2356.
192. Poganik, J. R.; Aye, Y., Electrophile Signaling and Emerging Immuno- and Neuro-modulatory Electrophilic Pharmaceuticals. *Front. Aging Neurosci.* **2020**, *12*, 1.
193. O'Brien, J.; Wendell, S. G., Electrophile Modulation of Inflammation: A Two-Hit Approach. *Metabolites* **2020**, *10* (11).
194. Mills, E. A.; Ogrodnik, M. A.; Plave, A.; Mao-Draayer, Y., Emerging Understanding of the Mechanism of Action for Dimethyl Fumarate in the Treatment of Multiple Sclerosis. *Front. Neurol.* **2018**, *9*, 5.
195. Brennan, M. S.; Matos, M. F.; Li, B.; Hronowski, X.; Gao, B.; Juhasz, P.; Rhodes, K. J.; Scannevin, R. H., Dimethyl fumarate and monoethyl fumarate exhibit differential effects on KEAP1, NRF2 activation, and glutathione depletion in vitro. *PLoS One* **2015**, *10* (3), e0120254.
196. Blewett, M. M.; Xie, J.; Zaro, B. W.; Backus, K. M.; Altman, A.; Teijaro, J. R.; Cravatt, B. F., Chemical proteomic map of dimethyl fumarate-sensitive cysteines in primary human T cells. *Sci Signal* **2016**, *9* (445), rs10.
197. Vucic, S.; Ryder, J.; Mekhael, L.; Rd, H.; Mathers, S.; Needham, M.; Dw, S.; Mc, K.; group, T. s., Phase 2 randomized placebo controlled double blind study to assess the efficacy and safety of tecfidera in patients with amyotrophic lateral sclerosis (TEALS Study): Study protocol clinical trial (SPIRIT Compliant). *Medicine (Baltimore)* **2020**, *99* (6), e18904.
198. Satoh, T.; Lipton, S., Recent advances in understanding NRF2 as a druggable target: development of pro-electrophilic and non-covalent NRF2 activators to overcome systemic side effects of electrophilic drugs like dimethyl fumarate. *F1000Res* **2017**, *6*, 2138.
199. Robledinos-Antón, N.; Fernández-Ginés, R.; Manda, G.; Cuadrado, A., Activators and Inhibitors of NRF2: A Review of Their Potential for Clinical Development. *Oxid Med Cell Longev* **2019**, *2019*, 9372182.
200. Cleasby, A.; Yon, J.; Day, P. J.; Richardson, C.; Tickle, I. J.; Williams, P. A.; Callahan, J. F.; Carr, R.; Concha, N.; Kerns, J. K.; Qi, H.; Sweitzer, T.; Ward, P.; Davies, T. G., Structure of the BTB domain of Keap1 and its interaction with the triterpenoid antagonist CDDO. *PLoS One* **2014**, *9* (6), e98896.
201. Del Prete, D.; Tagliatalata-Scafati, O.; Minassi, A.; Sirignano, C.; Cruz, C.; Bellido, M. L.; Muñoz, E.; Appendino, G., Electrophilic Triterpenoid Enones: A Comparative Thiol-Trapping and Bioactivity Study. *J. Nat. Prod.* **2017**, *80* (8), 2276-2283.
202. Sporn, M. B.; Liby, K. T.; Yore, M. M.; Fu, L.; Lopchuk, J. M.; Gribble, G. W., New synthetic triterpenoids: potent agents for prevention and treatment of tissue injury caused by inflammatory and oxidative stress. *J. Nat. Prod.* **2011**, *74* (3), 537-545.

203. Kim, J. E.; Park, H.; Lee, J. E.; Kang, T. C., CDDO-Me Inhibits Microglial Activation and Monocyte Infiltration by Abrogating NF $\kappa$ B- and p38 MAPK-Mediated Signaling Pathways Following Status Epilepticus. *Cells* **2020**, *9* (5), 1123.
204. Tran, T. A.; McCoy, M. K.; Sporn, M. B.; Tansey, M. G., The synthetic triterpenoid CDDO-methyl ester modulates microglial activities, inhibits TNF production, and provides dopaminergic neuroprotection. *J Neuroinflammation* **2008**, *5*, 14.
205. Dumont, M.; Wille, E.; Calingasan, N. Y.; Tampellini, D.; Williams, C.; Gouras, G. K.; Liby, K.; Sporn, M.; Nathan, C.; Flint Beal, M.; Lin, M. T., Triterpenoid CDDO-methylamide improves memory and decreases amyloid plaques in a transgenic mouse model of Alzheimer's disease. *J. Neurochem.* **2009**, *109* (2), 502-512.
206. Stack, C.; Ho, D.; Wille, E.; Calingasan, N. Y.; Williams, C.; Liby, K.; Sporn, M.; Dumont, M.; Beal, M. F., Triterpenoids CDDO-ethyl amide and CDDO-trifluoroethyl amide improve the behavioral phenotype and brain pathology in a transgenic mouse model of Huntington's disease. *Free Radic. Biol. Med.* **2010**, *49* (2), 147-158.
207. Hu, C.; Egger, A. L.; Mesecar, A. D.; van Breemen, R. B., Modification of Keap1 cysteine residues by sulforaphane. *Chem. Res. Toxicol.* **2011**, *24* (4), 515-521.
208. Dinkova-Kostova, A. T.; Fahey, J. W.; Kostov, R. V.; Kensler, T. W., KEAP1 and NRF2: Targeting the NRF2 Pathway with Sulforaphane. *Trends Food Sci. Technol.* **2017**, *69* (Pt B), 257-269.
209. Klomprens, E. A.; Ding, Y., The neuroprotective mechanisms and effects of sulforaphane. *Brain Circ.* **2019**, *5* (2), 74-83.
210. Egea, J.; Buendia, I.; Parada, E.; Navarro, E.; Rada, P.; Cuadrado, A.; López, M. G.; García, A. G.; León, R., Melatonin-sulforaphane hybrid ITH12674 induces neuroprotection in oxidative stress conditions by a 'drug-prodrug' mechanism of action. *Br. J. Pharmacol.* **2015**, *172* (7), 1807-1821.
211. Michalska, P.; Buendia, I.; Duarte, P.; FernandezMendivil, C.; Negredo, P.; Cuadrado, A.; López, M. G.; Leon, R., Melatonin-sulforaphane hybrid ITH12674 attenuates glial response in vivo by blocking LPS binding to MD2 and receptor oligomerization. *Pharmacol. Res.* **2020**, *152*, 104597.
212. Shin, J. W.; Chun, K. S.; Kim, D. H.; Kim, S. J.; Kim, S. H.; Cho, N. C.; Na, H. K.; Surh, Y. J., Curcumin induces stabilization of Nrf2 protein through Keap1 cysteine modification. *Biochem. Pharmacol.* **2020**, *173*, 113820.
213. Catanzaro, M.; Corsini, E.; Rosini, M.; Racchi, M.; Lanni, C., Immunomodulators Inspired by Nature: A Review on Curcumin and Echinacea. *Molecules* **2018**, *23* (11), 2778.
214. Singh, P. K.; Kotia, V.; Ghosh, D.; Mohite, G. M.; Kumar, A.; Maji, S. K., Curcumin modulates  $\alpha$ -synuclein aggregation and toxicity. *ACS Chem. Neurosci.* **2013**, *4* (3), 393-407.
215. Serafini, M. M.; Catanzaro, M.; Rosini, M.; Racchi, M.; Lanni, C., Curcumin in Alzheimer's disease: Can we think to new strategies and perspectives for this molecule? *Pharmacol. Res.* **2017**, *124*, 146-155.
216. Di Martino, R. M. C.; Pruccoli, L.; Bisi, A.; Gobbi, S.; Rampa, A.; Martinez, A.; Pérez, C.; Martinez-Gonzalez, L.; Paglione, M.; Di Schiavi, E.; Seghetti, F.; Tarozzi, A.; Belluti, F., Novel Curcumin-Diethyl Fumarate Hybrid as a Dualistic GSK-3 $\beta$  Inhibitor/Nrf2 Inducer for the Treatment of Parkinson's Disease. *ACS Chem. Neurosci.* **2020**, *11* (17), 2728-2740.
217. Magesh, S.; Chen, Y.; Hu, L., Small molecule modulators of Keap1-Nrf2-ARE pathway as potential preventive and therapeutic agents. *Med. Res. Rev.* **2012**, *32* (4), 687-726.
218. Nouredin, S. A.; El-Shishtawy, R. M.; Al-Footy, K. O., Curcumin analogues and their hybrid molecules as multifunctional drugs. *Eur. J. Med. Chem.* **2019**, *182*, 111631.
219. Luis, P. B.; Boeglin, W. E.; Schneider, C., Thiol Reactivity of Curcumin and Its Oxidation Products. *Chem. Res. Toxicol.* **2018**, *31* (4), 269-276.
220. Satoh, T.; McKercher, S. R.; Lipton, S. A., Nrf2/ARE-mediated antioxidant actions of pro-electrophilic drugs. *Free Radic. Biol. Med.* **2013**, *65*, 645-657.
221. Lipton, S. A., Pathologically activated therapeutics for neuroprotection. *Nat. Rev. Neurosci.* **2007**, *8* (10), 803-808.
222. Satoh, T.; Kosaka, K.; Itoh, K.; Kobayashi, A.; Yamamoto, M.; Shimojo, Y.; Kitajima, C.; Cui, J.; Kamins, J.; Okamoto, S.; Izumi, M.; Shirasawa, T.; Lipton, S. A., Carnosic acid, a catechol-type electrophilic compound, protects neurons both in vitro and in vivo through activation of the Keap1/Nrf2 pathway via S-alkylation of targeted cysteines on Keap1. *J. Neurochem.* **2008**, *104* (4), 1116-1131.
223. Lipton, S. A.; Rezaie, T.; Nutter, A.; Lopez, K. M.; Parker, J.; Kosaka, K.; Satoh, T.; McKercher, S. R.; Masliah, E.; Nakanishi, N., Therapeutic advantage of pro-electrophilic drugs to activate the Nrf2/ARE pathway in Alzheimer's disease models. *Cell Death Dis.* **2016**, *7* (12), e2499.
224. Sun, H.; Zhu, J.; Lin, H.; Gu, K.; Feng, F., Recent progress in the development of small molecule Nrf2 modulators: a patent review (2012-2016). *Expert Opin. Ther. Pat.* **2017**, *27* (7), 763-785.
225. Wardyn, J. D.; Ponsford, A. H.; Sanderson, C. M., Dissecting molecular cross-talk between Nrf2 and NF- $\kappa$ B response pathways. *Biochem. Soc. Trans.* **2015**, *43* (4), 621-626.
226. Ahmad, R.; Raina, D.; Meyer, C.; Kharbanda, S.; Kufe, D., Triterpenoid CDDO-Me blocks the NF- $\kappa$ B pathway by direct inhibition of IKK $\beta$  on Cys-179. *J. Biol. Chem.* **2006**, *281* (47), 35764-35769.

227. Kastrati, I.; Siklos, M. I.; Calderon-Gierszal, E. L.; El-Shennawy, L.; Georgieva, G.; Thayer, E. N.; Thatcher, G. R.; Frasor, J., Dimethyl Fumarate Inhibits the Nuclear Factor  $\kappa$ B Pathway in Breast Cancer Cells by Covalent Modification of p65 Protein. *J. Biol. Chem.* **2016**, *291* (7), 3639-3647.
228. Edwards, R. L.; Luis, P. B.; Varuzza, P. V.; Joseph, A. I.; Presley, S. H.; Chaturvedi, R.; Schneider, C., The anti-inflammatory activity of curcumin is mediated by its oxidative metabolites. *J. Biol. Chem.* **2017**, *292* (52), 21243-21252.
229. Abdeldayem, A.; Raouf, Y. S.; Constantinescu, S. N.; Moriggl, R.; Gunning, P. T., Advances in covalent kinase inhibitors. *Chem. Soc. Rev.* **2020**, *49* (9), 2617-2687.
230. Gupta, S. C.; Prasad, S.; Reuter, S.; Kannappan, R.; Yadav, V. R.; Ravindran, J.; Hema, P. S.; Chaturvedi, M. M.; Nair, M.; Aggarwal, B. B., Modification of cysteine 179 of I $\kappa$ B kinase by nimbolide leads to down-regulation of NF- $\kappa$ B-regulated cell survival and proliferative proteins and sensitization of tumor cells to chemotherapeutic agents. *J. Biol. Chem.* **2010**, *285* (46), 35406-35417.
231. Dong, T.; Li, C.; Wang, X.; Dian, L.; Zhang, X.; Li, L.; Chen, S.; Cao, R.; Huang, N.; He, S.; Lei, X., Ainsliadimer A selectively inhibits IKK $\alpha/\beta$  by covalently binding a conserved cysteine. *Nat. Commun.* **2015**, *6*, 6522.
232. Park, H.; Shin, Y.; Choe, H.; Hong, S., Computational design and discovery of nanomolar inhibitors of I $\kappa$ B kinase  $\beta$ . *J. Am. Chem. Soc.* **2015**, *137* (1), 337-348.
233. Elkamhawy, A.; Kim, N. Y.; Hassan, A. H. E.; Park, J. E.; Yang, J. E.; Oh, K. S.; Lee, B. H.; Lee, M. Y.; Shin, K. J.; Lee, K. T.; Hur, W.; Roh, E. J., Design, synthesis and biological evaluation of novel thiazolidinedione derivatives as irreversible allosteric IKK- $\beta$  modulators. *Eur. J. Med. Chem.* **2018**, *157*, 691-704.
234. Elkamhawy, A.; Kim, N. Y.; Hassan, A. H. E.; Park, J. E.; Paik, S.; Yang, J. E.; Oh, K. S.; Lee, B. H.; Lee, M. Y.; Shin, K. J.; Pae, A. N.; Lee, K. T.; Roh, E. J., Thiazolidine-2,4-dione-based irreversible allosteric IKK- $\beta$  kinase inhibitors: Optimization into in vivo active anti-inflammatory agents. *Eur. J. Med. Chem.* **2020**, *188*, 111955.
235. Deny, L. J.; Traboulsi, H.; Cantin, A. M.; Marsault, É.; Richter, M. V.; Bélanger, G., Bis-Michael Acceptors as Novel Probes to Study the Keap1/Nrf2/ARE Pathway. *J. Med. Chem.* **2016**, *59* (20), 9431-9442.
236. Widen, J. C.; Kempema, A. M.; Villalta, P. W.; Harki, D. A., Targeting NF- $\kappa$ B p65 with a Helenalin Inspired Bis-electrophile. *ACS Chem. Biol.* **2017**, *12* (1), 102-113.
237. Büchele, B.; Zugmaier, W.; Lunov, O.; Syrovets, T.; Merfort, I.; Simmet, T., Surface plasmon resonance analysis of nuclear factor- $\kappa$ B protein interactions with the sesquiterpene lactone helenalin. *Anal. Biochem.* **2010**, *401* (1), 30-37.
238. García-Piñeres, A. J.; Castro, V.; Mora, G.; Schmidt, T. J.; Strunck, E.; Pahl, H. L.; Merfort, I., Cysteine 38 in p65/NF- $\kappa$ B plays a crucial role in DNA binding inhibition by sesquiterpene lactones. *J. Biol. Chem.* **2001**, *276* (43), 39713-39720.
239. Pande, V.; Sousa, S. F.; Ramos, M. J., Direct covalent modification as a strategy to inhibit nuclear factor- $\kappa$ B. *Curr. Med. Chem.* **2009**, *16* (32), 4261-4273.
240. Yamamoto, M.; Horie, R.; Takeiri, M.; Kozawa, I.; Umezawa, K., Inactivation of NF- $\kappa$ B components by covalent binding of (-)-dehydroxymethylepoxyquinomicin to specific cysteine residues. *J. Med. Chem.* **2008**, *51* (18), 5780-5788.
241. Chen, K. M.; Spratt, T. E.; Stanley, B. A.; De Cotiis, D. A.; Bewley, M. C.; Flanagan, J. M.; Desai, D.; Das, A.; Fiala, E. S.; Amin, S.; El-Bayoumy, K., Inhibition of nuclear factor- $\kappa$ B DNA binding by organoselenocyanates through covalent modification of the p50 subunit. *Cancer Res.* **2007**, *67* (21), 10475-10483.
242. Switzer, C. H.; Cheng, R. Y.; Ridnour, L. A.; Murray, M. C.; Tazzari, V.; Sparatore, A.; Del Soldato, P.; Hines, H. B.; Glynn, S. A.; Ambs, S.; Wink, D. A., Dithiolethiones inhibit NF- $\kappa$ B activity via covalent modification in human estrogen receptor-negative breast cancer. *Cancer Res.* **2012**, *72* (9), 2394-2404.
243. Dhouafli, Z.; Cuanalo-Contreras, K.; Hayouni, E. A.; Mays, C. E.; Soto, C.; Moreno-Gonzalez, I., Inhibition of protein misfolding and aggregation by natural phenolic compounds. *Cell Mol Life Sci* **2018**, *75* (19), 3521-3538.
244. Giorgetti, S.; Greco, C.; Tortora, P.; Aprile, F. A., Targeting Amyloid Aggregation: An Overview of Strategies and Mechanisms. *Int. J. Mol. Sci.* **2018**, *19* (9).
245. Yang, F.; Lim, G. P.; Begum, A. N.; Ubeda, O. J.; Simmons, M. R.; Ambegaokar, S. S.; Chen, P. P.; Kaye, R.; Glabe, C. G.; Frautschy, S. A.; Cole, G. M., Curcumin inhibits formation of amyloid beta oligomers and fibrils, binds plaques, and reduces amyloid in vivo. *J. Biol. Chem.* **2005**, *280* (7), 5892-5901.
246. Thapa, A.; Jett, S. D.; Chi, E. Y., Curcumin Attenuates Amyloid- $\beta$  Aggregate Toxicity and Modulates Amyloid- $\beta$  Aggregation Pathway. *ACS Chem. Neurosci.* **2016**, *7* (1), 56-68.
247. Palhano, F. L.; Lee, J.; Grimster, N. P.; Kelly, J. W., Toward the molecular mechanism(s) by which EGCG treatment remodels mature amyloid fibrils. *J. Am. Chem. Soc.* **2013**, *135* (20), 7503-7510.
248. An, T. T.; Feng, S.; Zeng, C. M., Oxidized epigallocatechin gallate inhibited lysozyme fibrillation more strongly than the native form. *Redox Biol.* **2017**, *11*, 315-321.
249. Zhu, M.; Rajamani, S.; Kaylor, J.; Han, S.; Zhou, F.; Fink, A. L., The flavonoid baicalein inhibits fibrillation of alpha-synuclein and disaggregates existing fibrils. *J. Biol. Chem.* **2004**, *279* (26), 26846-26857.

250. Velandar, P.; Wu, L.; Ray, W. K.; Helm, R. F.; Xu, B., Amylin Amyloid Inhibition by Flavonoid Baicalein: Key Roles of Its Vicinal Dihydroxyl Groups of the Catechol Moiety. *Biochemistry* **2016**, *55* (31), 4255-4258.
251. Sato, M.; Murakami, K.; Uno, M.; Nakagawa, Y.; Katayama, S.; Akagi, K.; Masuda, Y.; Takegoshi, K.; Irie, K., Site-specific inhibitory mechanism for amyloid  $\beta$ 42 aggregation by catechol-type flavonoids targeting the Lys residues. *J. Biol. Chem.* **2013**, *288* (32), 23212-232124.
252. Takahashi, H.; Xia, P.; Cui, J.; Talantova, M.; Bodhinathan, K.; Li, W.; Saleem, S.; Holland, E. A.; Tong, G.; Piña-Crespo, J.; Zhang, D.; Nakanishi, N.; Larrick, J. W.; McKercher, S. R.; Nakamura, T.; Wang, Y.; Lipton, S. A., Pharmacologically targeted NMDA receptor antagonism by NitroMemantine for cerebrovascular disease. *Sci. Rep.* **2015**, *5*, 14781.
253. Talantova, M.; Sanz-Blasco, S.; Zhang, X.; Xia, P.; Akhtar, M. W.; Okamoto, S.; Dziejczapolski, G.; Nakamura, T.; Cao, G.; Pratt, A. E.; Kang, Y. J.; Tu, S.; Molokanova, E.; McKercher, S. R.; Hires, S. A.; Sason, H.; Stouffer, D. G.; Buczynski, M. W.; Solomon, J. P.; Michael, S.; Powers, E. T.; Kelly, J. W.; Roberts, A.; Tong, G.; Fang-Newmeyer, T.; Parker, J.; Holland, E. A.; Zhang, D.; Nakanishi, N.; Chen, H. S.; Wolosker, H.; Wang, Y.; Parsons, L. H.; Ambasadhan, R.; Masliah, E.; Heinemann, S. F.; Piña-Crespo, J. C.; Lipton, S. A., A $\beta$  induces astrocytic glutamate release, extrasynaptic NMDA receptor activation, and synaptic loss. *Proc. Natl. Acad. Sci. U S A* **2013**, *110* (27), E2518-2527.
254. Bernardo, A.; Minghetti, L., PPAR-gamma agonists as regulators of microglial activation and brain inflammation. *Curr. Pharm. Des.* **2006**, *12* (1), 93-109.
255. Chen, Y. C.; Wu, J. S.; Tsai, H. D.; Huang, C. Y.; Chen, J. J.; Sun, G. Y.; Lin, T. N., Peroxisome proliferator-activated receptor gamma (PPAR- $\gamma$ ) and neurodegenerative disorders. *Mol Neurobiol* **2012**, *46* (1), 114-24.
256. Yahfoufi, N.; Alsadi, N.; Jambi, M.; Matar, C., The Immunomodulatory and Anti-Inflammatory Role of Polyphenols. *Nutrients* **2018**, *10* (11), 1618.
257. Jan, A.; Adolfsson, O.; Allaman, I.; Buccarello, A. L.; Magistretti, P. J.; Pfeifer, A.; Muhs, A.; Lashuel, H. A., Abeta42 neurotoxicity is mediated by ongoing nucleated polymerization process rather than by discrete Abeta42 species. *J. Biol. Chem.* **2011**, *286* (10), 8585-8596.
258. Bernstein, S. L.; Dupuis, N. F.; Lazo, N. D.; Wyttenbach, T.; Condrón, M. M.; Bitan, G.; Teplow, D. B.; Shea, J. E.; Ruotolo, B. T.; Robinson, C. V.; Bowers, M. T., Amyloid- $\beta$  protein oligomerization and the importance of tetramers and dodecamers in the aetiology of Alzheimer's disease. *Nat. Chem.* **2009**, *1* (4), 326-331.
259. Laurén, J.; Gimbel, D. A.; Nygaard, H. B.; Gilbert, J. W.; Strittmatter, S. M., Cellular prion protein mediates impairment of synaptic plasticity by amyloid-beta oligomers. *Nature* **2009**, *457* (7233), 1128-1132.
260. Swomley, A. M.; Förster, S.; Keeney, J. T.; Triplett, J.; Zhang, Z.; Sultana, R.; Butterfield, D. A., Abeta, oxidative stress in Alzheimer disease: evidence based on proteomics studies. *Biochim. Biophys. Acta* **2014**, *1842* (8), 1248-1257.
261. Bitan, G.; Tarus, B.; Vollers, S. S.; Lashuel, H. A.; Condrón, M. M.; Straub, J. E.; Teplow, D. B., A molecular switch in amyloid assembly: Met35 and amyloid beta-protein oligomerization. *J. Am. Chem. Soc.* **2003**, *125* (50), 15359-15365.
262. Simoni, E.; Serafini, M. M.; Bartolini, M.; Caporaso, R.; Pinto, A.; Necchi, D.; Fiori, J.; Andrisano, V.; Minarini, A.; Lanni, C.; Rosini, M., Nature-Inspired Multifunctional Ligands: Focusing on Amyloid-Based Molecular Mechanisms of Alzheimer's Disease. *ChemMedChem* **2016**, *11* (12), 1309-1317.
263. Simoni, E.; Serafini, M. M.; Caporaso, R.; Marchetti, C.; Racchi, M.; Minarini, A.; Bartolini, M.; Lanni, C.; Rosini, M., Targeting the Nrf2/Amyloid-Beta Liaison in Alzheimer's Disease: A Rational Approach. *ACS Chem. Neurosci.* **2017**, *8* (7), 1618-1627.
264. Bu, X. L.; Rao, P. P. N.; Wang, Y. J., Anti-amyloid Aggregation Activity of Natural Compounds: Implications for Alzheimer's Drug Discovery. *Mol. Neurobiol.* **2016**, *53* (6), 3565-3575.
265. Tu, L. H.; Young, L. M.; Wong, A. G.; Ashcroft, A. E.; Radford, S. E.; Raleigh, D. P., Mutational analysis of the ability of resveratrol to inhibit amyloid formation by islet amyloid polypeptide: critical evaluation of the importance of aromatic-inhibitor and histidine-inhibitor interactions. *Biochemistry* **2015**, *54* (3), 666-676.
266. Emanuelsson, R.; Sterby, M.; Strømme, M.; Sjödin, M., An All-Organic Proton Battery. *J. Am. Chem. Soc.* **2017**, *139* (13), 4828-4834.
267. Le, T. N.; Cho, W. J., First total synthesis of the phenolic 7,8-dihydro-8-oxoprotoberberine alkaloid, cerasonine. *Chem. Pharm. Bull. (Tokyo)* **2008**, *56* (7), 1026-1029.
268. Li, Y.; Huang, Q.; Yu, X.; Liu, Y.; Li, L.; Li, B.; Zhang, X.; Chen, S.; Liu, Z.; Zhao, X.; Ma, J., Study of reactions of N $\epsilon$ -(carboxymethyl) lysine with o-benzoquinones by cyclic voltammetry. *Food Chem.* **2020**, *307*, 125554.
269. Scherzer-Attali, R.; Pellarin, R.; Convertino, M.; Frydman-Marom, A.; Egoz-Matia, N.; Peled, S.; Levy-Sakin, M.; Shalev, D. E.; Cafilisch, A.; Gazit, E.; Segal, D., Complete phenotypic recovery of an Alzheimer's disease model by a quinone-tryptophan hybrid aggregation inhibitor. *PLoS One* **2010**, *5* (6), e11101.

270. Convertino, M.; Pellarin, R.; Catto, M.; Carotti, A.; Caflich, A., 9,10-Anthraquinone hinders beta-aggregation: how does a small molecule interfere with Abeta-peptide amyloid fibrillation? *Protein Sci.* **2009**, *18* (4), 792-800.
271. Ginex, T.; Trius, M.; Luque, F. J., Computational Study of the Aza-Michael Addition of the Flavonoid (+)-Taxifolin in the Inhibition of  $\beta$ -Amyloid Fibril Aggregation. *Chemistry* **2018**, *24* (22), 5813-5824.
272. Forester, S. C.; Lambert, J. D., The role of antioxidant versus pro-oxidant effects of green tea polyphenols in cancer prevention. *Mol. Nutr. Food Res.* **2011**, *55* (6), 844-854.
273. Fiori, J.; Naldi, M.; Bartolini, M.; Andrisano, V., Disclosure of a fundamental clue for the elucidation of the myricetin mechanism of action as amyloid aggregation inhibitor by mass spectrometry. *Electrophoresis* **2012**, *33* (22), 3380-3386.
274. Wu, J.; Bie, B.; Yang, H.; Xu, J. J.; Brown, D. L.; Naguib, M., Activation of the CB2 receptor system reverses amyloid-induced memory deficiency. *Neurobiol. Aging* **2013**, *34* (3), 791-804.
275. Mangiatordi, G. F.; Intranuovo, F.; Delre, P.; Abatematteo, F. S.; Abate, C.; Niso, M.; Creanza, T. M.; Ancona, N.; Stefanachi, A.; Contino, M., Cannabinoid Receptor Subtype 2 (CB2R) in a Multitarget Approach: Perspective of an Innovative Strategy in Cancer and Neurodegeneration. *J. Med. Chem.* **2020**, *63*(23), 14448-14469.
276. Scheiner, M.; Dolles, D.; Gunesch, S.; Hoffmann, M.; Nabissi, M.; Marinelli, O.; Naldi, M.; Bartolini, M.; Petralla, S.; Poeta, E.; Monti, B.; Falkeis, C.; Vieth, M.; Hübner, H.; Gmeiner, P.; Maitra, R.; Maurice, T.; Decker, M., Dual-Acting Cholinesterase-Human Cannabinoid Receptor 2 Ligands Show Pronounced Neuroprotection in Vitro and Overadditive and Disease-Modifying Neuroprotective Effects in Vivo. *J. Med. Chem.* **2019**, *62* (20), 9078-9102.
277. Spinelli, F.; Capparelli, E.; Abate, C.; Colabufo, N. A.; Contino, M., Perspectives of Cannabinoid Type 2 Receptor (CB2R) Ligands in Neurodegenerative Disorders: Structure-Affinity Relationship (SAfiR) and Structure-Activity Relationship (SAR) Studies. *J. Med. Chem.* **2017**, *60* (24), 9913-9931.
278. Soto-Ortega, D. D.; Murphy, B. P.; Gonzalez-Velasquez, F. J.; Wilson, K. A.; Xie, F.; Wang, Q.; Moss, M. A., Inhibition of amyloid- $\beta$  aggregation by coumarin analogs can be manipulated by functionalization of the aromatic center. *Bioorg. Med. Chem.* **2011**, *19* (8), 2596-2602.
279. Huang, M.; Xie, S. S.; Jiang, N.; Lan, J. S.; Kong, L. Y.; Wang, X. B., Multifunctional coumarin derivatives: monoamine oxidase B (MAO-B) inhibition, anti- $\beta$ -amyloid (A $\beta$ ) aggregation and metal chelation properties against Alzheimer's disease. *Bioorg. Med. Chem. Lett.* **2015**, *25* (3), 508-513.
280. Turkman, N.; Shavrin, A.; Ivanov, R. A.; Rabinovich, B.; Volgin, A.; Gelovani, J. G.; Alauddin, M. M., Fluorinated cannabinoid CB2 receptor ligands: synthesis and in vitro binding characteristics of 2-oxoquinoline derivatives. *Bioorg. Med. Chem.* **2011**, *19* (18), 5698-5707.
281. Han, S.; Zhang, F. F.; Qian, H. Y.; Chen, L. L.; Pu, J. B.; Xie, X.; Chen, J. Z., Design, syntheses, structure-activity relationships and docking studies of coumarin derivatives as novel selective ligands for the CB2 receptor. *Eur. J. Med. Chem.* **2015**, *93*, 16-32.
282. Page, D.; Balaux, E.; Boisvert, L.; Liu, Z.; Milburn, C.; Tremblay, M.; Wei, Z.; Woo, S.; Luo, X.; Cheng, Y.; Yang, H.; Srivastava, S.; Zhou, F.; Brown, W.; Tomaszewski, M.; Walpole, C.; Hodzic, L.; St-Onge, S.; Godbout, C.; Salois, D.; Payza, K., Novel benzimidazole derivatives as selective CB2 agonists. *Bioorg. Med. Chem. Lett.* **2008**, *18* (13), 3695-3700.
283. Contestabile, A., Cerebellar granule cells as a model to study mechanisms of neuronal apoptosis or survival in vivo and in vitro. *Cerebellum* **2002**, *1* (1), 41-55.
284. Peña-Altamira, E.; Petralla, S.; Massenzio, F.; Virgili, M.; Bolognesi, M. L.; Monti, B., Nutritional and Pharmacological Strategies to Regulate Microglial Polarization in Cognitive Aging and Alzheimer's Disease. *Front. Aging Neurosci.* **2017**, *9*, 175.
285. Ma, L.; Jia, J.; Liu, X.; Bai, F.; Wang, Q.; Xiong, L., Activation of murine microglial N9 cells is attenuated through cannabinoid receptor CB2 signaling. *Biochem Biophys. Res. Commun.* **2015**, *458* (1), 92-97.
286. Swanson, C. R.; Joers, V.; Bondarenko, V.; Brunner, K.; Simmons, H. A.; Ziegler, T. E.; Kemnitz, J. W.; Johnson, J. A.; Emborg, M. E., The PPAR- $\gamma$  agonist pioglitazone modulates inflammation and induces neuroprotection in parkinsonian monkeys. *J. Neuroinflammation* **2011**, *8*, 91.
287. Breidert, T.; Callebert, J.; Heneka, M. T.; Landreth, G.; Launay, J. M.; Hirsch, E. C., Protective action of the peroxisome proliferator-activated receptor-gamma agonist pioglitazone in a mouse model of Parkinson's disease. *J. Neurochem.* **2002**, *82* (3), 615-624.
288. Quinn, L. P.; Crook, B.; Hows, M. E.; Vidgeon-Hart, M.; Chapman, H.; Upton, N.; Medhurst, A. D.; Virley, D. J., The PPARgamma agonist pioglitazone is effective in the MPTP mouse model of Parkinson's disease through inhibition of monoamine oxidase B. *Br. J. Pharmacol.* **2008**, *154* (1), 226-233.
289. Schedin-Weiss, S.; Inoue, M.; Hromadkova, L.; Teranishi, Y.; Yamamoto, N. G.; Wiehager, B.; Bogdanovic, N.; Winblad, B.; Sandebring-Matton, A.; Frykman, S.; Tjernberg, L. O., Monoamine oxidase B is elevated in Alzheimer disease neurons, is associated with  $\gamma$ -secretase and regulates neuronal amyloid  $\beta$ -peptide levels. *Alzheimers Res. Ther.* **2017**, *9* (1), 57.

290. Binda, C.; Aldeco, M.; Geldenhuys, W. J.; Tortorici, M.; Mattevi, A.; Edmondson, D. E., Molecular Insights into Human Monoamine Oxidase B Inhibition by the Glitazone Anti-Diabetes Drugs. *ACS Med. Chem. Lett.* **2011**, *3* (1), 39-42.
291. Watson, G. S.; Cholerton, B. A.; Reger, M. A.; Baker, L. D.; Plymate, S. R.; Asthana, S.; Fishel, M. A.; Kulstad, J. J.; Green, P. S.; Cook, D. G.; Kahn, S. E.; Keeling, M. L.; Craft, S., Preserved cognition in patients with early Alzheimer disease and amnesic mild cognitive impairment during treatment with rosiglitazone: a preliminary study. *Am. J. Geriatr. Psychiatry* **2005**, *13* (11), 950-958.
292. Sato, T.; Hanyu, H.; Hirao, K.; Kanetaka, H.; Sakurai, H.; Iwamoto, T., Efficacy of PPAR- $\gamma$  agonist pioglitazone in mild Alzheimer disease. *Neurobiol. Aging* **2011**, *32* (9), 1626-1633.
293. Catanzaro, M.; Lanni, C.; Basagni, F.; Rosini, M.; Govoni, S.; Amadio, M., -Light on Age-Related Macular Degeneration: Targeting Nrf2-Pathway as a Novel Therapeutic Strategy for Retinal Pigment Epithelium. *Front. Pharmacol.* **2020**, *11*, 844.
294. De Nuccio, C.; Bernardo, A.; Troiano, C.; Brignone, M. S.; Falchi, M.; Greco, A.; Rosini, M.; Basagni, F.; Lanni, C.; Serafini, M. M.; Minghetti, L.; Visentin, S., NRF2 and PPAR- $\gamma$  Pathways in Oligodendrocyte Progenitors: Focus on ROS Protection, Mitochondrial Biogenesis and Promotion of Cell Differentiation. *Int. J. Mol. Sci.* **2020**, *21* (19), 7216.
295. Rosini, M.; Simoni, E.; Caporaso, R.; Minarini, A., Multitarget strategies in Alzheimer's disease: benefits and challenges on the road to therapeutics. *Future Med. Chem.* **2016**, *8* (6), 697-711.
296. Geldenhuys, W. J.; Darvesh, A. S.; Funk, M. O.; Van der Schyf, C. J.; Carroll, R. T., Identification of novel monoamine oxidase B inhibitors by structure-based virtual screening. *Bioorg. Med. Chem. Lett.* **2010**, *20* (17), 5295-5298.
297. Jamali, B.; Bjørnsdottir, I.; Nordfang, O.; Hansen, S. H., Investigation of racemisation of the enantiomers of glitazone drug compounds at different pH using chiral HPLC and chiral CE. *J. Pharm. Biomed. Anal.* **2008**, *46* (1), 82-87.
298. Davis, R. A., Isolation and structure elucidation of the new fungal metabolite (-)-xylariamide A. *J. Nat. Prod.* **2005**, *68* (5), 769-772.
299. Goel, A.; Parihar, A.; Mishra, P.; Varshney, S.; Nag, P.; Beg, M.; Gaikwad, A.; Rath, S. K., Design and synthesis of novel pyranone-based insulin sensitizers exhibiting *in vivo* hepatoprotective activity. *Med. Chem. Commun.* **2013**, *4*, 1532-1536.
300. Santillo, M. F.; Liu, Y.; Ferguson, M.; Vohra, S. N.; Wiesenfeld, P. L., Inhibition of monoamine oxidase (MAO) by  $\beta$ -carbolines and their interactions in live neuronal (PC12) and liver (HuH-7 and MH1C1) cells. *Toxicol. In Vitro* **2014**, *28* (3), 403-410.
301. Lipton, S. A., Failures and successes of NMDA receptor antagonists: molecular basis for the use of open-channel blockers like memantine in the treatment of acute and chronic neurologic insults. *NeuroRx* **2004**, *1* (1), 101-110.
302. Müller, M. K.; Jacobi, E.; Sakimura, K.; Malinow, R.; von Engelhardt, J., NMDA receptors mediate synaptic depression, but not spine loss in the dentate gyrus of adult amyloid Beta ( $A\beta$ ) overexpressing mice. *Acta Neuropathol. Commun.* **2018**, *6* (1), 110.
303. Gasparini, L.; Dityatev, A., Beta-amyloid and glutamate receptors. *Exp. Neurol.* **2008**, *212* (1), 1-4.
304. National Institute of Health ClinicalTrials.gov. <https://clinicaltrials.gov/> (accessed 20/12/2020).
305. Song, X.; Jensen, M.; Jogini, V.; Stein, R. A.; Lee, C. H.; Mchaourab, H. S.; Shaw, D. E.; Gouaux, E., Mechanism of NMDA receptor channel block by MK-801 and memantine. *Nature* **2018**, *556* (7702), 515-519.
306. Xia, P.; Chen, H. S.; Zhang, D.; Lipton, S. A., Memantine preferentially blocks extrasynaptic over synaptic NMDA receptor currents in hippocampal autapses. *J. Neurosci.* **2010**, *30* (33), 11246-11250.
307. Figueiredo, C. P.; Clarke, J. R.; Ledo, J. H.; Ribeiro, F. C.; Costa, C. V.; Melo, H. M.; Mota-Sales, A. P.; Saraiva, L. M.; Klein, W. L.; Sebollela, A.; De Felice, F. G.; Ferreira, S. T., Memantine rescues transient cognitive impairment caused by high-molecular-weight  $A\beta$  oligomers but not the persistent impairment induced by low-molecular-weight oligomers. *J. Neurosci.* **2013**, *33* (23), 9626-9634.
308. Wu, H. M.; Tzeng, N. S.; Qian, L.; Wei, S. J.; Hu, X.; Chen, S. H.; Rawls, S. M.; Flood, P.; Hong, J. S.; Lu, R. B., Novel neuroprotective mechanisms of memantine: increase in neurotrophic factor release from astroglia and anti-inflammation by preventing microglial activation. *Neuropsychopharmacology* **2009**, *34* (10), 2344-2357.
309. Marotta, G.; Basagni, F.; Rosini, M.; Minarini, A., Memantine Derivatives as Multitarget Agents in Alzheimer's Disease. *Molecules* **2020**, *25* (17), 4005.
310. Fagiani, F.; Catanzaro, M.; Buoso, E.; Basagni, F.; Di Marino, D.; Raniolo, S.; Amadio, M.; Frost, E. H.; Corsini, E.; Racchi, M.; Fulop, T.; Govoni, S.; Rosini, M.; Lanni, C., Targeting Cytokine Release Through the Differential Modulation of Nrf2 and NF- $\kappa$ B Pathways by Electrophilic/Non-Electrophilic Compounds. *Front. Pharmacol.* **2020**, *11*, 1256.
311. Chanput, W.; Mes, J. J.; Wichers, H. J., THP-1 cell line: an in vitro cell model for immune modulation approach. *Int. Immunopharmacol.* **2014**, *23* (1), 37-45.



312. Simoni, E.; Daniele, S.; Bottegoni, G.; Pizzirani, D.; Trincavelli, M. L.; Goldoni, L.; Tarozzo, G.; Reggiani, A.; Martini, C.; Piomelli, D.; Melchiorre, C.; Rosini, M.; Cavalli, A., Combining galantamine and memantine in multitargeted, new chemical entities potentially useful in Alzheimer's disease. *J. Med. Chem.* **2012**, *55* (22), 9708-9721.
313. Rosini, M.; Simoni, E.; Caporaso, R.; Basagni, F.; Catanzaro, M.; Abu, I. F.; Fagiani, F.; Fusco, F.; Masuzzo, S.; Albani, D.; Lanni, C.; Mellor, I. R.; Minarini, A., Merging memantine and ferulic acid to probe connections between NMDA receptors, oxidative stress and amyloid- $\beta$  peptide in Alzheimer's disease. *Eur. J. Med. Chem.* **2019**, *180*, 111-120.
314. Mobbili, G.; Crucianelli, E.; Barbon, A.; Marcaccio, M.; Pisani, M.; Dalzini, A.; Ussano, E.; Bortolus, M.; Stipa, P.; Astolfi, P., Liponitroxides: EPR study and their efficacy as antioxidants in lipid membranes. *RSC Adv.* **2015**, *5*, 98955-98966.
315. Bartolini, M.; Naldi, M.; Fiori, J.; Valle, F.; Biscarini, F.; Nicolau, D. V.; Andrisano, V., Kinetic characterization of amyloid-beta 1-42 aggregation with a multimethodological approach. *Anal. Biochem.* **2011**, *414* (2), 215-225.
316. Bartolini, M.; Bertucci, C.; Bolognesi, M. L.; Cavalli, A.; Melchiorre, C.; Andrisano, V., Insight into the kinetic of amyloid beta (1-42) peptide self-aggregation: elucidation of inhibitors' mechanism of action. *ChemBioChem* **2007**, *8* (17), 2152-2161.
317. Naiki, H.; Higuchi, K.; Hosokawa, M.; Takeda, T., Fluorometric determination of amyloid fibrils in vitro using the fluorescent dye, thioflavin T1. *Anal. Biochem.* **1989**, *177* (2), 244-249.
318. Catani, V. M.; Gasperi, V., Assay of CB<sub>1</sub> Receptor Binding. In *Endocannabinoid Signaling: Methods and Protocols*, Maccarrone, M., Ed. Springer Science: New York, 2016; Vol. 1412, pp 41-55.
319. Mukherjee, S.; Adams, M.; Whiteaker, K.; Daza, A.; Kage, K.; Cassar, S.; Meyer, M.; Yao, B. B., Species comparison and pharmacological characterization of rat and human CB<sub>2</sub> cannabinoid receptors. *Eur. J. Pharmacol.* **2004**, *505* (1-3), 1-9.
320. Dolles, D.; Nimczick, M.; Scheiner, M.; Ramler, J.; Stadtmuller, P.; Sawatzky, E.; Drakopoulos, A.; Sotriffer, C.; Wittmann, H.; Strasser, A.; Decker, M., Aminobenzimidazoles and Structural Isomers as Templates for Dual-Acting Butyrylcholinesterase Inhibitors and hCB(2)R Ligands To Combat Neurodegenerative Disorders. *ChemMedChem* **2016**, *11* (12), 1270-1283.
321. Uliassi, E.; Peña-Altamira, L. E.; Morales, A. V.; Massenzio, F.; Petralla, S.; Rossi, M.; Roberti, M.; Martinez Gonzalez, L.; Martinez, A.; Monti, B.; Bolognesi, M. L., A Focused Library of Psychotropic Analogues with Neuroprotective and Neuroregenerative Potential. *ACS Chem. Neurosci.* **2019**, *10* (1), 279-294.
322. Di Paolo, M. L.; Cozza, G.; Milelli, A.; Zonta, F.; Sarno, S.; Minniti, E.; Ursini, F.; Rosini, M.; Minarini, A., Benextramine and derivatives as novel human monoamine oxidases inhibitors: an integrated approach. *FEBS J.* **2019**, *286* (24), 4995-5015.

# APPENDIX

Copies of  $^1\text{H}$  and  $^{13}\text{C}$  NMR spectra of final compounds 1-30.

